2.05
Mantle Samples Included in Volcanic Rocks: Xenoliths and Diamonds

D. G. Pearson
Durham University, UK
D. Canil
University of Victoria, BC, Canada
and
S. B. Shirey
Carnegie Institution of Washington, DC, USA

2.05.1 MANTLE XENOLITHS: THE NATURE OF THE SAMPLE

2.05.1.1 Occurrence and Classification

Fragments of the Earth's mantle are frequently transported to the surface via volcanic rocks that are dominantly alkaline in nature. These fragments range up to sizes in excess of 1 m across. The term "mantle xenoliths" or "mantle nodules" is applied to all rock and mineral inclusions of presumed mantle derivation that are found within host rocks of volcanic origin. The purpose of this contribution is to review the geochemistry of mantle xenoliths. For detailed petrological descriptions of individual locations and suites, together with their geological setting, the reader is referred to the major reference work by Nixon (1987).

Despite peridotite xenoliths in basalts being recognized for several centuries and comparisons being made to lherzolite massifs (Lacroix, 1893), it was not until work on garnet peridotites and diamonds in kimberlites by Fermor (1913) and Wagner (1914) that such xenoliths were conceptually associated with a peridotite zone in the Earth beneath the crust, i.e., the zone that we now identify as the mantle. Mantle xenoliths provide snapshots of the lithospheric mantle beneath particular regions at the time of their eruption and hence are crucial direct evidence of the nature of the mantle beneath regions where no samples have been exposed by tectonic activity. As such, xenoliths are an essential compliment to tectonically exposed bodies of mantle (orogenic peridotites and ophiolites) that occur at plate boundaries (see Chapter 2.04). One obvious contrast between the mantle samples provided by xenoliths and those provided by peridotite massifs is the lack of field relationships available for xenoliths. Other drawbacks include the small size of many xenoliths. This makes accurate estimation of bulk compositions difficult and accentuates modal heterogeneities. The frequent infiltration of the host magma also complicates their chemical signature. Despite these drawbacks, xenoliths are of immense value, being the only samples of mantle available beneath many areas. Because they are erupted rapidly, they freeze in the mineralogical and chemical signatures of their depth of origin, in contrast to massifs which tend

to re-equilibrate extensively during emplacement into the crust. In addition, many xenolith suites, particularly those erupted by kimberlites, provide samples from a considerably greater depth range than massifs. Over 3,500 mantle xenolith localities are currently known. The location and nature of many of these occurrences are summarized by Nixon (1987). A historical perspective on their study is given by Nixon (1987) and Menzies (1990a). Mantle xenoliths from any tectonic setting are most commonly described from three main igneous/pyroclastic magma types (where no genetic relationships are implied):

(i) Alkalic basalts sensu-lato (commonly comprising alkali basalt-basanites and more evolved derivatives), nephelinites and melilitites.

(ii) Lamprophyres and related magmas (e.g., minettes, monchiquites, and alnoites) and lamproites.

(iii) The kimberlite series (Group I and Group II or orangeites; Mitchell, 1995).

Although mantle xenoliths most commonly occur in primitive members of the above alkaline rocks, rare occurrences have been noted in more evolved magmas such as phonolites and trachytes (e.g., Irving and Price, 1981).

To simplify matters and to circumvent the petrographic complexities of alkaline volcanic rocks in general, we will use the term "alkalic and potassic mafic magmas" to include alkalic basalts, nephelinites, melilitites, and lamprophyres. Occurrence of xenoliths in such magmas can be compared to those occurring in kimberlites and related rocks. As a general rule, the spectrum of mantle xenoliths at a given location varies with host rock type. In particular, alkalic and potassic mafic magmas tend to erupt peridotites belonging predominantly to the spinel-facies, whereas kimberlites erupt both spinel and garnet-facies peridotites (Nixon, 1987; Harte and Hawkesworth, 1989).

Even within either "group" of volcanic rocks the variety of possible xenolith types is great. Table 1 presents a summary of the most common mantle xenolith groups that are found in kimberlitic hosts and within the alkalic and potassic mafic magmas. The significance and abundance of these groups will be discussed below.

Although widespread in the literature, classification of xenoliths on the basis of their host magma is not fully informative. It is more geologically useful to subdivide xenoliths in terms of their tectonic setting. A basic subdivision of xenolith occurrences is between those erupted in oceanic settings and those erupted in continental settings. The continental occurrences far outnumber the oceanic occurrences. The continental occurrences can be further subdivided depending on age of the crust and the tectonic history of the area being sampled. Xenoliths from stable cratonic and circum-cratonic regions are distinctly different in petrology from those occurring in areas that have experienced significant lithospheric rifting, generally in noncratonic crust, in the recent geological past. As such, we will utilize the terms cratonic/circum-cratonic to refer to xenoliths occurring on and around craton margins and the term noncratonic in referring to mantle sampled away from cratons, often in areas that have experienced recent lithospheric thinning. There is a link back to the host rock in that, as a general rule, cratonic and circum-cratonic xenoliths are erupted by kimberlites and noncratonic xenoliths are erupted by alkalic and potassic mafic magmas.

2.05.1.1.1 *Mantle xenoliths in continental volcanic rocks*

Xenoliths found in Archean cratonic regions are characterized by the lithological types reported in Table 1(a). Garnet-facies peridotites dominate the peridotite xenolith inventory in these locations. In contrast, away from cratons, there is a scarcity of garnet-facies peridotites (Table 1(b)). In addition, cratonic xenolith suites contain samples derived from depths ranging from crustal levels to >200 km, whereas noncratonic xensoliths come from less than 140 km deep. There can be distinct differences between xenoliths erupted on craton and those erupted in stable areas of Proterozoic crust marginal to cratons. For instance, subcalcic-garnet harzburgites occur on most cratons but do not occur in circum-cratonic suites (Boyd *et al.*, 1993). In addition, the maximum depths of equilibration of circum-cratonic peridotite suites are less than for cratonic peridotite suites (e.g., Finnerty and Boyd, 1987). These differences warrant the distinction between "cratonic" and "circum-cratonic" xenoliths. In addition, young rift-related magmatism, marginal to cratons, samples very thin lithosphere compared to cratonic and circum-cratonic lithosphere. The xenoliths sampled in this environment fall into the loose category of "noncratonic" xenoliths. A more detailed and complex tectonic classification is provided by Griffin *et al.* (1999a).

2.05.1.1.2 *Mantle xenoliths in oceanic volcanic rocks*

The nature of the suboceanic mantle is largely constrained from geochemical studies of its partial melts (see Chapter 2.08) because occurrences of mantle xenoliths in the ocean basins are much rarer than on the continents. The host rocks for these xenoliths are exclusively alkalic and

Table 1 Major groups of mantle xenoliths in kimberlite-related and alkali basalt series volcanic rocks (after Harte and Hawkesworth, 1989). Textural classification follows that of Harte (1977). Terminology for phlogopite-rich mafic mantle xenoliths from Gregoire *et al.* (2002). For supplementary data and classifications see Nixon (1987), table 62.

Type	*Characteristics*	*Examples*	*Mg# olivine*
(**A**) *Cratonic/circum-cratonic xenoliths erupted by Kimberlite-related volcanics*			
AI: Coarse Mg-rich, low-*T* peridotites	Often abundant. Mostly harzburgites and lherzolites with varying but low modal diopside and garnet. Wide range of orthopyroxene abundance, Kaapvaal examples notably enriched. Crystals typically 0.2 mm with equant or tabular shapes, irregular grain boundaries, rarely granoblastic (Harte, 1977). Bulk compositions typically highly depleted in Fe, Ca, and Al, enriched in Mg. Mineralogy: Cr-rich pyrope, Cr-diopside. Orthopyroxene in garnet facies characterized by >1.0 wt.% Al_2O_3. Cr-spinel sometimes evident. Minor phlogopite common grading into type VIII phlogopite peridotites. Phlogopite often surrounds garnet and is strongly correlated with the presence of diopside. Estimated equilibration temperatures less than 1,100 °C. Equilibration pressures can vary widely within a pipe and range from c. 2 GPa to >6 GPa. Rarely diamondiferous (e.g., Dawson and Smith, 1975), more commonly contain graphite (Pearson *et al.*, 1994).	N. Lesotho (Nixon and Boyd, 1973a), Kaapvaal craton (Gurney and Harte, 1980; Boyd and Nixon, 1978; Boyd and Mertzman, 1987; Nixon, 1987), Siberia (Sobolev, 1974; Boyd *et al.*, 1993); Jericho Slave craton (Kopylova *et al.*, 1999)	Av 92.8 (91–95)
	Subcalcic garnet (high Cr-pyrope; knorringitic) bearing harzburgite varieties scarce but can contain diamond and graphite. Can be megacrystalline. Textures similar to type I. Equilibration temperatures and pressures intermediate between low-*T* and high-*T* lherzolites, i.e., 1,150 °C, 5–6 GPa, but vary widely.	Udachnaya, Siberia (Sobolev *et al.*, 1973; Pokhilenko *et al.*, 1993), Kaapvaal (Boyd *et al.*, 1993)	92–95.5
	Spinel facies widespread but less abundant. Textures as for garnet variety, spinel texture symplectitic or irregular. Equilibration temperatures <800 °C. Can also be orthopyroxene enriched, like garnet facies. Spinel composition can vary widely in Cr# but mostly aluminous. Cr-rich spinels coexist with garnet. Orthopyroxenes in spinel facies have >1.0 wt.% Al_2O_3. Similar range in bulk composition to garnet facies.	Kaapvaal craton (Carswell *et al.*, 1984; Boyd *et al.*, 1999)	91.5–94

AII: coarse, Fe-rich low-*T* peridotites and pyroxenites	Widespread, normally rare but locally abundant. Mainly garnet lherzolites and garnet websterites but also clinopyroxenites and orthopyroxenites ("bronzitites"). Ilmenite can be present in pyroxenites. Coarse grained to "megacrystalline" (at Jericho). Textures and equilibration temperatures as for type I. Sometimes modally layered. Wide ranging bulk and mineral compositions, with high Fe, Ca, Al, and Na relative to type I. Rare fine-grained "quench textured" ilmenite/garnet pyroxenites.	Matsoku, Kaapval craton (Gurney *et al.*, 1975); Jericho, Slave craton (Kopylova *et al.*, 1999); Mzongwana, SE margin Kaapvaal craton (Boyd *et al.*, 1984a)	83–89
AIII: dunites	Widespread, locally common. Two varieties: (i) Highly depleted, coarse to ultracoarse >50 mm olivine (megacrystalline) dunites, often containing chromite or sub calcic high-Cr pyrope and frequently diamondiferous.	Siberia, notably Udachnaya (Pokhilenko *et al.*, 1993)	93–95
		Kimberley (Boyd *et al.*, 1983; Dawson *et al.*, 1981)	85–93
	(ii) Often fine to medium grained more Fe-rich dunites, mineral zoning indicates "metasomatism." Mostly deformed textures. Orthopyroxene, garnet, phlogopite, diopside, chromite present.		
AIV: deformed low-*T* peridotites and pyroxenites	Widespread, locally common. Porphyroclastic or mosaic-porphyroclastic textures. Modal abundances, chemical characteristics and *P*–*T* equilibration conditions similar to those of type I.	Jericho, Slave craton (Kopylova *et al.*, 1999)	91–95
AV: deformed high-*T* peridotites	Widespread but variable abundance in group I kimberlites, absent/scarce in group II kimberlites. Commonly deformed; porphyroclastic and mosaic-porphyroclastic textures with fine neoblasts of olivine. Although generally more depleted than pyrolite, bulk rocks and minerals generally enriched in Fe and Ti compared to type I (low-*T*) and significant compositional overlap of minerals with megacrysts (type X). Equilibration temperatures 1,100 °C to >1,500 °C, equilibration pressures generally 4.5 GPa to >6.5 GPa. Garnets and pyroxenes frequently zoned.	N. Lesotho (Nixon and Boyd, 1973a); Jagersfontein, Kaapvaal craton (Burgess and Harte, 1999); Siberia (Sobolev, 1974; Boyd *et al.*, 1993); Slave (Kopylova *et al.*, 1999); Somerset Island, Churchill Province (Schmidberger and Francis, 1999)	87–92
AVI: phlogopite-rich mafic mantle xenoliths	Widespread and locally common. Olivine poor/absent rocks. Two main subdivisions of this group (Gregoire *et al.*, 2002) are: (i) MARID suite (mica–amphibole–rutile–ilmenite–diopside) with accessory zircon common. Probable genetic link to group II kimberlites. Medium to coarse grained, undeformed to deformed, sometimes modal banding. Amphibole always K-richterite.	Kimberley (Dawson and Smith, 1977; Gregoire *et al.*, 2002)	NA
	(ii) PIC suite (phlogopite–ilmenite–clinopyroxene) with minor rutile. Diopside or Al- and Ti-poor augites. Probable genetic link to group I kimberlites. K-richterite is absent; grade to glimmerites as phlogopite mica reaches >90%. Coarse grained, variably deformed.	Kimberley (Gregoire *et al.*, 2002)	NA

(continued)

Table 1 (continued).

Type	*Characteristics*	*Examples*	*Mg# olivine*
AVII: pyroxenite sheets rich in Fe and Ti	Restricted to Matsoku. Orthopyroxene and clinopyroxene rich rocks with widely variable olivine and garnet compositions, often with ilmenite and phlogopite (the IRPS suite: see type VIII). Bulk compositions Fe and Ti rich. Form magmatic intrusions (<16 cm thick) into type I rocks which become metasomatized.	Matsoku (Gurney *et al.*, 1975; Harte *et al.*, 1975, 1987)	
AVIII: modally metasomatized peridotites	Wide spread, variable abundance. Mostly metasomatized variants of type I. Diverse mineralogies, Two most commonly recognized groups are phlogopite peridotites (PP) and phlogopite–K-richterite–Peridotites (PKP) of Erlank *et al.* (1987). Can be harzburgite or lherzolite, typically coarse grained, undeformed but some display porphyroclastic textures. Assemblages vary with location. Cr-titanate "LIMA" minerals (Lindsleyite–Mathiasite) relatively common at Bultfontein; edenite-phlogopite association at Jagersfontein; ilmenite–rutile–phlogopite–sulfide (IRPS) suite at Matsoku associated with pyroxenitic sheets (type VII). Metasomatic clinopyroxene link to type AI.	Matsoku (Gurney *et al.*, 1975); Kimberley pipes (Erlank *et al.*, 1987; Gregoire *et al.*, 2002); Jagersfontein (Winterburn *et al.*, 1990)	Same as type I, to more Fe-rich.
AIX: eclogites, grospydites, alkremites, and variants	Very widespread, rare to locally abundant. Eclogites (omphacite and pyrope-almandine garnet). Garnet composition widely variable, in grospydites garnet has a large grossular component. At some locations (e.g., Jagersfontein), unusual assemblages of garnet + spinel (Alkremites), garnet + corundum (Corganites) and corundum + garnet + spinel (Corgaspinites) occur (Mazzone and Haggerty 1989). Accessory phases in eclogites include kyanite, corundum, ilmenite, rutile, sanidine, coesite, sulfides, graphite and diamond. Eclogites classified on texture: group I large subhedral to rounded garnets in matrix of omphacite. High Cr, Ca, Fe, and Mn in omphacite. Garnets more Na (avg. 0.1 wt.% Na_2O) and Mg rich. Group II have interlocking texture of anhedral garnet and omphacite and are less altered. Garnets are lower in Na_2O (0.05 wt.%). Common hosts for diamond, especially group I. Not all eclogites of obvious mantle origin and some grade into garnet granulites and pyroxenites of crust origin.	Roberts Victor (MacGregor and Carter, 1970; McCandless and Gurney, 1989); Jagersfontein (Nixon *et al.*, 1978; Mazonne and Haggerty, 1989); Orapa (Robinson *et al.*, 1984), all Kaapvaal craton. Udachnaya, Siberian craton (Sobolev, 1974; Ponomarenko, 1975); Koidu, W. African craton (Tompkins and Haggerty, 1984; Hills and Haggerty, 1989)	NA

AX: megacrysts (discrete nodules)	Single crystals or monomineralic polycrystalline aggregates (sometimes exsolved) weighing up to 15 kg. Rare mutual lamellar or granular intergrowths. Large range in Mg#, Cr, and Ti in a given suite.		
	Cr-poor variety: widespread, locally abundant (e.g., Monastery). Garnets, clino- and orthopyroxenes, phlogopite and ilmenite most common, zircon and olivine rarer. Debatable whether phlogopite and olivine are members of Cr-poor suite. Wide range in chemistry but Cr-poor, Fe–Ti-rich relative to type I (low-*T*) peridotite minerals. Mineral chemistry and estimated equilibration P/Ts overlap those of type V (high-*T*) lherzolites. Some Slave craton "Cr-poor megacrysts" show mineral chemistry links to type II megacrystalline pyroxenite xenoliths. See review of Schulze (1987).	N. Lesotho (Nixon and Boyd 1973b); Monastery (Gurney *et al.*, 1979), Jagersfontein (Hops *et al.*, 1992), Kaapvaal craton; The Malaita megacryst suite (Nixon and Boyd, 1979), occurs in an ocean plateau alnoite, but has many similarities with the kimberlitic low-Cr suite	
	Cr-rich variety: (i) A suite comprising garnet plus ortho- and clinopyroxene, mostly restricted to kimberlites from Colorado-Wyoming. Mineralogically similar to type I lherzolites.	Colorado-Wyoming craton (Eggler *et al.*, 1979)	
	(ii) "Granny Smith" diopsides; bright green Cr-diopside, may contain blebs/intergrowths of ilmenite and phlogopite. Can be polycrystalline.	Kimberley and Jagersfontein (Boyd *et al.*, 1984b)	
	Miscellaneous: mostly garnets and pyroxenes with no clear paragenetic association or links to other megacryst suites. May represent disrupted peridotites/eclogites/pyroxenites.		
AXI: polymict aggregates	Polymict aggregates of peridotite, eclogite and megacrysts, of variable grain size, some containing quenched melt. Mineral assemblages not in elemental or isotopic equilibrium.	Bultfontein, De Beers and Premier mines, Kaapvaal (Lawless *et al.*, 1979). Malaita	Highly variable
AXII: diamond and inclusions in diamonds	Widespread and closely related to cratons. Abundance varies from $<$1 ppm to 100 ppm by weight. Size $\ll$0.1 g to c. 750 g. Type I diamonds contain abundant N, type II low N (Harris, 1987).	All cratons (Harris, 1987; Meyer, 1987)	93–96
	Inclusion suites divided into peridotitic (P-type) and eclogitic (E-type) parageneses.		
	P-type inclusions: high-Cr, low Ca garnet, Cr-diopside, Fo-rich olivine, orthopyroxene, chromite, wustite, Ni-rich sulfide, have restricted, high Mg, high Ni chemistry. Equilibration temperatures 900–1,100 °C.		
	E-Type inclusions: pyrope-almandine, high Na garnet ($>$0.1 wt.%), omphacite, coesite, low-Ni sulfide.		

(continued)

Table 1 (continued).

Type	*Characteristics*	*Examples*	*Mg# olivine*
AXIII: ultra-deep peridotites	Rare and restricted to Jagersfontein (Kaapvaal Craton) and Koidu (W. African craton). Four-phase garnet lherzolite. Close association of pyrope-garnet (~70% py; 2 wt.% Cr_2O_3) and jadeite-rich clinopyroxene (20% Jd, & 4% Di). Clinopyroxene forms either orientated rods in garnet host or as discrete grains attached to garnet in cuspate contact. Both pyroxenes exsolved from garnet at 100–150 km depth. Recombination of garnet gives original depths of derivation of 300–400 km. Discrete garnets and "lherzolites" with eclogitic affinities also found (Sautter *et al.*, 1991).	All samples so far from the Jagersfontein kimberlite, S. Africa (Haggerty and Sautter, 1990; Sautter *et al.*, 1991) and Koidu, Sierra Leone (Deines and Haggerty, 2000)	91.6
(**B**): *Non-cratonic xenoliths erupted by alkalic and potassic mafic magmas sensu lato*[a]			
BI: Cr-diopside lherzolite group	Very widespread and common in a variety of tectonic settings, off-craton. Dominantly spinel-facies (Al or Cr-spinel) lherzolites but can be garnet-facies and garnet-spinel facies (e.g., Vitim). Coarse grained, commonly little deformed, sometimes show preferred orientation. Include harzburgites, orthopyroxenites, clinopyroxenites, websterites, and wehrlites. Pargasite and phlogopite may also be common. Both low TiO_2 and high TiO_2 amphiboles can occur at the same locality. Accessory apatite, can be common locally (e.g., Bullenmerri, Victoria). Interstitial silicate glass can be present. Garnet and spinel facies significantly more olivine-rich and orthopyroxene poor than peridotites from cratons such as Kaapvaal and Siberia. Bulk rocks less depleted in Ca, Al, Fe, and lower in Mg than cratonic peridotites. Minerals generally higher Mg# and Cr# and lower Na and Ti than those of the Al-Augite group. Can be subdivided into type IA (LREE depleted clinopyroxene) and type IB (LREE enriched clinopyroxene).	Victoria, SE Australia (Frey and Green, 1974); Vitim (Ionov *et al.*, 1993a); San Carlos and other W. USA localities (Frey and Prinz, 1978; Wilshire and Shervais, 1975); Eifel (Stosch and Seck, 1980); Hawaii (Jackson and Wright, 1970); Scotland (Menzies and Halliday, 1988) Garnet facies: Thumb, Navajo field (Ehrenberg, 1982a,b); Pali-Aike, Patagonia (Stern *et al.*, 1989); Vitim, S. Siberia (Ionov, 1993a,b)	>0.85, Avg. ~90
BII: Al-augite wehrlite-pyroxenite group	Widespread and common. Frequently clinopyroxene-rich rocks but widely variable: wehrlites, clinopyroxenites, dunites, websterites, lherzolites, lherzites, gabbros. Al-spinel is the typical aluminous phase but may contain plagioclase. Kaersutite common along with apatite, Fe–Ti oxides, and phlogopite. Some igneous and metamorphic textures. Composite xenoliths relatively common (in contrast to kimberlite-related xenoliths). Cross-cutting pyroxene-rich veins and layers may occur in olivine-rich hosts. Olivine-rich aggregates also found in pyroxene-rich xenoliths. Minerals generally lower Mg# and Cr#, higher Ti than those of the type I (Cr-diopside group).	Victoria, SE Australia (Frey and Green, 1974); San Carlos and other W. USA localities (Frey and Prinz, 1978; Wilshire and Shervais, 1975; Irving, 1980); Hawaii (Jackson and Wright, 1970; Irving, 1980)	<0.85

BIII: garnet pyroxenite group	Widespread but not abundant. Garnet clinopyroxenites and websterites plus clinopyroxenites and websterites where pyroxenes commonly show exsolution of garnet and/or spinel as well as Ca-rich or Ca-poor pyroxene. Accessory ilmenite and sometimes apatite. Coarse grained, undeformed textures, sometimes layered. "Basaltic" bulk compositions.	Delegate, SE Australia (Lovering and White, 1969; Irving, 1974), Salt Lake Crater, Hawaii (Beeson and Jackson, 1970)	NA
BIV: modal metasomatic group	Widespread varieties of the above groups showing evidence for modal (or "patent") metasomatism. Wehrlite-clinopyroxenites with mica, glimmerites. Typical metasomatic phases include pargasite/ kaersutite, phlogopite, apatite, and grain-boundary oxides e.g., rutile. Apatite only in some cases. Silicate glass as melting product of amphibole, clinopyroxene, or phlogopite common. Composite xenoliths occur.	Nunivak, Alaska (Francis, 1976), SE Australia (O'Reilly *et al.*, 1991), Menzies and Murthy, 1980a, Vitim (Ionov *et al.*, 1993a), Loch Roag and Fife Scotland (Menzies *et al.*, 1989)	NA
BV: megacrysts	Widespread with variable abundance. Usually large (>1 cm) single crystals. Large range in Mg#, Cr, and Ti in a given suite. Group A: Al-augite, Al-bronzite, olivine, kaersutite, pyrope, pleonaste, plagioclase; some of which may have crystallized from the host magma Group B: Anorthoclase, Ti-mica, Fe–Na salite, apatite, magnetite, ilmenite, zircon, rutile, sphene, and corundum, all of which are likely xenocrysts. Some coarse crystals are undoubtedly derived from disaggregated type I and type II xenoliths.	SE Australia (Binns *et al.*, 1970; Irving and Frey, 1984; Schulze, 1987), Loch Roag, Scotland (Menzies *et al.*, 1989)	NA

[a] Based on Harte and Hawkesworth (1989) with nomenclature from Frey and Green (1974), Wilshire and Shervais (1975), Frey and Prinz (1978), Irving (1980), and Menzies (1983).

potassic mafic magmas. The xenolith suite of the Hawaiian volcanic chain is perhaps the best characterized (Jackson and Wright, 1970) of the ocean islands, while extensive suites have also been found in the Canary Islands (Neumann *et al.*, 1995), Samoa (Hauri *et al.*, 1993), Grande Comore (Coltorti *et al.*, 1999), and Tahiti. Most of these occurrences sample the oceanic lithosphere directly below the islands and those of type I (Table 1) are proposed to be residues of partial melting that have been variably metasomatized, with carbonatite-like fluids frequently being invoked (Hauri *et al.*, 1993; Coltorti *et al.*, 1999). The Hawaiian suite is more complex. Pyroxenites of type II and type III are common and iron-rich peridotites, some with garnet, are thought to be physical mixtures of spinel lherzolites with the pyroxenite suite (Sen and Leeman, 1991).

Some xenolith localities sample the mantle lithosphere beneath oceanic plateaux. The most extensive and varied xenolith suite in this regard is that from Malaita (Solomon Islands) on the margin of the Ontong Java Plateau (Nixon and Boyd, 1979). This locality is hosted by an alnoite and contains both garnet and spinel-facies lherzolites together with a spectacular megacryst suite. Although in an oceanic setting, the variety of the xenolith suite provided by the Malaita alnoite, in particular the megacrysts, show strong similarities to suites from kimberlites (Nixon and Boyd, 1979).

2.05.1.1.3 Mantle xenoliths in subduction zone environments

Although xenoliths from subduction-related tectonic settings have been known for sometime, their detailed relationship to the subduction zone system has been a matter of debate. Most samples are type-I spinel lherzolites and modal metasomatic variants of type IV, most commonly kaersutite and phlogopite. Among the best-known examples are from Itinome-Gata, Japan (Aoki, 1968) and Simcoe, NW, USA (Brandon *et al.*, 1999), although spinel lherzolites from Grenada, Lesser Antilles, also occur. It is not well established whether these xenoliths actually represent parts of the metasomatized mantle wedge above the subduction zone, or simply mantle lithosphere not intimately related to the subduction zone process. McInnes and Cameron (1994) have reported xenoliths from the Tabar–Lihir–Tanga–Feni arc, Papua New Guinea, that are purported to be mantle wedge compositions.

2.05.1.2 Lithologies

2.05.1.2.1 Nomenclature and abundance

An important point to note in the discussion of mantle xenoliths is the varying petrographic nomenclature used. Workers studying noncratonic peridotite xenoliths and orogenic peridotites use the IUGS nomenclature proposed by Streckeisen (1976), i.e., a harzburgite can contain up to 5 modal % clinopyroxene. In contrast, those who study xenoliths from kimberlites use the more thermodynamically consistent "clinopyroxene-free" definition of a harzburgite. This is based on the reasoning that the presence of even the smallest amount of an extra phase, in this case clinopyroxene, reduces the number of degrees of freedom of the system by one (O'Hara *et al.*, 1975).

The terms "parent" or "modal" metasomatism are usually used to infer the presence of minerals additional to those commonly observed in peridotites (e.g., Harte, 1983). There is a growing body of evidence indicating the addition of certainly clinopyroxene and possibly garnet to peridotites during metasomatic events (Erlank *et al.*, 1987; Pearson *et al.*, 2002; Shimizu, 1999; Simon *et al.*, in press). As suggested by Erlank *et al.* (1987), this possibility and its implications for nomenclature should be kept in mind when discussing metasomatic processes and events.

Both mono- and polyminerallic fragments occur as mantle xenoliths. Monominerallic aggregates whose relationship to the host rock is uncertain are generally referred to as "megacrysts" (Table 1), whereas the term "xenolith" is most commonly applied to polyminerallic aggregates that are unlikely to have crystallized directly from the host magma. Many megacrysts, sometimes referred to as discrete nodules/xenoliths, are thought to have some genetic/temporal relationship with the host volcanic rock or magmatic activity associated with producing the host rock (Table 1). As such, they do not generally represent fragments of the Earth's mantle that have been accidentally sampled and their geochemistry will not be described in detail here. The reader is referred to Schulze (1987) for a review of megacrysts petrology and to Harte (1983), Irving and Frey (1984), Hops *et al.* (1992), and Nowell *et al.* (in press) for a discussion of megacryst geochemistry.

Studies of mantle xenoliths have confirmed the view from seismology that peridotite is volumetrically the dominant component of the Earth's shallow mantle (<400 km) (see Chapter 2.02). This is because xenolith suites in almost all tectonic environments are dominated by peridotites. Even at localities where other lithologies such as eclogite dominate the intact xenolith suite, mineral concentrate studies show that peridotite dominates the inventory of entrained mantle material (Schulze, 1989). Major- and trace-element studies of mineral concentrates from mined kimberlites have also been used to illustrate

how the distribution of lithologies varies with depth within a given mantle section (Griffin *et al.*, 1999a).

2.05.1.2.2 Noncratonic xenoliths

Lithologies most common in this tectonic environment are summarized in Table 1(b) and detailed descriptions and summaries of their petrology can be found in Nixon (1987) and Harte and Hawkesworth (1989). The dominant xenolith lithology is spinel lherzolite belonging to type I but garnet-facies xenoliths also occur, such as at Vitim, Siberia (Ionov *et al.*, 1993a) and Pali-Aike, S. America (Stern *et al.*, 1989). Garnet-facies peridotites carried by the Thumb minette, Arizona (Ehrenberg, 1982a) and the Lashaine ankaramitic scoria and carbonantite tuff in Tanzania (Rudnick *et al.*, 1994) bear close similarities to kimberlite-derived xenoliths. This might be expected for Lashaine given the cratonic setting. Noncratonic xenoliths are generally less than 30 cm in size, although exceptions occur. They are on average smaller than at many kimberlite-bone cratonic xenolith locations. Type I peridotites are commonly lherzolites. Type II or Al-augite wehrlite–pyroxenite groups have lower Mg/(Mg + Fe) and Cr/(Cr + Al) but higher titanium than those of type I.

In contrast to cratonic xenoliths, the main two groups of noncratonic xenoliths commonly have overlapping equilibration temperatures and may occur in close association as composite xenoliths, with the Al-augite group showing intrusive relationships into the Cr-diopside group (e.g., Wilshire and Shervais, 1975; Irving, 1980). The type II pyroxenites are interpreted as intrusive magmatic activity within the mantle. However, their bulk compositions are not melts but are a function of magma–wallrock interaction and crystal plating onto the walls of magma conduits (Wilshire and Shervais, 1975; Irving, 1980). Metasomatism, involving introduction of amphibole and biotite as well as variations in mineral chemistry, are common in the vicinity of Al-augite series intrusions.

The most common and widely studied metasomatic phases in noncratonic type I and II xenoliths are amphibole and mica plus, less commonly, apatite, and carbonate. These phases occur as intergranular material or in veins in association with other metasomatic minerals. Amphibole is frequently contained in melt pockets (glass), e.g., Francis (1976). Primary carbonates have been found in peridotite, pyroxenite, and eclogite xenoliths (Ionov *et al.*, 1993b; Pyle and Haggerty, 1994; Ionov, 1998; Lee *et al.*, 2000b). Experimental evidence suggests that carbonate should be a stable mantle phase in peridotitic assemblages, but it is still relatively scarce considering the geochemical evidence suggesting carbonatite metasomatism in mantle peridotites (see review by Menzies and Chazot, 1995). Canil (1990) interprets the general absence of carbonate in mantle xenoliths to dissociation of carbonate during syn-entrainment decompression.

2.05.1.2.3 Cratonic and Circum-cratonic Xenoliths

Much of our knowledge of cratonic and circum-cratonic xenoliths is based on the extensive studies of samples from southern African kimberlites, particularly the diamondiferous kimberlites of the Kaapvaal craton and surrounding areas (Nixon, 1987; Gurney *et al.*, 1991). Similar xenolith suites have now been described from other cratons such as Siberia (Sobolev, 1974; Boyd *et al.*, 1997), the Slave (Kopylova *et al.*, 1999) and Colorado–Wyoming (Eggler *et al.*, 1979) cratons. In addition, kimberlites located on craton margins (Somerset Island; Mitchell, 1977; Schmidberger and Francis, 1999) or in Proterozoic regions surrounding cratons, e.g., Namibia (Mitchell, 1984) can have excellent peridotite suites that mirror those on craton.

Cratonic xenolith suites provided by kimberlites have two main populations of mantle xenoliths that can be distinguished on the basis of their equilibration pressure, temperature, and textures. Type I, or "low-temperature" peridotites, are generally coarse grained, with low levels of deformation and yield equilibration temperatures generally below 1,100 °C (Table 1; Boyd, 1973; Nixon and Boyd, 1973; Harte, 1983; Finnerty and Boyd, 1987). In contrast, "high-temperature" (type V) peridotites are generally finer grained, highly deformed and yield equilibration temperatures between 1,100 °C and 1,500 °C (Boyd, 1973; Nixon and Boyd, 1973; Harte, 1983; Finnerty and Boyd, 1987). Iron-rich (type II) peridotites and deformed, low-temperature peridotite/pyroxenites (type IV) show intermediate features between type I and type V end-members. In contrast to certain noncratonic xenolith suites, composite xenoliths are much scarcer in cratonic xenolith populations. This may be a function of the differing properties of the contrasting host magmas in the two environments. In particular, no clear examples of xenoliths exhibiting contact relations between common type I peridotites and eclogites (and variants) have been found, despite overlaps in their equilibration conditions (Harte and Hawkesworth, 1989). The Matsoku kimberlite is exceptional in its sampling of composite xenoliths, where iron- and titanium-rich pyroxenite sheets (type VII) show intrusive relationships to low-temperature (type I)

peridotites, analogous to the relationships seen in noncratonic type I and type II xenolith groups (Harte *et al.*, 1987).

Harzburgites (clinopyroxene-free assemblages) are relatively common within the low-temperature garnet facies group of kimberlite xenoliths. However, despite a lack of clinopyroxene in hand specimen, mineral chemistry indicates that many of these single-pyroxene garnet peridotite xenoliths equilibrated with clinopyroxene. Kimberlite-derived xenoliths also host a variety of phlogopite-rich mafic xenoliths such as the MARID suite (Table 1; Dawson and Smith, 1977; Gregoire *et al.*, 2002) that show geochemical similarities to kimberlites. Eclogite xenoliths are abundant in some kimberlites (Table 1) and are described in detail in Section 2.05.3.

The megacryst suite is far more common and distinct in kimberlites than in Alkali Basalt Series xenoliths, the one exception being the Malaita megacryst suite (Nixon and Boyd, 1979). Most kimberlitic megacrysts are type X(a) and are believed to be the products of deep crystallization from magma (Nixon and Boyd, 1973b; Menzies, 1983; Harte, 1983). The relationship of this parental megacryst magma to the host kimberlite is debated but must be related in time and space. The mineral chemistry and equilibration conditions of the chromium-poor megacrysts are similar to those of high-temperature type V peridotites (Harte, 1983; Burgess and Harte, 1999). Megacrysts are typically 1, to a few centimeters in diameter. Some localities, such as Monastery, S. Africa, are renown for larger (10 cm and above) samples. Low-chromium garnet megacrysts have been reported from Malaita weighing up to 15 kg (Nixon, 1987).

An unusual variety of ultrahigh pressure xenoliths has been described from the Jagersfontein kimberlite (Haggerty and Sautter, 1990; Sautter *et al.*, 1991). These xenoliths (type XIII, Table 1) comprise four-phase lherzolite, discrete garnets, or iron-rich "lherzolites" with eclogitic affinities (Sautter *et al.*, 1991). Their key characteristic is that the garnets of all varieties contain rods of clinopyroxene that were apparently exsolved from a higher pressure, silicon-rich, majoritic garnet. Equilibration pressures of these samples are 4–5 GPa, but recombination of original garnet compositions before clinopyroxene exsolution gives pressure estimates of 13–15 GPa, equivalent to depths of derivation up to 500 km. Haggerty and Sautter (1990) suggest that similar xenoliths might also be present at other kimberlites such as Koidu, Sierra Leone.

2.05.2 PERIDOTITE XENOLITHS

2.05.2.1 Textures

Mantle xenoliths are metamorphic tectonites whose textures reflect the temperature (T), pressure (P) and differential stress conditions under which they were sampled accidentally by their host magma. The grain size, orientation and interrelationships amongst different minerals with varying strength in peridotites and eclogites will vary depending on the deformation history experienced by the sample, and are used to classify the texture of the rock according to set criteria. Nixon and Boyd (1973a) were some of the first workers to note the relationship between chemistry and texture in peridotite xenoliths. Various classification systems have been devised (e.g., Boullier and Nicolas, 1975; Harte *et al.*, 1975) but the terminology of Harte (1977) is used by most workers (Tables 1 and 2) and will be adopted here.

Xenoliths most commonly show coarse or porphyroclastic textures, or some continuum between the two. The former is defined by a grain size of greater than 2 mm (Table 2) and is commonly equigranular (Figure 1(a)). This texture represents a stable grain size developed under differential stresses that are small and constant over millions of years in the lithosphere. The grain size in olivine, the most abundant but weakest mineral in peridotite xenoliths, can be a measure

Table 2 Brief summary of textural classifications for xenoliths.

Texture	*Grain size*	*Grain boundaries*	*Related terminology*
(1) Coarse	Avg. >2.0 mm	Straight to smoothly curving	Equant, tabular, protogranular,[a] granular[a]
(2) Porphyroclastic (>10% olivine as porhyroclasts)	Two populations: larger p.clasts in finer grained matrix of neoblasts	Straight in neoblasts, irregular in p.clasts	Disrupted, fluidal, sheared[a]
(3) Mosaic porphyroclastic	As in (2)	As in (2)	Fluidal
(4) Granuloblastic	Avg. <2.0 mm	Straight or smooth, polygonal	Equant, tabular

[a] Other terms used in the literature to describe the same texture.

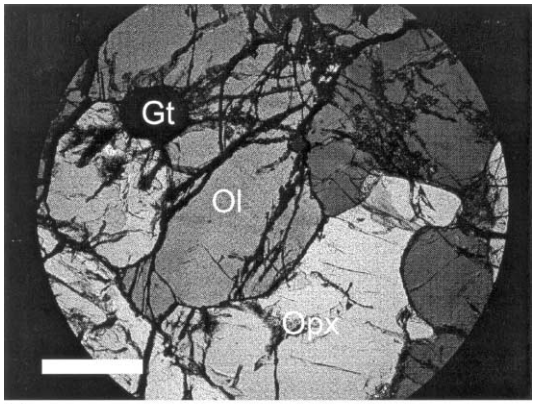

(a)

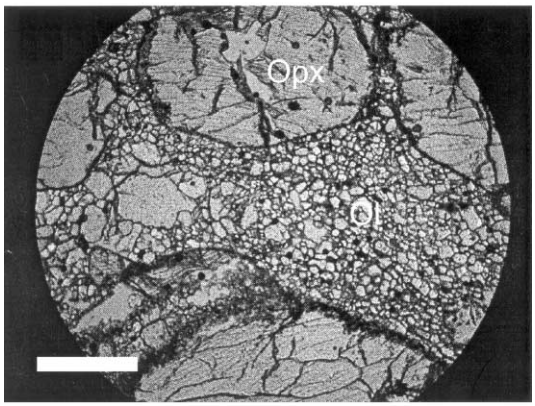

(b)

Figure 1 Common petrographic textures in peridotite xenoliths. Other textural details given in Table 1. (a) Coarse texture in cross-polarized light of garnet peridotite containing olivine (ol), orthopyroxene (opx), and garnet (gt). (b) Mosaic porphyroclastic texture in plane polarized light of garnet peridotite. Both samples are from the Torrie kimberlite, Slave Province (scale bar is 1 mm).

of the state of differential stress. This property of olivine has been calibrated by experiment (Ross *et al.*, 1980) and applied as a grain size "piezometer" to infer states of stress, viscosity, and strain rate in the mantle lithosphere as functions of depth or tectonic setting (Ave Lallement *et al.*, 1980; Mercier, 1980; Ross, 1983). Stress estimates based on this technique are open to interpretation (Twiss, 1977) and may not be entirely representative because the piezometer has been calibrated mainly for aggregates consisting only of olivine, and not multiphase samples.

At higher differential stresses, coarse textures evolve into porphyroclastic, which are defined by the development of smaller neoblasts of olivine amongst stronger pyroxenes, garnet, or spinel (Figure 1(b)). At much higher differential stress or in the presence of melt, fluidal porphyroclastic textures develop, exhibited most classically in garnet peridotite PHN1611. The significance of the latter texture in kimberlite-hosted garnet peridotite xenoliths has been of much interest since its original recognition by Nixon and Boyd (1973a). Proposals for the generation of such textures include shear heating or deformation during related diapiric upwelling. Whatever the cause, porphyroclastic textures cannot be retained for long periods at the high temperatures attendant in the mantle lithosphere, due to the rate at which olivine grains recrystallize and coarsen (Goetze, 1975). Porphyroclastic textures are thus a transient phenomena experienced by samples on a short timescale before entrainment in their host magma, as is also indicated by zoning patterns in minerals from these rocks (Smith and Boyd, 1992).

Gradations between coarse and porphyroclastic textures are observed in some xenolith populations and represent how this recrystallization process can be arrested during sampling by the host magma. In many suites, the change from coarse to porphyroclastic texture occurs as a function of depth, with porphyroclastic textures generally occurring at high temperatures and depths of sampling, although the opposite trend is observed in some suites (Boyd and Nixon, 1978; Franz *et al.*, 1996a).

2.05.2.2 Modal Mineralogy

The modal mineralogy of xenoliths has been used to estimate primitive mantle compositions (Carter, 1970), to constrain the source region of basaltic magmas (Yoder, 1976) and the density of mantle lithosphere (Boyd and McAllister, 1976). Modes in xenoliths are derived by point counting of thin sections or by mass balancing whole-rock compositions with mineral chemical data for all phases present in the xenolith. The former technique is prone to larger uncertainty because standard thin sections (9 cm^2) are not representative of the coarse-grained textures in xenoliths. Larger thin sections can obviate this problem. The mass balance method is more quantitative but uncertainty can arise in coarse rocks if the sample is too small. In addition, minute intergranular secondary phases can contribute significantly to the bulk rock analysis of an element but are not accounted for by the mineral chemistry of the major phases (Boyd and Mertzman, 1987). The mean and median modal mineralogy of cratonic and noncratonic peridotites is summarized in Table 3.

By definition, peridotites contain greater than 40% olivine with lesser amounts of orthopyroxene and clinopyroxene. An aluminous phase, plagioclase, spinel, or garnet may be present depending on the pressure of equilibration and defines the "facies" from which the peridotite xenolith was sampled (Figure 2). Plagioclase-peridotites are generally rare in continental xenolith suites

because this facies is stable only at depths shallower than the Moho (~35 km) in most sections of mantle lithosphere sampled by volcanic rocks. Spinel peridotite is very common in off-craton localities. Although garnet peridotites are most frequently studied in on-craton xenolith suites, spinel-facies peridotites can be common (Boyd *et al.*, 1999). In contrast, garnet peridotites are scarce in off-craton mantle xenolith localities. Transitions between the facies are encountered in some xenolith suites. Accessory amounts of ilmenite, amphibole, phlogopite, apatite, monazite, and even zircon are recognized in some xenolith suites as veins, texturally equilibrated grains or grain boundary phases. These grains are usually interpreted as due to chemical modification (metasomatism) of the original peridotite residue.

Xenoliths may also show a spatial association of minerals. Spinel–pyroxene clusters on centimeter-scales are recognized in some samples and are interpreted to reflect conversion of garnet peridotite through the garnet–spinel-facies transition, either by heating or decompression (Smith, 1977). In some cratonic xenoliths, a spatial association of garnet and pyroxenes has been recognized on scales of up to 8 cm^2 (Boyd and Mertzman, 1987; Cox *et al.*, 1987; Saltzer *et al.*, 2001). The spatial association was originally thought to be of exsolution origin (Cox *et al.*, 1987). At high temperatures along the mantle solidus, orthopyroxene is calcium- and aluminum-rich, and on cooling these components exsolve to produce spatially associated garnet and clinopyroxene (Canil, 1991, 1992). The exsolution origin, however, is inconsistent with isotopic disequilibria recorded between pyroxenes and garnet (Gunther and Jagoutz, 1997). Some xenoliths also contain too much clinopyroxene and garnet to account for by this process alone (Canil, 1992), or from a simple melt depletion perspective (Pearson *et al.*, 2002). This evidence argues for a late introduced component of these minerals, as is also evidenced by trace-element studies reviewed below (Shimizu, 1999; Simon *et al.*, 2003). The spatial associations in xenoliths emphasize the potential heterogeneity problem in the chemical analysis of coarser-grained xenoliths. The implication is that xenoliths with small sizes may not be mineralogically representative of the volume of mantle they sample.

Boyd (1989) compiled modes of major minerals in peridotite xenoliths from on and off-craton localities and compared the results with mantle residues from oceanic mantle represented by

Table 3 Mean and median modal mineralogy of xenoliths.

	ol	*opx*	*cpx*	*sp*	*gt*
Off-craton ($n = 98$)					
Average	63.7	21.5	11.7	1.8	9.6
Median	62.9	21.8	12.9	1.7	11.4
1σ	8.4	6.6	5.2	0.8	6.1
On-craton ($n = 210$)					
Average	71.9	20.8	3.3	1.1	6.2
Median	72.0	20.6	2.0	0.8	5.3
1σ	11.6	10.3	4.5	1.0	3.8

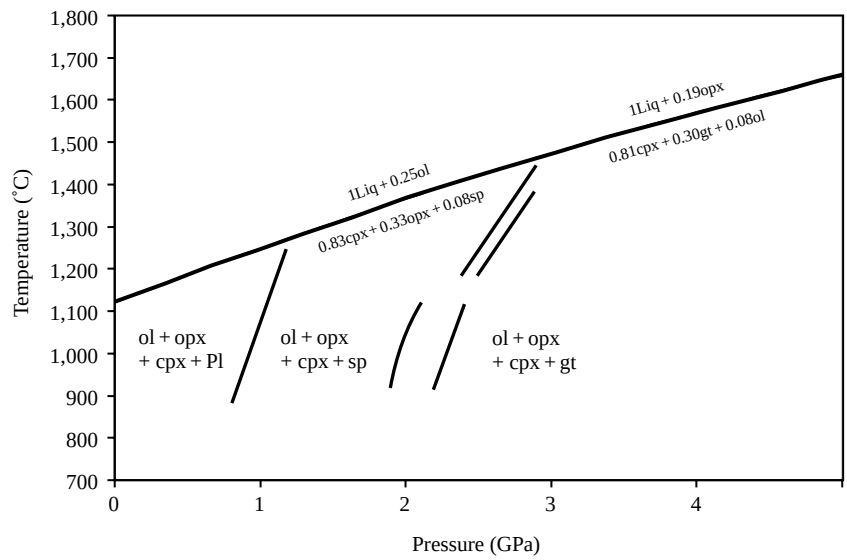

Figure 2 Pressure–temperature diagram showing solidus (after Hirschmann, 2000) and phase boundaries (after Koga *et al.*, 1999) defining the plagioclase-, spinel-, and garnet- facies of peridotite from various experimental studies (Green and Hibberson, 1970; Green and Ringwood, 1970; Nickel, 1986; O'Neill, 1980). Two different versions of the spinel–garnet phase boundary are shown. The stoichiometry of melting reactions on the solidus at different pressures is after Robinson *et al.* (1998) and Walter (1998).

ophiolites and abyssal peridotites. Boyd (1989) showed that in off-craton suites, ophiolites and abyssal peridotites, the amount of olivine shows a good correlation with the degree of depletion in the xenolith, defined by the Mg/(Mg + Fe) (i.e., Mg#) in olivine. In contrast, xenoliths from the Kaapvaal craton have far less olivine and far more orthopyroxene than expected from simple melt depletion (see Chapter 2.08). The latter attribute is reflected by the lower Mg/Si ratio of these rocks (Section 2.05.2.5).

The modal abundances of olivine, orthopyroxene, clinopyroxene and spinel observed for spinel peridotites from six well-characterized off-craton xenolith suites are plotted against a depletion index in Figures 3(a)–(c). The amount of olivine correlates negatively with degree of depletion, as expected because olivine is a product of the reaction that produces melt at the solidus (Figure 2) (see Chapter 2.08). The number of samples compiled ($n = 143$) may not be completely representative, but there is nonetheless a suspicious population gap at ~2 wt.% Al_2O_3. At higher levels of depletion, the rocks are harzburgites (<5% cpx), and the slope of the negative correlation between olivine and Al_2O_3 is steeper (Figure 3(a)), suggesting a change in melting reaction, as is observed in peridotite melting experiments (Baker and Stolper, 1994; Robinson *et al.*, 1998). All five xenolith suites have samples within this group (Figure 3(a)) and thus exhibit bimodality, as noted previously (Shi *et al.*, 1998) but reasons for its origin are unclear.

The trend for orthopyroxene with depletion is more constant, whereas clinopyroxene and spinel show good positive correlations (Figures 3(a)–(c)). In melting reactions on the solidus, clinopyroxene contributes the most to the melt phase (Figure 2) and thus is consumed most rapidly with depletion until it is exhausted after ~20% melting.

Differences between the modes observed in spinel peridotite xenoliths and those predicted by experiment may result because the former are not simple residues, and have had components introduced after their original formation.

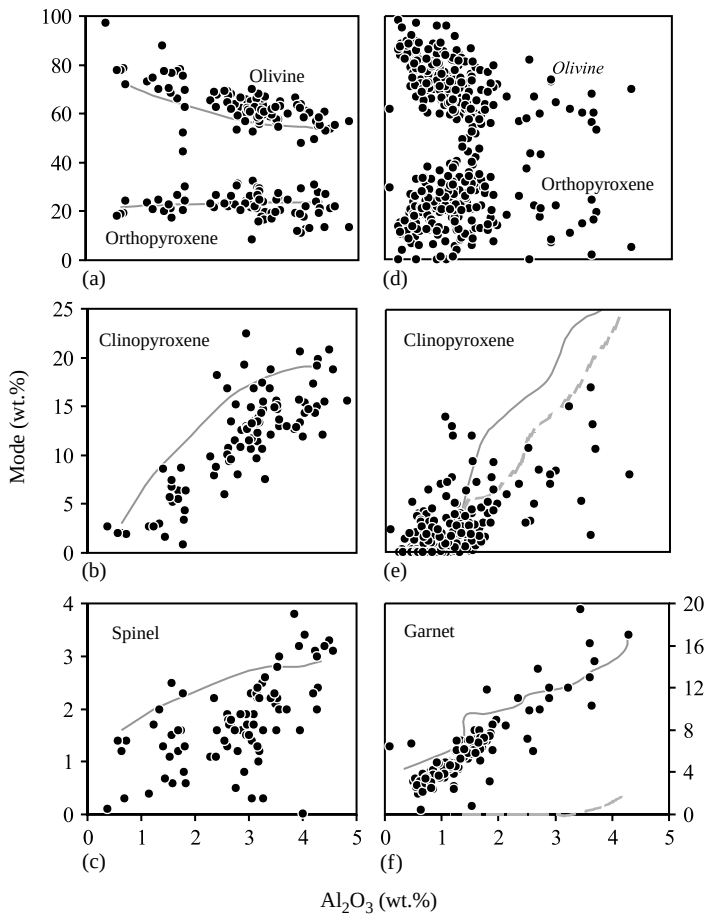

Figure 3 Modal abundances in (a–c) off-craton and (d–f) on-craton xenoliths as a function of depletion (indexed by wt.% Al_2O_3). Shown for illustrative purposes are calculated modal variations in residues as a function of melt fraction for melting at 1.5 GPa (a–c) and 3 GPa and 7 GPa (d–f) using empirical methods in Canil (2002). Data sources in Table 6.

More likely, however, is that modes measured experimentally at high T along the solidus cannot be directly compared with those observed in xenoliths that have cooled hundreds of degrees, changing their modal proportions slightly. Furthermore, the model melting trends and reactions vary in detail depending on the model source mineralogy or melting process (equilibrium versus fractional). Nonetheless, the trends observed in xenoliths generally correlate with those determined in experiment, reiterating the basic tenet that the modal proportions in peridotite xenoliths are due to a source–residue relationship with basaltic/komatiitic melt extraction (Carter, 1970; Walter, 1998; see also Chapter 2.08).

Figures 3(d)–(f) compares modes observed in four well-characterized on-craton xenolith suites ($n = 189$) with degree of depletion. When compared to the off-craton samples, trends are far more scattered for olivine and orthopyroxene, and a significant population of samples are orthopyroxene-rich, as originally remarked by Boyd (1989). The trend for garnet is remarkably regular and uniform, whereas many samples contain far more clinopyroxene than expected for their level of depletion. This excess clinopyroxene may be of exsolution origin, or introduced to the rock after its original formation as a residue (Canil, 1992; Shimizu, 1999; Simon *et al.*, 2003). Comparison with trends expected from peridotite melting models is complicated by the fact that orthopyroxene is replaced at the solidus by a low calcium clinopyroxene, and is a product of the melting reaction at $P > 3$ GPa (Walter, 1998). The mean and median modes of off-craton and on-craton xenoliths from Figure 3 are summarized in Table 2.

2.05.2.3 Mineral Chemistry

2.05.2.3.1 Olivine

Olivine is the main constituent of peridotite xenoliths and is a major host for magnesium, iron, and nickel. The Mg# of olivine reflects that of the whole rock which in turn is related to the degree of melt depletion or enrichment in iron. The Mg# of peridotitic olivine is between 88–92, and 91–94 for off- and on-craton mantle xenoliths, respectively, reflecting the generally more iron-depleted nature of the latter (Boyd and Mertzman, 1987; Boyd, 1997). Xenoliths that have been metasomatized by silicate melt, or that are the crystallization products of silicate melts are generally iron-enriched relative to depleted peridotite and hence have lower olivine Mg# (Table 1). Iron-rich olivines are also found in iron-rich lherzolite xenoliths from Hawaii, where they are interpreted as resulting from physically mixing iron-rich pyroxenites with normal peridotite followed by subsequent re-equilibration (Sen and Leeman, 1991). Carbonatite metasomatism may increase Mg# in secondary olivines due to introduction of magnesium (Hauri and Hart, 1993; Ionov *et al.*, 1993b). Typical analyses are listed in Tables 4 and 9.

2.05.2.3.2 Orthopyroxene

The Mg# of orthopyroxene is similar or slightly greater than that of olivine, due to a relative Fe–Mg partition coefficient (K_D) of ~1 that is independent of P and T (von Seckendorff and O'Neill, 1993). The calcium content of orthopyroxene also varies depending on the temperature of equilibration of the sample and its bulk composition. In both the spinel- and garnet-facies, the CaO content increases with T and varies between 0.2 wt.% and 2.0 wt.%. Orthopyroxenes with very low CaO occur in harzburgites and/or in low-T samples in many kimberlite-borne xenolith suites.

The Al_2O_3 content of orthopyroxene varies greatly in xenoliths depending on the T and P of equilibration of the sample, as well as its bulk composition. In the spinel peridotite facies, the Al_2O_3 content is controlled by T and varies between 1 wt.% and 6 wt.%. In the garnet-facies, the Al_2O_3 content is controlled by both P and T, and is usually below 2 wt.%. Very depleted harzburgites have low Al_2O_3 in orthopyroxene regardless of facies, as evident in samples from the Colorado Plateau (Smith *et al.*, 1999) and in many cratonic xenoliths (Boyd and Mertzman, 1987). The Cr_2O_3 of orthopyroxene is low (<0.6 wt.%); this element can substitute for aluminum and so may vary with T and P (Nickel, 1986). The Fe_2O_3 is generally very low (<0.15 wt.%) but can increase in high-T porphyroclastic xenoliths such as PHN1611 (>0.3 wt.%) and hence affect P–T estimates (Brey and Köhler, 1990; Carswell, 1991; Taylor, 1998). Representative analyses of orthopyroxene in different peridotite facies are shown in Tables 4 and 9.

2.05.2.3.3 Clinopyroxene

Clinopyroxene is a major host for sodium, calcium, chromium, and titanium in mantle xenoliths and shows extensive solid solution toward orthopyroxene and/or garnet at high P and T in the mantle (Boyd, 1969, 1970; Brey and Köhler, 1990). The Mg# of clinopyroxene is usually slightly greater than that of coexisting olivine, due to a K_D greater than 1. The calcium content of clinopyroxene is strongly T-dependent and is between 40 mol.% and 50 mol.% wollastonite component. Subcalcic clinopyroxenes

Table 4 Representative major element mineral chemical data for peridotite xenoliths from different facies (wt.%).

Mineral	*Sample #*	*Facies*	SiO_2	TiO_2	Al_2O_3	Cr_2O_3	FeO	Fe_2O_3	NiO	MnO	MgO	CaO	Na_2O	*Total*	*Location*	*Data source*
Plagioclase	RH07-217c	Plag-sp	48.64		33.71		0.03					16.28	2.19		Antarctica	Zipfel and Worner (1992)
Clinopyroxene	RH07-217c	Plag-sp	52.32	0.48	5.71	0.84	3.08			0.15	16.02	20.75	1.01	100.12	Antarctica	Zipfel and Worner (1992)
	Pali No. 2 35-H	Plag-sp	50.19	0.65	6.77	1.82	3.3			0.05	16.05	19.81	0.92	99.56	Hawaii	Sen (1988)
	Pali No. 2 36-H	Plag-sp	51.8	0.85	6.37	0.28	4.84				16.61	17.91	1.22	99.88	Hawaii	Sen (1988)
	2905	Sp	52.4	0.39	6.18	0.89	2.35	0.5		0.05	15.3	20.3	1.57		Noorat, Australia	Canil and O'Neill (1996)
	313-37	Sp-gt	52.21	0.45	6.04	1	2.9				15.43	19.12	1.87	99.02	Vitim	Ionov (1996)
	314-74	Sp-gt	52.6	0.28	6.24	1.06	2.72				16.08	19.48	1.47	99.93	Vitim	Ionov (1996)
	313-1	gt	52.82	0.5	5.67	1.29	2.78				15.41	19.04	1.92	99.43	Vitim	Ionov (1996)
	313-3	gt	52.84	0.57	5.81	1.32	3				15.52	18.77	1.99	99.82	Vitim	Ionov (1996)
	FRB 1350	Sp-gt	54.9	0.03	2.04	0.9	1.5	0.23			17.3	22.9	1.23	101	Kaapvaal	Canil and O'Neill (1996)
	BD 1150	gt	54.3	0.18	2.62	1.74	1.97	1.03			16.2	19.7	1.74	99.5	Kaapvaal	Canil and O'Neill (1996)
	PHN 5267	gt	56.8		1.35	0.57	2.89	0.48			21.5	16.8	0.75	101.1	Kaapvaal	Canil and O'Neill (1996)
	PHN 1611	gt	55	0.34	2.46	0.53	5.43				20.9	14.2	1.52	99.7	Kaapvaal	Smith *et al.* (1991)
Orthopyroxene	RH07-217c	Plag-sp	57.32	0.02	3.06	0.31	6.32			0.15	34.64	0.51	0	102.33	Antarctica	Zipfel and Worner (1992)
	Pali No.2 35-H	Plag-sp	55.27	0.14	3.87	0.26	6.72			0.08	33.6	0.61	0.22	100.77	Hawaii	Sen (1988)
	Pali No.2 36-H	Plag-sp	55.5	0.12	2.93	0.15	7.9				33.4	0.2	0.1	100.3	Hawaii	Sen (1988)
	2905	Sp	56	0.05	4.18	0.18	5.9	0.42		0.1	34	0.55	0.1		Noorat, Australia	Canil and O'Neill (1996)
	313-37	Sp-gt	55.53	0.14	3.96	0.49	5.92		0.11		32.51	0.8	0.17	99.63	Vitim	Ionov (1996)
	314-74	Sp-gt	55.61	0.08	4.44	0.52	5.54		0.06		33.21	0.75	0.12	100.33	Vitim	Ionov (1996)

(continued)

Table 4 (continued).

Mineral	*Sample #*	*Facies*	*SiO_2*	*TiO_2*	*Al_2O_3*	*Cr_2O_3*	*FeO*	*Fe_2O_3*	*NiO*	*MnO*	*MgO*	*CaO*	*Na_2O*	*Total*	*Location*	*Data source*
	313-1	gt	55.41	0.19	3.85	0.55	5.88		0.09		32.94	0.75	0.14	99.8	Vitim	Ionov (1996)
	313-3	gt	55.16	0.17	3.73	0.53	5.98		0.03		32.94	0.76	0.11	99.41	Vitim	Ionov (1996)
	FRB 1350	Sp-gt	58	0.03	1.13	0.22	4.89	0.35			36.5	0.27		101.3	Kaapvaal	Canil and O'Neill (1996)
	BD 1150	gt	56.9	0.07	0.72	0.2	5.08	0.63			35.2	0.75	0.1	99.7	Kaapvaal	Canil and O'Neill (1996)
	PHN 5267	gt	56.4		0.91	0.24	4.53	0.44			35	1.38	0.16	99.1	Kaapvaal	Canil and O'Neill (1996)
	PHN 1611	gt	56.1	0.23	1.36	0.22	6.71				32.5	1.59	0.33	99	Kaapvaal	Smith *et al.* (1991)
Spinel	RH07-217c	Plag-sp		0.01	56.86	13.34	10.44			0.1	20.13			100.91	Antarctica	Zipfel and Worner (1992)
	Pali No.2 35-H	Plag-sp		0.2	39.76	25.97	16.96			0.11	17.04	0.78		100.82	Hawaii	Sen (1988)
	Pali No.2 36-H	Plag-sp	0.08	0.62	53.1	8.6	15.6			0.06	19.03	0.06		97.16	Hawaii	Sen (1988)
	2905	Sp		0.5	57.4	11.5	9.1	1.79			20.3					Canil and O'Neill (1996)
	313-37	Sp-gt	0.13	0.43	43.47	22.37	13.42		0.22		18.55			98.59	Vitim	Ionov (1996)
	314-74	Sp-gt	0.12	0.27	47.61	18.25	12.66		0.27		20.12			99.3	Vitim	Ionov (1996)
	313-3	gt	0.11	0.45	44.79	23.05	13.6		0.18		18.92			101.1	Vitim	Ionov (1996)
	FRB 1350	Sp-gt		0.1	19.3	49.4	14.8	2.78			13.4			99.7	Kaapvaal	Canil and O'Neill (1996)
Garnet	313-37	Sp-gt	42.28	0.13	23.42	1.18	7.01			0.33	20.97	5.18		100.5	Vitim	Ionov (1996)
	314-74	Sp-gt	43.41	0.13	23.86	1.18	6.34			0.24	21.47	5.14		101.77	Vitim	Ionov (1996)
	313-1	gt	42.53	0.12	23.62	1.18	7.21			0.24	20.77	4.82		100.49	Vitim	Ionov (1996)
	313-3	gt	42.67	0.19	23.25	1.14	7.51			0.19	20.91	4.9		100.76	Vitim	Ionov (1996)
	FRB 1350	Sp-gt	42	0.03	22.1	2.07	7.95	0.31			20.1	5.43		100	Kaapvaal	Canil and O'Neill (1996)
	BD 1150	gt	41.6	0.02	21.3	2.64	8.09	0.81			19.9	4.54		98.9	Kaapvaal	Canil and O'Neill (1996)
	PHN 5267	gt	42.3	0.03	20.5	3.54	5.63	0.85			22.3	4.93	0.02	100.1	Kaapvaal	Canil and O'Neill (1996)
	PHN 1611	gt	42.6	0.67	21.1	2.22	8.65			0.22	21.1	4.63	0.06	101.3	Kaapvaal	Smith *et al.* (1991)

(Wo $<35\%$) occur in cratonic suites as megacrysts or discrete nodules, and indicate very high T of equilibration, perhaps in equilibrium with melt (Boyd, 1969, 1970; Boyd and Nixon, 1978).

The Al_2O_3 content of clinopyroxene varies between 1 wt.% and 7 wt.% and shows a positive correlation with both T of equilibration and the bulk composition. Up to 3 wt.% Cr_2O_3 is observed in xenolith clinopyroxenes. The molar Cr/Al in clinopyroxene is nearly identical to that of the bulk rock and correlates positively with the level of depletion. Up to 35% of all iron in clinopyroxene is Fe^{3+} and the partition of this cation between clinopyroxene and garnet may vary with T or f_{O_2} (Luth and Canil, 1993; Canil and O'Neill, 1996).

In a given facies, the sodium and titanium content of clinopyroxene shows a negative correlation with depletion (or chromium content) and can increase substantially in metasomatized xenoliths. The substitution of sodium, chromium, and aluminum has a complex relationship with T, P and degree of depletion but in general, clinopyroxene from higher P samples contains more sodium. Representative analyses for different peridotite facies are shown in Table 4.

Many xenoliths can show two generations of clinopyroxene. Second generation clinopyroxene can occur as a minor phase on primary rims or along grain boundaries, and is usually related to infiltration of the host magma. When compared to primary clinopyroxene, secondary clinopyroxene is usually very high in calcium and low in sodium, aluminum, and/or Mg#. The contribution of secondary clinopyroxene to bulk rock sodium, calcium, or iron contents can be considerable (Boyd *et al.*, 1997).

Pyroxenites (as opposed to eclogites) commonly have sodium-rich aluminous augite as their clinopyroxene. Clinopyroxenes from MARID xenoliths are aluminum- and titanium-poor Mg-augites or diopsides (Dawson and Smith, 1977).

2.05.2.3.4 Spinel

The chemical systematics of spinel in peridotite xenoliths and xenocrysts have been reviewed at length (Arai, 1994; Roeder, 1994; Barnes and Roeder, 2001). The Cr/(Cr + Al) and Fe/Mg ratio of spinel in xenoliths shows a strong positive correlation (Figure 4). For a nearly constant mantle olivine composition, the Fe/Fe + Mg) of spinel increases with decreasing T of equilibration. The Cr/(Cr + Al) reflects both the degree of depletion of the bulk rock and also the T and P (and/or facies) of equilibration. Spinels crystallized from depleted xenoliths or at high P in the garnet-facies have high Cr/(Cr + Al), whereas spinel from less depleted xenoliths or at lower T or P in the spinel-facies

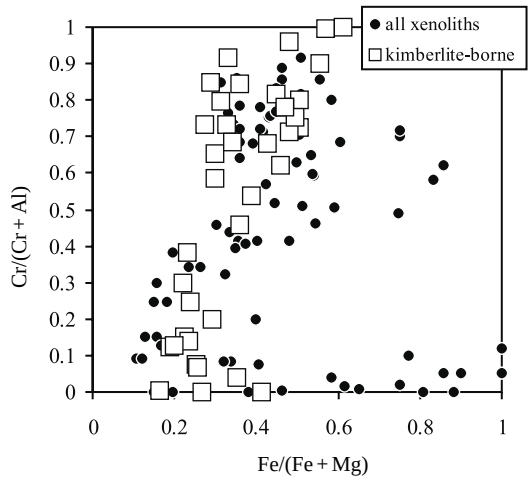

Figure 4 Covariation of Cr/(Cr + Al) and Fe/(Fe + Mg) in spinels from mantle xenoliths in kimberlites and other volcanic rocks. The data points are representative of the extremities of fields for a database of 2.5×10^4 analyses (source Barnes and Roeder, 2001).

have low Cr/(Cr + Al) (Roeder, 1994). The TiO_2 contents of mantle spinels are low (<0.5 wt.%) and correlate with level of depletion in the xenolith.

The Fe^{3+} content in xenolith spinels is large and unlike garnet or pyroxenes can be measured reliably from electron microprobe methods (Wood and Virgo, 1989) and is useful for oxygen barometry of spinel peridotites (Wood *et al.*, 1990; Ballhaus *et al.*, 1991). Representative analyses from different peridotite facies are shown in Table 3.

2.05.2.3.5 Garnet

The major-element systematics of mantle garnets were recently reviewed by Griffin *et al.* (1999a) using a database of over 12,000 analyses. A database of over 900 garnets is used in plots here for illustrative purposes. The Mg# of garnets from peridotite xenoliths ranges from 0.75 to 0.90 and is sensitive to T-dependent exchange with coexisting olivine, but these correlations can be obscured by bulk composition effects (Griffin *et al.*, 1999a). Typical analyses are given in Table 4.

The different trends of garnets on a CaO versus Cr_2O_3 plot (Figure 5) are useful for distinguishing the protolith of garnet xenocrysts (Gurney and Switzer, 1973; Sobolev *et al.*, 1973; Schulze, 1995) and garnets from spinel-bearing peridotite (Kopylova *et al.*, 2000). The positive correlation of CaO with Cr_2O_3 in peridotite garnets arises from a complex interplay of P, T, bulk composition and reciprocal solid solution effects between

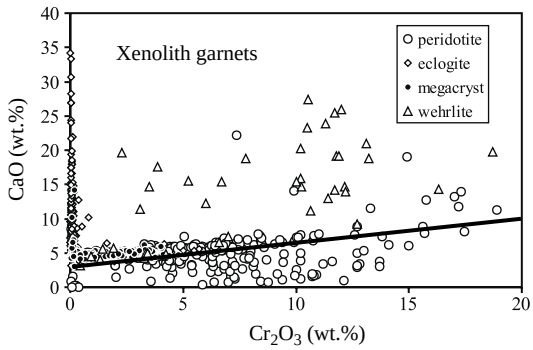

Figure 5 Covariation of CaO with Cr_2O_3 in garnets from a large database ($n = 900$) from a wide variety of xenoliths in kimberlites and other alkaline rocks. Note the positive correlation of calcium and chromium in peridotite garnets. Garnets below the line are "harzburgitic," whereas those above it are lherzolitic or wehrlitic.

Ca–Mg–Fe and Al–Cr end-member components in garnets (Wood and Nicholls, 1978; Nickel, 1986; Girnis and Brey, 1999). To a first order the Cr_2O_3 of peridotitic garnet is controlled by the level of depletion, as shown by a good negative correlation with bulk rock Al_2O_3 (Griffin *et al.*, 1999b), whereas the Ca/Cr ratio depends on $P-T$ of equilibration as well as the Cr/Al ratio of the bulk rock. The high Cr/Al observed in many peridotitic garnets requires a protolith with high Cr/Al, which cannot be achieved by melting in the garnet facies. Protoliths to these chromium-rich garnets must have formed in the spinel peridotite facies (Bulatov *et al.*, 1991; Canil and Wei, 1992; Stachel *et al.*, 1998). Subcalcic (harzburgitic) garnets are confined mainly to lithosphere sampled beneath terrains older than 2.5 Ga and are commonly associated with the presence of diamond (Gurney and Switzer, 1973; Sobolev *et al.*, 1973; Pokhilenko *et al.*, 1993). These subcalcic and chromium-rich garnets are far less abundant in suites from 2.5 Ga to 1 Ga terrains and are absent from mantle beneath terrains less than <1 Ga (Griffin *et al.*, 1999a).

Mantle garnets have $Fe^{3+}/\sum Fe$ ratios of 0.02–0.15 (Luth *et al.*, 1990). The Fe^{3+} content in garnet correlates with T of equilibration and Fe_2O_3 of the bulk rock (Canil and O'Neill, 1996) and is also a useful oxygen barometer for garnet peridotites (Luth *et al.*, 1990; Gudmundsson and Wood, 1995).

2.05.2.3.6 Plagioclase

Plagioclase occurs only in peridotite xenoliths sampled from areas of high geothermal gradient and thinned crust, where the plagioclase-facies is stable and can be sampled from beneath the Moho (Figure 2). It may also occur in shallow lithosphere that has been impregnated by melts (Sen and Leeman, 1991). Plagioclase in peridotite xenoliths is typically calcic (An60–90) due to the low Na_2O levels of most peridotites.

2.05.2.3.7 Amphibole

Amphiboles in most noncratonic xenoliths are essentially (Ti,Cr)-pargasites or, less commonly, kaersutites (Ionov *et al.*, 1997). Those in cratonic xenoliths are typically K-richterites (in MARID/PKP rocks; Gregoire *et al.* (2002); see Table 1 for definitions) or pargasite (Winterburn *et al.*, 1990). Mg# in most cases is close to coexisting pyroxenes (89–91) but vein amphiboles can be lower (Ionov *et al.*, 1997). Mg# for K-richterites in MARID xenoliths is in the range 87.2–92.8. Titanium contents of disseminated amphibole are also generally lower than in vein amphibole. K_2O contents of vein pargasite (1–2%) are higher than disseminated crystals in non-cratonicxenoliths. K-richterites from MARIDS have significantly higher but homogenous K_2O (4.25–4.95 wt.%).

2.05.2.3.8 Mica

Mica in mantle xenoliths is usually phlogopite in composition (Carswell, 1975; Ionov *et al.*, 1997). Mg# usually mimics coexisting pyroxenes, generally being high. MARID phlogopites have Mg# from 87.3 to 88.4 and Al_2O_3 from 10.95 wt.% to 11.2 wt.% (Gregoire *et al.*, 2002). As with amphibole, vein phlogopite can have lower Mg# but higher titanium compared to that disseminated in a peridotite matrix. K_2O contents are generally between 8 wt.% to 10.5 wt.% for phlogopites from veins, metasomatized peridotites or MARID/PIC assemblages (Table 1).

2.05.2.4 Thermobarometry

Defining the distribution of temperature at depth within the Earth as a function of both space and time is the basis for understanding many geological processes (Verhoogen, 1956). Xenoliths have a very central place in this effort because they are pieces of lithosphere and chemical exchange amongst the minerals in these rocks record the physical conditions at the time of their entrainment. In this way xenoliths have become ground-truth information for remote sensing studies of the state of the lithosphere by geophysical techniques.

Thermobarometry is the estimation of the equilibrium temperatures and pressures (depths) recorded by mineral chemical equilibria.

Thermobarometry of mantle xenoliths has been a fruitful endeavour since the pioneering work of Boyd (1973) and serves many purposes:

(i) It provides an estimation of the depth interval and minimum thickness of the lithosphere sampled by a volcanic rock. Because xenoliths are accidentally sampled, not all depth intervals are necessarily represented in a xenolith population.

(ii) The pressures and temperatures provide some spatial context amongst samples within a xenolith population, which may perhaps be divisible according to their textures and/or compositions. This is the basis for the commonly used low (<1,100 °C) versus high (>1,100 °C) T classification of xenoliths from cratonic lithosphere (Boyd and Mertzman, 1987; Boyd, 1989). The depth estimates also provide some insight into the scale of heterogeneity in the textures or bulk chemistry in a xenolith population.

(iii) In many circumstances, xenolith suites may record a regular P–T gradient which can be used to define paleogeothermal gradients in the lithosphere, which vary with tectonic setting and/or age of the crustal province, and provide some insight into the thermal state of the mantle in these environments.

A number of experimentally calibrated thermobarometers are available to estimate the P and T of polymineralic mantle xenoliths, depending on the mineral assemblage present (Table 5). Brey (1990) estimates that for rocks equilibrated within the P and T range of experiments used to construct the Brey *et al.* (1990) thermobarometer combination, accuracy is ±60 °C and 0.45 GPa. Not all methods necessarily agree for all exchange equilibria amongst all minerals in a given sample. Geobarometry of peridotites has mainly been confined to garnet-facies samples, utilizing the P dependence of chromium or aluminum solubility in pyroxenes coexisting with garnet (Brey *et al.*, 1990; MacGregor, 1974; Nickel and Green, 1985; Nimis and Taylor, 2000). In general, there are few geobarometers available for spinel-facies rocks. The exchange of calcium between olivine and clinopyroxene is P-dependent but is also highly T-sensitive and so late stage heating in xenoliths can be a problem for this method. Currently this geobarometer is the only quantitative method for spinel-facies rocks, but its application can also be analytically challenging. Accurate results, however, are obtainable with careful work (Köhler and Brey, 1990).

The accuracy of xenolith thermobarometry has been critically evaluated several times (Finnerty, 1989; Carswell, 1991), most recently by Smith (1999). Smith (1999) finds that most thermobarometers agree in the range between 900 °C and 1,100 °C and 2–5 GPa. Deviations between thermobarometers below and above that T range partly relate to shortcomings in the experimental calibrations for some exchange equilibria, to the lack of constraints on Fe^{3+} contents of minerals, or to the variable kinetic responses for different cations during chemical exchange amongst minerals (e.g., aluminum exchange versus Fe–Mg exchange). The latter problem can be exploited to unravel the thermal history of individual samples or sections of mantle sampled (Smith *et al.*, 1991; Smith and Boyd, 1992; Franz *et al.*, 1996a,b) but relies on an experimental database for diffusion that is not particularly well-constrained for some cations in mantle minerals (aluminum, chromium). Some limits can be placed on these quantities using

Table 5 Some thermobarometers applicable to xenoliths.[a]

Method[b]	*Assemblage*	*Equilibria*	*Comments/caveats*	*Accuracy*[c]
Barometers				
P_{BKN}	gt–opx	Al exchange	gt-facies only	0.5 GPa
P_{NT}	cpx–gt	Cr/Al exchange	gt-facies only	0.3 GPa
P_{KB}	ol–cpx	Ca exchange	Very T sensitive, analytically challenging	0.7
Thermometers				
T_{WS}	opx–sp	Al exchange	sp-facies only	
T_{Ball}	ol–sp	Fe–Mg exchange	Very T sensitive, fast response	30 °C
T_{BKN}	opx–cpx	Ca–Mg exchange	Insensitive to Fe^{3+}	60 °C
T_{TA}	opx–cpx	Ca–Mg exchange	Insensitive to Fe^{3+}	62 °C
T_{Caopx}	opx	Ca–Mg exchange	Insensitive to Fe^{3+}	60 °C
T_{Kr}	cpx–gt	Fe–Mg exchange	Fe^{3+} sensitive[d]	100 °C
T_{OW}	ol–gt	Fe–Mg exchange	Fe^{3+} sensitive[d]	180 °C
T_{HA}	opx–gt	Fe–Mg exchange	Fe^{3+} sensitive[d]	92 °C
T_{LG}	opx–gt	Fe–Mg exchange	Fe^{3+} sensitive[d]	96 °C

[a] Only the most commonly used are listed. For a more extensive list see Taylor (1998) or Brey *et al.* (1990). [b] P_{BKN}, T_{BKN}, T_{Caopx}: Brey and Köhler (1990); P_{KB}: Kohler and Brey (1990); P_{NT}: Nimis and Taylor (2000); T_{WS}: Witt-Eickschen and Seck (1991); T_{Ball}: Ballhaus *et al.* (1991); T_{TA}: Taylor (1998); T_{Kr}: Krogh (1988); T_{OW}: O'Neill and Wood (1979); T_{HA}: Harley (1984); T_{LG}: Lee and Ganguly (1988). [c] The 2σ accuracies are based on ability to reproduce experimental data (Brey and Köhler, 1990; Taylor, 1998). [d] The sensitivity to Fe^{3+} content of one or both phases is reviewed by Canil and O'Neill (1996).

zoning patterns in natural xenolith minerals (Smith and Barron, 1991).

The number of extant $P-T$ estimates for mantle samples is enormous. The pressures and temperatures recorded by garnet peridotite xenoliths compiled and reviewed recently by Rudnick and Nyblade (1999) are shown with additional data in Figure 6. Many of these suites have regular $P-T$ arrays that are reasonably assumed to record the steady-state paleogeothermal gradient at the time of eruption. The latter information has been central to studies of heat flow in the lithosphere and the distribution of heat producing elements in the crust and mantle (Rudnick and Nyblade, 1999; Russell *et al.*, 2001; Russell and Kopylova, 1999), which in turn constrain models for the bulk composition of the continental crust (Rudnick *et al.*, 1998).

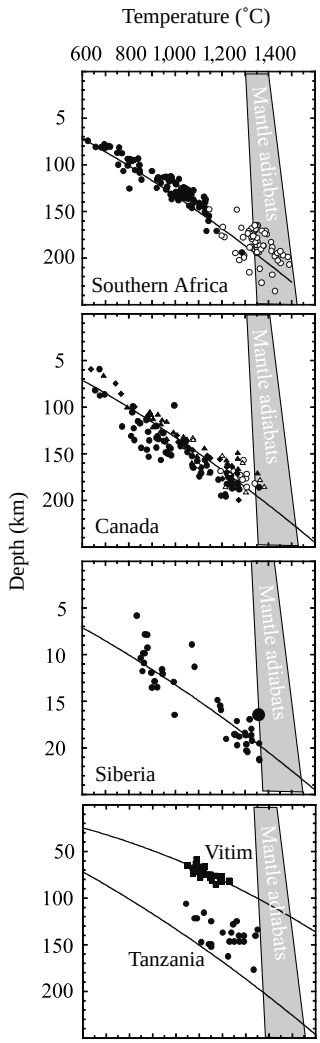

Figure 6 $P-T$ arrays compiled for garnet peridotite xenoliths from several suites using two-pyroxene thermometry and Al-in-orthopyroxene barometry (T_{BKN} and P_{BKN} methods, Table 5). Data sources given in Rudnick and Nyblade with additional data here for Vitim (Ionov *et al.*, 1993a) and Canada (MacKenzie and Canil, 1999; Schmidberger and Francis, 1999). The best-fit line for the Kaapvaal data is plotted in each figure for reference. Intersection of $P-T$ array with mantle adiabats (shaded field) represents an estimate of the thickness of lithosphere at the time of sampling.

The samples shown in Figure 6 reveal a number of features about the lithosphere sampled by xenoliths. The $P-T$ arrays, when projected to a mantle adiabat, can be used to define the maximum depth of mantle lithosphere beneath a locality at the time of eruption. Beneath cratons the lithosphere is at least 220 km deep, whereas below more active tectonic areas (e.g., Vitim) it is much thinner. Paleogeothermal gradients also vary between some cratons, or even within the same craton, as evident in the spread in some data sets (e.g., the Slave samples). Irregularities are evident in some $P-T$ arrays. Some of this variation may be due to lack of mineral equilibrium, perhaps because of recent diopside growth (Brey, 1990; Simon *et al.*, 2003). In other instances the $P-T$ variations signal a transient state of heat advection in the mantle shortly before the sampling process. For example, in many localities, the porphyroclastic xenoliths (open symbols in Figure 4) are displaced to higher temperatures away from the $P-T$ gradient for coarse samples. This is interpreted to be related to heating attended by melt infiltration and recrystallization as recorded by zoning and textural studies of these samples (Smith *et al.*, 1991; Smith and Boyd, 1992; Franz *et al.*, 1996a,b).

2.05.2.5 Bulk Rock Chemistry

The mantle comprises 68% by mass of Earth, and an accurate estimate for its composition is the very basis for unraveling the origin and differentiation of our planet. The bulk chemical analysis of xenoliths has been central to understanding the composition of the Earth's mantle, the genesis of basalt and the physical properties in the lithosphere that bear on its stability in the rigid part of the mantle system.

In view of the inhomogeneities observed for peridotite outcrops in ophiolites and orogenic massifs (Dick and Sinton, 1979; Chapter 2.04), there is some uncertainty as to how representative the bulk analysis of a centimeter-scale sample is of the volume of mantle sampled by a host magma. Furthermore, most peridotite xenoliths are coarse-textured and some contain spatial associations on the centimeter-scale (see above). Compilations discussed or presented here make no distinction for sample size but larger samples (>500 g) are

likely to be more representative (Boyd and Mertzman, 1987; Cox *et al.*, 1987).

2.05.2.5.1 Major elements

The database for major-element analyses of mantle xenoliths numbers in the hundreds and has been used in several estimates of average mantle compositions or of the primitive upper mantle (Kuno and Aoki, 1970; Maaloe and Aoki, 1977; Jagoutz *et al.*, 1979; Sun, 1982; Palme and Nickel, 1985; Hart and Zindler, 1986; McDonough and Sun, 1995). Differences in the bulk chemistry of xenoliths as functions of the tectonic environment or tectonothermal age of the crust through which xenolith-bearing magmas have sampled are highlighted in more recent compilations (Boyd, 1989, 1997; Griffin *et al.*, 1999b).

The covariation of Mg/Si and Al/Si for a large database of xenoliths (Table 6) is plotted in Figure 7 and compared with compositions of chondritic meteorites. The xenoliths form an array with negative slope. Melting reactions at low P (<2.5 GPa) along the peridotite solidus produce olivine and liquid at the expense of pyroxenes and spinel (Figure 2). Residues become enriched in magnesium and depleted in silicon and aluminum, explaining the array of compositions in Figure 7 as a partial melting trend to form lithosphere. Scatter in the trend may be due to spatial inhomogeneities, perhaps due to the sample size problem, or to chemical modification (metasomatism) that postdates the original partial melting and depletion process. The chondrite trend shows an opposite slope in Figure 7, which may represent variable compositions in the solar nebula (Jagoutz *et al.*, 1979; Palme and Nickel, 1985). The intersection of the peridotite xenolith and chondrite arrays is interpreted to be "primitive upper mantle" (PUM), or the bulk composition of the silicate earth. This approach, together with studies of other refractory elements known to be in chondritic proportions, has been used to derive some of the various estimates for PUM shown in Table 7 (see Chapter 2.01).

The covariation of Mg/Si with Mg# in a suite of xenoliths from off-craton localities is shown in Figure 8. The negative correlation on this plot parallels that observed for residues from ocean basins and ophiolites and defines the "oceanic" trend of Boyd (1989). With increasing depletion away from "model" primitive mantle compositions (Table 7) more iron is extracted in the residue relative to magnesium and the olivine content of the rock increases, reflected by higher Mg/Si. In the large data set of xenoliths, there is significant scatter in this trend, compared to a much more coherent one which would be observed for orogenic massif or abyssal peridotites (Chapter 2.04). Some of the scatter is due to a subparallel alignment of individual suites on this plot, or to metasomatic effects within each suite, where depleted rocks have had iron added to the rock, shifting it below the oceanic trend (Boyd, 1997). The term "oceanic" for the compositional array of noncratonic xenoliths in this plot may be somewhat misleading, because it is not clear if most of the subcontinental lithosphere originated in an oceanic environment (Griffin *et al.*, 1999b). Noncratonic lithospheric mantle is not as depleted in general and shows different depletion trends in detail than do abyssal peridotites, as will be shown below.

The covariation of Mg/Si and Mg# for xenoliths from six Archean cratons plotted in Figure 8 is quite distinguishable from most of the noncratonic samples by having much higher (Mg#). Despite their higher Mg#, many cratonic xenoliths have low FeO and Mg/Si irrespective of whether they crystallized in the garnet- or spinel-facies. This is especially so for samples from the Kaapvaal and Siberian cratons, but other cratons also have samples within this field. Boyd (1989) and Boyd *et al.* (1997) recognized that cratonic peridotites from the Kaapvaal and Siberian cratons defined a "cratonic" trend. The low Mg/Si in the bulk rock analysis is reflected petrographically by their high modal orthopyroxene contents (compare Figure 3). The origin of the high degrees of depletion but low Mg/Si in cratonic peridotites has been much debated (Boyd, 1989; Herzberg, 1999; Kelemen *et al.*, 1998; Walter, 1999; see Chapter 2.08).

Both calcium and aluminum are refractory lithophile elements during condensation processes in the solar nebula and show relatively constant element-ratios in all classes of chondritic meteorites (Palme and Nickel, 1985). Chondritic meteorites are the presumed starting material from which the mantle is derived (Ringwood, 1966) and so it is surprising that most peridotite xenoliths do not have chondritic Ca/Al ratios, irrespective of their degree of depletion (Figure 9). Some samples have near chondritic ratios but the mean and median for mantle xenoliths are clearly above that (Table 7). In contrast, samples of cratonic mantle have a generally lower than chondritic Ca/Al (Figure 9).

The superchondritic Ca/Al ratio in the upper mantle might be balanced by a slightly differing lower mantle composition, if the latter region accumulated majorite or perovskite during a magma ocean early in Earth evolution (Palme and Nickel, 1985). There is now little evidence to support this suggestion (McDonough and Sun, 1995). Hart and Zindler (1986) interpreted the high Ca/Al of xenoliths as a sampling bias, with preferential sampling and analysis of clinopyroxene-rich (and thus more calcium-rich) xenoliths by most investigators due to their attractive

Table 6 Data sources for major and minor element compositions of xenoliths.

Location	*Authors*
Ocean island	
Samoa	Hauri *et al.* (1993)
Kerguelen	Gregoire *et al.* (2000)
Hawaii	Sen and Leeman (1991)
Oceanic arc	
Lihir, Papua New Guinea	McInnes *et al.* (2001)
Batan, Phillipines	Maury *et al.* (1992)
Bismarck, Papua New Guinea	Franz *et al.* (2002)
Continental rift	
Tariat, Mongolia	Press *et al.* (1986)
East African Rift, Ethiopia	Bedini *et al.* (1997)
Vitim, Russia	Ionov *et al.* (1993a)
Continental intraplate	
Grand Canyon, USA	Smith *et al.* (1999)
Green Knobs, USA	Smith and Levy (1976)
Green Knobs, USA	Aoki (1981)
Bandera, USA	Smith *et al.* (1999)
Puerco Necks, USA	Smith *et al.* (1999)
Thumb, USA	Ehrenberg (1982)
Various locations	Jaguotz *et al.* (1979)
E. Australia	Stolz and Davies (1991)
W. Hungary	Embey-Isztin *et al.* (1989)
Romania	Vaselli *et al.* (1995)
Hannuoba, China	Song and Frey (1999)
Italy	Morten (1987)
N. Africa	Dautria *et al.* (1992)
N. Africa	Dupuy *et al.* (1985)
Sardinia	Dupuy *et al.* (1987)
S.E. Australia	Frey and Green (1974)
S.E. Australia	Yaxley *et al.* (1992)
Yukon, Canada	Francis (1987)
N. British Columbia, Canada	Shi *et al.* (1998)
West Kettle River, Canada	Xue *et al.* (1990)
Massif Central, France	Zangana *et al.* (1999)
Massif Central, France	Zangana *et al.* (1999)
Sahara basin, N. Africa	Dautria *et al.* (1992)
Continental arc	
W. Mexico	Luhr and Aranda-Gomez (1997)
Patagonia	Laurora *et al.* (2001)
Cratonic	
Labait, Tanzania	Lee and Rudnick (1999)
Olmani, Tanzania	Rudnick *et al.* (1994)
Lashaine, Tanzania	Rudnick *et al.* (1993)
Wiedemann, E. Greenland	Bernstein *et al.* (1998)
W. Australia	Jaques *et al.* (1990)
Jericho, Canada	Kopylova and Russell (2000)
Nikos, Canada	Schmidberger and Francis (2000)
Jagersfontein, S, Africa	Winterburn *et al.* (1990)
Kaapvaal, S.Africa	Boyd and Mertzman (1987)
Udachnaya, Siberia	Boyd *et al.* (1997)
Kimberley, S. Africa	Boyd *et al.* (1993)
Premier. S. Africa	Boyd (1999)

appearance in hand sample. This may be part of the problem, but calcium and aluminum are not depleted equably during earlier stages of partial melting (McDonough, 1990). More aluminum is extracted than calcium, and the ratio becomes greater than chondritic with increasing depletion. Furthermore, petrographic or geochemical evidence of metasomatism by carbonatitic melts in some mantle xenoliths show that infiltration of ephemeral, low-melt-fraction carbonatitic melts can greatly elevate Ca/Al in mantle lithosphere (Rudnick *et al.*, 1993; Yaxley *et al.*, 1998).

Neither of these proposals, however, can explain the subchondritic Ca/Al of most cratonic peridotites. If the latter are residues at higher *P*, more aluminum remains in the residue relative to calcium, the opposite trend of lower *P* residues. The anomalously low Ca/Al of cratonic peridotites may be unique to the formation of subcratonic mantle, or is a secondary feature with unexplained origin.

Al_2O_3 is a convenient depletion index in peridotites because it is immobile during serpentinization, marine weathering and metamorphic processes that ensue during the exhumation of these rocks (Coleman and Keith, 1971; Snow and Dick, 1995). It thus permits comparison of samples from many different settings in variable states of preservation. Figure 10 shows the mean and median Al_2O_3 content of xenoliths subdivided by sample type or tectonic setting (Table 8). These data are compared with mantle peridotites from orogenic massifs and from known tectonic settings in the ocean basins (abyssal peridotites, pre-oceanic margins and forearcs).

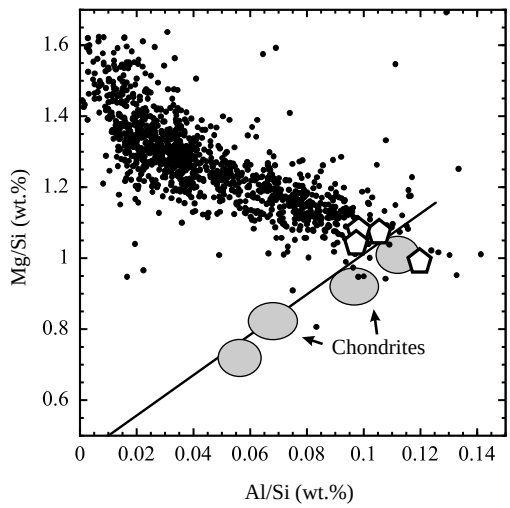

Figure 7 Mg/Si versus Al/Si plot (wt.%) for 593 xenoliths compared with the compositions of chondrites. Data sources in Table 6. Also plotted are various estimates for primitive upper mantle (polygons from Table 7) (source Jagoutz *et al.*, 1979).

On average, the mantle sampled in noncratonic xenolith suites in continental intraplate regions and in young rifts shows a similar limited level of depletion, relative to PUM. Similar, small levels of depletion are also observed for pre-oceanic rifts and orogenic massif peridotites. In contrast, the mean compositions of cratonic, oceanic arc and oceanic island suites are quite depleted. Similar levels of depletion are observed in oceanic forearcs and abyssal peridotites. The 1σ error bars shown in Figure 10 signify considerable overlap between these groups. Unfortunately, there are few published data for ocean island, or continental and oceanic arc suites in the literature (Table 5) to augment the global trends observed in Figure 10.

The Mg# is also another measure of depletion, but is more susceptible to modification by secondary metasomatic processes in the mantle, or to alteration by serpentinization and/or marine weathering. Olivine Mg# is sometimes used to avoid problems of grain-boundary

Table 7 Major and minor elements in xenolith averages and primitive upper mantle (PUM) models.

Sample	*HZ86 PUM*	*J79 PUM*	*PN85 PUM*	*M90 Xeno. avg.*	*M95 PUM*
SiO_2	45.96	45.14	46.20	44.00	44.92
Al_2O_3	4.06	3.97	4.75	2.27	4.44
FeO	7.54	7.82	7.70	8.43	8.05
MgO	37.78	38.30	35.50	41.40	37.80
CaO	3.21	3.50	4.36	2.15	3.54
Na_2O	0.33	0.33	0.40	0.24	0.36
K_2O	0.03	0.03		0.05	0.29
Cr_2O_3	0.47	0.46	0.43	0.39	0.38
MnO	0.13	0.14	0.13	0.14	0.14
TiO_2	0.181	0.217	0.230	0.090	0.201
NiO	0.28	0.27	0.23	0.28	0.25
CoO	0.013	0.013	0.012	0.014	
P_2O_5	0.02			0.06	0.02
Mg/Si	1.06	1.09	0.99	1.21	1.09
Al/Si	0.10	0.10	0.12	0.06	0.11
Mg#	0.90	0.90	0.89	0.90	0.89
Sc (ppm)		17	19	12	16
V (ppm)		77		56	82
Ga (ppm)		3		2	4
References	1	2	3	4	5

References: 1. Hart and Zindler (1986); 2. Jagoutz *et al.* (1979); 3. Palme and Nickel (1985); 4. McDonough (1990); 5. McDonough and Sun (1995).

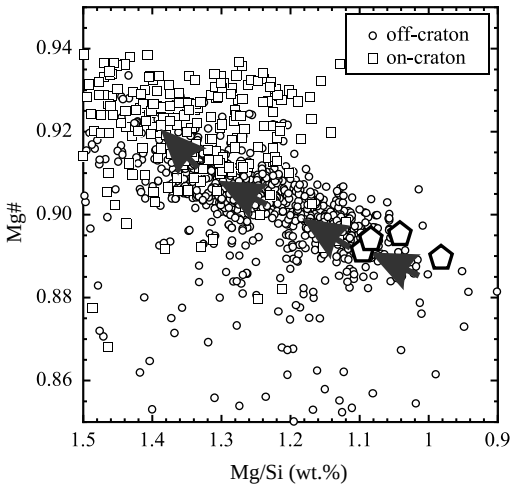

Figure 8 Mg/(Mg + Fe) versus Mg/Si for: (a) off-craton spinel peridotite xenoliths and (b) cratonic garnet and spinel peridotite xenoliths. Arrows mark the "oceanic" trend (Boyd, 1989, 1997) defined by abyssal peridotites. Also shown are various estimates for primitive upper mantle (polygons from Table 7).

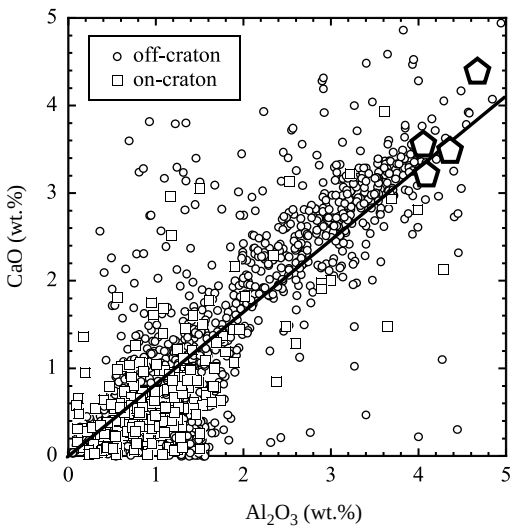

Figure 9 Covariation of CaO and Al_2O_3 in off-craton and on-craton xenoliths. Data sources in Table 6. Shown for reference are various estimates for primitive upper mantle (polygons) and the ratio in chondritic meteorites.

iron-introduction (Boyd, 1989). A summary of the Mg# for xenoliths in different settings shows the same trends as when Al_2O_3 is used as a depletion index (Figure 11). The larger range in Mg# observed for ocean island xenolith suites when compared to other settings is due to secondary melt impregnation in this setting (Boyd, 1997). This plot also emphasizes the depletion of cratonic peridotite xenoliths in FeO.

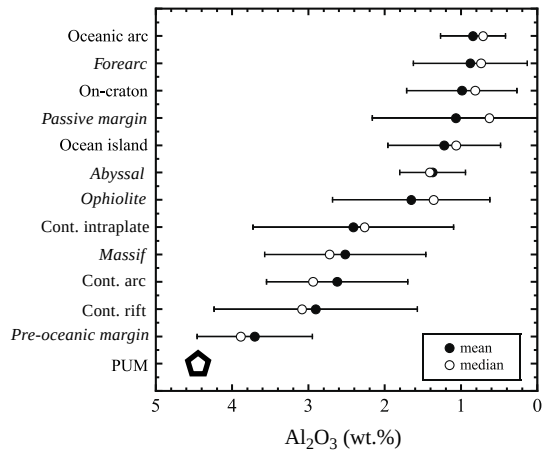

Figure 10 Mean and median Al_2O_3 (wt.%) for peridotite xenoliths from different settings, compared with samples from known modern tectonic settings (in italics; Table 8).

2.05.2.5.2 *Minor and trace elements*

Compatible trace elements. Both nickel and cobalt in xenoliths show good correlations with depletion parameters such as Al_2O_3 or MgO (Figures 12(a) and (b)). Both elements partition into olivine, which is enriched in the residue during melting and so these elements have bulk distribution coefficients greater than one during partial melting. The Ni/Co ratio in peridotites is nearly constant and approximately chondritic for xenoliths over a range of depletion. This is one of the strongest arguments for heterogeneous accretion of the Earth (Jagoutz *et al.*, 1979). Because nickel is highly siderophile but cobalt only slightly so, a near chondritic Ni/Co ratio requires a late "veneer" be added to Earth's mantle shortly after accretion (O'Neill, 1991). Alternatively, nickel may become less siderophile at extreme T and P during homogeneous accretion (see Chapter 2.10 and references therein).

Unlike nickel and cobalt, chromium shows a nearly constant level of depletion in xenoliths (Figure 12(c)). There is considerable scatter in mantle data sets for chromium that is beyond that attributable to analytical error and much greater than the scatter in nickel or cobalt (Liang and Elthon, 1990). This likely reflects the heterogeneous distribution of chromium in xenoliths, which is contained mainly in a very minor phase (spinel). Small xenolith specimens may over- or under-represent this mineral in peridotite bulk analyses (Liang and Elthon, 1990). The nearly constant chromium levels with varying depletion suggest a bulk distribution coefficient that is ~1 during melting, very different from the bulk distribution coefficient (D) for chromium during crystallization of mafic magmas that are the partial melt complement to the residues represented by

Table 8 Mean and median whole rock compositions of xenoliths.

Sample type	*SiO_2*	*TiO_2*	*Al_2O_3*	*FeO^**	*MnO*	*MgO*	*CaO*	*LOI*	*Al/Si* (wt.%)	*Mg/Si* (wt.%)	*Ca/Al* (wt.%)	*Fe/Al* (wt.%)	*Mg#*	*Ni*	*Co*	*Cr*	*Sc*	*V*	*Cr/Al*	*V/Al*	*n*
Ocean islands																					
Mean	43.72	0.08	1.22	9.27	0.13	44.25	1.10		0.03	1.31	1.36	14.13	0.895	2,410	153	2,794	8	40	0.494	0.0063	16
Median	44.61	0.04	1.07	8.04	0.12	44.73	0.82		0.03	1.30	1.10	10.94	0.908	2,399	141	2,601	9	32	0.433	0.0064	
σ	2.01	0.08	0.74	2.05	0.04	2.34	0.75		0.02	0.11	0.92	9.50	0.022	187	26	806	2	16	0.379	0.0019	
Oceanic arc																					
Mean	44.49	0.02	0.84	8.33	0.14	44.61	0.89	2.67	0.02	1.30	1.75	20.66	0.905	2,262	149	3,326	13	38	0.627	0.0056	21
Median	44.74	0.02	0.71	8.10	0.14	44.66	0.89	2.11	0.02	1.29	1.55	14.97	0.906	2,404	139	2,998	12	40	0.660	0.0000	
σ	1.77	0.02	0.43	0.77	0.01	1.87	0.48	0.90	0.01	0.09	1.32	24.83	0.007	298	33	1,021	5	11	0.677	0.0071	
Continental rifts																					
Mean	44.58	0.10	2.91	7.91	0.13	41.17	2.79	0.13	0.07	1.19	1.28	5.03	0.902	2,152		2,749	11	54	0.246	0.0028	23
Median	44.43	0.11	3.08	7.88	0.13	41.21	2.62	0.13	0.08	1.19	1.17	3.40	0.903	2,160		2,703	10	51	0.159	0.0018	
σ	0.87	0.07	1.33	0.42	0.01	3.43	1.65	0.03	0.03	0.11	0.49	3.71	0.008	220		640	5	20	0.183	0.0030	
Continental intraplate																					
Mean	44.33	0.10	2.41	8.07	0.13	41.84	4.85	0.23	0.06	1.17	1.46	6.10	0.899	2,147	102	2,819	12	59	0.216	0.0037	273
Median	44.42	0.08	2.26	8.12	0.13	41.70	2.57	0.02	0.06	1.20	1.19	4.76	0.900	2,135	104	2,740	12	61	0.182	0.0041	
σ	1.39	0.09	1.31	1.79	0.03	2.96	10.14	0.27	0.03	0.26	0.93	4.51	0.014	263	8	625	4	19	0.190	0.0024	
Continental arc																					
Mean	44.41	0.10	2.62	8.60	0.13	41.14	2.41		0.07	1.20	1.25	5.88	0.895	2,110	108	2,521		53	0.214	0.0041	28
Median	44.71	0.09	2.94	8.20	0.13	40.72	2.52		0.07	1.17	1.24	3.70	0.898	2,066	105	2,552		55	0.179	0.0039	
σ	1.17	0.05	0.92	1.47	0.03	2.80	1.00		0.02	0.10	0.25	6.08	0.018	282	11	499		17	0.110	0.0010	
Cratonic																					
Mean	43.27	0.05	0.99	7.20	0.14	46.19	0.70	3.29	0.03	1.38	0.88	16.62	0.919	2,579	120	3,778	4	29	0.636	0.0043	232
Median	43.39	0.04	0.82	7.01	0.13	46.52	0.49	2.27	0.02	1.39	0.82	11.60	0.921	2,570	116	2,861	4	27	0.456	0.0042	
σ	1.63	0.05	0.72	1.11	0.04	2.94	0.72	2.55	0.02	0.11	0.66	18.18	0.014	324	19	2,720	3	14	0.858	0.0044	
																				Total	593

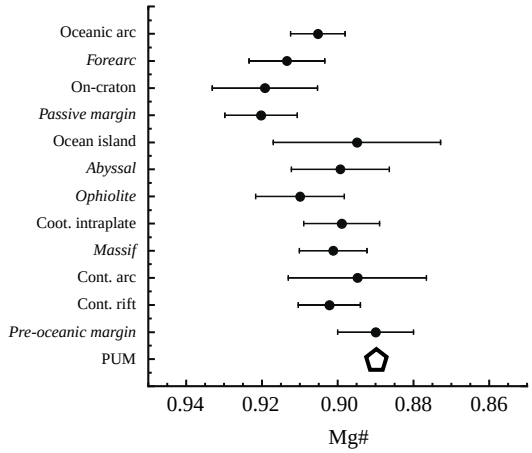

Figure 11 Mean and median Mg/(Mg + Fe) for the same samples in Figure 10 (in italics; Table 8). Error bar represents 1σ of the mean.

xenoliths. The latter feature requires that most magma extracted from the mantle be picritic (Liang and Elthon, 1990). Cratonic peridotite suites show a lower chromium level for a given level of depletion compared to noncratonic xenoliths, but reasons for this are not clear. More than 50% of the cratonic samples plotted are spinel-free and so the reduced scatter in these suites may arise because chromium is more equably partitioned amongst the garnet and pyroxenes in these samples.

The mean and median Cr/Al ratio of various xenoliths varies with tectonic setting, but there are large standard deviations due to the sampling problem for chromium (Figure 13). Despite the scatter, it becomes clear that the high Cr/Al of protoliths required to form low calcium, high chromium harzburgitic garnets in xenoliths occur in the arc or abyssal tectonic setting, at pressures within the spinel-stability field.

Due to the equable partitioning of manganese amongst peridotite minerals, this element shows a much tighter cluster with depletion than does chromium. Like chromium, manganese has a nearly constant abundance in a range of xenolith types and in orogenic massifs (Figure 12(d)). The near parallel trend indicates a bulk D during melting that is ~1. Cratonic peridotites show generally lower manganese contents for a given degree of depletion.

Mildly incompatible elements. The abundance of V in several different mantle residues was recently reviewed by Canil (2002). The trends for abyssal and massif peridotites are compared with on- and off-craton xenolith suites in Figure 14. Abyssal peridotites contain the most V at a given degree of depletion. Massif peridotites are shifted from the abyssal samples and parallel the off-craton samples, but the latter show considerable scatter. Arc xenoliths, although few in number, are the most impoverished in V for a given degree of depletion. Some cratonic peridotites overlap the abyssal samples but many project toward or along the trend for arc xenoliths (Figure 14(b)).

The distinct trends for V abundances in peridotite xenoliths may exist because this element is f_{O_2}-sensitive during melting. Canil (2002) interprets these trends to represent the primary f_{O_2} during melting, with f_{O_2} during partial melting increasing in the following order: abyssal peridotites < massif peridotites ~ off-craton xenoliths < arc and cratonic xenoliths. Scatter in the off-craton xenolith suites is not likely due to metasomatism (Canil and Fedortchouk, 2000) but rather can be attributed to analytical errors or real f_{O_2} variations in residues from a range of tectonic environments. Further effort to apply V abundances as paleo-redox indicators during lithosphere formation will require more analyses for V in xenoliths from a broader range of tectonic settings (arc xenoliths are very underrepresented), and an evaluation of interlaboratory accuracy for analysis of this element in peridotites. There are surprisingly many trace-element data sets for xenoliths where V is not measured.

There are few measurements of the Fe^{3+} (Fe_2O_3) abundance in mantle xenoliths (O'Neill *et al.*, 1993; Canil *et al.*, 1994; Canil and O'Neill, 1996). Wet chemical determinations for Fe_2O_3 in peridotites are fraught with errors, but better and more precise results are obtainable with Mossbauer spectroscopy of individual minerals (O'Neill *et al.*, 1993). Fe^{3+} behaves as a mildly incompatible element during melting with a bulk D of ~0.1, similar to that of scandium or V (Figure 12(e)).

Scandium and sodium are very compatible in clinopyroxene. The covariation of Sc or sodium with depletion follows that of V or Fe^{3+} (Figures 12(f) and (h)) and correlates with the decreasing clinopyroxene abundance with increased melting (Figure 3). The kink in the trend for scandium in xenoliths at ~2 wt.% Al_2O_3 may signal exhaustion of clinopyroxene from residues after ~20% melting (Figure 3). Both Sc and sodium show far more scatter in xenoliths than in massif peridotites (Figures 12(f) and (h)), likely because the former samples have experienced more metasomatism, but also possibly because they are contaminated with small amounts of intergranular material (from host volcanic rock) which concentrate these elements and contribute them to the bulk analysis. Scatter due to these effects is particularly pronounced for more depleted xenolith samples with less than ~2 wt.% Al_2O_3. These effects pose even greater problems for the abundances of highly incompatible elements in xenoliths (Zindler and Jagoutz, 1988).

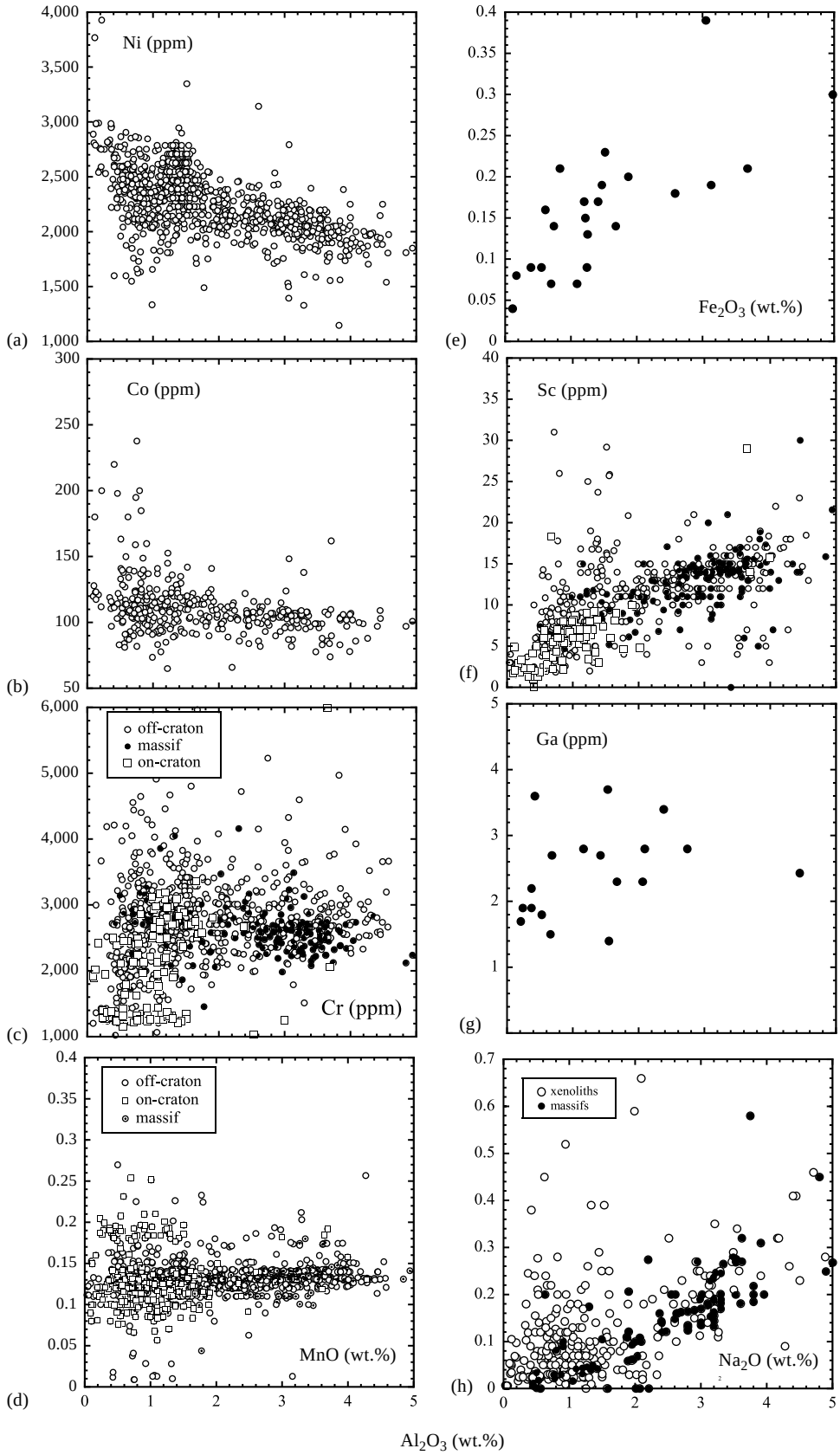

Figure 12 Covariation of: (a) Ni, (b) Co, (c) Cr, (d) MnO, (e) Fe_2O_3, (f) Sc, (g) Ga, (h) Na_2O with Al_2O_3 (wt.%) in on- and off-craton xenolith suites. Samples from all settings are grouped together in the panels where no legend is shown. Data sources in Table 6.

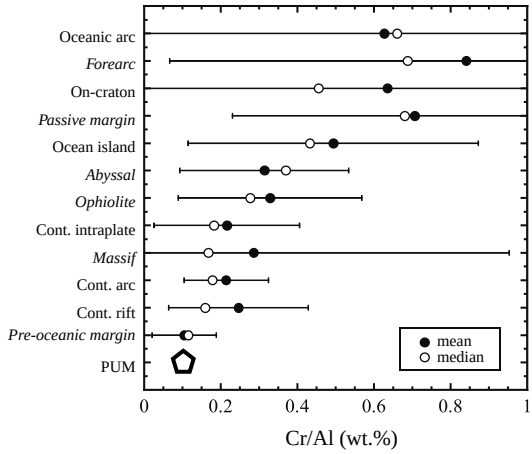

Figure 13 Mean and median Cr/Al for the same samples in Figure 10 (in italics; Table 8). Error bar represents 1σ of the mean.

The few analyses of gallium in xenoliths (Rhodes and Dawson, 1975; Kurat *et al.*, 1980; McKay and Mitchell, 1988) shows that the element has a distribution similar to that of Fe_2O_3, but there are too few data to define any trends (Figure 12(g)). Gallium also partitions itself amongst mantle minerals in the same order as Fe_2O_3.

Incompatible elements (rare-earth elements, large-ion lithophile elements, high-field-strength-elements)

(i) *Peridotites*. The high levels of incompatible element enrichment in almost all mantle xenolith host volcanic rocks results in a high probability that levels of these elements in the bulk xenoliths are compromised by infiltration of the host magma during entrainment and eruption. For this reason and because of the effects of weathering on the whole-rock geochemistry of some highly incompatible elements such as rubidium and strontium, the most reliable data for mantle xenoliths are generally thought to be obtained from mineral studies. However, the possibility that some minerals in certain xenolith suites may have crystallized recently, from the host volcanic rock, complicates the issue further. The effects of weathering and host rock infiltration are discussed further from an isotopic perspective in Section 2.05.2.7. Exceptional to these misgivings are mica- and amphibole-rich rocks such as the MARID suite (Table 1), which have inherently high levels of incompatible elements and are thus more immune from host rock infiltration (Erlank *et al.*, 1987; Gregoire *et al.*, 2002; Pearson and Nowell, 2002).

Detailed studies of the incompatible trace-element budget of mantle xenoliths illustrate the problems. Mass balance studies that use modal analyses and mineral compositions to calculate

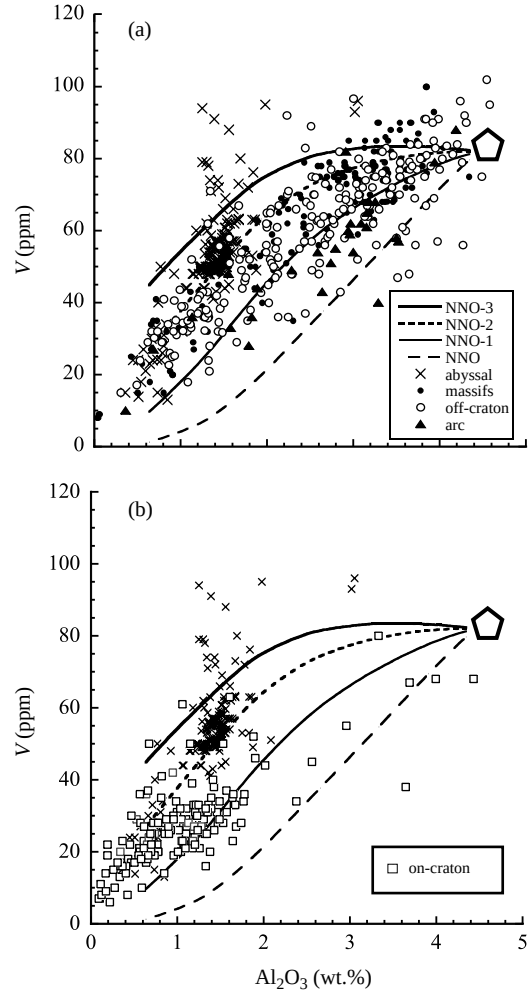

Figure 14 Covariation of V with Al_2O_3 in: (a) abyssal peridotites, orogenic massifs, off-craton xenoliths, arc xenoliths, and (b) cratonic xenoliths (data sources in Table 6). Shown for illustrative purposes are residue trends for partial melting at 1.5 GPa as a functions of f_{O_2} (expressed relative to the nickel-nickel oxide (NNO) buffer) calculated using methods described in Canil (2002).

peridotite bulk compositions show large deficiencies between calculated whole-rocks and those measured (McDonough *et al.*, 1992; Pearson and Nowell, 2002). Schmidberger and Francis (2001) show that calculated whole-rock LREE abundances in peridotites from Somerset Island, Canada, are 70–99% lower than measured whole-rock REE concentrations. The discrepancies can be explained by infiltration of between 0.4 wt.% and 2 wt.% kimberlite (Figure 15). Not all the "interstitial" component in xenoliths is host-rock melt. Bodinier *et al.* (1996) and Bedini and Bodinier (1999) have shown the presence of a very thin (<10 μm thick) reaction layer coating the surfaces of spinel crystals in several suites of

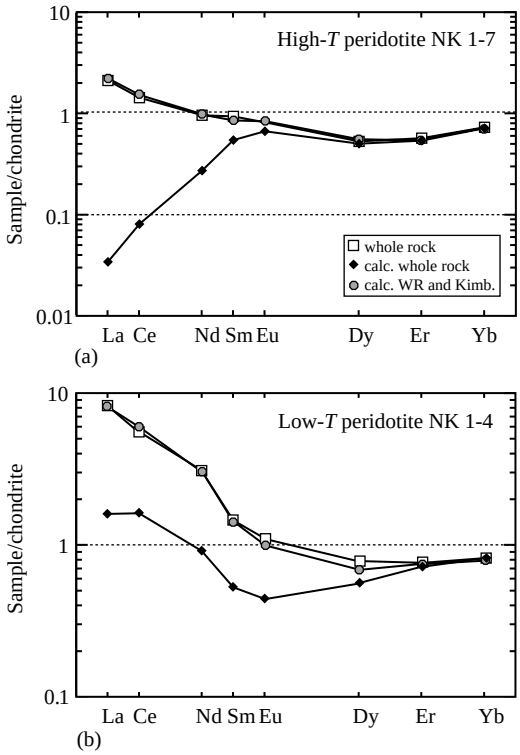

Figure 15 Illustration of the effects of host-rock contamination on whole-rock REE geochemistry. Chondrite-normalized REE patterns of measured whole-rock peridotites compared with REE abundances calculated from modal data plus mineral compositions. Also compared are mixtures of calculated whole-rock and kimberlite for each diagram. Two specimens, (a) and (b) are high-*T* and low-*T* garnet lherzolites from Somerset Island, Nunuvut (Canada) (after Schmidberger and Francis, 2001).

spinel lherzolite xenoliths of noncratonic origin. This layer comprises titanium oxides and phlogopite and can account for 45–90% of the whole-rock budget of rubidium, barium, niobium, and tantalum (Figure 16). Bodinier *et al.* (1996) and Bedini and Bodinier (1999) suggest that spinel rims are likely to be present in most noncratonic spinel lherzolite xenolith suites and attribute the feature to a metasomatic process involving percolation of silica-rich and potassium-rich small melt fractions in the lithospheric mantle. However, a study of peridotite mineral and bulk rock trace-element budgets in two Southeast Australian xenoliths by Eggins *et al.* (1998) did not find evidence for a significant grain boundary component. Detailed studies within individual minerals show that they can contain fluid inclusions that are enriched in uranium, thorium, lead, rubidium, strontium, neodymium, barium, and alkalis. This will significantly affect whole-rock geochemical budgets (Rosenbaum *et al.*, 1996).

Schiano and Clocchiatti (1994) have also demonstrated the ubiquitous presence of volatile, silica- and potassium-rich small melt fractions trapped as inclusions in silicate minerals in noncratonic peridotite xenoliths that affect whole-rock and mineral trace-element budgets. Such inclusions have $SiO_2 > 60$ wt.%, $TiO_2 < 1$ wt.%, $K_2O > 6$ wt.%, $K_2O/Na_2O > 1$ and have high contents of H_2O, CO_2 plus Cl. The inclusions have minimum trapping temperatures of 1,220 °C at 0.7 GPa, corresponding to entrapment at oceanic upper mantle depths. The widespread occurrence of these inclusions in off-craton peridotites is consistent with the continuous infiltration of small melt fractions into the lithospheric mantle as proposed by McKenzie (1989). Recently, it has been shown that infiltration of the host basaltic magma and subsequent reaction may produce glassy veins and pockets whose composition encompasses that of a variety of proposed metasomatic agents (Ciuff *et al.*, 2002). These results suggest caution when drawing inferences about mantle processes from glass pockets and veins in xenoliths.

Mass-balance inversion of a suite of noncratonic type I xenoliths from SE Ethiopia (Bedini and Bodinier, 1999) show that the trace-element composition of some whole-rock peridotites may be controlled by five distinct components:

- The silicate minerals account for all the HREE budget and 50–90% of the LREE, strontium, and Zr–Hf in apatite-free peridotites.
- Mineral hosted fluid inclusions contribute significantly to rubidium (20–25%) and to lesser extents the LILE budgets.
- A pervasive grain-boundary component that is selectively enriched in highly incompatible elements, contributing 25–90% of the whole-rock budget for barium, thorium, uranium, and 10–50% for niobium and LREE in apatite-free samples.
- Thin reaction layers (<10 μm thick) coating spinel surfaces that are composed of titanium oxides and phlogopite. These phases dominate the budget for niobium, tantalum (45–60%), and rubidium plus barium (30–80%) in all the xenoliths studied.
- Apatite dominates the budget of thorium, uranium, strontium, and LREE (25–75%), when present.

Similar findings were made by Kalfoun *et al.* (2002) who suggest that only 1–5% of niobium in spinel lherzolites from S.E. Siberia reside in silicate phases with the remainder hosted in finely disseminated rutile.

Despite these uncertainties and complications, some systematics are evident for whole-rock incompatible element data in xenolith suites.

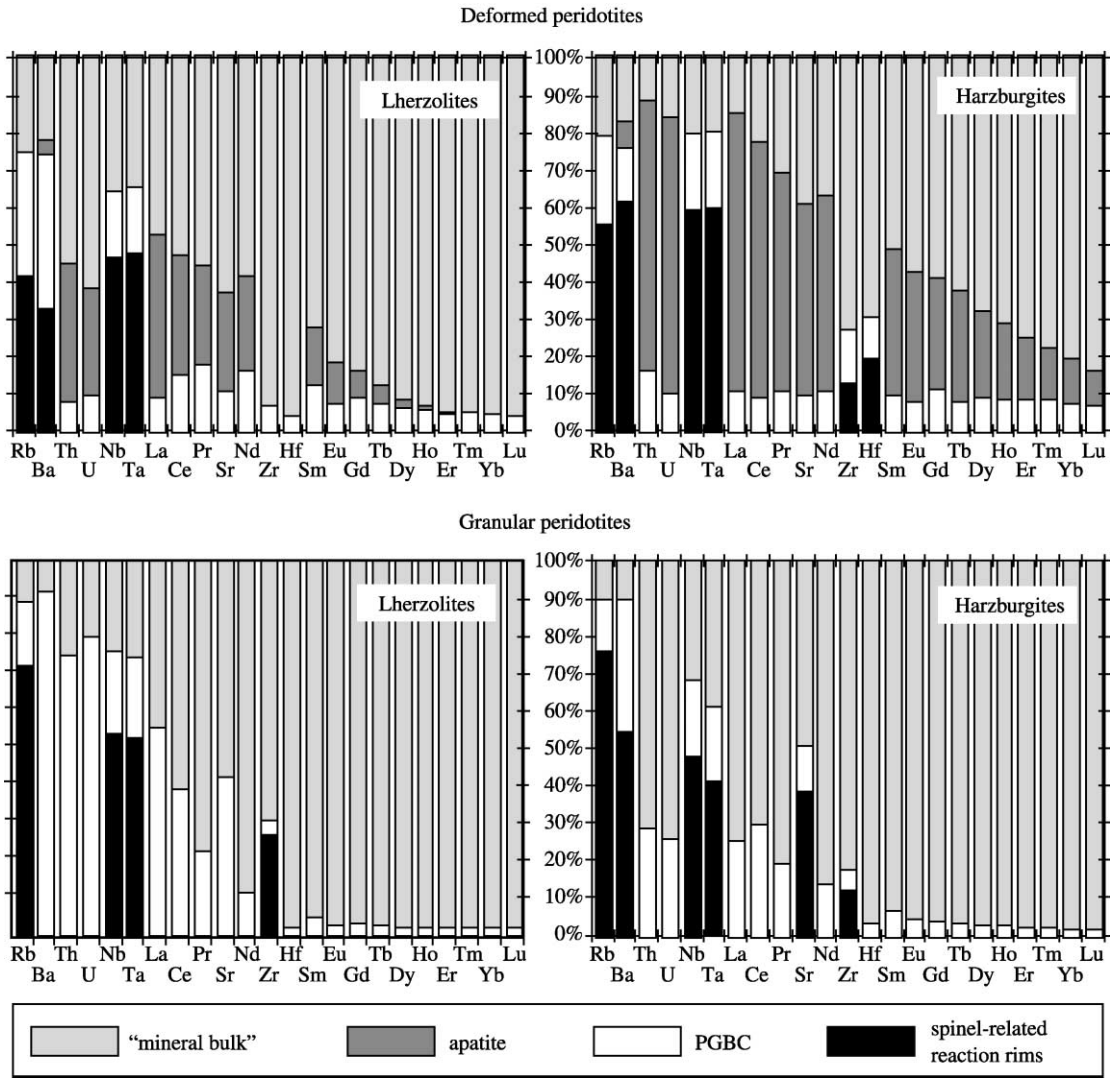

Figure 16 Trace-element mass-balance for deformed and granular lherzolites and harzburgites from E. Africa illustrating the contribution of a pervasive grain boundary component (PGBC), apatite and spinel reaction rims in wt.% of the total elemental whole-rock budget (after Bedini and Bodinier, 1999).

REE and other incompatible element studies of both cratonic (Nixon *et al.*, 1981) and noncratonic xenoliths (Frey and Green, 1974; Stosch and Seck, 1980; McDonough, 1990) have led to the notion that despite their overall major-element depletion, peridotite xenoliths are enriched (relative to chondrites) in incompatible elements, notably LREE. The fact that these samples have higher Mg# and nickel contents than primitive mantle, yet many have LREE enriched signatures, led Frey and Green (1974) to suggest a multistage history whereby the peridotites were initially melt depleted due to basalt extraction and this residue was later enriched by small amounts of incompatible element enriched melt. This basic model is still accepted as commonly applicable to many peridotite xenoliths from a wide variety of tectonic settings.

The concept of incompatible element enrichment has been extended as a general characteristic of the whole lithospheric mantle. While the whole-rock analyses of many peridotites are LREE enriched, the above discussion suggests that this feature could be imposed very recently and that the original character of many of the peridotites and by inference, the lithospheric mantle, is not as incompatible element rich as generally thought. For instance, for a selection of cratonic and circum-cratonic peridotites, Pearson and Nowell (2002) find that the mantle-normalized incompatible element patterns for calculated whole-rock peridotites range from very LREE depleted to slightly LREE enriched, but are generally characterized by very low abundances of the highly incompatible elements barium and lanthanum.

Noncratonic type I (Cr-diopside group) spinel lherzolites (Table 1) have whole-rock REE patterns that are commonly LREE-enriched or less commonly, LREE depleted (Figure 17). This bulk rock chemistry is reflected in their clinopyroxene chemistry such that those with bulk rock LREE-depletion have LREE-depleted clinopyroxene patterns (type IA; Menzies, 1983) and those with bulk rock LREE- enrichment have LREE-enriched clinopyroxene patterns (type IB; Menzies, 1983; Figure 17). The difference between the two groups may well be related to late stage melt/fluid infiltration before/during eruption. Variations in degree of LREE enrichment also correlate with peridotite texture in some spinel lherzolite suites (Downes and Dupuy, 1987). For instance, Xu *et al.* (1998) observed that deformed harzburgites and lherzolites from Wangqing, NE China, were consistently LREE enriched compared to equigranular lherzolites and harzburgites. The type II Al-augite group xenoliths show a wide variety of incompatible element characteristics that are generally enriched, relative to PUM and seem coupled to their relatively fertile major-element compositions.

For cratonic, kimberlite-derived xenoliths, relationships between texture/equilibration temperature and geochemistry also exist. The low-temperature (granular) type I peridotites have generally more LREE enriched compositions than the high-temperature (sheared) type V peridotites (Nixon *et al.*, 1981; Figure 17). These systematics are partly a function of the fact that garnets and diopsides in low-temperature peridotites are more variably LREE enriched than in high temperature peridotites (Figure 17).

Heavy rare earth elements (HREE), in particular ytterbium, are less affected by host rock interaction and show significant positive correlations with CaO, Al_2O_3, scandium, and vanadium contents of noncratonic spinel lherzolites (McDonough, 1990). This is taken as a reflection of the similarity of bulk distribution coefficients of these elements during partial melting. Trends for "hydrous" (amphibole and phlogopite-bearing) spinel peridotites are more scattered than for anhydrous peridotites, probably due to introduction of both aluminum and ytterbium during metasomatism (McDonough, 1990). Cratonic and circum-cratonic peridotites show much less coherency in terms of Al–Ca–Yb correlations (Irvine, 2002), probably due to their more complex metasomatic and magmatic histories. However, Kelemen *et al.* (1998) have argued that low ytterbium levels in cratonic peridotites correlate with low CaO and suggest that this is a function of initial melting in the spinel stability field, releasing ytterbium into the melt, followed by subduction and incorporation into the CLM.

High-quality data for high-field-strength element (HFSE) ratios such as Zr/Hf and Nb/Ta have shown that bulk rock noncratonic spinel lherzolites have ratios similar to primitive mantle (Jochum *et al.*, 1989). This data, together with that from basalts, is used to argue against significant fractionation of these elements during normal mantle melting.

Studies of the HFSE abundances in peridotite xenoliths and their metasomatized variants have also been relevant to arguments concerning flood basalt genesis. Many basaltic rocks erupted through continental areas have distinctive incompatible trace-element signatures compared with basalts erupted in oceanic areas. Continental basalts have characteristic enrichment in large-ion-lithophile (LILE) elements such as barium and depletion of high-field-strength elements (HFSE) such as titanium and niobium (Thompson *et al.*, 1983). This feature has been used to suggest that the CLM is the source region for certain continental basalts (e.g., Hawkesworth *et al.*, 1983; Hergt *et al.*, 1991) although numerous counter arguments have been raised (e.g., Menzies, 1992). McDonough (1990) followed by Arndt and Christensen (1992) examined available trace-element data for off-craton spinel lherzolites and concluded that the CLM, as represented by xenoliths, does not have trace-element characteristics consistent with it being the source of continental basalts because they are not characterized by HFSE depletion. These conclusions have been extended to cratonic peridotites and phlogopite-rich metasomatic mafic xenoliths by Pearson and Nowell (2002), who note that mantle xenoliths containing hydrous minerals such as amphibole and mica have positive HFSE anomalies. Any melt where these phases contribute to the melt fraction will therefore have positive HFSE anomalies. Models involving residual rutile and/or hydrous phases are possible but are of doubtful validity because such phases should be the first to contribute to the melt (e.g., Foley, 1992).

Modeling of the whole-rock and mineral trace-element compositions in xenoliths that have experienced metasomatic infiltration of melts led Ionov *et al.* (2002a) to conclude that the REE and HFSE element compositions of peridotites adjacent to veins bear the chemical fingerprints of the metasomatic agent closest to its source (e.g., a melt vein). Further away, signatures are increasingly dominated by fractionation processes related to melt percolation.

Noncratonic Al-augite group Pyroxenites (type BII). In contrast to the pyroxenites within orogenic massifs (Chapter 2.04) relatively few bulk rock trace-element studies have been performed on noncratonic (or cratonic) pyroxenite xenoliths. The most extensive geochemical studies are of

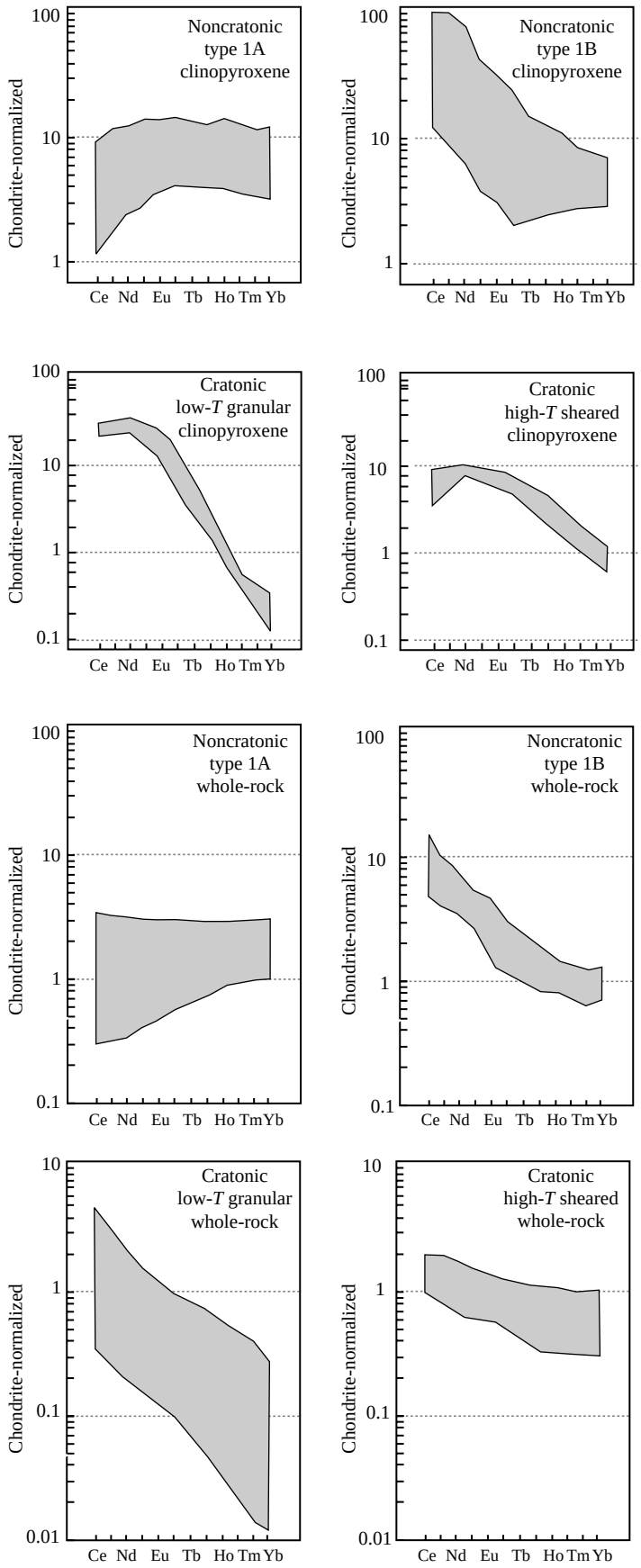
Noncratonic type 1A clinopyroxene
Noncratonic type 1B clinopyroxene
Cratonic low-T granular clinopyroxene
Cratonic high-T sheared clinopyroxene
Noncratonic type 1A whole-rock
Noncratonic type 1B whole-rock
Cratonic low-T granular whole-rock
Cratonic high-T sheared whole-rock
Chondrite-normalized
Ce Nd Eu Tb Ho Tm Yb

occurrences in southeastern Australia (Irving, 1974; Griffin *et al*., 1988) the western USA (Irving, 1980); Hawaii (Frey, 1980). Pyroxene-rich sheets from Kilbourne Hole and San Carlos have greater than chondritic abundances of all REE, with chondrite-normalized patterns that are convex upwards, with maxima between neodymium and samarium (Irving, 1980). Other samples show more variability, ranging from LREE depleted to enriched patterns. Pyroxenites from Salt Lake Crater, Hawaii, have a wide range in nickel contents and Mg together with the convex upward rare earth element distributions relative to chondrites. These features were interpreted by Frey (1980) to be produced by formation of the pyroxenites as "cumulates" from the Honolulu Volcanic Series. As expected, orthopyroxenites and websterites have lower REE abundances and LREE-depleted patterns are common compared with xenoliths dominated by clinopyroxene (McDonough and Frey, 1989). There is general consensus that the REE patterns and abundances reflect pyroxene accumulation on the walls of magma conduits during "flow crystallization" of magma passing through the mantle (Irving, 1980). Clear evidence of host rock contamination is observed in some samples.

Cratonic mica and amphibole-rich "metasomatic" rocks. Incompatible element abundances in these rocks are probably at sufficient levels to minimize the effects of host rock contamination. The phlogopite-rich mafic xenoliths (type VI) are LREE-enriched (10 and 50 times PUM; Figure 18, Erlank *et al*., 1987; Gregoire *et al*., 2002; Pearson and Nowell, 2002). Glimmerites (phlogopite-rich rocks—Table 1) have the lowest absolute REE abundances, due to the low levels of REE in phlogopite, but the presence of apatite in glimmerites greatly enhances their REE and strontium content. Virtually all samples display strong positive rubidium, niobium, and tantalum anomalies (Figure 18), making these lithologies unlikely sources for continental basaltic magmatism (Pearson and Nowell, 2002). Variable contents of minor phases such as apatite, allanite and barite cause substantial variations in lanthanum, cerium, barium, and thorium abundances (Gregoire *et al*., 2002). MARID xenoliths contain ubiquitous K-richterite, which imposes a negative strontium anomaly on most rocks of this type. HFSE ratios such as Zr/Hf, that are normally relatively constant in peridotites, vary widely in these rock types due to the presence of ilmenite and other phases.

2.05.2.5.3 *Platinum group elements and rhenium*

The platinum group elements (PGEs) comprise osmium, iridium, ruthenium, rhodium, platinum, and palladium. Rhenium is often discussed along with the PGEs because of its similar geochemical behavior and because it forms part of the important Re–Os isotope decay system. The pioneering work on PGE abundances in mantle xenoliths was performed by Morgan *et al.* (1981, 1986). Recent advances in analytical geochemistry allow the routine determination of high-precision PGE data in mantle-derived rocks. In particular, techniques are now available that permit analysis of rhenium and osmium along with all the other PGEs (except rhodium), by isotope dilution (Pearson and Woodland, 2000). Here we discuss recent PGE determinations of mantle xenoliths that contrast the PGE compositions of cratonic and noncratonic xenoliths.

PGEs in fertile, unmelted mantle predominantly reside in base metal sulfides (Jagoutz *et al*., 1979) and this is supported by positive correlations between bulk rock PGE content and selenium (Lorand and Alard, 2001). Experiments and observation indicate that monosulfide solid solution (mss) preferentially accommodates refractory PGEs (osmium, iridium, ruthenium, rhodium) relative to Cu-sulfides, which concentrate palladium and rhenium (Lorand and Alard, 2001; Pearson *et al*., 1998b). Once sulfide has been removed from a melt residue, the difference in solid–liquid silicate partition coefficients ($D^{Solid/melt}$) between the I-PGEs (osmium, iridium, ruthenium) and the platinum-group PGEs (P-PGEs; rhodium, platinum, palladium) leads to fractionated PGE patterns, with progressive depletion of P-PGEs, while I-PGEs remain in the residue. This results in a decrease of P-PGE/I-PGE ratios such as Pd/Ir with progressive melting while ratios of I-PGEs, such as Os/Ir, remain close to 1 (Lorand *et al*., 1999; Handler and Bennett, 1999; Rehkämper *et al*., 1999; Pearson *et al*., 2002, 2004). The progressive interelement PGE

Figure 17 Summary fields of chondrite-normalized REE patterns for whole-rock peridotites and clinopyroxenes for peridotite xenoliths. Noncratonic whole-rock peridotites are either LREE-depleted (type IA; least common) or LREE-enriched (type IB; most common). Data sources from Stosch and Seck (1980), Stosch and Lugmair (1986), Menzies *et al.* (1985). Clinopyroxenes from these rocks also show LREE enrichment or depletion. Cratonic peridotite whole rocks are ubiquitously LREE-enriched. Low-*T* (granular) suite show greater LREE/HREE compared to high-*T* (sheared) suite and this is reflected in the more LREE-enriched clinopyroxene compositions in the low-*T* suite. Data sources from Shimizu (1975), Nixon *et al.* (1981), and Irvine (2002). Low-*T* whole-rock suite includes 19 samples from Letseng, N. Lesotho (Irvine, 2002).

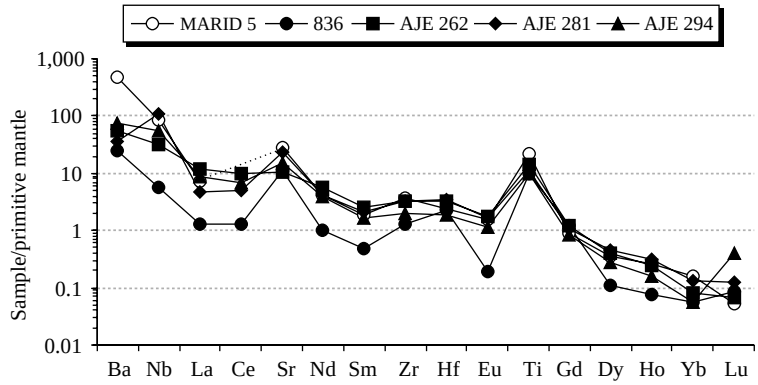

Figure 18 Primitive mantle normalized trace-element abundance patterns for whole-rock MARID xenoliths from kimberlites. Primitive mantle values used for normalisation in this plot and subsequent plots are those of McDonough and Sun (1995) (sources Pearson and Nowell, 2002; Gregoire *et al.*, 2002).

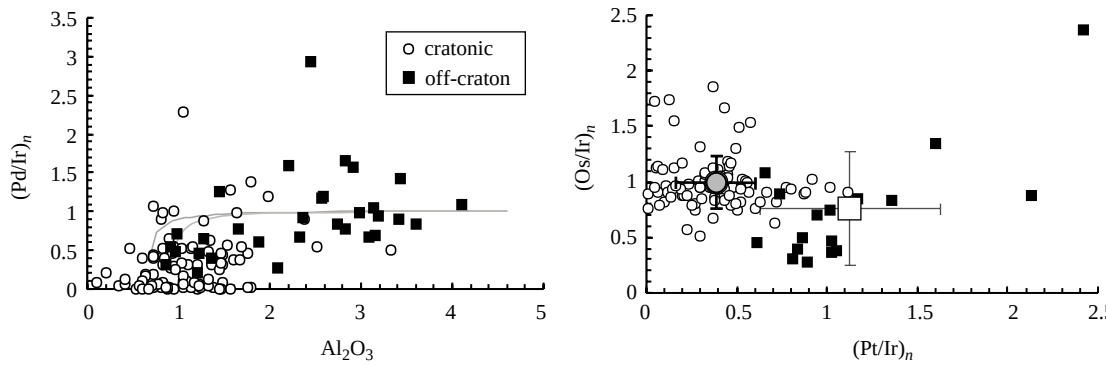

Figure 19 Left: $(Pd/Ir)_n$, where *n* refers to values normalized to primitive mantle values (McDonough and Sun, 1995) versus bulk rock Al_2O_3. Right: $(Os/Ir)_n$ versus $(Pt/Ir)_n$ plot of cratonic and off-craton whole-rock peridotites. Curves on left-hand plot are trends expected for progressive melting of mantle peridotite. On the right-hand plot, large circle with error bars = mean and 1 SD for cratonic peridotites. Large square with error bars = mean and 1 SD for off-craton peridotites. Cratonic peridotite data are isotope dilution data from Pearson *et al.* (2002), Irvine (2002), Pearson *et al.* (2004), and Irvine *et al.* (2003). Off-craton xenolith data from Handler and Bennett (1999) and Pearson *et al.* (2004).

fractionation during partial melting can be correlated with major-element depletion indices such as Al_2O_3 (Figure 19). If cratonic peridotites represent highly depleted melt residues then they should have very low Pd/Ir ratios to complement the depleted nature of their major-element compositions Pearson *et al.* (in press). Should melt/fluid re-enrichment or some other form of disturbance affect a peridotite subsequent to melting then this should be reflected in PGE patterns and PGE-major-element systematics. Modeling of melt re-enrichment involving the addition of new sulfides to variably depleted melt residues during magma–solid interaction produces elevation of the $(Pd/Ir)_n$ ratio to supra-chondritic levels and elevated P-PGE contents (Rehkämper *et al.*, 1999).

Cratonic peridotite xenoliths from Lesotho, S. Africa, the Jericho kimberlite, Slave craton, and Somerset Island, Churchill Province, northern Canada, along with selected samples from Kimberley, S. Africa, have been analyzed for PGEs plus rhenium (Irvine, 2002; Irvine *et al.*, 2003; Pearson *et al.*, 2002, 2004). Data from the Lesotho suite illustrates the typical within-suite PGE variation (Figure 20; Irvine, 2002; Pearson *et al.*, 2004). The simplest chondrite-normalized PGE-Re patterns to interpret are those of group A, defined by Irvine (2002) as being highly depleted in platinum, palladium, and rhenium but unfractionated in terms of Os–Ir and ruthenium (Figure 20). This signature correlates with the highly depleted major-element characteristics of cratonic xenoliths and reflects the more incompatible nature of the low-melting point or P-PGE members of the PGE group. The P-PGEs and rhenium quantitatively partition into the melt phase during high degrees of melting (>30%) thought to be responsible for generating the major-element characteristics of cratonic peridotites, probably due to the breakdown of

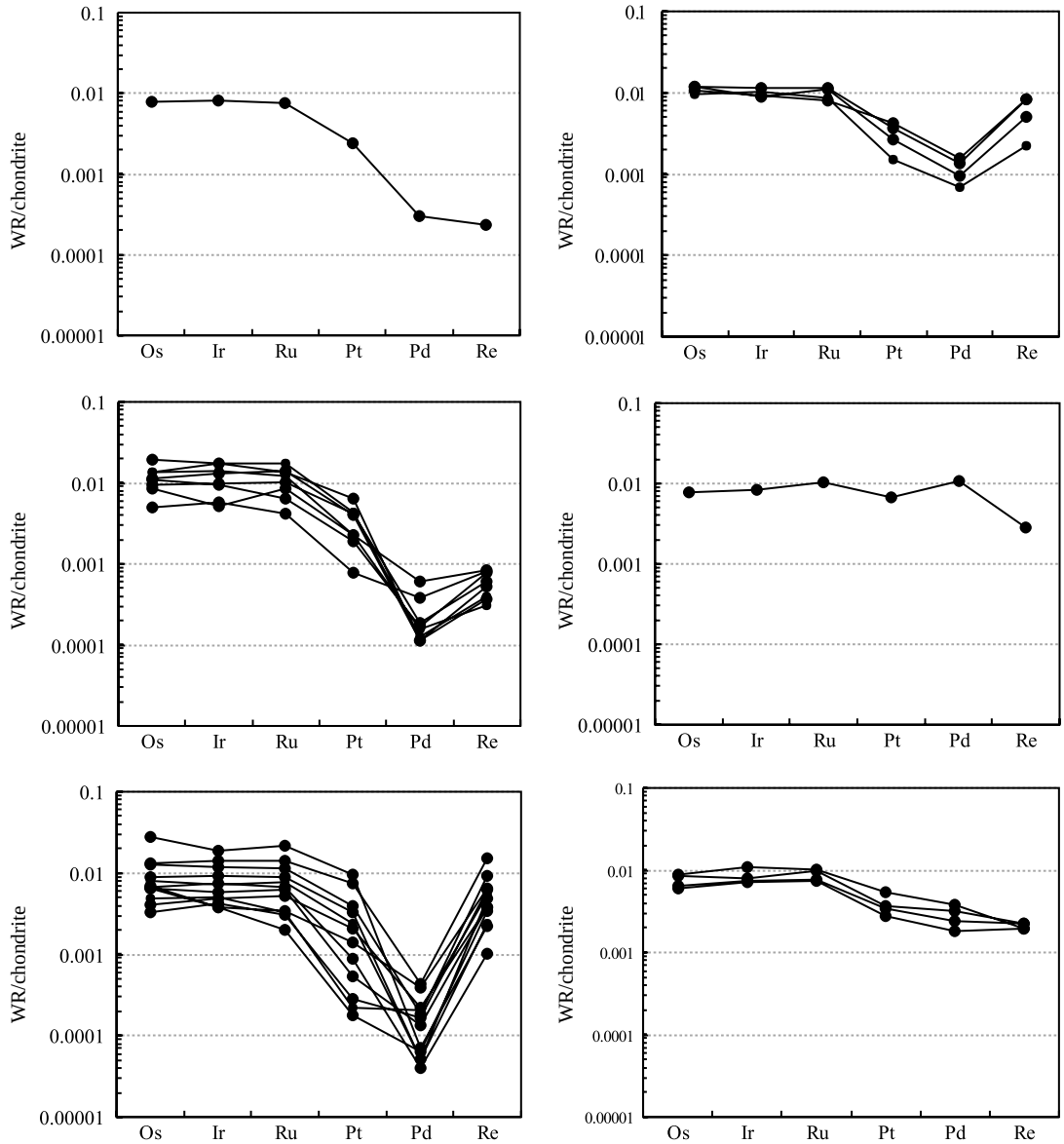

Figure 20 Primitive mantle normalized extended PGE patterns (including rhenium) for cratonic whole-rock garnet peridotite xenoliths from the Letseng kimberlite (Lesotho) (sources Irvine, 2002 and Pearson *et al.*, 2004).

the monosulfide solid solution (mss). In contrast, the higher melting point I-group PGEs remain in the residue and are stabilized in either alloy phases or high melting point residual Ru–Os–Ir sulfides. This produces a highly P-PGE depleted residual peridotite that is considerably more depleted in P-PGEs (Pearson *et al.*, 2004). These peridotites have lower $(Pt/Ir)_n$, and rhenium than fertile, noncratonic spinel lherzolite xenoliths (Figure 19: Handler and Bennett, 1999) or massif peridotites (Lorand *et al.*, 1999). Variations on these scenarios are PGE patterns that still show marked P-PGE depletion, with $(Pd/Ir)_n = 0.007$ to 0.117, but slight rhenium enrichments may occur, probably due to infiltrating melt, that produce small upward kinks at rhenium in the extended PGE pattern (group Bi of Irvine, 2002; Figure 20). Other samples show much greater increases in rhenium abundance with minimal effect on the depleted P-PGEs (e.g., $(Pd/Ir)_n = 0.004$ to 0.102; group Bii of Irvine, 2002; Figure 20). Subgroup Biii has higher Pd abundances and enhanced rhenium. These peridotites have either undergone lower levels of melt depletion or have experienced some palladium re-enrichment following melt depletion. Groups C and D show much less fractionation of P-PGEs from I-PGEs and higher abundances of P-PGEs plus rhenium such that

$(Pd/Ir)_n$ values are greater than 1. Both these groups are likely to have experienced P-PGE enrichment, perhaps by a sulfide melt.

Examination of all data for cratonic peridotites (Figure 19) shows similar features to the Lesotho suite (Irvine, 2002). Highly depleted cratonic peridotites generally have low Al_2O_3 and very low $(Pd/Ir)_n$ values. Variation in Al_2O_3 at very low, constant $(Pd/Ir)_n$ appears characteristic of cratonic peridotites and may be related to the introduction of late-stage diopside by the host kimberlite (Pearson *et al.*, 2002a; Simon *et al.*, 2003). Positive slopes at moderate angles may be related to silicate melt-metasomatism, whereas subvertical trends of increasing Al_2O_3 and $(Pd/Ir)_n$ are indicative of sulfide addition (Rehkämper *et al.*, 1999). Hence, the bulk rock PGE systematics of cratonic peridotites are indicative of their major-element depleted characters, but with metasomatic effects superimposed on this signature to varying degrees.

The best characterized noncratonic, spinel peridotite xenoliths for PGEs are those from southeastern Australia (Handler and Bennett, 1999), the Massif Central, France (Lorand and Alard, 2001), Western USA (Morgan *et al.*, 1981; Lee, 2002) and Vitim, Siberia (Pearson *et al.*, 2004). In general, $(Pd/Ir)_n$ values for noncratonic peridotites are considerably higher than those of cratonic xenoliths (Figure 19), in keeping with their much less depleted nature (Figures 10 and 19). The fertile lherzolites have broadly chondritic PGE interelement ratios with little fractionation of P-PGEs from I-PGEs, in contrast to cratonic peridotites. Some of the more depleted, lower Al_2O_3 peridotites have lower $(Pd/Ir)_n$ but systematics are complicated by metasomatism and alteration processes (e.g., Lee, 2002). Both fertile and depleted peridotites have elevated $(Ir/Os)_n$ that scatter much more than cratonic peridotites (Figure 19). Positive correlation of $(Ir/Os)_n$ with Cu/S suggests late-stage osmium mobility in the southeastern Australian suite (Handler *et al.*, 1999). Similar, but less well developed trends are also seen in western USA xenoliths. In the southeastern Australian and Massif Central peridotites suites, peridotites containing metasomatic phases (amphibole, mica, apatite) have similar PGE systematics to those that do not contain metasomatic phases (Handler *et al.*, 1999; Lorand and Alard, 2001). This has been interpreted as indicating that PGEs were not greatly affected by the melt infiltration events that cause crystallization of mica and amphibole.

Where peridotites show both textural and geochemical evidence for pervasive interaction with percolating melts, PGE and selenium abundances are greatly reduced. PGE abundances decrease by ~80%, probably because of dissolution of intergranular sulfides (Lorand and Alard, 2001). In contrast, peridotites metasomatized by small melt fractions show enrichment in platinum and palladium and elevated $(Pd/Ir)_n$. Bulk mineral separate PGE-Re analyses of two fertile xenoliths from southeastern Australia indicate less than 6% of the whole-rock PGE budget resides in either silicate or oxide phases and further implicates sulfides and alloys as the main controls of PGE-Re abundance. Comparison of sulfide versus whole-rock budgets by Lorand and Alard (2001) demonstrates the dominance of sulfide as the main PGE host in relatively fertile peridotites. This confirms the results of earlier studies of xenolith PGE mass balance (Hart and Ravizza, 1996; Mitchell and Keays, 1981) plus xenolith-derived and diamond inclusion sulfide studies (Jagoutz *et al.*, 1979; Pearson *et al.*, 1998b). As with cratonic xenoliths, sulfur-PGE and major-element-PGE correlations in more depleted noncratonic peridotites indicate that I-PGEs are probably not hosted entirely by sulfide (Lee, 2002).

One striking feature to emerge from the preponderance of high quality rhenium and osmium abundance data resulting from Re–Os isotope work on xenoliths is that the mean osmium concentration for cratonic peridotite xenoliths (3.8 ± 2.6 ppb) is significantly higher than that for noncratonic peridotites (both spinel and garnet facies; 2.0 ± 1.1 ppb; Figure 21 Pearson *et al.* (2004)). Because osmium is compatible, residues from large degrees of melting should have higher osmium than PUM and this is the case for cratonic peridotites. However, the off-craton peridotites are also residual yet they have significantly lower osmium than PUM, with many samples having concentrations below 1 ppb. The reason for this difference is not well understood. Melt percolation through peridotites can dissolve residual sulfides and hence lower osmium and this process may be more prevalent in the off-craton suites studied so far. Lee (2002) suggested multiple processes, including mobilization by aqueous fluids/secondary loss associated with sulfide breakdown were required to account for the osmium (and rhenium, palladium, and platinum) depletion in western USA peridotites. It is clear that noncratonic peridotite xenolith suites are much more susceptible to these processes than cratonic peridotites. The large degrees of melt extraction that have affected cratonic peridotites means that their osmium is likely to be hosted in alloy phases and refractory sulfides that may be more resistant to syn-eruption sulfide breakdown and alteration/leaching. However, we note that nonchondritic Ir/Os values are not a feature of massif peridotites that have experienced similar levels of depletion to noncratonic peridotites (e.g., Burnham *et al.*, 1998).

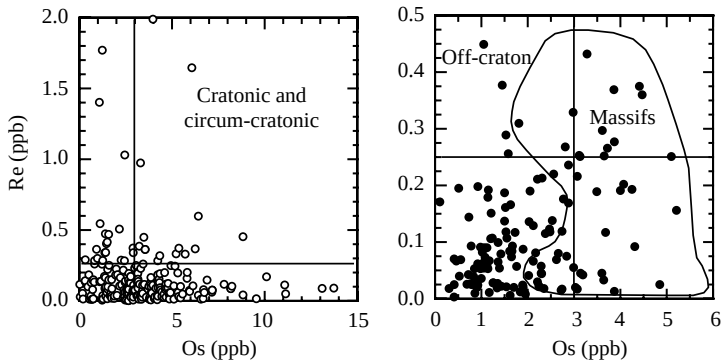

Figure 21 Covariation of rhenium versus osmium in whole-rock cratonic and circum-cratonic peridotite xenoliths (left) and off-craton peridotite xenoliths (right). Off-craton suite is compared to range in Massif peridotites (shown by field). Cratonic values extend to >15 ppb Os and >2 ppb Re. Lines denote Primitive Mantle values of Morgan *et al.* (1986) (source Walker *et al.*, 1989a; Carlson and Erving, 1994; Carlson *et al.*, 1999a; Pearson *et al.*, 1994, 1995a,b, 2002; Reisberg and Lorand, 1995; Handler *et al.*, 1997; Burnham *et al.*, 1998; Chesley *et al.*, 1999; Burton *et al.*, 2000; Peslier *et al.*, 2000; Meisel *et al.*, 2001; Hanghoj *et al.*, 2001; Irvine *et al.*, 2001, 2003; Irvine, 2002).

In summary, PGE studies of peridotite xenoliths from a variety of tectonic settings to date (Morgan *et al.*, 1981; Rehkämper *et al.*, 1997; Lorand and Alard, 2001; Handler and Bennett, 1999; Irvine, 2002; Irvine *et al.*, 2003) reveal a similar history to that indicated from incompatible elements such as REE. The depletion in P-PGE relative to I-PGE correlates broadly with melt depletion indices such as Al_2O_3 and shows that once sulfide-mss has disappeared at high degrees of melting, such as in cratonic peridotites, P-PGE partition quantitatively into the melt. Suprachondritic $(Pd/Ir)_n$ and $(Ru/Ir)_n$, or $(Os/Ir)_n$ values are indicative of metasomatic disturbance of PGEs by later melt infiltration or alteration. However, in contrast to REE studies, where whole-rock peridotites are ubiquitously LREE enriched, whole-rock PGE patterns frequently retain the signature of melt depletion, even when significant LREE enrichments are present in the bulk rock (Lorand and Alard, 2001; Irvine, 2002). This confirms earlier suggestions that PGEs and the Re–Os isotope system are much more robust to the effects of metasomatism than lithophile elements.

2.05.2.6 Mineral Trace-element Geochemistry

2.05.2.6.1 Olivine

Olivine is a major reservoir for divalent transition metal cations in xenoliths. Nickel, manganese, cobalt, and zinc all show correlations with Fo content in olivine from xenoliths. Nickel is positively correlated with Fo content, whereas cobalt, manganese, and zinc are negatively correlated suggesting the latter behave moderately incompatibly during the melting process. The calcium content of olivine is very *T* sensitive and is often zoned by heating and cooling effects. Typical abundances are listed in Table 9. High magnesium and calcium contents in secondary olivines within some peridotite xenoliths have been suggested to result from carbonatite metasomatism (Hauri *et al.*, 1993; Ionov *et al.*, 1993a).

There are far fewer data for trace-element cations because they are usually at levels below the detection limit of most analytical instruments. Trivalent cations (aluminum, scandium, vanadium, chromium, ytterbium) are all highly correlated with one another in olivine, suggesting crystal chemical effects for their substitution, with general trends of increasing concentration with equilibration temperature (Norman, 1998, 2001). The very few REE analyses in olivine show flat chondrite-normalized profiles that are several orders of magnitude lower in abundance than coexisting clinopyroxene (Figure 22). Li levels in olivine are generally higher than other minerals in mantle peridotite and so olivine will probably dominate the lithium budget in anhydrous peridotites (Eggins *et al.*, 1998; Glaser *et al.*, 1999).

2.05.2.6.2 Orthopyroxene

Orthopyroxene partitions nickel, cobalt, and manganese less than olivine and there are no clear correlations amongst these elements. Although low in abundance, orthopyroxene can be a significant reservoir for the trivalent cations vanadium, scandium plus tetravalent titanium, due to its high modal abundance, especially in depleted xenoliths with little or

Table 9 Representative trace element analyses of minerals from peridotite xenoliths.

Mineral	*Setting*	*Type*	*Lithology*	*Notes*	*Sample no.*	*Reference*	*Element*												
							Li	*Be*	*B*	*Sc*	*Ti*	*V*	*Rb*	*Sr*	*Y*	*Zr*	*Nb*	*Ba*	*La*	*Ce*
gt	C	AI	gt Lherz	Low-T	8604 gt3	1	0.048		0.25		199			0.272	6.37	14.9	0.005	0.139	0.023	0.220
gt	C	AI	gt Lherz	Low-T	FRB135	1					191			0.511	2.01	37.7	0.665	0.021	0.039	0.984
gt	C	AV	gt Lherz	Low-T	UV128/91	1					958			0.406	3.04	19.4	0.706	0.100	0.060	0.481
gt	C	AI	gt Harz	Low-Ca	RV174	2					73.2			6.13	1.69	7.99		0.010	1.92	7.93
gt	OC	BI	gt-lherz		Vi313-105	3				111	1,260		0.025	28.9		28.9	0.071	0.040	0.009	0.075
cpx	C	AI	gt Lherz	Low-T	8604 Di3	1	0.554	0.289	0.364		401			221	0.884	33.0	0.581	0.168	17.2	41.8
cpx	C	AI	gt Lherz	Low-T	FRB 135	1					104			342	0.205	11.7	0.901	0.686	6.97	27.8
cpx	C	AV	gt Lherz	High-T	UV128/91	1	0.451	0.18	0.324		405			99.1	1.09	4.55	0.232	0.358	2.46	7.79
cpx	OC	AI	gt-lherz		Vi313-105	3				29	3,420		0.011	78.5		21.2	0.50	0.13	1.03	3.58
cpx	OC	BI	sp. Lherz		ET80	4					3,120		0.003	26.9	17.1	13.0	0.027	0.090	0.240	0.950
cpx	OC	BI	sp. Lherz	fertile	2905	9	1.31			31.2	2,704	244	0.008	57.9	21.1	33.4	0.229	0.182	0.774	2.920
cpx	OC	BI	sp. Harz	depleted	84-402	9	1.95			94.4	1,512	219	0.034	155	12.3	50.4	1.46	0.210	5.780	1.340
cpx	OC	BIV	Amph-Sp.	Lherz	DW56-19	5					2,664		0.900	180	20.3	68.1	0.640	0.130	12.0	37.6
cpx	C	AVI	MARID		AJE282	6				43	676	333	0.650	509	7.70	40.0	0.190	11.8	16.0	41.0
opx	C	AI	gt-lherz		8604 En	1					142			0.186	0.017	0.230	0.109	0.039	0.032	0.046
opx	OC	BI	gt. Lherz		Vi313-105	3				8.2	1,050		0.010	0.49		1.58	0.061	0.04	0.010	0.026
opx	OC	BI	sp. Lherz		ET80	4					730		0.006	0.270	0.950	0.650	0.015		0.014	0.020
opx	OC	BI	sp. Lherz		2905	9	0.105			60.2	568	75	0.005	0.129	1.070	1.600	0.006	0.059	0.001	0.010
olv	OC	BI	sp. Lherz		ET80	4					36.1		0.050	0.076	0.040	0.124	0.116	0.1	0.016	
olv	OC	BI	sp. Lherz		2905	9	1.7			3.9	23.6	3	0.023	0.025	0.045	0.118	0.002	0.112	0.001	0.005
olv	OC	BI	gt-lherz		Vi313-105	3				1.5			0.016	0.034		0.044	0.019	0.013	0.0019	0.0037
Spinel	OC	BI	sp. Lherz		ET80	4					416		0.1080	0.0180	0.0005	0.0050	0.0060	0.1700		
Spinel	OC	BI	sp. Lherz		2905	9	0.72			2.1	720	346	0.328		0.200	0.716	0.085	0.312	0.012	0.033
amph	OC	BII	Pxite		SF93803	10	1.16			15.9	26,280	219		249	9.04	98.8	15.9		2.22	10.3
amph	C	AVI	MARID	K-Rich.	AJE288	6				24	978	128	21.0	570	0.650	25.0	3.90	78.0	2.90	7.10
amph	C	AVI	PKP	K-Rich.	BD2346	6					795	51	20.0	294	1.64	67.0	1.50	98.0	3.10	7.10
amph	OC	BIV	Vein		313-103	7				21.2	26,640		3.90	269		123	74.8	88.0	2.34	8.70
amph	OC	BIV	Amph-sp.	Lherz	DW56-19	6					15,300		16.0	470	22.1	82.6	83.9	327	16.1	50.1
phlog.	C	AVI	MARID		FRB836	1	6.90	3.38	3.59		5,036		379	1.14	0.020	1.14	5.36	424	0.127	0.040
phlog.	C	AVI	MARID		AJE288	6					2,385	60	545	4.20	0.280	1.80	14.0	439	0.460	0.200
phlog.	OC	BIV	Phl-sp-	Lherz	Mo4230-16	7				5.1	28,260		97.8	662		3.59	7.08	14,610		0.150
phlog.	OC	AIV	Phl-sp-	Lherz	SG96B11	10	7.7			4.42	27,600	199	154	77.5	0.78	28.1	34.4	824		0.520
Apatite	OC	BI	sp. Lherz		ET49	4							0.400	20,850	147	11.6	4.98	1,240	3,925	4,295
Apatite	OC	BI	Mica vein		4334-lu	4							0.105	4,087	92	0.870	2.66	118	765	623
Zircon	C	AVI	MARID		FRB836	1								14.3	303	58,20,000	10.6	0.253	0.353	18.8
Ilmenite	C	AVI	MARID		AJE288	6					3,20,700	837				53.0	1,318			
Rutile	C	AVI	MARID		AJE262	6					5,64,900	1,236				1,159	1,024			
Lindsleyite	C	AVIII	Phlog.	Lherz	AJE285	6					3,54,720	2,175		20,379		14,952	1,278	20,599		
Carbonate	OC	BIV	Amph-sp-	lherz	4-90-9	8					10.00			1,900	0.71	0.580	0.200	389	0.550	0.770

Element																				
Pr	*Nd*	*Sm*	*Eu*	*Gd*	*Tb*	*Dy*	*Ho*	*Er*	*Yb*	*Lu*	*Hf*	*Ta*	*Pb*	*Th*	*U*	*Rb/Sr*	*Sm/Nd*	*Lu/Hf*	*U/Pb*	*Th/Pb*
0.081	0.921	0.460	0.156	0.718	0.125	1.25	0.211	0.924	1.50	0.342	0.114	0.071					0.499	3		
0.469	0.391	1.5	0.471	1.4	0.113	0.605	0.0865	0.143	0.121		0.159						3.84			
0.156	1.34	0.728	0.19	0.673	0.0849	0.604	0.121		0.906	0.18	0.326						0.543	0.552		
1.21	4.93	0.750	0.200	0.670	0.090	0.350	0.070	0.200	0.210	0.040							0.152			
0.032	0.387	0.572	0.394	2.09	0.54	4.62	1.16	3.62	3.66	0.60	0.48	0.002	0.119	0.001	0.0032	0.0009	1.478	1.260	0.027	0.012
5.01	17.5	2.17	0.495	2.23	0.164	0.678	0.025	0.235	0.359	0.002	1.13	0.039					0.124	0.002		
5.28	28.6	4.27	0.557	0.324	0.087	0.088	0.051	0.163	0.260		0.619						0.149			
1.31	5.83	1.09	0.342	0.543	0.082	0.449	0.044		0.146	0.002	0.233		3.43		0.022		0.187	0.010	0.007	
0.742	4.30	1.50	0.546	1.68	0.232	1.15	0.176	0.358	0.202	0.025	0.99	0.040	0.039	0.022	0.0063	0.0001	0.350	0.025	0.160	0.572
0.280	2.34	1.27	0.560	2.36	0.450	3.33	0.740	2.19	1.96	0.310	0.730	0.002		0.016	0.003	0.0001	0.543	0.425		
	3.69	1.61	0.645	2.52		3.28		2.14	1.9	0.280	1.020	0.041		0.031	0.010	0.0001	0.436	0.275		
	10.1	2.83	0.960	2.85		2.280		1.11	0.893	0.131	1.320	0.215		0.620	0.136	0.0002	0.280	0.099		
6.29	27.2	7.14	1.83	6.22	0.820	4.31	0.970	2.15	1.46	0.254	1.41	0.083				0.0050	0.263	0.180		
6.00	28.0	5.30	1.60	3.60	0.390	1.90	0.350	0.680	0.440	0.040	2.7	0.01	1.5	0.120	0.030	0.0013	0.189	0.015	0.020	0.080
0.012	0.027	0.050	0.018	0.079		0.064	0.006	0.032	0.035	0.003	0.088						1.898	0.035		
0.008	0.048	0.029	0.013	0.052	0.010	0.071	0.015	0.040	0.038	0.006	0.063	0.007	0.035	0.0016	0.0002	0.0199	0.606	0.097	0.007	0.046
0.004	0.033	0.021	0.011	0.052	0.013	0.128	0.037	0.148	0.247	0.051	0.035	0.001		0.002	0.001	0.0222	0.636	1.457		
	0.020	0.019	0.009	0.042		0.116		0.137	0.215	0.041	0.045	0.001			0.001	0.0388	0.950	0.911		
0.001	0.008		0.001	0.004		0.005	0.002	0.009	0.018	0.005	0.004	0.002		0.002		0.6579	0.000	1.190		
	0.002		0.0002	0.001		0.003		0.007	0.018	0.005	0.003	0.007		0.001	0.0004	0.9200		1.660		
	0.003		0.0013	0.004	0.0008	0.0068	0.002	0.0053	0.001	0.0047	0.0012	0.0033	0.0012	0.015	0.0003	0.4838	0.000	3.757	0.251	12.169
0.0001			0.0002			0.0007			0.0003		0.0002	0.0001		0.0001		6.000				
	0.017	0.011	0.004	0.016		0.032		0.024	0.015	0.002	0.020	0.058		0.005	0.001		0.647	0.100		
1.88	10.8	3.360	1.280	3.350	0.540	2.550	0.400	0.790	0.320	0.032	4.85	1.33		0.034	0.001		0.311	0.007		
0.850	3.40	0.500	0.120	0.250	0.025	0.130	0.020	0.050	0.050	0.010	0.990	0.060	3.30	0.300	0.210	0.037	0.147	0.010	0.064	0.091
0.780	3.00	0.740	0.120	0.540	0.060	0.320	0.050	0.120	0.080	0.010	1.800	0.060	4.30	0.670	0.280	0.068	0.247	0.006	0.065	0.156
1.62	9.22	2.88	1.02	2.99	0.39	1.83	0.26	0.46	0.21	0.019	7.54	6.65	0.590	0.072	0.017	0.014	0.312	0.003	0.029	0.122
8.14	32	6.70	2.53	6.53	0.715	4.28	0.762	1.97	1.23	0.265	2.07	2.79				0.034	0.209	0.128		
0.006	0.031	0.026								0.006	0.180		4.38	1.15	0.088	332.5	0.818	0.032	0.020	0.263
																129.8				
0.027	0.29				0.006	0.056	0.011	0.059	0.120	0.026	0.130	0.370	15.4	0.008	0.009	0.148	0.000	0.200	0.001	0.001
											0.780									
315	1035	127	32.3	78.8	10.4	40.2	5.80	11.4	6.1	0.740	0.187	0.120		661	126		0.123	3.957		
	87.0	13.9							5.7		0.022			97.0			0.160			
0.859	9.77	9.28	3.26	19.2	5.88	49.8	12.8		54.5	10.9	14900		18.5	71.2	86.2		0.950	0.001	4.659	3.849
											1.00	40.0								
											28.0	46.0								
											407	90								
0.180	0.900			0.470											0.160					

gt = garnet, cpx = clinopyroxene, opx = orthopyroxene, olv = olivive, amph = amphibole, phlog = phlogopite.
1 = this study; 2 = Stachel *et al.* (1998); 3 = Ionov (1996); 4 = Bedini and Bodinier (1999); 5 = Johnson *et al.* (1996); 6 = Gregoire *et al.* (2002); 7 = Ionov *et al.* (1997); 8 = Ionov (1998); 9 = Eggins *et al.* (1998); 10 = Glaser *et al.* (1999). c = cratonic, oc = off-craton. Type refers to classification of Table 1.

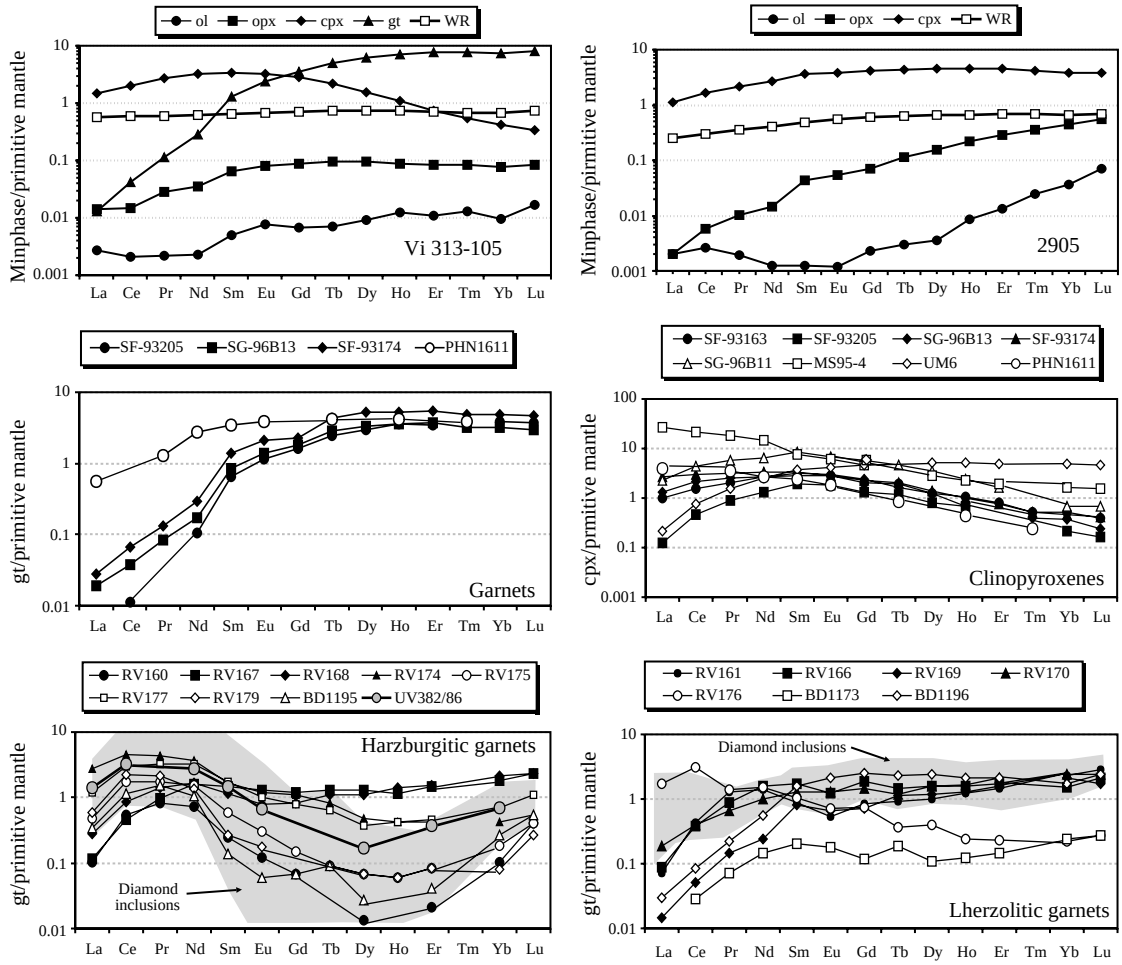

Figure 22 Primitive mantle normalized REE patterns in minerals from peridotite xenoliths and diamond inclusions. Upper two diagrams show coexisiting minerals in a noncratonic garnet lherzolite (Vi 313-105; Vitim suite, Ionov, 1996, 2004; Table 9) and a noncratonic spinel lherzolite (2905, SE Australia; Eggins *et al.*, 1998; see also Table 9). Middle left diagram shows REE data for garnets from noncratonic garnet lherzolites (SF-93205, SG-96B13, SF-93174; Glaser *et al.*, 1999) and high-*T* cratonic garnet lherzolite (PHN1611; Shimizu, 1975). Middle right diagram shows REE data for clinopyroxenes from off-craton (Vitim) garnet lherzolites (SG93163, SF-93205, SG-96B13, SF-93174, SG-96B11; Glaser *et al.*, 1999), off-craton (SE Australia) spinel lherzolites (MS95-4, UM-6; Norman, 1998) and cratonic high-*T* garnet lherzolite (PHN1611; Shimizu, 1975). Lower diagrams show REE patterns for garnets from cratonic lherzolites and harzburgites. Lower left diagram shows garnets in harzburgite xenoliths from the Roberts Victor mine, S. Africa (Stachel *et al.*, 1998). Also shown is a garnet from a diamondiferous low-calcium garnet dunite from Udachnaya, Siberia (UV382/86; Pearson *et al.*, 1995a). Shaded field is for the range of harzburgitic garnet inclusions in diamonds from Akwatia, Guinea (Stachel and Harris, 1997). Lower right diagram shows garnets in lherzolite xenoliths from the Roberts Victor mine, S. Africa (Stachel *et al.*, 1998). Shaded field is for the range of lherzolitic garnet inclusions in diamonds from Akwatia, Guinea (Stachel and Harris, 1997).

no clinopyroxene (Bedini and Bodinier, 1999; Eggins *et al.*, 1998; McDonough *et al.*, 1992). The abundances of strontium, niobium, zirconium, and yttrium in orthopyroxenes are near or below the ppm-level and show no clear correlations. A general feature is enrichment of titanium, zirconium, and niobium relative to coexisting clinopyroxene (Eggins *et al.*, 1998; Norman, 1998, 2001; Simon *et al.*, 2003). The few measurements of the REE patterns in orthopyroxene are typically LREE-depleted, with all REE one to two orders of magnitude below clinopyroxene (Figure 22). There is far more scatter and far less coherent variation amongst many incompatible trace elements in orthopyroxene, likely reflecting more heterogeneity on the micro-scale (Shimizu, 1999) as well as temperature effects that are not well understood with the paucity of data available (Norman, 2001).

2.05.2.6.3 Clinopyroxene

Clinopyroxene is a major host for many incompatible trace elements in peridotite xenoliths (Table 9) and as such its trace-element composition is a useful indicator of chemical modification in the mantle. Clinopyroxene partitions titanium and vanadium equably with spinel but is a major host for strontium and scandium. The partition of the latter element is *T* sensitive. The trivalent elements all show strong correlations in clinopyroxene from all types of xenoliths. There are significant depletions of zirconium, titanium, and yttrium relative to elements with similar compatibilities (REE), but coexisting orthopyroxene shows a complementary enrichment in these elements (McDonough, 1990). Clinopyroxene generally has lower niobium than garnet or mica/amphiboles (Figure 23). Nb/Ta is close to the PUM value in most instances, despite very variable abundances of both elements. Clinopyroxenes from metasomatic assemblages such as MARID xenoliths show very large negative HFSE anomalies due to equilibration with HFSE-rich phases such as ilmenite, amphibole, mica, and rutile.

Clinopyroxene shows a range of REE patterns from extremely enriched to very depleted LREE signatures (Figure 22). Noncratonic peridotites are subdivided on the basis of clinopyroxene REE patterns into LREE-depleted (type IA) and LREE-enriched (type IB; Menzies, 1983; Figure 17). LREE-enriched type IB pyroxenes are the norm in most suites. LREE-depleted varieties are relatively scarce. Very few clinopyroxenes show simple LREE-depleted REE patterns that can be interpreted solely in terms of melt depletion, i.e., LREE depletion, flat, unfractionated MREE-HREE patterns (e.g., UM-6 or 2905; Figure 22). For peridotites that do have LREE-depleted clinopyroxenes, a correlation of HREE with other incompatible trace elements (e.g., yttrium, strontium, zirconium) in xenoliths suites worldwide requires fractional melting to be the principal means of depletion in the mantle (Norman, 2001).

Clinopyroxenes that have equilibrated with garnet in off-craton garnet peridotites show

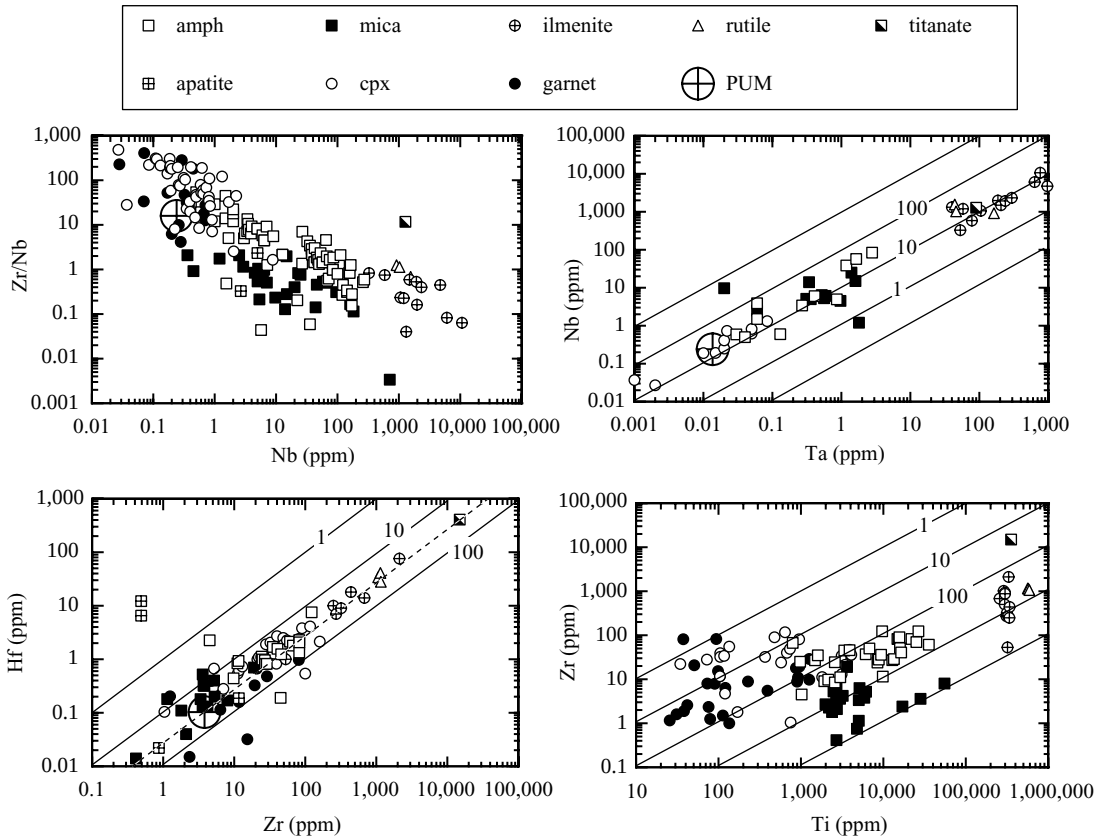

Figure 23 High field strength element (HFSE) variations in mantle xenolith minerals. Primitive mantle values plotted are from McDonough and Sun (1995). Dashed lines extend from PM values at constant ratios, e.g., at Nb/Ta = 17.6, Zr/Hf = 37. Solid lines are constant elemental ratios (1–100 labeled) (sources Moore *et al.*, 1992; Witt-Eickschen and Harte, 1994; Vannucci *et al.*, 1995; Ionov and Hoffman, 1995; Johnson *et al.*, 1996; Chazot *et al.*, 1996; Vaselli *et al.*, 1996; Ionov *et al.*, 1997; Shimizu *et al.*, 1997; Norman, 1998; Glaser *et al.*, 1999; Pearson and Nowell, 2002; Gregoire *et al.*, 2002; Kalfoun *et al.*, 2002; Table 9).

substantially lower levels of HREE than those from spinel-facies peridotites (compare Vi313-105 and 2905; Figure 22). Clinopyroxene REE systematics are linked to texture/equilibration temperature (Figure 17). Clinopyroxene in low-T (granular) peridotites is more LREE enriched and HREE depleted than that from high-T (sheared) peridotites. The relationship between garnet and clinopyroxene in high-T peridotites is close to equilibrium (e.g., PHN1611 shown in Figure 22) and mirrors the relationship shown by off-craton garnet peridotites (e.g., Vi313-105). In contrast, the HREE-depleted clinopyroxenes from the low-T peridotites are often not in equilibrium with their coexisting garnets (Shimizu *et al.*, 1997; Shimizu, 1999; Simon *et al.*, 2003).

LREE enrichment in clinopyroxene is widely linked to metasomatism by either silicate melts or carbonatitic fluids, usually via cryptic (in the sense of no new phase being introduced) metasomatism, although there is a strong possibility that the diopside itself could have precipitated from the melt. This is strongly favored for much of the ubiquitously LREE-enriched diopside found in cratonic peridotites (Figure 17) which are not in trace-element equilibrium with their coexisting garnets and for which equilibrium melts for the diopside closely resemble kimberlite (Simon *et al.*, 2003).

Metasomatism has also fractionated trace-element ratios such as Ti/Eu or Zr/Hf in clinopyroxene that are invariant to the melting process. Samples with fractionated Ti/Eu and or Zr/Hf and possessing extreme LREE-enrichment (near 100 × chondrite) show patent or cryptic evidence for metasomatism by carbonatitic liquid (Yaxley *et al.*, 1998). This process has also been suggested to impart low aluminum (Hauri *et al.*, 1993; Rudnick *et al.*, 1993) and high sodium (Yaxley *et al.*, 1998) to secondary clinopyroxenes. Some xenolith clinopyroxenes, particularly from low-T cratonic xenoliths, show extreme heterogeneity in trace elements. Incompatible element abundances can vary by factors of 2–10 on millimeter scales in clinopyroxenes. Diffusion should erase these gradients over longer time periods at high T in the mantle (Van Orman *et al.*, 2001), requiring that some component of clinopyroxene crystallized late in the history of the xenolith before sampling (Shimizu, 1999).

2.05.2.6.4 Garnet

Garnet can also be a major host for trace elements in peridotite xenoliths, especially in harzburgites. A large data set was recently summarized by Griffin *et al.* (1999a). The abundances of manganese and nickel in peridotitic garnets change due to T-dependent partitioning with coexisting olivine (Sachtleben and Seck, 1981; Griffin *et al.*, 1989; Smith *et al.*, 1991; Canil, 1999). The levels of scandium, titanium, and vanadium in xenolith garnets are commonly correlated with their level of depletion (as measured by the chromium content of the garnet) and to T-sensitive partitioning with coexisting pyroxenes, but the former effect is not well constrained. Trends of zirconium and yttrium in garnets are also correlated with different styles of depletion and/or chemical modification in the mantle (Griffin *et al.*, 1999c). Levels of yttrium in mantle garnet show a strong correlation with depletion (chromium content) and garnets very depleted in this element (<10 ppm) mainly occur in mantle sampled beneath Archean terrains (Griffin *et al.*, 1999a). Because yttrium is compatible in garnet, a low yttrium content implies that this phase was absent during the melting process, but has exsolved during cooling. The positive correlation of yttrium with titanium, gallium, and zirconium, suggests that all of these elements are sensitive to melt depletion. Correlations of the latter three elements with chromium, however, are weak, likely due to the effects of metasomatism. At $T < 1000$°C, metasomatism is interpreted to lead to preferential introduction of zirconium over titanium and yttrium (Figure 24). There are strong correlations of zirconium, titanium, yttrium, and gallium in garnets equilibrated at $T > 1{,}000$ °C that suggest a major contribution from melt-related metasomatism at higher T (Griffin *et al.*, 1999a). Zr/Nb is close to, or higher than PUM while Ti/Zr is very variable (Figure 23) and linked to garnet type

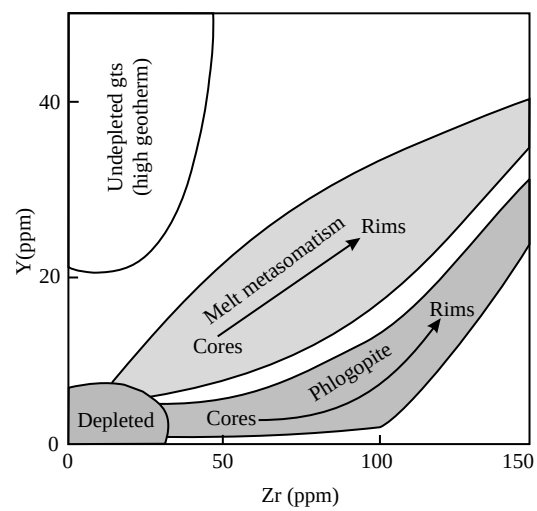

Figure 24 Covariation of yttrium and zirconium in mantle garnets showing fields ascribed to different mantle protoliths (undepleted, depleted) and processes (high-T melt metasomatism, low-T phlogopite metasomatism) and zonation patterns from cores to rims of garnets (after Griffin *et al.*, 1999c).

(Shimizu *et al.*, 1997). Levels of niobium in some garnets can equal those of clinopyroxene.

Two distinct REE patterns are recognized in mantle garnets (Figure 22). Garnets with normal heavy rare earth element (HREE) enriched patterns and garnets with sinuous REE patterns. The normal garnets show depletion in the LREE, steady enrichment from Sm_N to Yb_N and are most frequent in noncratonic xenolith suites or high-*T* cratonic xenoliths (Shimizu, 1975; Glaser *et al.*, 1999; Figure 22). These garnet REE systematics are compatible with those expected from melt-residues, or garnets that have equilibrated with silicate melts. In contrast, the sinuous REE patterns peak at either neodymium or samarium, Sm_N is greater than Dy_N, and can have fairly flat trends between the HREE or Yb_N is greater than Er_N (Shimizu, 1975; Shimizu and Richardson, 1987; Shimizu *et al.*, 1997; Stachel *et al.*, 1998; Figure 22). This garnet REE pattern is commonly recognized in low-*T* cratonic xenoliths (harzburgites) or diamond inclusion garnets that are depleted in calcium and have not equilibrated with clinopyroxene (Shimizu and Richardson, 1987; Hoal *et al.*, 1994; Pearson *et al.*, 1995b; Stachel *et al.*, 1998).

Various hypotheses have been proposed to explain the origin of the sinuous REE patterns. Two-stage models of melt depletion followed by metasomatism have been proposed. For instance, Stachel *et al.* (1998) suggest that the high chromium content (>5%) of these garnets is a reflection of the protolith origin as a residue from polybaric melting to create Archean ocean lithosphere. As the oceanic lithosphere is subducted, garnets growing from this depleted protolith were over-printed by a metasomatic fluid with high LREE/HREE. Although attractive, these models have problems. The wide range of HREE shown by subcalcic garnets is difficult to account for. In addition, where overprinting of LREE enrichment occurs in other LREE-depleted minerals such as clinopyroxene or olivine, "spoon-shaped" patterns, with maxima at lanthanum occur rather than sinuous patterns with peaks at neodymium or samarium. Hoal *et al.* (1994) found sinuous REE patterns in calcium-saturated pyrope garnets as well as in subcalcic garnets. These authors propose disequilibrium effects to develop sinuous garnet REE patterns that cause the LREE to diffuse and readjust faster than the HREE during chemical modification of garnet in the mantle. While differences in the diffusion coefficients of LREE and HREE have been measured for diopside (Van Orman *et al.*, 2001), that could account for some of the more complex REE patterns measured in this mineral, experimental determinations have not found any difference in LREE-HREE diffusion coefficients for garnet (Van Orman *et al.*, 2002). Normal and sinuous REE patterns can be present in different parts of the same garnet (Shimizu, 1999; Griffin *et al.*, 1999c), arguing for a disequilibrium feature, arrested shortly before sampling. This is supported by the widely ranging and often unsupported neodymium isotope systematics of these garnets (Pearson *et al.*, 1995a). The origin of the sinuous REE pattern in mantle garnets remains to be unequivocally demonstrated.

The considerable REE heterogeneity in many cratonic garnets is also reflected in other trace elements. Abundances of zirconium, yttrium, hafnium, cerium, and strontium can vary by over a factor of two, and correlate positively, both for multiple analyses of the same garnet grain, or for analyses of different garnet grains from the same sample. The peculiar and varied REE partitioning of mantle garnets leads to highly variable Sm/Nd and Lu/Hf (Figures 25 and 26), many of which are

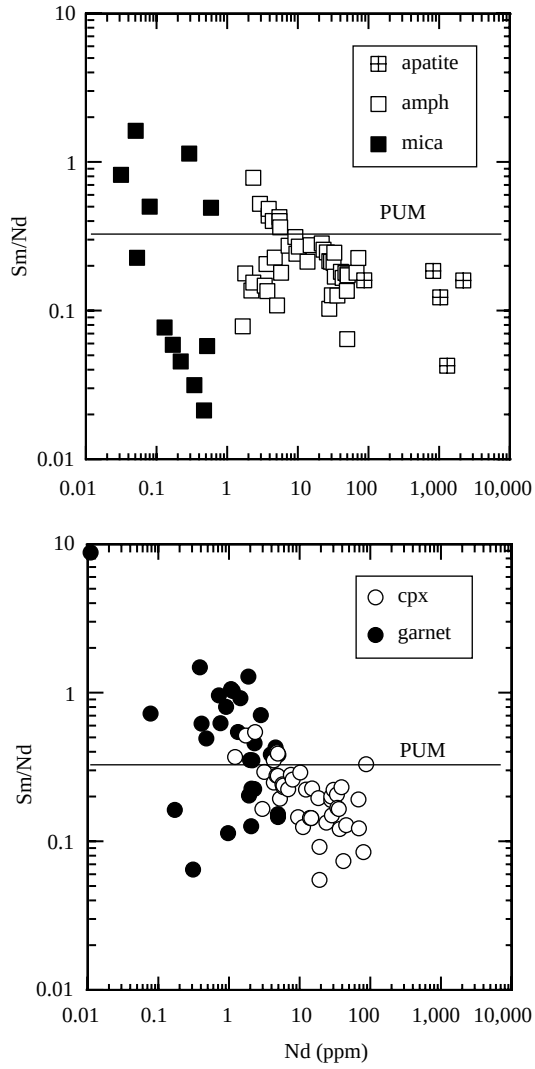

Figure 25 Covariation of Sm/Nd versus Nd for mantle xenolith minerals. Primitive mantle (PUM) line for Sm/Nd marked. Data sources as in Figure 23.

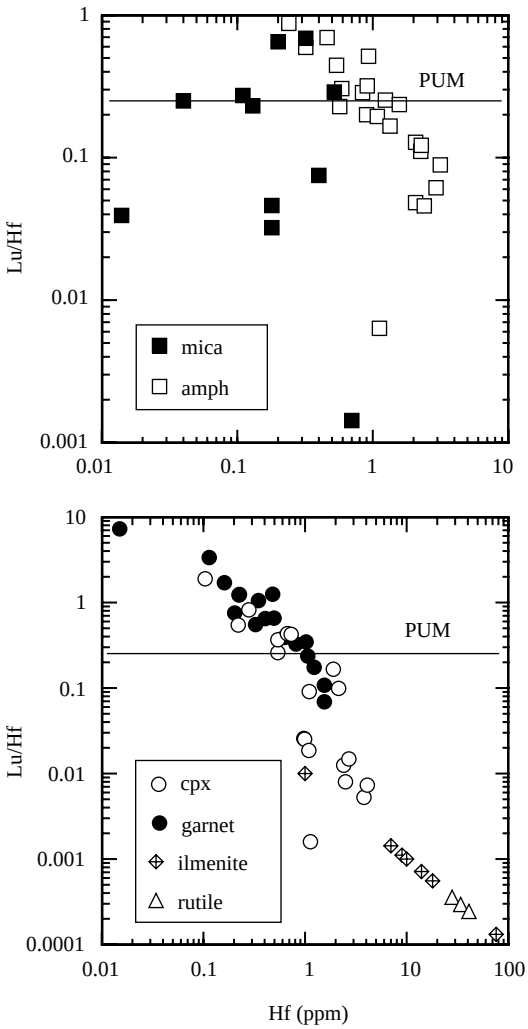

Figure 26 Covariation of Lu/Hf versus Hf for mantle xenolith minerals. Primitive mantle (PUM) line for Lu/Hf marked. Data sources as in Figure 23.

not those expected for equilibrium with a silicate melt. The strontium contents of mantle garnets range widely (0.1 ppm to >40 ppm) and often correlate positively with the sinuosity of the REE pattern (e.g., $(Nd/Yb)_N$). The very high levels of strontium are all from subcalcic, high-chromium garnets of the low-calcium harzburgite/dunite suite or diamond inclusions and have been linked to equilibration with a carbonate-melt fraction possibly during diamond genesis (Pearson *et al.*, 1995c).

2.05.2.6.5 Spinel

Because spinel is a very minor phase in peridotites, it makes up only a very small proportion of the trace-element budget (Eggins *et al.*, 1998; Norman, 2001). Spinel has a limited database for trace cations. The compatible trace-element data for nickel, cobalt, manganese, titanium, vanadium, scandium, zinc, and gallium are shown in Table 9. The nickel and zinc contents are sensitive to *T*-dependent partitioning with olivine, and zinc can be a useful single mineral trace-element geothermometer (Griffin *et al.*, 1993). Experimental work indicates the partition of vanadium into spinel is f_{O_2} sensitive (Horn *et al.*, 1994; Canil, 2002). Moderate concentrations of zirconium and niobium can also be present. Zr–Nb enriched reaction rims have also been found on spinels from numerous off-craton spinel lherzolites (Bedini and Bodinier, 1999; Figure 16).

2.05.2.6.6 Amphibole, phlogopite, apatite, zircon, rutile, ilmenite, titanate, and carbonate

Volatile-bearing minerals (mica, amphibole, apatite) together with titanium-rich phases such as ilmenite, rutile and titanates, are the major manifestation of modal or "patent" metasomatism in mantle xenoliths. The effects of carbonatite metasomatism are widely inferred in many xenolith suites from trace-element systematics (e.g., Hauri *et al.*, 1993; Rudnick *et al.*, 1993; Coltorti *et al.*, 1999) but carbonate of mantle origin is rare in xenoliths (Ionov, 1998). Mantle xenolith studies have allowed direct measurement of both inter-mineral and mineral–melt (through the presence of interstitial glass) trace-element partitioning (Chazot *et al.*, 1996; Ionov *et al.*, 1997). For brevity we will not specifically deal with partitioning data here.

In an extensive review of the geochemistry of volatile-bearing minerals in mantle xenoliths, Ionov *et al.* (1997) have pointed out that although minerals such as mica, amphibole, and apatite are often referred to as "hydrous," in many cases they have very low H_2O contents (Boettcher and O'Neill, 1980). In such cases, these minerals may have significant amounts of fluorine, chlorine and CO_2. Mica, amphibole, and apatite, together with the oxide phases, are important hosts for titanium, potassium, rubidium, strontium, barium, and niobium (Table 9).

Amphibole. Mantle amphibole equilibrated with clinopyroxene generally has lower Rb/Sr (<0.03) than PUM, whereas amphibole within veins and some amphibole-rich peridotites have considerably higher Rb/Sr (Table 9). The weighted mean Rb/Sr (0.036) is very close to the PUM value of 0.03 but values vary widely (Figure 27). Typical strontium contents vary from 200 ppm to 2,000 ppm, averaging close to 500 ppm and are generally higher than those of mica (Figure 27). Ba in mantle xenolith amphiboles typically varies from 100 ppm–1,500 ppm (Table 9;

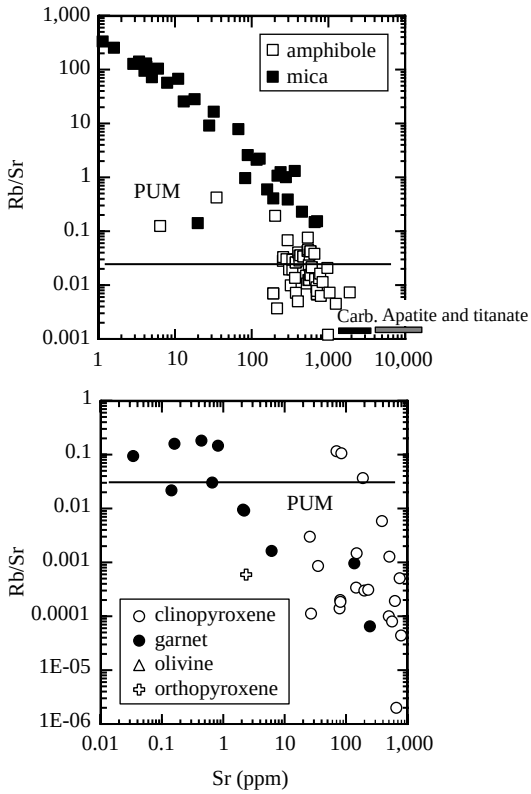

Figure 27 Covariation of Rb/Sr versus Sr for mantle xenolith minerals. Primitive mantle (PUM) line for Rb/Sr marked. Data sources as in Figure 23 (Carb. = carbonate).

Ionov *et al.*, 1997). Both strontium and barium are higher in amphibole from xenoliths than those from massif peridotites (e.g., Vannucci *et al.*, 1995). Numerous ion-probe and laser/solution ICP-MS studies have found wide variation in amphibole REE patterns depending on textural context and tectonic setting (Witt- Eickschen and Harte, 1994; Vannucci *et al.*, 1995; Ionov and Hofmann, 1995; Johnson *et al.*, 1996; Chazot *et al.*, 1996; Vaselli *et al.*, 1995; Ionov *et al.*, 1997; Pearson and Nowell, 2002; Gregoire *et al.*, 2002).

Amphiboles show a wide variety of REE patterns that cannot be uniformly related to modal abundance. Ionov *et al.* (1997) suggest that where the mineral has equilibrated extensively with silicate melt, LREE-enrichment and convex REE patterns occur. Hence, vein amphiboles from noncratonic xenoliths are enriched in LREE and MREE over HREE and thus have convex REE patterns (e.g., Figure 28). Disseminated amphiboles have lower MREE/HREE in some instances but those in xenoliths from the W. Eifel region are much more LREE-enriched than amphibole from other locations. Disseminated amphibole can be either LREE enriched or depleted relative to PUM (Figure 28). The transition from convex-shaped REE patterns in vein amphibole to LREE-depleted disseminated amphibole in vein wall rock has been clearly documented (Vaselli *et al.*, 1995; Zanetti *et al.*, 1996). K-richterites from MARID xenoliths are characteristically LREE-enriched with convex patterns (Gregoire *et al.*, 2002; Figure 28). In contrast to amphibole from xenoliths, disseminated amphibole from massif peridotites is almost exclusively LREE depleted (Vannucci *et al.*, 1995; Zanetti *et al.*, 1996), possibly reflecting more extensive equilibration with other phases. Most xenolith-derived amphibole has Sm/Nd < PUM (Figure 25) and hence, with time, will develop unradiogenic neodymium isotopic signatures with respect to PUM. However, a large proportion of disseminated amphibole has Sm/Nd close to, or above PUM. Hence, the presence of amphibole in a peridotite is no guarantee of the generation of "enriched" neodymium isotopic signatures with time.

Vein amphiboles are generally richer in TiO_2 than disseminated varieties, with Ti/Zr close to the PUM value (112) or above (Figure 23). LREE-enriched disseminated amphiboles from the W. Eifel peridotite xenoliths are low in TiO_2 (<1%) and have lower Ti/Zr than PUM (Witt-Eickschen and Harte, 1994). Multielement patterns are characterized by positive titanium and niobium anomalies (Figure 28). Amphibole has high but variable levels of both zirconium and niobium compared to pyroxenes and garnets. Niobium values vary from <1 ppm to 270 ppm (mean ~ 25 ppm) and zirconium varies from <1 ppm to 300 ppm (mean ~ 45 ppm). Zr/Nb is lower than clinopyroxene and generally significantly less than PUM for most amphiboles. This is largely a function of the high niobium contents of amphiboles and means that bulk rock Zr/Nb will be lower than PUM for amphibole-rich samples. Consequently, melts of amphibole-peridotite should have low Zr/Nb.

Amphibole HFSE characteristics are sensitive to the presence of ilmenite and rutile. In MARID samples where rutile dominates over ilmenite, Gregoire *et al.* (2002) note that K-richterites display large negative niobium and tantalum anomalies, whereas when ilmenite dominates, these anomalies are positive. Nb/Ta ratios of amphibole vary from close to the PUM value (17.6) up to ~25 (Figure 23). Zr/Hf values are generally lower than the PUM value of 37 (Figure 23). Differences in HFSE contents between vein and disseminated amphibole (and mica) in spinel peridotites may be explained by a model in which Zr–Nb rich amphibole and mica crystallize close to, or within a melt vein in the mantle. The fractionated, chlorine-rich aqueous residual fluids from the evolved melt then crystallize low Zr–Nb, LREE-depleted amphibole or

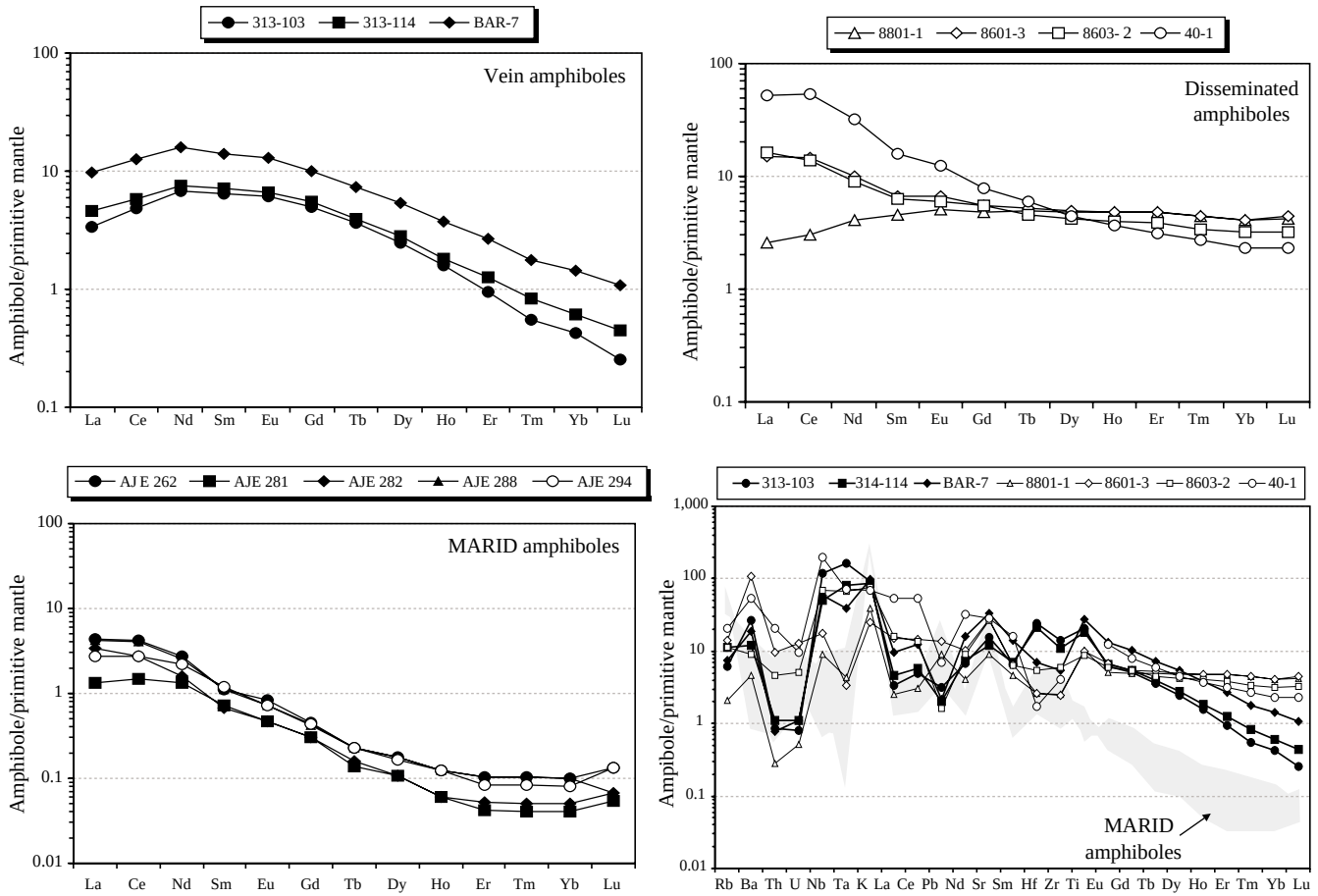

Figure 28 Primitive mantle normalized REE and multi-element patterns for amphiboles from mantle xenoliths. Vein amphibole and disseminated amphibole data from off-craton spinel lherzolite xenoliths (Ionov and Hofmann, 1995; Ionov *et al.*, 1997). MARID amphibole data from Gregoire *et al.* (2002).

mica at a distance from the feeder, as disseminated metasomatic phases within peridotite (Ionov *et al.*, 1997). The residual chlorine-rich fluids are effective at transporting LILE and so disseminated mica crystallising away from the vein in this model is barium and lead rich.

Amphibole in spinel peridotites can have similar zirconium and hafnium contents to clinopyroxene. Lu/Hf ratios span the range of clinopyroxene and can be greater or less than PUM (Figure 26). In the absence of more exotic phases (see below), amphibole and mica dominate the niobium, tantalum, and titanium budget of peridotites (Ionov *et al.*, 1997). To this extent, Pearson and Nowell (2002), have pointed out that any hydrous peridotite proposed as a source for flood basalt volcanism is unlikely to yield melts with the negative HFSE anomalies measured in flood basalts (e.g., Thompson *et al.*, 1983). Amphibole has lead contents in the upper range, to well in excess of those commonly measured in clinopyroxenes (Figure 29), with only mica, of the silicate phases, containing more lead. U/Pb ratios are predominantly greater than PUM but clinopyroxene commonly has a higher U/Pb ratio. Lithium and boron in amphibole are commonly around 1 ppm and thus significantly lower than the levels observed in phlogopite (Table 9; Glaser *et al.*, 1999).

In summary, amphibole, along with mica, is the dominant silicate host for niobium in peridotitic xenoliths. In mica-absent assemblages amphihole also dominates the barium and tantalum budgets (Ionov *et al.*, 1997; Eggins *et al.*, 1998) and its presence strongly affects the bulk rock Zr/Nb ratio.

Mica. Mica, usually phlogopite, is the dominant host for rubidium and barium in the mantle but has highly variable Rb/Sr (0.13–60) and Ba/Sr ratios (Ionov *et al.*, 1997). As with amphibole, the geochemistry of mantle mica varies with texture and hence probably proximity to melt veins (Ionov *et al.*, 1997). Rb contents of micas in peridotites vary from 10 ppm to ~800 ppm. Strontium contents vary from ~1 ppm to almost 1,000 ppm and this variation creates highly variable Rb/Sr that is significantly higher than PUM in most cases (Figure 27). Phlogopites from cratonic type VI and VIII xenoliths, e.g., MARIDs, are exceptionally rubidium-rich compared those found in noncratonic xenoliths (Table 9). Ba contents are very variable and are probably related to the nature of the parental fluid and its evolution away from silicate melt veins. Micas from noncratonic peridotite xenoliths have been reported with 0.5–10 wt.% BaO (Ionov *et al.*, 1997). MARID micas are relatively barium poor, with 300–700 ppm. Along with amphibole, mica dominates the niobium and tantalum budget of silicate-hosted trace elements. Nb/Ta can be close to PUM but shows some scatter (Figure 23) that could be partly related to analytical problems at low tantalum levels. As expected, Ti/Zr is higher than clinopyroxene and largely overlaps the amphibole range, but at lower zirconium contents. As with amphibole, Zr/Nb is low, from a combination of relatively low zirconium and high niobium. Niobium levels are comparable with amphibole. Zr/Hf scatters around PUM values. Mica hafnium levels are lower than amphibole and clinopyroxene (<1 ppm). Lu/Hf ranges widely because of wide variations in both elements (Figure 26). Some of the scatter could be analytical.

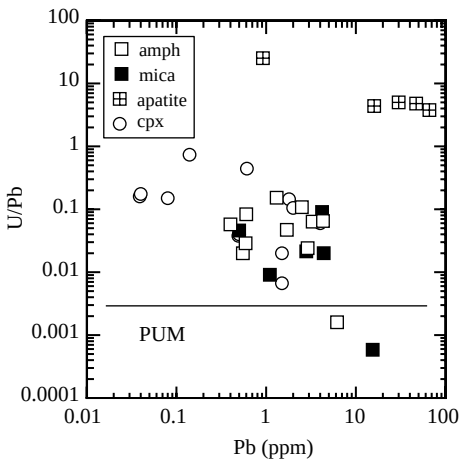

Figure 29 Covariation of U/Pb versus Pb for mantle xenolith minerals. Primitive mantle (PUM) line for U/Pb marked. Data sources as in Figure 23.

Mica from mantle xenoliths is very poor in REE, especially LREE (Table 9). Where reported, Sm/Nd values vary widely both above and below the PUM values (Figure 25); however, the low levels present could be easily influenced by small inclusions or analytical artifacts. Neodymium levels are so low that even the presence of tens of percent mica in a peridotite mineralogy do not significantly influence the neodymium budget of the rock. As such, the presence of mica in a peridotite is not sufficient to generate LREE enrichment and hence its presence alone, is unlikely to cause a bulk peridotite to evolve to "enriched" neodymium isotopic compositions (Pearson and Nowell, 2002).

LREE enrichment relative to PUM in whole-rock peridotites is more likely to be a product of grain-boundary enrichment or clinopyroxenes becoming LREE enriched. Micas are poor in thorium and uranium but high in lead compared to clinopyroxene so that U/Pb is low. Some micas can have up to 20 ppm lead and Rosenbaum (1993) proposes that they are the main mantle lead repository. More recent data have shown that amphiboles can have comparably high lead (Table 9).

Of the volatile-rich minerals, mica has the highest affinity for the light elements lithium and

boron, being 3–5 times more enriched than amphibole or pyroxenes (Table 9; Glaser *et al.*, 1999) and hence will affect the light element budget of any peridotite. However, the large modal abundance of olivine together with its moderately high lithium content means that olivine will dominate the budget overall.

Apatite. Apatite is relatively common in noncratonic continental and oceanic peridotite xenoliths (Menzies and Wass, 1983; Ionov *et al.*, 1997). Most apatites are chlorine-rich (2–4.3%) with low F/Cl (0.1–0.3). High fluorine (~5%) and low chlorine (~0.25%) have been reported for apatite in spinel lherzolites from Pacific OIB (Hauri *et al.*, 1993). Extremely high strontium contents, commonly $>2 \times 10^4$ ppm and up to 7 wt.% (Ionov *et al.*, 1997; Table 9) are common in mantle apatites meaning that this phase is a major repository for strontium when present in peridotites at abundances of 0.1% or above. Rb/Sr is very low. Apatites have high levels of REE and are LREE-enriched (Table 9). Lanthanum and cerium concentrations can reach >1 wt.% and neodymium concentrations can be above 1,000 ppm. Sm/Nd is below PUM. HFSE are low and so the presence of this phase does not affect bulk rock HFSE chemistry.

Thorium and uranium contents of apatite vary widely but are normally very high compared to other mantle phases (generally >10 ppm; Table 9; Ionov *et al.*, 1997). Apatites in MARID xenoliths tend to have lower uranium (Kramers *et al.*, 1983), possibly due to uranium partitioning into rutile or zircon. Lead contents are the highest reported for the "common" mantle minerals but U/Pb is generally >> PUM.

Zircon, monazite, rutile, ilmenite, and titanate. Zircons in upper mantle xenoliths have been reported in MARID and PKP xenoliths and glimmerites (Kinny and Dawson, 1992; Konzett *et al.*, 1998; Hamilton *et al.*, 1998; Rudnick *et al.*, 1999). In contrast to rutile, its high blocking temperature and low common Pb have made zircon attractive for U–Pb dating of MARID assemblages. Zircon seems to be found associated with metasomatism characterized by the precipitation of phlogopite and phases such as ilmenite, rutile, monazite, and apatite (Rudnick *et al.*, 1999). Trace-element data are limited but it is apparent that PKP and MARID zircons have higher thorium and uranium contents than zircon megacrysts found in kimberlite (Konzett *et al.*, 1998). Zircons from glimmerites have higher U/Th than zircons from MARID/PKP xenoliths. Recent studies link both the geochemistry and geochronology of MARID xenoliths to the crystallization products of group II kimberlites in the lithospheric mantle (Hamilton *et al.*, 1998; Konzett *et al.*, 2000; Gregoire *et al.*, 2002). Monazite has been reported from metasomatized mantle xenoliths and is also useful for U–Pb geochronology (Rudnick *et al.*, 1993; Carlson and Irving, 1994).

Macrocrystalline rutile is a rare phase in peridotite xenoliths (Haggerty, 1987) but is an essential constituent of MARID xenoliths (Dawson and Smith, 1977). As such, the only published trace-element data for rutiles is from MARIDs (Gregoire *et al.*, 2002; Table 9). In addition to containing substantial vanadium (>1,000 ppm), the other two main elements hosted by rutile are zirconium and niobium, both of which occur at the 1,000 ppm level; Figure 23. In addition, elevated levels of hafnium and tantalum are present. Thus, rutile exerts a huge influence on the HFSE budget of peridotites. Rutile Nb/Ta ratios (~22) are slightly more elevated than PUM (17.6). Lu/Hf values are extremely low (<0.001) such that the mineral should be of great utility in tracing mantle initial hafnium isotope compositions. The potential for U–Pb geochronology using rutile has been hampered in mantle settings by the low closure temperature of the U–Pb system in rutile and its high common (nonradiogenic) lead content. Microcrystalline rutile, plus loveringite and armalcolite, are increasingly found as very finely disseminated phases, sometime coating spinels, in noncratonic lherzolites. These phases are major hosts for niobium and tantalum when compared to silicates (Bodinier *et al.*, 1996; Bedini and Bodinier, 1999; Kalfoun *et al.*, 2002) and have variable Nb/Ta (11–37). Despite high ZrO_2 contents (up to 7 wt.%), in most instances, rutiles do not dominate bulk rock zirconium contents because of the zirconium-rich nature of modally abundant clinopyroxene (Kalfoun *et al.*, 2002).

Ilmenite is a widespread titanium-rich oxide phase in mantle xenoliths, occurring in both metasomatized peridotites, pyroxenites, MARIDs and eclogites in cratonic and noncratonic suites. As with rutile, ilmenite is a HFSE-rich phase and its low Lu/Hf ratio (Figure 26) makes it attractive for determining initial hafnium isotope ratios and for controlling/defining the low Lu/Hf region of Lu–Hf isochrons (Nowell *et al.*, in press). Nb/Ta in ilmenites varies. Those from MARID rocks can be considerably greater than PUM (32; Gregoire *et al.*, 2002; Table 9), whereas megacryst ilmenite Nb/Ta may scatter either side of PUM values (Moore *et al.*, 1992).

Titanates are another group of oxide phases occurring in metasomatized peridotites and MARID assemblages (Jones *et al.*, 1982; Haggerty *et al.*, 1983; Haggerty, 1987). So far, these phases have not been recognized in noncratonic continental or oceanic xenoliths and hence are characteristic of kimberlite-related xenolith sampling. LIMA minerals are members

of the lindsleyite (barium-specific) and mathiasite (potassium-specific) series in the crichtonite (strontium-specific) group. As such these phases are hugely enriched in LILE and also HFSE (Table 9). For instance, ZrO_2 contents of up to 4 wt.% and LREE contents of 1–2 wt.% are common in mathiasite (Haggerty, 1989). Strontium concentrations are high (over 2 wt.%), with very low Rb/Sr. Niobium, tantalum, and hafnium are all highly abundant compared to silicate mantle minerals but Nb/Ta values (~15) are close to PUM. The large enrichments of strontium, neodymium, and hafnium in these minerals make them obvious targets for isotopic measurements. K–Ba titanates of the LIMA group are typical of metasomatic associations in cratonic xenoliths of type VI and VII (Table 1) and probably originate from kimberlite-like melts.

Carbonate. Increasing recognition of carbonate within noncratonic peridotite xenoliths in particular has lead to improved geochemical documentation of this phase in the mantle (Ionov, 1998; Lee *et al*., 2000; Ionov and Harmer, 2002). Of the incompatible elements, carbonate is most enriched in strontium (generally 1,000–5,000 ppm) and Rb/Sr is very low (Figure 30 and Table 9). HFSE are characteristically very low but Ionov and Harmer (2002) report unusual niobium values of ~100 × PUM in carbonates from Mongolian peridotites (Figure 30). U and Th contents are significantly higher than in silicate mantle phases (5–20 ppm) and lead is also generally elevated (10–30 ppm), reflecting the ease of substitution of Pb^{2+} for Ca^{2+}. REE contents are mostly low and not as LREE-enriched as carbonatites. The characteristics of carbonates from mantle xenoliths are similar to early-crystallized calcite phenocrysts in carbonatites (Ionov and Harmer, 2002) and led Ionov (1998), Lee *et al*. (2000) and Ionov and Harmer (2002) to conclude that carbonate grains and pockets in peridotites are crystal "cumulates" from carbonate-rich melts rather than quenched carbonatitic liquids.

2.05.2.7 Radiogenic Isotope Geochemistry

Radiogenic isotope studies of mantle xenoliths have been used to determine their age and to better constrain the origin of the various metasomatic events that have affected them. Extensive reviews on the subject have been published: Menzies (1990a); Menzies and Hawkesworth (1987); Pearson (1999a,b); and Pearson and Nowell (2002). The reader is referred to these works for a more detailed explanation of the isotope systematics.

2.05.2.7.1 Primary and secondary signatures

When ultramafic rocks were initially analyzed for strontium isotopes (Hurley *et al*., 1964; Roe, 1964; Stueber and Murthy, 1966; Lanphere, 1968) only whole rocks were analyzed. Such data led to numerous erroneous conclusions about the relationship between mantle samples and basalts due to the pervasive alteration suffered by many ultramafic rocks, enhancing the amount of radiogenic strontium present. Subsequent studies have shown that acid-washed mineral separates, particularly diopside and garnet, are the most reliable means of obtaining the primary, unaltered

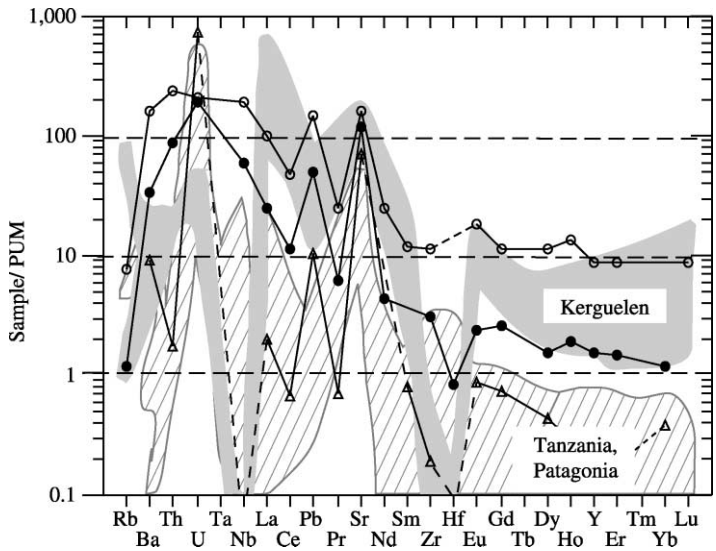

Figure 30 Primitive mantle normalized multielement patterns for carbonates from mantle xenoliths, modified from Ionov and Harmer (2002). Data shown as points are from Mongolia peridotite xenoliths, compared to carbonates in xenoliths from Kerguelen, Tanzania, and Patagonia. See Ionov (1998) and Ionov and Harmer (2002) for data sources.

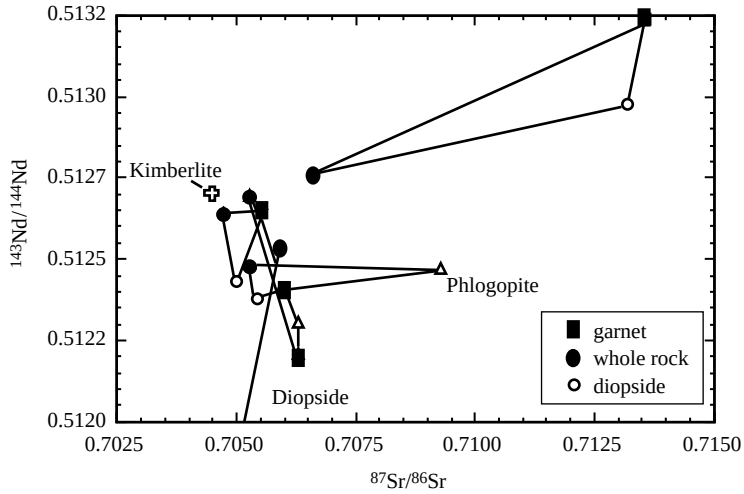

Figure 31 Whole-rock versus mineral separate Nd–Sr isotopic compositions for kimberlite derived xenoliths from Bultfontein (Richardson *et al.*, 1985) and one sample from Jagersfontein (Walker *et al.*, 1989a). Lines connect coexisting phases/whole-rocks. Initial isotopic composition of the Bultfontein kimberlite is also plotted. Jagersfontein cpx plots well off scale on Nd axis.

isotopic composition of mantle material (Bruekner, 1974; Basu and Murthy, 1977; Basu and Tatsumoto, 1980; Jagoutz *et al.*, 1980; Menzies and Murthy, 1980a,b; Richardson *et al.*, 1985; Zindler and Jagoutz, 1988). Even with apparently "clean" mineral separates from mantle rocks, detailed studies have shown that sequential acid leaching procedures are necessary for many minerals in order to obtain the primary (mantle) isotopic composition, unaffected by crustal contamination (Richardson *et al.*, 1985; Zindler and Jagoutz, 1988; Pearson *et al.*, 1993). In general, for isotopic analysis, mineral fragments are selected that are clear, as free of mineral and fluid inclusions as possible and that are bounded by fresh fractures induced by sample preparation, i.e., avoiding grains that retain their primary margins.

In cratonic xenoliths, both low-T secondary alteration and kimberlite contamination have been identified as major concerns to be addressed during the analysis of mineral separates (Richardson *et al.*, 1985). Acid washed mineral separates give considerably different Nd–Sr isotope compositions than their whole-rocks for both peridotites (Richardson *et al.*, 1985; Walker *et al.*, 1989a) and eclogites (Neal *et al.*, 1990; Figure 31), the isotopic signature of the whole-rocks is dominated by small amounts of infiltrated host kimberlite. The whole-rock isotopic signatures of some samples however, appear to be dominated by a component distinctly different to the host kimberlite. This component usually is characterized by much more radiogenic strontium isotopes and appears to be due to the effects of addition of phlogopite mica, which may not be related to the host kimberlite (Figure 31). Also, the nature of kimberlite/xenolith alteration often

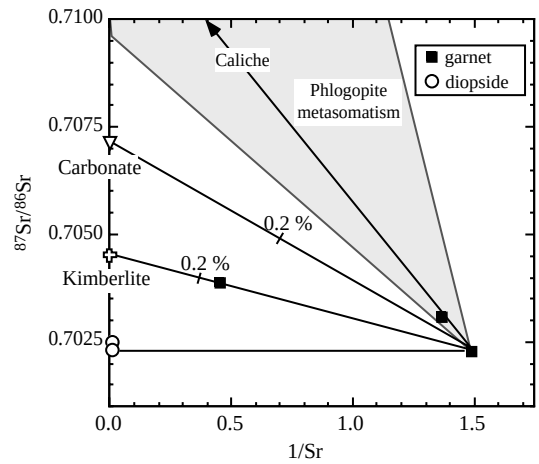

Figure 32 Strontium isotope and abundance systematics of "pure" and altered/metasomatized garnet and diopside separates from the Bultfontein kimberlite (after Richardson *et al.*, 1985). Shaded region indicates the area defined by phlogopite addition. Tick marks on mixing lines illustrate % of component added.

produces almost undetectable films of high-strontium material on mineral grain-boundaries and fractures. This can dramatically affect the measured strontium isotope composition of a low-strontium mineral such as garnet if not properly removed (Figure 32).

Because of the numerous secondary effects that modify the whole-rock elemental and isotopic compositions, our discussion below will focus solely on mineral-separate analyses for the Rb–Sr, Sm–Nd, Lu–Hf, and U–Pb isotope systems. In comparison, the Re–Os system is much more robust to the effects of

alteration than the highly incompatible-element-based isotope systems and less affected by invasion of the host rock. For instance, ingress of between 0.5% and 1.5% kimberlite to a host xenolith, as suggested by Schmidberger *et al.* (2001) on the basis of incompatible elements, changes the $^{187}Os/^{188}Os$ ratio of a late Archean peridotite by 0.15%, an insignificant amount. In contrast, the neodymium isotope systematics would be drastically altered because the kimberlite might contribute 70% of the measured whole-rock neodymium (Figure 15). Despite its relatively robust nature, mantle metasomatic events do affect the Re–Os isotope system in mantle xenoliths, just as they do the other radiogenic isotope systems. This will be outlined below.

2.05.2.7.2 Mineral isotope equilibria and parent–daughter fractionation

Peridotites that are residues from melt extraction, i.e., the majority of mantle xenolith peridotites, should contain pyroxenes and garnets that have LREE-depleted compositions such that their low Rb/Sr and high Sm/Nd relative to PUM should plot in the "depleted" field of Figure 33. Clearly, only a small proportion of peridotite xenolith minerals still reflect this depleted history because of either metasomatism, or because some minerals, e.g., certain diopsides in kimberlite-derived xenoliths, have crystallized from melts passing through the peridotite following initial depletion (Shimizu *et al.*, 1997; Shimizu, 1999; Simon *et al.*, 2003). This relationship is also true for the Lu/Hf isotope system where garnets can have either high Lu/Hf, characteristic of melt depletion or low Lu/Hf, indicative of a more complex history (Figure 26). Furthermore, although the minerals within some noncratonic peridotite xenoliths show inter-mineral equilibrium trace-element partitioning relationships (Figure 22), this is not the case for most cratonic peridotites (Shimizu *et al.*, 1997; Shimizu, 1999; Simon *et al.*, 2003).

A consequence of this varied elemental partitioning and hence parent–daughter isotope fractionation, is that the extent to which isotopic equilibria is achieved by xenoliths is also very variable, despite the high equilibration temperatures of mantle rocks. This indicates that many of the processes that affect the incompatible element isotope systematics in mantle xenoliths are of a relatively recent nature compared to the age of the rock. Hence, it is difficult to simply use the measured parent/daughter element ratios of xenoliths and their minerals to predict what their measured isotopic compositions should be.

One of the first studies to show this was performed on Kilbourne Hole spinel lherzolites (Jagoutz *et al.*, 1980). Equilibrated neodymium isotopes in orthopyroxene and diopside defined essentially zero age isochrons, consistent with the very recent eruption age of the host volcanic rocks, while strontium isotopes were un-equilibrated. Stolz and Davies (1988) found varying degrees of equilibration between amphibole, clinopyroxene and apatite in peridotite xenoliths from S.E. Australia. Several samples contained coexisting amphibole and clinopyroxene and had almost reached isotopic equilibrium for strontium but displayed disequilibrium relations for lead and neodymium isotopes. This was taken to indicate more rapid diffusion of strontium than lead and neodymium. Some peridotite and eclogite

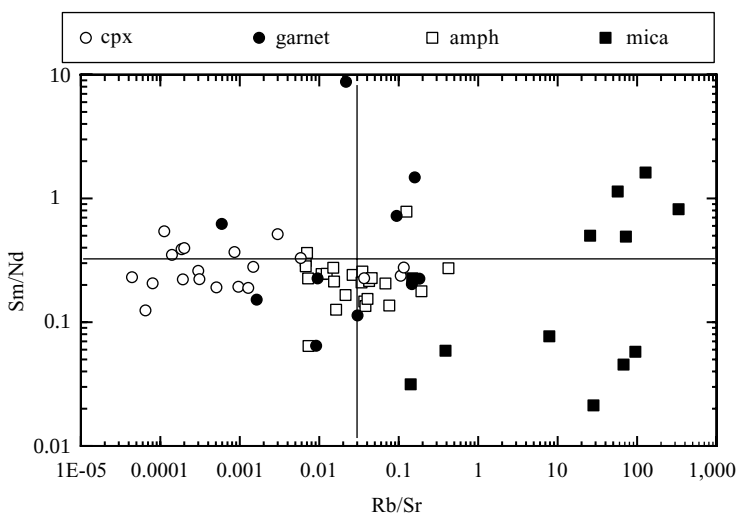

Figure 33 Sm/Nd versus Rb/Sr plot of minerals from mantle xenoliths. Data sources as for Figure 23 and Table 9. Lines denote primitive mantle values.

samples have resided in the mantle at sufficient temperature to equilibrate neodymium isotopes so that the difference in isotopic compositions measured today purely reflects radiogenic decay since eruption (Richardson *et al.*, 1985; Walker *et al.*, 1989; Snyder *et al.*, 1993; Pearson *et al.*, 1995a,b). For instance, Pearson *et al.* (1995b) obtained a relatively precise 1,150 ± 41 Myr (2σ) clinopyroxene–orthopyroxene–garnet Sm–Nd isochron for a garnet peridotite xenolith from the Proterozoic Premier kimberlite (Figure 34). The equilibration temperature of this xenolith is below 800 °C and the close agreement of the isochron with the eruption age of the Premier kimberlite suggests that the peridotite was above the blocking temperature of the Sm–Nd system in these minerals. Despite the apparent inter-mineral isotopic equilibria, mineral REE studies of the same sample by Shimizu (1999) suggests that they were not in elemental equilibrium and had been disturbed just prior to eruption.

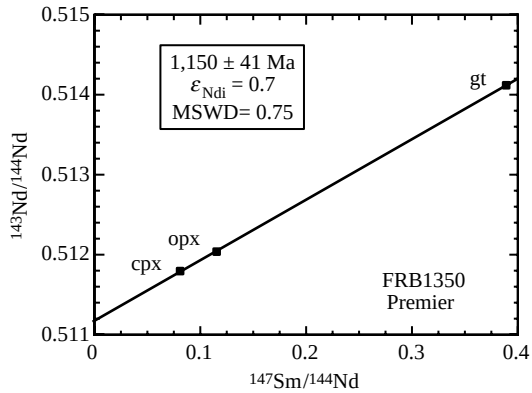

Figure 34 Sm–Nd garnet–orthopyroxene–clinopyroxene mineral isochron for a cratonic garnet lherzolite from Premier, S. Africa. Errors are 2σ (source Pearson *et al.*, 1995b).

More ancient mineral isochrons, significantly in excess of eruption ages, have been determined for diopside-garnet pairs in cratonic peridotites (Gunther and Jagoutz, 1997; McCulloch, 1989; Pearson *et al.*, 1995a,c; Zhuravlev *et al.*, 1991) and eclogites (Jacob *et al.*, 1994; Jagoutz, 1988; Jagoutz *et al.*, 1984). Two-point peridotite mineral isochrons from a single kimberlite pipe can vary widely in slope, giving apparent ages hundreds of Myr different (Figure 35). The geochronological information provided by these isochrons is unclear. The wide variations in xenolith isochron ages from a single kimberlite are unlikely to represent closure ages (Pearson *et al.*, 1995a). Contamination by the host kimberlite can alter peridotite mineral isochrons and this can usually be identified. Gunther and Jagoutz (1997) proposed that the oldest mineral isochrons in Siberian peridotites, of ~2 Ga, represent closure ages. Younger ages represent partial closure/re-equilibration during either lithospheric residence or during eruption.

In situ trace-element measurements of minerals from some of these peridotites provide a different perspective. The frequent presence of both fine-scale (100 μm) zonation and nonequilibrium partitioning behavior for REE between many garnets and clinopyroxenes from Siberian peridotites (Shimizu *et al.*, 1997; Shimizu, 1999) has two possible implications. One is the probable recent

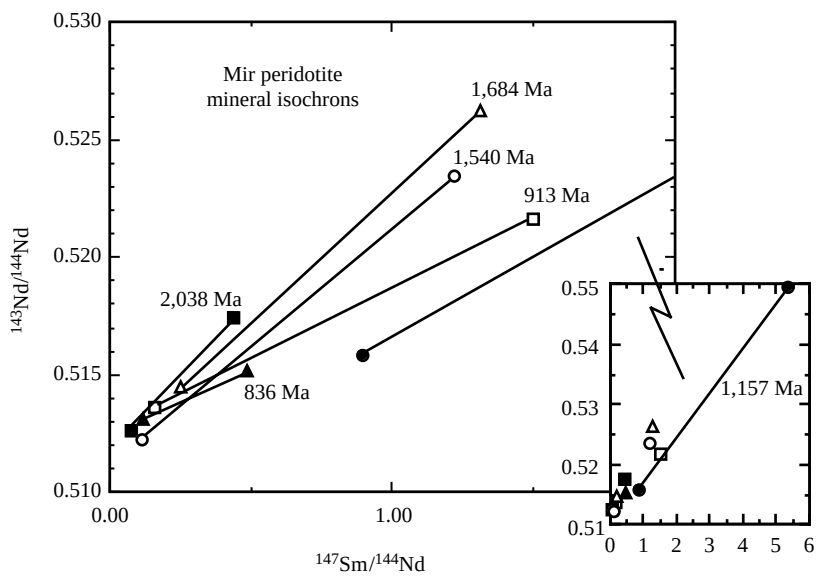

Figure 35 Garnet-diopside Sm–Nd mineral isochrons for peridotites from the Mir kimberlite pipe, Siberia. Ages relating to the slope of each line are given (after Pearson, 1999b).

disruption of isotope systematics in many peridotite minerals due to recent mineral growth. Secondly, in numerous cases it is likely that diopside and garnet have not coexisted long enough to have even partly equilibrated in terms of trace elements and isotopes. A good example of the type of isotopic complexity that this can lead to is shown by reversed mineral "isochrons" in some cratonic peridotites (Figure 36). The Sm–Nd isotope systematics of garnet–orthopyroxene–clinopyroxene clusters in Kimberley peridotites show distinctly more radiogenic neodymium for both clino- and orthopyroxenes compared to the garnet, despite much higher Sm/Nd of the garnet (Figure 36). This feature has been observed in other Kaapvaal low-*T* peridotites and suggests recent garnet growth from a LREE enriched precursor (Gunther and Jagoutz, 1994) and/or that the clinopyroxene has been newly introduced. Hence, without detailed petrography and mineral elemental chemistry it is unwise to interpret cooling age information from two-point mineral isochrons in mantle rocks.

Carlson and Irving (1994) found correlated Sm–Nd systematics in minerals from Wyoming peridotites that scatter around a 1.8 Ga reference isochron. The neodymium in these cratonic samples is consistently very unradiogenic compared to primitive upper mantle, with an initial ε_{Nd} of −9, indicative of an ancient metasomatic prehistory. The Sm–Nd isochron age agrees well with U–Th–Pb ages for zircon and monazite metasomatic phases in the Wyoming peridotite suite and must clearly reflect the time of a major, regional metasomatic enrichment event in the lithosphere (Carlson and Irving, 1994). This study and others make a clear case for multiple enrichment events following the initial depletion of peridotitic lithosphere sampled by xenoliths (e.g., Pearson *et al.*, 1995a; Pearson, 1999b).

2.05.2.7.3 Rb–Sr, Sm–Nd, Lu–Hf, U–Pb, and Re–Os isotopic signatures

Major-element compositions of most lithospheric peridotites reflect an origin as melt-residues. However, as with parent–daughter isotope ratios, compilation of their strontium and neodymium mineral isotopic compositions reveals that very few samples show the characteristics of ancient melt residues (Figure 37). Osmium isotopes are the exception and dominantly reflect ancient extraction of high Re/Os melts, leaving rhenium-depleted residues to develop time integrated low $^{187}Os/^{188}Os$. The huge isotopic diversity shown by peridotite Nd–Sr isotope systematics (Figure 38) is a reflection of the diverse parent–daughter elemental fractionation shown by mantle silicate minerals coupled with ancient, multiple-stage histories involving melt depletion and subsequent interaction with melts passing through the lithospheric mantle.

Peridotite xenoliths from continental regions show substantial overlap with oceanic mantle for isotopic compositions of lithophile elements such as strontium and neodymium (Menzies, 1990a; Pearson, 1999b; Figure 37). The frequency distribution for neodymium isotopes in peridotite xenoliths that represent the continental lithospheric mantle (CLM) ranges from highly radiogenic compositions (relatively high values of $^{143}Nd/^{144}Nd$; high ε_{Nd}), indicative of long-term parent–daughter depletion, to highly enriched compositions (relatively low values of

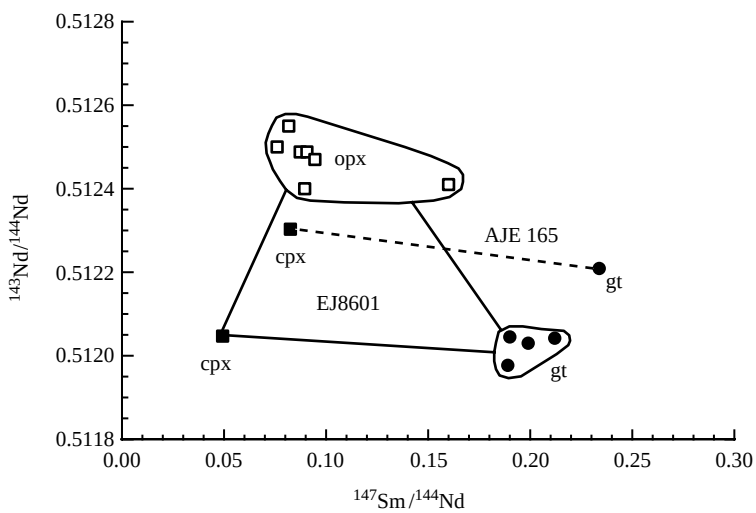

Figure 36 Sm–Nd isotope systematics of minerals from Kimberley peridotites. Data for AJE165 from Richardson *et al.* (1985), and for EJ8601 from Gunther and Jagoutz (1994).

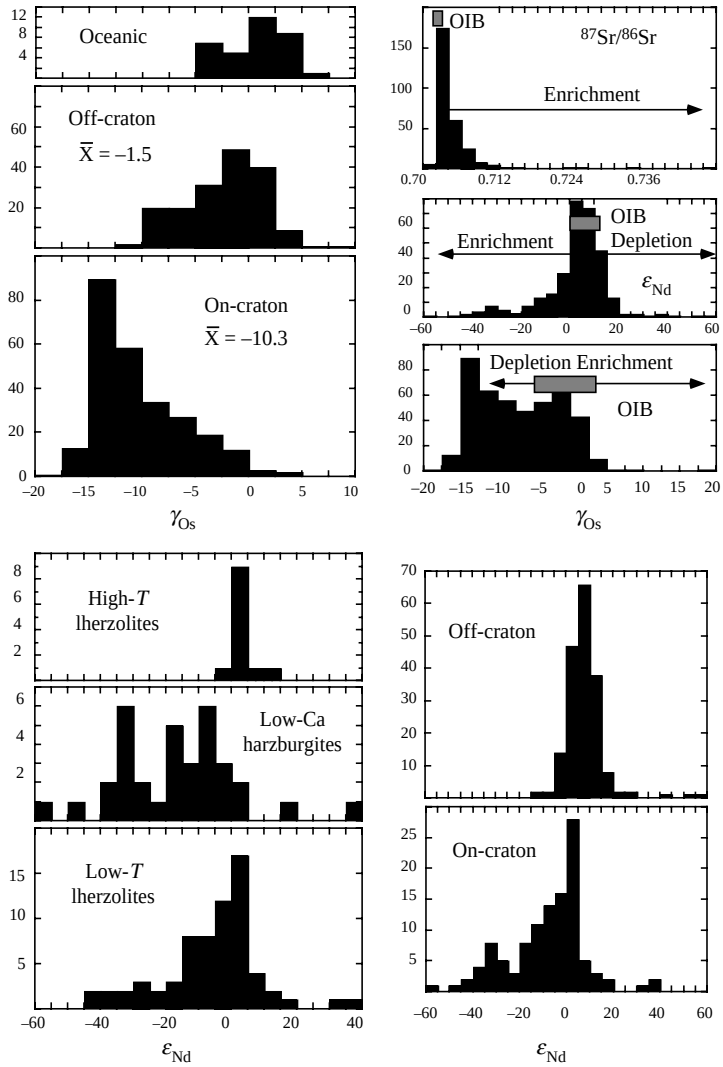

Figure 37 Frequency distribution plots for Os, Nd, and Sr isotope compositions of cratonic and noncratonic peridotite xenoliths. Upper right plots give the range for ocean island basalts (OIB) and arrows show the direction of isotopic evolution for melt depletion and enrichment events. Data compiled from sources cited in Menzies (1990b), Pearson (1999a,b), and those given in Figure 21 (after Pearson and Nowell, 2002).

$^{143}Nd/^{144}Nd$; low ε_{Nd}) that require ancient parent–daughter enrichment. Despite this wide spread in neodymium isotopic compositions, the remarkable aspect of the frequency distribution for CLM as a whole is that the pronounced mode is within 5ε units of bulk Earth and the mean ε_{Nd} value is 1.8. On this basis, the dominant neodymium isotopic characteristic of CLM is not "enriched" but is close to, or slightly more depleted than bulk Earth. Of course, if Depleted Mantle is used as a reference point then the CLM mode is "enriched." The strontium isotope frequency distribution has a long tail out to very radiogenic ("enriched") compositions but the mean $^{87}Sr/^{86}Sr$ is 0.7047; very close to estimates of bulk Earth. It is important to bear in mind that this statistical view of CLM geochemistry could be heavily influenced by samples that have geochemical signatures dominated by their host magmas; i.e., the xenolith sample set could be very biased and the real CLM composition grossly different.

If continental peridotite xenoliths are divided into cratonic and noncratonic compositions, the vast majority of highly enriched neodymium isotope compositions originate in cratonic mantle and very few are evident in noncratonic mantle. Enriched neodymium isotope compositions can also be found in mantle sampled by orogenic peridotites (Reisberg and Zindler, 1986; Pearson *et al.*, 1993; Chapter 2.04) but not the extreme values evident in cratonic CLM. This is expected, given the great antiquity of cratonic CLM. Further subdivision of cratonic samples (Figure 37) shows

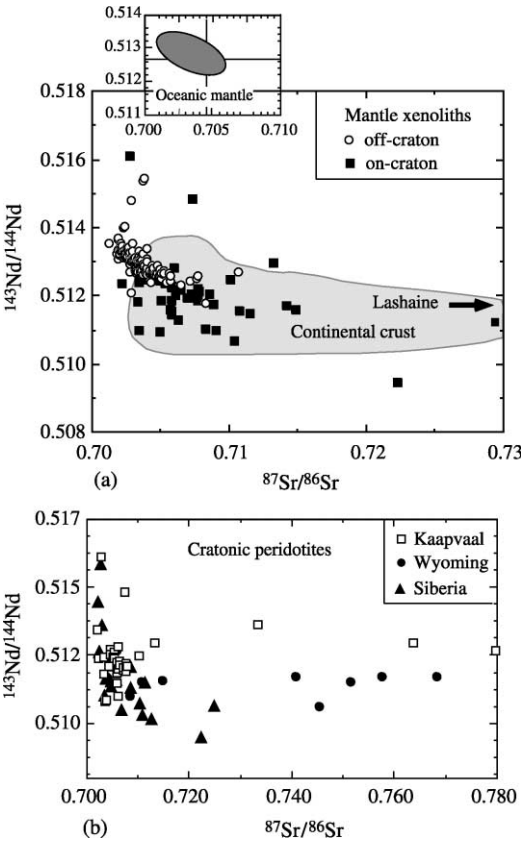

Figure 38 Nd–Sr isotope variation of clinopyroxenes and garnet in peridotite xenoliths. (a) Compares cratonic and noncratonic peridotite xenoliths with continental crust. Inset shows restricted field for oceanic mantle. Arrow points to a peridotite from Lashaine, Tanzania, that lies at an $^{87}Sr/^{86}Sr$ value of 0.83. (b) Compares cratonic peridotites from the Kaapvaal, Wyoming, and Siberian cratons.

that garnets from the low-calcium harzburgite subgroup of type I xenoliths have the most extreme neodymium isotopic variations (Pearson *et al.*, 1995c; Jacob *et al.*, 1998a), whereas the mode for typical low-temperature cratonic lherzolites (type I) is close to bulk Earth and the distribution more restricted. The more tightly clustered lherzolite distribution is probably influenced by the recent formation of diopside, from the host magma, in many of these rocks. Jacob *et al.* (1998a) have shown that low-calcium garnets from an individual kimberlite (Udachnaya) are extremely heterogeneous in their Nd–Sr isotope compositions on a single grain basis, with a range in initial ε_{Nd} of 42 units between grains. The total range for low-calcium garnets, as composites (Pearson *et al.*, 1995a) or single grains from the Udachnaya kimberlite alone is over 60ε units for neodymium, i.e., ~3 times the range found in the convecting mantle, emphasizing the extreme isotopic heterogeneity shown by CLM xenoliths.

Some intracratonic distinctions can be made on the basis of Sr–Nd isotope systematics that reflect differing extents and styles of lithospheric enrichment processes. Peridotites from the Kaapvaal and Wyoming lithospheric roots have strontium isotope compositions that range up to very radiogenic compositions. Probably the most extreme strontium isotope composition of a mantle rock to date comes from a clinopyroxene from a Tanzanian peridotite ($^{87}Sr/^{86}Sr = 0.836$; Cohen *et al.*, 1984), but an insufficient number of Tanzanian samples have been analyzed to make comparisons meaningful. Most of these extreme strontium isotope compositions measured for clinopyroxene and garnet are un-supported by the very low Rb/Sr of these phases (Figure 27). This may indicate that the garnet and/or clinopyroxenes formed from a high Rb/Sr precursor that had sufficient time to evolve radiogenic strontium. The garnet and pyroxene inherited the strontium isotope composition of the precursor but excluded Rb from their lattice. Rubidium-rich phlogopite is a possible candidate to form part of the precursor assemblage. Alternatively, radiogenic strontium could be inherited during H_2O-rich fluid metasomatism via some unspecified mechanism.

In contrast to the Kaapvaal and Wyoming cratons, minerals within Siberian peridotites rarely have $^{87}Sr/^{86}Sr$ over 0.720, with most below 0.710. This possibly correlates with a general paucity of phlogopite in Siberian peridotites (Boyd *et al.*, 1997), indicating that hydrous-fluid-dominated metasomatism has not been as extensive in the Siberian lithosphere. The range in ε_{Nd} for Siberian peridotites is comparable to that of Kaapvaal peridotites (Figure 38(b)), reflecting both ancient LREE depletion and enrichment. Development of very unradiogenic neodymium isotope compositions, relative to bulk Earth, while retaining relatively moderate/low enrichment of $^{87}Sr/^{86}Sr$ is also a characteristic of peridotite and pyroxenite–glimmerite xenoliths from Loch Roag, Scotland, erupted at the margin of the N. Atlantic craton (Menzies and Halliday, 1988). LREE enrichment without marked increase of Rb/Sr is thought to be a characteristic of carbonatite metasomatism, and appears to be a clearly identifiable signature in xenoliths from various cratons, though usually via elemental geochemistry (see Sections 2.05.2.5 and 2.05.2.6).

Xenoliths from the Wyoming craton have consistently very low ε_{Nd} coupled with radiogenic strontium. This radiogenic strontium signature is largely a reflection of the preponderance of mica-peridotites, mica pyroxenites and glimmerites in the xenolith suite analyzed compared to the lherzolite–harzburgite lithologies that dominate xenolith suites from Kaapvaal and Siberia. The radiogenic strontium isotopic signature has been interpreted as the result of shallow

slab-derived fluid fluxing during the Archean, soon after formation of the protoliths (Carlson and Irving, 1994).

From the diversity of observed isotopic compositions a number of different metasomatic agents have been inferred, that are thought to produce shifts of Nd–Sr isotope systematics in distinct directions. The three main enrichment processes thought to affect the lithospheric mantle, identifiable from petrographic evidence are silicate melt addition, H_2O-fluid-rich metasomatism, which may result in phlogopite/amphibole metasomatism and may ultimately be linked to silicate melt intrusion (Ionov *et al.*, 1997), and carbonatite metasomatism. These processes operate to different extents in differing tectonic environments and leave a multitude of effects. The reader is referred to Menzies and Hawkesworth (1987) and Menzies and Chazot (1995) for reviews. Recently, Ionov *et al.* (2002a,b) have noted that chromatographic effects related to porous flow during melt percolation can decouple strontium from neodymium isotopes in peridotite xenoliths, creating enrichment in $^{87}Sr/^{86}Sr$ at relatively constant neodymium isotope composition. These authors note that the frequently observed decoupling of strontium from neodymium isotopes, which is often attributed to metasomatism by subduction-related fluids, can be a signature only of silicate melt percolation without the need for subduction zone fluids. Hence, as with trace-element signatures, it may be dangerous to identify the nature of a metasomatic agent solely on isotopic criteria. Coupled petrographic, mineral chemical, elemental and isotopic studies are required to fully understand these processes.

The high-temperature peridotites that appear to occupy the basal portions of CLM, either as a layer (Nixon and Boyd, 1973a), or as local zones surrounding magma intrusions (Gurney and Harte, 1980), have very restricted neodymium isotopic compositions, with a pronounced mode within 1 epsilon unit of bulk Earth. The higher equilibration *P*/*T*'s determined for high-temperature peridotites indicate that they occupy the lowermost lithospheric mantle. It is clear that this region has neodymium isotope compositions indistinguishable from bulk Earth (Figure 37) although the data set is small and data from other continents are needed. Strontium isotopic compositions in southern African and Siberian high-*T* peridotites are usually close to bulk Earth values (Richardson *et al.*, 1985; Walker *et al.*, 1989; Pearson *et al.*, 1995a,b) but clinopyroxenes from high-*T* peridotites at Somerset Island (Churchill Province, northern Canada) have more radiogenic strontium than the low-*T* peridotites (Schmidberger *et al.*, 2001). The generally more primitive Nd–Sr isotope systematics of the high-*T* peridotite suite indicates that their incompatible element isotope systematics have been recently influenced by melts infiltrating from the convecting mantle. This is in agreement with major and trace-element zonation studies. However, the age of the infiltrated protolith has been shown from osmium isotope studies to be much more ancient and probably part of the original Archean lithospheric mantle (Walker *et al.*, 1989; Pearson *et al.*, 1995a,b). A summary of the Sr–Nd–Os isotope characteristics of cratonic and off-craton continental xenoliths and their relation to major-element parameters and density is shown in Figure 39.

Four cratonic, ultradeep xenoliths from S. Africa and Sierra Leone have been analyzed for their strontium and neodymium isotopic compositions (Macdougall and Haggerty, 1999). The neodymium isotopic compositions of minerals from these xenoliths suggest that they were emplaced into the African lithosphere at times ranging from approximately the time of kimberlite eruption to hundreds of millions of years earlier. The samples show a complex history of melt

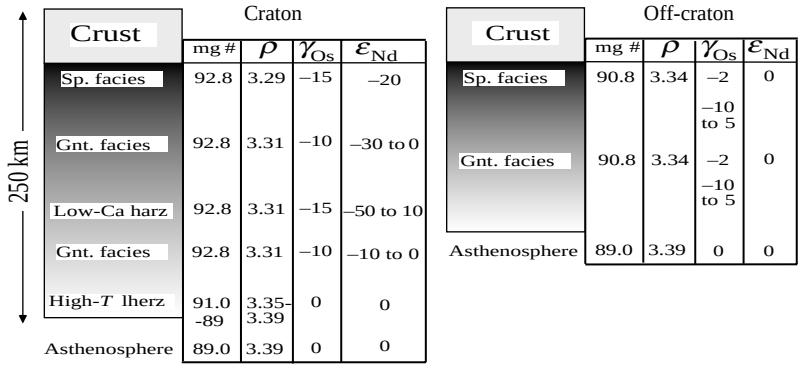

Figure 39 Cross-section of "typical" cratonic and noncratonic lithospheres as sampled by xenoliths showing the variation in olivine Mg#, density (ρ), Os and Nd isotope compositions with depth.

depletion and enrichment. Macdougall and Haggerty (1999) propose that the complex isotope systematics of these samples indicate a heterogeneous deep mantle. Detailed oxygen isotope work on these samples by Deines and Haggerty (2000) concluded that they experienced a series of metasomatic alterations, including an event a few million years before eruption of the host kimberlite. Because of the complicated history experienced by these xenoliths, further studies on additional samples are needed before we can be confident that the data are representative of the Transition zone and deeper.

Few systematic Sr–Nd isotope studies have been performed on ocean island xenolith suites. Ducea *et al.* (2002) analyzed clinopyroxenes from plagioclase-spinel and spinel peridotites from Pali, (Oahu, Hawaii) and found relatively depleted strontium and neodymium isotope systematics that they interpret as representing their evolution as residues from the extraction of Pacific Ocean crust. Consistent with this is a 61 ± 20 Ma errorchron defined by the pyroxene separates that is within error of the 80–85 Ma age of Pacific lithosphere beneath Hawaii.

Compared with neodymium and strontium, there are relatively few studies of the lead isotopic compositions of mantle xenoliths and the systematics are probably biased towards samples that show some degree of patent metasomatism in the form of introduction of amphibole and/or mica. Much of the data come from noncratonic metasomatized peridotites (e.g., Stolz and Davies, 1988) and cratonic MARID xenoliths. Some type I xenoliths that do not have patent metasomatism, from cratonic and noncratonic settings (Kramers, 1977; Galer and O'Nions, 1989; Walker *et al.*, 1989; Lee *et al.*, 1996) together with various pyroxenites and megacrysts have also been analyzed (Ben Othman *et al.*, 1990; Tatsumoto *et al.*, 1992). Only mineral data are considered. As with strontium and neodymium, lead isotopic compositions are extremely variable in mantle xenoliths (Figure 40). Peridotites and their metasomatized variants show most of the heterogeneity while pyroxenites and megacrysts have more constant compositions that relate closely to the host magmas and suggest a genetic link (Ben Othman *et al.*, 1990; Tatsumoto *et al.*, 1992). As expected from their greater antiquity, cratonic xenoliths show considerably more lead isotope variation than their noncratonic counterparts. Both suites define broad positive correlations on a $^{207}Pb/^{204}Pb$ versus $^{206}Pb/^{204}Pb$ diagram that are subparallel to the northern hemisphere reference line (NHRL) defined by Atlantic MORB, but displaced to higher $^{207}Pb/^{204}Pb$ except for two samples from the Cameroon line (Lee *et al.*, 1996). Almost all noncratonic peridotites plot to the right of the Geochron. A number of cratonic peridotites plot well to the left of this reference point, suggesting ancient U/Pb depletion. Cratonic samples also range up to very radiogenic $^{206}Pb/^{204}Pb$. Most noncratonic peridotites have $^{206}Pb/^{204}Pb < 19$ except several samples from the Cameroon Line (Lee *et al.*, 1996) that have HIMU characteristics (Figure 40). Apart from peridotites from the Cameroon Line, Pb–Sr isotope systematics are characterized by heterogeneity. The variability is such that the end-member mantle "components" HIMU, EMI and EMII (Zindler and Hart, 1986) are all strongly developed in some xenolith suites, with those from the Wyoming craton (Carlson and Irving, 1994) and Tanzania (Cohen *et al.*, 1984) showing particularly strong EMII-like characteristics of high $^{87}Sr/^{86}Sr$ at

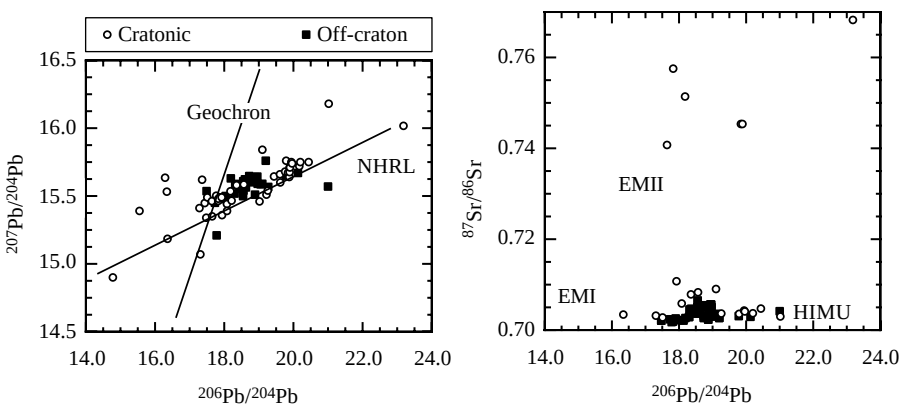

Figure 40 $^{207}Pb/^{204}Pb$ versus $^{206}Pb/^{204}Pb$ isotope plot and $^{87}Sr/^{86}Sr$ versus $^{206}Pb/^{204}Pb$ plot of cratonic and noncratonic peridotite xenoliths minerals. For cratonic peridotites, only clinopyroxenes are plotted. For noncratonic peridotites, amphibole or clinopyroxene are plotted. Metasomatic rocks such as MARIDs from cratons are not plotted. NHRL = Northern Hemisphere Reference Line, EMI = Enriched Mantle I hypothetical mantle component, EMII = Enriched Mantle II hypothetical mantle component and HIMU = the hypothetical mantle component with high time-integrated U/Pb proposed by Zindler and Hart (1986).

moderate $^{206}Pb/^{204}Pb$ (Figure 40). HIMU-type lead isotope characteristics seem to be restricted to cratonic peridotites despite the high measured U/Pb and Th/Pb of some noncratonic peridotites (Meijer *et al.*, 1990). This is further indication of the decoupling of parent–daughter ratios from isotopic compositions in xenoliths, probably due to recent processes. Many noncratonic peridotite xenoliths show well developed EMI and/or EMII characteristics (Tatsumoto *et al.*, 1992). Menzies (1990) has proposed detailed models of lithospheric chemical "domains" related to different times and styles of metasomatism, and suggests that a significant fraction of the lower lithosphere is of HIMU isotopic character.

Improved analytical capabilities have led to the analysis of several hundred xenoliths for osmium isotopic composition. The compatible nature of osmium during mantle melting means that, unlike incompatible-element-based isotope systems, peridotite residues have much higher osmium contents than mantle melts and thus the system is less readily disturbed by later metasomatism (see Section 2.05.2.5.3). This is clearly shown by rhenium and osmium abundances (Figure 21). The vast majority of rhenium contents of both cratonic and noncratonic peridotite xenoliths are below the PUM value proposed by Morgan *et al.* (1981) and many are P-PGE depleted. This contrasts with almost universal LREE enrichment of whole-rock peridotites. That the Re–Os system is not immune from the effects of metasomatism is illustrated by the consideration of extended PGE patterns (Figure 20; Section 2.05.2.5.3; Pearson *et al.*, 2002, 2004). Disruption of both rhenium and osmium in some mantle environments may have occurred (Chesley *et al.*, 1999), especially where sulfide metasomatism is involved (Alard *et al.*, 2000). However, Pearson *et al.* (2002, 2004) and Irvine *et al.* (2003) have shown that coupled PGE and Re–Os isotope analyses can effectively assess the level of osmium isotope disturbance in peridotite suites.

The compatible-element nature of osmium is illustrated by the correlation of osmium isotope composition with indices of melt depletion such as bulk rock Al_2O_3 (Figure 41). Numerous other melt depletion indices show equally good, or sometimes better correlations for a given suite. Meisel *et al.* (2001) use the upper intercept of $^{187}Os/^{188}Os$ at $Al_2O_3 = 4.23\%$ to estimate the primitive mantle osmium isotope composition and find good agreement between seven suites of peridotites (0.1296). More work is required to establish the extent to which these trends are disturbed by melt re-enrichment before accepting this method as the best way to define the PUM osmium isotope composition. Reisberg and Lorand (1995) suggested that the lower intercept of the trends might be used to define the initial $^{187}Os/^{188}Os$ of a given peridotite suite and hence derive a model age. The scatter for the off-craton compilation is then a function of different, subparallel trends for suites of different ages. Pearson (1999a) has pointed out that extrapolation of $^{187}Os/^{188}Os$ to zero Al_2O_3 will lead to an overestimation of model ages because Al_2O_3 is unlikely to be reduced to zero in any melt-residue suite. Sulfur and selenium provide better analogues from this point of view because their abundance should approach zero on the disappearance of sulfide at high levels of melting. However, both these elements suffer from metasomatic disturbance.

Cratonic and circum-cratonic kimberlite-derived xenoliths show poor correlations of $^{187}Os/^{188}Os$ and Al_2O_3 compared to noncratonic peridotites (Figure 41). Although some scatter is present within the total noncratonic data set, individual suites show much better correlations, the suite from Vitim being an excellent example (Pearson *et al.*, 1998a, 2004; Figure 41). Carlson *et al.* (1999b) suggest that the lack of correlation between $^{187}Os/^{188}Os$ and Al_2O_3 in cratonic peridotites is due to a rhenium-rich, aluminum-poor metasomatic component such as a carbonatitic fluid.

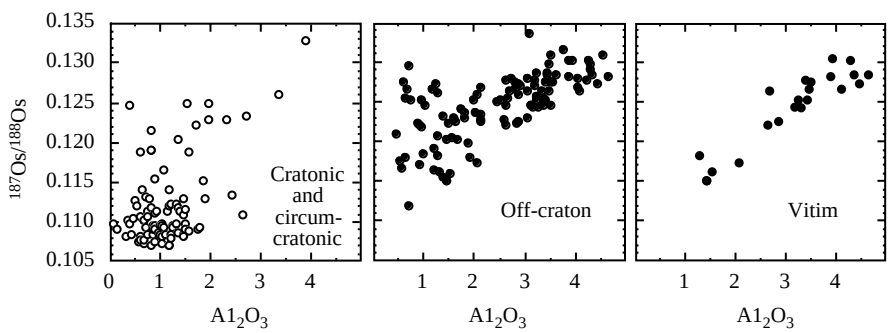

Figure 41 $^{187}Os/^{186}Os$ versus bulk rock Al_2O_3 for cratonic plus circum-cratonic peridotites, off-craton peridotites and the Vitim subset of off-craton peridotites. Data sources as for Figure 21. Vitim data set is from Pearson *et al.* (2002, 2004).

Radiogenic isotope studies of oceanic peridotite xenoliths are relatively few compared to continental peridotite xenoliths. In general, compositions are much more restricted than continental xenoliths, as might be expected for younger lithospheric mantle. However, recent studies are finding examples of very unradiogenic osmium isotopic compositions even in the oceanic environment. One example is the peridotite suite from the Kerguelen plateau, southern Indian Ocean. Unradiogenic osmium isotopes in these peridotites ($^{187}Os/^{188}Os$ ratios as low as 0.119) have been interpreted as indicating that the mantle beneath the Kerguelen plateau is ancient (>1 Ga old) and of continental rather than oceanic origin (Hassler and Shimizu, 1998), although similarly low values have also been reported from some abyssal peridotites (Snow and Reisberg, 1995; Brandon *et al.*, 2001). Even less radiogenic $^{187}Os/^{188}Os$ ratios (as low as 0.113 up to 0.129) have been reported for lherzolites from Salt Lake Crater, Hawaii (Griselin and Lassiter, 2002). These values extend to less radiogenic compositions than reported from abyssal peridotites. Possibilities to explain this data are that the xenoliths sample exotic fragments of subcontinental mantle in the Pacific, or that the xenoliths are derived from a heterogeneous Hawaiian plume that contains ancient, recycled oceanic lithosphere. A further possibility is that the unradiogenic Os isotopes are a result of an melting event that did not lead to lithospheric accretion. The fragment of mantle remained in the convecting mantle to be accreted to lithosphere during some later, more recent differentiation event.

The osmium isotope compositions of oceanic peridotite xenoliths significantly overlap the range for noncratonic continental peridotite xenoliths (Figure 37) although some of the latter suites have less radiogenic compositions that relate to their older ages (see below). The osmium isotopic mode and mean for noncraton peridotite xenoliths ($\gamma_{Os} = -1.5$) are close to chondritic (Figure 37). In contrast, cratonic peridotite xenoliths have extremely unradiogenic osmium isotope compositions with a frequency distribution that is strongly negatively skewed; mean $\gamma_{Os} = -10.3$ and values extending to -17 (Figure 37). Extremely unradiogenic osmium isotope compositions in cratonic xenoliths, even those sampled by Alkali Basalt Series magmas in cratonic settings (Chesley *et al.*, 1999; Hanghoj *et al.*, 2001) set them apart from peridotites from other tectonic settings and are a highly distinctive feature of Archean mantle sampled as peridotite xenoliths (Figure 39). Highly unradiogenic osmium isotope compositions of some cratonic high-*T* peridotites have shown that although they have experienced recent metasomatic disturbance, the protoliths were attached to the mantle root in the Archean (Walker *et al.*, 1989; Pearson *et al.*, 1995a; Carlson *et al.*, 1999). The osmium isotope compositions of almost all lithospheric peridotite suites are completely distinct from those of their host magmas.

Lithologies other than peridotites have not received significant attention from isotope geochemists. Wehrlites and pyroxenites from the off-craton locality of Bullenmerri (southeastern Australia) have strontium, neodymium, and lead isotopic compositions that are generally similar to those found in the regional alkali basalts (Porcelli *et al.*, 1992) indicating a likely origin as the crystallization products of magmas related to the host volcanism. Similarities in the Sr–Nd–Pb isotope data of erupted magma, pyroxenite/amphibole veins and megacrysts in noncratonic xenolith suites support a genetic link between these phenomena (Menzies *et al.*, 1985; Ben Othman *et al.*, 1990).

There are few published Lu–Hf isotope studies of mantle xenoliths because of difficulties in efficient ionization of hafnium by thermal ionization mass spectrometers. Multicollector plasma mass spectrometers are a solution to this problem and data are emerging that promise to be a more revealing tool in mantle environments than neodymium isotopes. The variety of Lu/Hf fractionation displayed by mantle minerals (Figure 42) indicates that, as with other isotope systems, isotopic variation should be considerable and initial results are confirming this. Salters and Zindler (1995) found very radiogenic $^{176}Hf/^{177}Hf$ at relatively unradiogenic neodymium isotope compositions in spinel peridotites from Salt Lake Crater, Hawaii. Radiogenic $^{176}Hf/^{177}Hf$ also characterizes low-*T* circum-cratonic

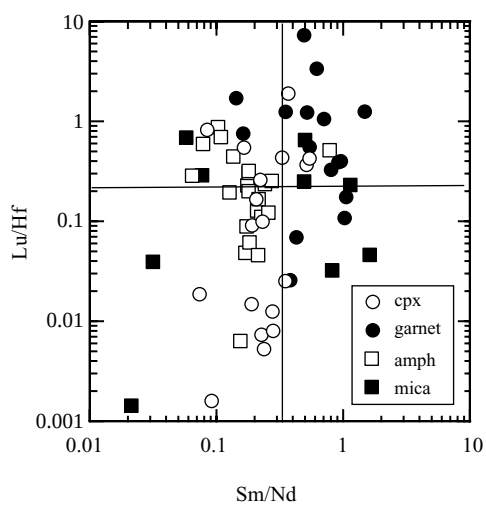

Figure 42 Covariation of Lu/Hf versus Sm/Nd for minerals from mantle peridotite xenoliths. Lines marked are the primitive mantle ratios.

peridotites from the Somerset Island kimberlite (Churchill Province, N. Canada; Schmidberger *et al.*, 2002). ε_{Hf} values range up to +160 at relatively unradiogenic neodymium isotopic compositions, forming a subvertical trend on an Nd–Hf isotope diagram (Figure 43). Radiogenic $^{176}Hf/^{177}Hf$ has also been measured in clinopyroxenes from Vitim peridotites (Blichert-Toft *et al.*, 2000) with compositions that lie consistently on, or well above the mantle Nd–Hf array (Figure 43). Clinopyroxenes from low-*T* Kaapvaal peridotite xenoliths have Hf–Nd isotope systematics that lie within, to just below the terrestrial array (Simon *et al.*, 2002). This is probably consistent with a late, metasomatic origin for many of these clinopyroxenes (Simon *et al.*, 2003). Some clinopyroxenes from Kaapvaal low-*T* lherzolites have ε_{Hf} values up to +70 (Bedini *et al.*, 2002) and are more consistent with a melt depletion origin. In contrast, garnets from cratonic peridotites commonly have highly radiogenic hafnium isotopic compositions that lie well above the mantle Nd–Hf isotope array, with ε_{Hf} values between +100 and +2,500. Thus, it seems clear from the relatively few (<100) data points obtained so far, that continental lithospheric mantle as sampled by xenoliths is characterized by highly radiogenic $^{176}Hf/^{177}Hf$ and by compositions that plot mostly well above the mantle Nd–Hf array, often in subvertical trends. This trend is similar to that found recently for cpx in spinel peridotites from the Beni Bousera orogenic peridotite (Pearson and Nowell, 2003; Figure 43) and hence is not just restricted to xenoliths, but appears a universal characteristic of lithospheric mantle. The highly radiogenic Hf isotopic compositions must be a product of ancient depletion involving residual garnet while the relatively unradiogenic neodymium isotopes are probably a function of more recent metasomatic disturbance that has not greatly affected the Lu–Hf system.

The robustness of the Lu–Hf isotope system in some mantle environments is demonstrated by the precise Lu–Hf isochron of 1,413 ± 67 Myr defined by clinopyroxene separates from the Beni Bousera peridotite massif (Pearson and Nowell, 2003). This age probably dates the time of melt extraction from these rocks and is considerably more precise than the Sm–Nd isochron or the scattered Re–Os isotope systematics of these rocks. This indicates the potential power of this system in dating mantle rocks. The initial results from the Lu–Hf isotope system indicate that of the incompatible element isotope systems, it is the more robust to metasomatic effects, with signatures frequently recording the time-integrated response to melt depletion.

2.05.2.7.4 *The age of mantle peridotites*

The first modern isotopic studies of continental lithospheric mantle (CLM) revealed that it must have been isolated from the convecting mantle for billion-year timescales (Kramers, 1977; Menzies and Murthy, 1980a; Richardson *et al.*, 1984).

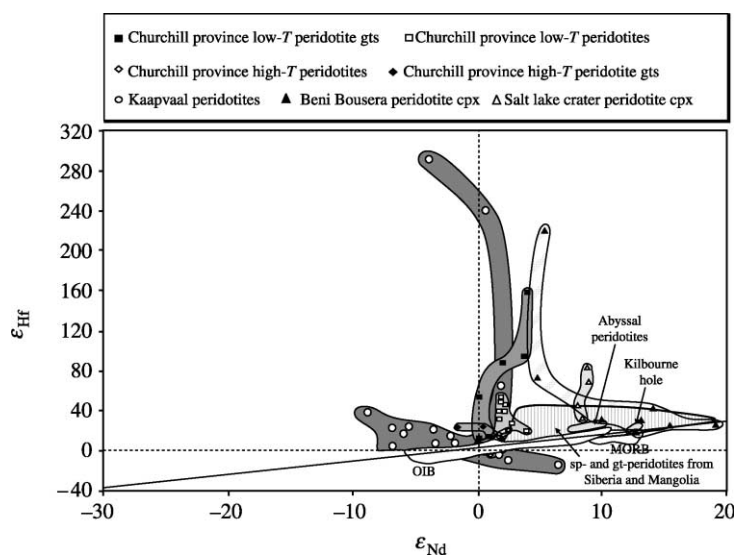

Figure 43 ε_{Hf} versus ε_{Nd} isotope diagrams for lithospheric mantle peridotite minerals. Kaapvaal peridotite data are all garnets and clinopyroxenes (Simon *et al.*, 2002). Slave peridotite data are garnets and whole rocks from Schmidberger *et al.* (2002). Salt Lake Crater peridotites (Hawaii), Kilbourne Hole and Abyssal peridotites, are from Salters and Zindler (1995). Siberian and Mongolian peridotite field are clinopyroxene data from cratonic and off-craton peridotites (field taken from Ionov and Weis, 2002). Fields for MORB (N-MORB) and OIB are from Nowell *et al.* (1998). Field for Beni Bousera peridotites from Pearson and Nowell (2003).

The incompatible element isotope systems used in these studies also showed that the parent-daughter isotope ratios for the respective systems must have been enriched relative to bulk Earth over such timescales. The ages obtained were "enrichment" ages and give rise to the "old enriched mantle" label for CLM. Further detailed work using incompatible-element-based isotopic systems revealed much detailed information concerning the complex, multiphase enrichment history of some peridotites (Richardson *et al.*, 1985; Stosch and Lugmair, 1986; McDonough and McCulloch, 1987; McCulloch, 1989; Gunther and Jagoutz, 1994; Pearson *et al.*, 1995a,b; Xu *et al.*, 1998) but because of these disturbances, the data do not constrain their formation ages.

Although the Re–Os isotope system is not immune from the effects of post-melt depletion processes such as metasomatism (Alard *et al.*, 2000; Burton *et al.*, 2000; Chesley *et al.*, 1999; Pearson *et al.*, 1995c) this system is by far the most reliable we have for estimating the formation ages of peridotites (Pearson, 1999a), although in certain instances, the Lu–Hf isotope system is proving very powerful (Pearson and Nowell, 2003). The Re–Os isotope system has been widely applied to both cratonic and noncratonic peridotite xenoliths. In particular, new developments using either analysis of sulfide inclusions in primary minerals, (Alard *et al.*, 2000; Pearson *et al.*, 2002), chromites (Chesley *et al.*, 1999) or combined osmium-isotope–PGE systematics (Pearson *et al.*, 2002) give us more confidence in the interpretation of Re–Os isotope ages for CLM peridotites.

Cratonic mantle peridotites. Over 230 whole-rock cratonic xenoliths have now been analyzed for Re–Os isotope compositions. Given that many peridotite xenoliths have experienced relatively recent rhenium introduction, it is generally best to use rhenium-depletion model ages (T_{RD}) that do not rely on the measured rhenium content of the rock for model age calculation. For cratonic peridotite xenoliths, the frequency distribution of rhenium-depletion ages shows a wide range, with a pronounced mode at 2.5–2.75 Gyr and some samples that have T_{RD} ages of >3.5 Gyr (Figure 44) With no data filtering, this is a first order observation that the lithospheric mantle underlying Archean cratons is also Archean in age. The Re–Os isotope system has been applied to the dating of seven different cratonic keels; the Kaapvaal craton (Walker *et al.*, 1989; Carlson and Irving, 1994; Pearson *et al.*, 1995b; Carlson *et al.*, 1999b; Irvine *et al.*, 2001), the Siberian craton (Pearson *et al.*, 1995a), the North Atlantic craton (Hanghoj *et al.*, 2001), the Wyoming craton (Carlson and Irving, 1994), the Tanzanian craton (Chesley *et al.*, 1999), the North China craton (Gao *et al.*, 2002), and the Slave craton (Irvine *et al.*, 1999, 2003) which have all produced Archean Re–Os model ages. Some model ages range to in excess of 3.5 Ga but most are in the region between 2.7 Ga and 3.2 Ga (Figure 44). Archean ages are obtained from peridotites derived from well into the diamond stability field.

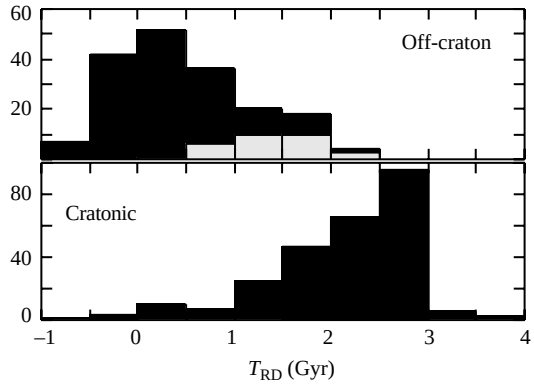

Figure 44 Frequency distribution plots of Re–Os isotope T_{RD} model ages (calculated assuming Re/Os = 0) for cratonic and off-craton peridotite xenoliths and massifs. The light-shaded field in the off-craton plot shows the range for kimberlite-derived peridotites from Namibia and East Griqualand. Data sources as in Figure 21 plus Pearson (unpublished).

Re-Os data for peridotite xenoliths erupted by Paleozoic kimberlites of the North China craton indicate the presence of refractory, chemically buoyant Archean lithospheric mantle beneath the craton at that time. Younger, post-Archean Re–Os model ages obtained from peridotite xenoliths erupted by Tertiary alkali basalts in the same craton indicate that the deeper section of the cratonic keel was replaced by more fertile lithospheric mantle sometime after the Palaeozoic (Gao *et al.*, 2002).

Circum-cratonic mantle. The mantle beneath areas adjacent to cratons is also sampled by kimberlite in numerous locations, allowing comparison of the age of CLM beneath circum-cratonic regions with that beneath the cratons. In southern Africa, kimberlites intrude to the West and Southeast of the exposed craton in Namibia and East Griqualand respectively and also to the south, in the Karoo. Rhenium depletion model ages for peridotite xenoliths sampled by these kimberlites are all post-Archean, with maximum ages in the range 2–2.2 Gyr (Pearson *et al.*, 2002a), equivalent to the age of the oldest exposed crust in these areas. Peridotite xenoliths erupted by alkali basalts in the Vitim region of Russia provide samples of CLM adjacent to the Siberian craton (Ionov *et al.*, 1993a). Rhenium depletion ages of up to 2.1 Gyr have been reported from this xenolith suite (Pearson *et al.*, 1998a, 2004).

In all these cases, the circum-cratonic mantle immediately surrounding Archean cratons gives younger rhenium depletion ages, consistent with the younger crustal ages in these regions. Such coherency of ages indicates a general coupling of the crust-mantle systems in and around some cratons (Pearson *et al.*, 2002).

Peridotites from younger lithosphere. Noncratonic peridotite xenoliths are often erupted in areas characterized by significant recent extensional tectonic activity. Re–Os model ages for these samples are predominantly younger than cratonic and circum-cratonic samples (e.g., Peslier *et al.*, 2000), however, peridotites from some localities such as southeastern Australia (Handler *et al.*, 1997) and the Sierra Nevada of the western USA (Lee *et al.*, 2001) have rhenium depletion ages as old as meso-Proterozoic, significantly older than the latest crust generation episodes in these areas. This indicates that old CLM in these cases survives the rifting and crustal differentiation events imposed on them. The old remnant lithospheric mantle found beneath the Sierra Nevada is used to support a model of delamination of deep, unstable lithosphere produced due to collisional thickening (Lee *et al.*, 2000a). Most of the xenoliths analyzed from these areas are spinel-facies xenoliths that are likely to be derived from depths less than 60–70 km deep. Thus, it is only the shallower Proterozoic mantle in general that survives these reworking episodes.

U–Pb ages on high-U/Pb, high-Th/Pb phases. Re–Os model ages record, to varying degrees of precision and accuracy, the timing of melt depletion in peridotites. The presence of high U/Pb and Th/Pb phases such as zircon and monazite in rare peridotite, MARID/PKP and glimmerite xenoliths allow precise U–Th–Pb ages to obtained (Carlson and Irving, 1994; Hamilton *et al.*, 1998; Konzett *et al.*, 1998, 2000; Rudnick *et al.*, 1999). Because the zircon and monazite are associated with metasomatic enrichment events the ages obtained date the timing of melt enrichment in the host rock. Some of these ages are highly precise, e.g., Carlson and Irving (1994) obtain an age of 1,779 ± 2 Myr for a monazite crystal in a glimmerite from the Montana xenolith suite. This age is in agreement with a zircon U–Pb age of 1,784 ± 20 Myr from a peridotite from the same xenolith suite (Rudnick *et al.*, 1999). These ages are suggested to record an enrichment event coincident with the formation of the Great Falls tectonic zone. In contrast, zircons from a phlogopite vein in a harzburgite from the Labait tuff cone, Tanzania record a very young, 400 ± 200 kyr metasomatic event affecting Archean peridotite. Thus, the potential for these phases to yield precise geochronological information in mantle assemblages is clear, if they can be found. These minerals appear to retain their radiogenic Pb because they are the principal sinks for Pb in the host rock. They do not significantly exchange with their surrounding minerals and hence they record ancient ages even though residing at mantle temperatures. In this sense, their "blocking" temperatures in the mantle environment are high, even for monazite.

2.05.2.8 Stable Isotope Chemistry: Oxygen, Carbon, and Sulfur Isotopes

In comparison to radiogenic isotope data, stable isotope data for minerals in peridotites are sparse. As with radiogenic isotopes, alteration processes and invasion by the host rock means that the most reliable data are derived from mineral separate analyses. Initial studies of the variation and inter-mineral fractionation of oxygen isotopes between mantle xenolith minerals were interpreted as due to varying equilibration temperatures (Kyser *et al.*, 1981). Gregory and Taylor (1986) re-interpreted this complex data set in terms of open-system exchange between the minerals and metasomatic fluids. In this model, olivine and spinel exchange oxygen more rapidly than pyroxenes and hence show larger variations in isotope composition. A problem with the Gregory and Taylor (1986) model is how a fluid with a distinct $\delta^{18}O$ can percolate through mantle consisting of 80% olivine without being rapidly buffered to the composition of the ambient mantle. A problem for both models, and for most pre-1990 oxygen isotope data on mantle minerals, is the relatively imprecise data obtained by convention fluorination techniques for mantle minerals, especially olivine, which made interpretation of small inter-mineral isotopic fractionations difficult to do with confidence.

The advent of laser-fluorination techniques dramatically improved capabilities for precise analyses of these phases and led to the observation that olivine from a wide range of peridotites, including hydrous and anhydrous variants, has a very constant $\delta^{18}O$ (Mattey *et al.*, 1994). In addition, olivine and pyroxene data obtained using laser-fluorination show much smaller, more systematic fractionations than conventional fluorination data on the same samples (Figure 45). This observation has been confirmed by subsequent studies (Chazot *et al.*, 1997; Xu *et al.*, 1998).

Because of the buffering effect of mantle olivine on the oxygen isotope composition of metasomatic fluids, oxygen isotopes are not, in most cases, effective tracers of mantle–fluid interaction (Mattey *et al.*, 1994; Menzies and Chazot, 1995). One exception to this is the fluid-process that creates diamond. Comparison of the oxygen isotope compositions of garnets in typical

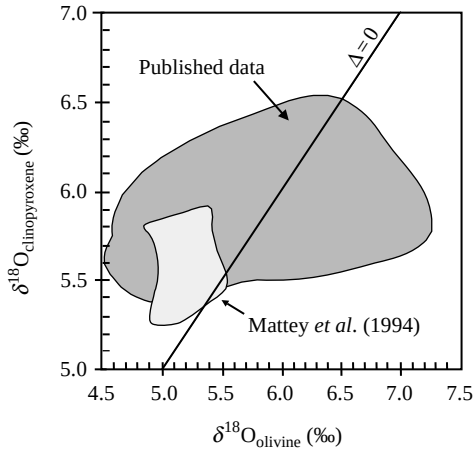

Figure 45 δ^{18}O clinopyroxene versus δ^{18}O olivine for peridotite mantle xenoliths. The large-shaded field is for cratonic and noncratonic peridotites analyzed by conventional fluorination techniques cited in Mattey *et al.* (1994). The light-shaded smaller field is for laser-fluorination analyses of a wide-range of cratonic and noncratonic peridotite (source Mattey *et al.*, 1994).

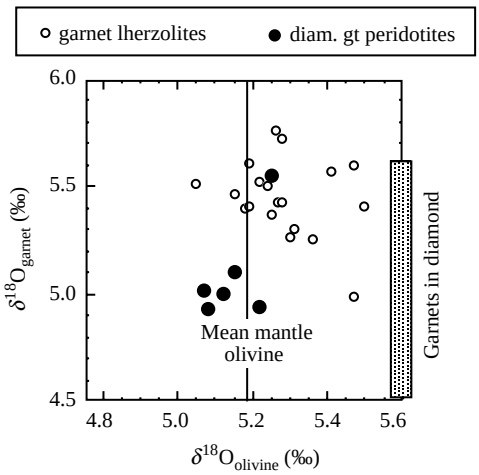

Figure 46 δ^{18}O garnet versus δ^{18}O olivine plot for garnet lherzolites (cratonic and noncratonic), subcalcic garnet harzburgite/dunites, and subcalcic garnet inclusions in diamonds. Data from Mattey *et al.* (1994), Lowry *et al.* (1999), and Mattey and Pearson (unpublished). The range for garnets included in diamonds and some xenolith garnets with no corresponding olivine analyses are plotted on the right-hand axis of the diagram. The mean value for mantle olivine is from Mattey *et al.* (1994).

lherzolite xenoliths with peridotitic garnet inclusions in diamonds and garnets from diamondiferous peridotite xenoliths shows that garnets associated with diamonds have significantly lower δ^{18}O than garnets in nondiamondiferous peridotites (Figure 46; Lowry *et al.*, 1999). Olivines from the diamondiferous peridotites also appear shifted to lower δ^{18}O than typical for the nondiamondiferous garnet lherzolites but are within the range of mantle olivines from spinel lherzolites (Mattey *et al.*, 1994). In addition, reversed oxygen isotope fractionation between garnet and olivine in both diamond inclusions and diamondiferous peridotites suggests that garnet preserves subtle isotopic disequilibrium related to the genesis of chromium-rich garnet and/or diamond (Lowry *et al.*, 1999). It is also possible to explain the anomalously low δ^{18}O values of low-calcium harzburgite/dunite assemblages in terms of a subduction model. High bulk rock Cr/Ca and high Cr/Al in garnet in these assemblages may require a low-pressure melting origin, consistent with formation as oceanic lithosphere, followed by subduction (Section 2.05.2.5.2; Schulze, 1986; Canil and Wei, 1992). The δ^{18}O values are shifted lower than typical mantle, which is consistent with high-T hydrothermal alteration operative in the deep oceanic lithosphere. Subduction of such material could, therefore, account for the low δ^{18}O values of olivine in subcalcic garnet harzburgites. Further studies are required to better constrain these possibilities.

A detailed laser-fluorination study of individual minerals from ultradeep xenoliths (Deines and Haggerty, 2000) revealed significant oxygen isotopic variation. While evidence for oxygen isotopic equilibrium is observed between some garnet–olivine, garnet–orthopyroxene and clinopyroxene–orthopyroxene pairs, fractionation between garnet and clinopyroxene tends to be out of equilibrium. Deines and Haggerty (2000) concluded from diffusion modeling that the xenoliths had experienced a series of metasomatic alterations, including an event that lowered the δ^{18}O value of the pyroxenes, a few million years before eruption by the host kimberlites. The mean δ^{18}O values of garnets in these transition-zone rocks are argued to be unaltered by the metasomatic processes and are indistinguishable from upper-mantle values.

In the oceanic setting, spinel lherzolite xenoliths from Pali (Hawaii) have olivine δ^{18}O values of 5.09–5.12 per mil, typical of olivines from other oceanic and continental mantle rocks (Ducea *et al.*, 2002). In contrast, olivines from plagioclase peridotites are enriched by ~0.5 per mil. This is interpreted to be due to the formation of plagioclase by reaction with or crystallization from melts intruding the Pacific lithospheric mantle.

Hydrogen isotope data for mantle xenoliths is usually acquired on hydrous minerals such as amphibole and mica. One problem is that early studies did not texturally characterize mica occurrences and so the information is of limited value. Perhaps the best-documented study is that

of Boettcher and O'Neil (1980), who analyzed megacrystic phlogopite from kimberlites and phlogopite from peridotites. These authors found a restricted range in δD (−70 per mil to −63 per mil), typical of mantle derived magmas. In megacrysts and veins, amphibole often has lower δD and δ^{18}O than coexisting phlogopite but the reason for this is not well understood (Kyser, 1990).

The systematics of sulfur isotopes in mantle xenoliths have been reviewed by Kyser (1990). Most sulfide data have so far been obtained by *in situ* analyses using SIMS or laser probe and this is less prone to alteration effects than whole-rock analyses. Chaussidon *et al.* (1989) found that considerable sulfur isotope variation exits in mantle minerals (δ^{34}S −5 to 8 per mil), which they attributed to fractionation between residual sulfide and the melt during melting. However, it is megacrysts that show most variation in their data set, possibly due to magmatic processes while sulfide from the garnet peridotites has a much more restricted range, of between −1 per mil and +4 per mil, typical of mantle values. Wilson *et al.* (1996) found elevated δ^{34}S in peridotites from Dish Hill, which they proposed was due to metasomatic introduction of subducted crustal sulfur.

2.05.2.9 Noble Gases

2.05.2.9.1 He isotopes

Initial studies of xenoliths from both continental (Porcelli *et al.*, 1986) and oceanic (Vance *et al.*, 1989) settings showed a remarkable consistency of ^{3}He/^{4}He, in contrast to their widely variable strontium isotope compositions. For example, peridotite xenoliths from the Canary Islands, Gough, Kerguelen, and Madeira studied by Vance *et al.* (1989) had a restricted ^{3}He/^{4}He range of 5.2–7R/R_A (where R_A is the atmospheric ^{3}He/^{4}He value), comparable to MORB. In contrast, their clinopyroxene strontium isotope compositions extended over almost the entire range of oceanic basalts. ^{3}He/^{4}He in Hawaiian xenoliths is slightly higher, 8.2–9.5R/R_A, possibly reflecting a sampling bias towards pyroxenites compared to peridotites. The Hawaiian pyroxenites are probably linked to the host magmatism, which has elevated ^{3}He/^{4}He. In contrast, Poreda and Farley (1992) found ^{3}He/^{4}He ratios of up to 21.6 ± 1 in Samoan peridotite xenoliths. The highest xenolith ^{3}He/^{4}He ratios are comparable to those measured in Samoan lavas and the data are most easily interpreted in a model where the xenoliths trap volatiles from the high ^{3}He/^{4}He lava sources.

The continental samples analyzed by Porcelli *et al.* (1986) had ^{3}He/^{4}He ranging from ~6 to just above 10, with a mean value well within the MORB range. These samples had extremely variable strontium isotope compositions. These initial studies clearly showed that helium and lithophile element isotope compositions in mantle xenoliths from both oceanic and continental settings are decoupled. This was confirmed by a more extensive study of continental peridotites from the Massif Central, The Eifel region, Spitzbergen and Kapfenstein by Dunai and Baur (1995), who analyzed exclusively mineral separates. The mean ^{3}He/^{4}He values of these four suites were 6.5, 6.0, 6.7, and 6.1 times R_A and hence within the MORB range, but lower than the average MORB value of 8. Dunai and Baur (1995) suggested that the helium isotope signature preserved in the xenoliths is inherited from their host magma and reflects a MORB-like source. A recent, extensive review of noble gases from continental peridotite xenoliths and basalts found a mean R/R_A value of 6.1 ± 0.9 compared to the MORB source ratio of 8 ± 1 and proposed that this difference is significant (Gautheron and Moreira, 2002). The difference between the continental mantle, as portrayed by the xenoliths, and MORB cannot be accounted for by uranium-decay, leading Gautheron and Moreira (2002) to postulate a model where the residence time for helium in continental lithospheric mantle is around 100 Ma. If such a residence time is correct then the continental mantle cannot be used to track helium isotopes, or other noble gases through time and is completely overprinted by the MORB-source.

2.05.2.9.2 Neon, argon, and xenon isotopes

Neon isotope data from Samoan lavas show elevated ^{20}Ne/^{22}Ne relative to atmosphere. The data are not consistent with a model of mixing between a degassed MORB mantle with high ^{20}Ne/^{22}Ne and a deeper, undegassed plume source with atmospheric ^{20}Ne/^{22}Ne. The similarity of neon isotopes between the Samoan plume-like source and MORB supports the idea that neon isotopes in the mantle as a whole more closely resemble the solar composition than that of the atmosphere (see Chapter 2.06). "Plume-like" neon isotopic signatures have been identified in an apatite from a southeastern Australian spinel lherzolite xenolith (Matsumoto *et al.*, 1997).

^{40}Ar/^{36}Ar in the least contaminated Samoan xenoliths varies from 4,000 to 12,000, with the highest values found in samples with the highest ^{3}He/^{4}He values. There is little evidence for atmosphere-like argon in the source of Samoan lavas, with values likely to be in excess of 5,000 (Poreda and Farley, 1992). These data, combined with ^{129}Xe and ^{136}Xe anomalies 6% greater than the atmospheric value, contradict the idea that

high $^{3}He/^{4}He$ mantle domains have pristine, near-atmospheric heavy rare gas isotope compositions and suggests that much of the mantle could have non-atmospheric noble gas isotopic compositions.

High uranium and thorium contents of metasomatic minerals in pyroxenites and peridotites from southeastern Australia produce radiogenic ^{4}He and nucleogenic ^{21}Ne and ^{22}Ne (Matsumoto *et al.*, 2000). Accounting for this and the effects of atmospheric contamination, the heavy noble gas isotope systematics of peridotites from this region and the European continental peridotites analyzed by Dunai and Baur (1995) are MORB-like in character, i.e., with elevated $^{40}Ar/^{36}Ar$, $^{20}Ne/^{22}Ne$, $^{129}Xe/^{130}Xe$, and $^{136}Xe/^{130}Xe$. Thus, the heavy noble gas isotope data from continental lithospheric mantle support models where the volatile budget of this reservoir is dominated by fluxing from the underlying MORB source (Gautheron and Moreira, 2002) and/or that many of the samples formed from MORB-source mantle, accreting to the continental lithosphere during melt depletion. In contrast, Dunai and Baur (1995) have suggested that the He–Ar systematics of some European peridotite xenoliths reflect mixing of recycled crustal material with a MORB-like source during the Variscan orogeny. If data from massif peridotites and peridotite xenoliths are considered together, the continental lithospheric mantle can be argued to have lower $^{3}He/^{4}He$ values than the convecting MORB-source mantle but with dominantly MORB-like argon, neon, and xenon isotope systematics.

2.05.3 ECLOGITE XENOLITHS

2.05.3.1 Classification, Mineralogy, and Petrography

All kimberlites within cratonic areas of southern Africa that have been well sampled contain eclogite (Gurney *et al.*, 1991) but at most localities it is a rare xenolith type. Consequently, studies of eclogites have been confined to a few kimberlites, e.g., Newlands, Bellsbank/Bobbejaan, Roberts Victor and Orapa on the Kaapvaal craton (Table 1(a); MacGregor and Carter, 1970; Robinson *et al.*, 1984; Hatton and Gurney, 1987; Taylor and Neal, 1989) and Udachnaya plus Mir from the Siberian craton (Sobolev, 1974; Snyder *et al.*, 1993; Jacob *et al.*, 1994; Beard *et al.*, 1996). Assessing the relative abundance of eclogite within the whole lithospheric mantle is not easy due to considerations of preferential disaggregation of certain types of xenoliths. On the basis on mineral concentrate studies, Schulze (1989) estimates eclogite to be less than 2% on average of a given continental lithospheric mantle section, as sampled by kimberlites. In exceptional circumstances, such as at the Roberts Victor kimberlite (S. Africa), eclogite comprises 95–98% of the mantle xenolith inventory, however, even here, mineral concentrate studies show that peridotite is abundant.

In noncratonic xenolith suites, eclogite is much scarcer and it is notable if this lithology is present. Pyroxenites and garnet pyroxenites are more common in noncratonic xenolith suites.

Eclogites consist of omphacitic clinopyroxene and pyrope-almandine garnet. Their grospydite variants (Table 1) are defined as containing garnets with a large grossular component together with kyanite. Accessory phases vary widely but rutile is perhaps the most common (Table 1). At some localities, such as Roberts Victor, coesite is more common than originally thought (Schulze *et al.*, 2000) and orthopyroxene is sometimes present. Other exotic related rocks such as alkremites contain spinel and/or corundum as major phases associated with garnet (Table 1; type IX). Olivine is unknown. Diamond can be present as a significant component of eclogites at some localities (Gurney *et al.*, 1991).

There are several different classification schemes for eclogites. Roberts Victor eclogites have been divided into group I and group II rocks (MacGregor and Carter, 1970), based on their textures (Table 1). Taylor and Neal (1989) subdivided the Bellsbank/Bobbejaan eclogites into three groups (A–C) on the basis of their mineral chemistry and used this classification in subsequent studies to help assign crust or mantle origins to eclogites. A modified version of the MacGregor and Carter terminology is probably the most widely applied, at least to southern African eclogites. That cratonic eclogites are erupted from mantle depths is confirmed by the presence of diamond in group I variants (Table 1(a)). In addition, the incorporation of relatively high levels of sodium into group I eclogitic garnets and potassium into group I clinopyroxenes (McCandless and Gurney, 1989) requires a high pressure, mantle origin. Eclogites occurring in circum-cratonic and craton-margin kimberlites, often containing feldspar and associated with granulitic assemblages are widely accepted to be of crustal origin (e.g., Gurney *et al.*, 1991). Alkremites (spinel–garnet assemblages; Table 1(a)) probably represent an end-member of the eclogite suite (Nixon *et al.*, 1978).

2.05.3.2 Mineral Chemistry and Equilibration Conditions

Eclogites have widely varying garnet compositions that are less chromium- and magnesium-rich than those of peridotite xenoliths (Figure 47). As a general guideline, eclogite garnets have

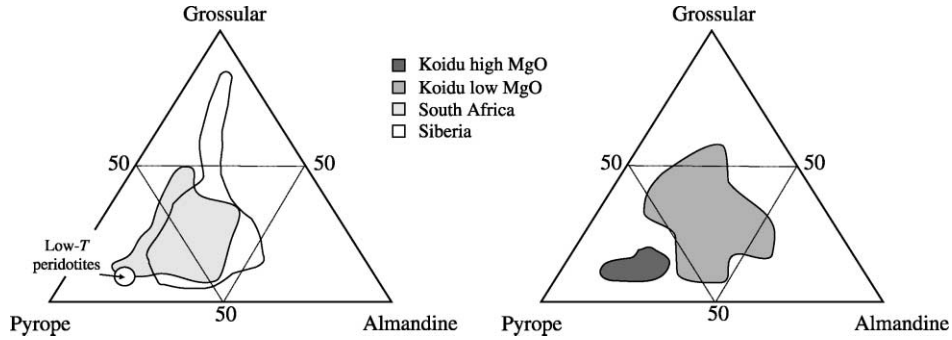

Figure 47 Garnet compositions for eclogites from Siberia, South Africa, and Koidu (Sierra Leone) compared to low-*T* Kaapvaal peridotites, in terms of their pyrope, grossular, and almandine calculated end-members (sources Sobolev, 1974; Hatton and Gurney, 1987; Mazonne and Haggerty, 1989; Taylor and Neal, 1989; Jacob *et al.*, 1994; Hills and Haggerty, 1989; Viljoen *et al.*, 1996; Pyle and Haggerty, 1998; and Barth *et al.*, 2001).

<2 wt.% Cr_2O_3, whereas peridotitic garnets exceed this value (Figure 5; Gurney *et al.*, 1991). The most common garnet compositions are in the pyrope–almandine range but their grossular contents can vary widely. When grossular is dominant over pyrope in the garnet composition in eclogites, the lithology is termed grospydite (Sobolev, 1974). Na_2O contents of garnets from group I eclogites exceed 0.07 wt.% (Schulze *et al.*, 2000) and this feature is interpreted to reflect high-pressure equilibration conditions (>5 GPa; McCandless and Gurney, 1989). Garnets from group II eclogites have <0.07 wt.% Na_2O. Garnets from alkremites and related rocks are generally grossular-rich pyrope–almandine–grossular solid solutions with negligible spressartine (Mazonne and Haggerty, 1989).

Clinopyroxenes are omphacitic, with large jadeite and minor pyroxene quadrilateral components that clearly distinguish them from the clinopyroxene found in pyroxenite xenoliths or pyroxenites from massif peridotites (Figure 48). Omphacite Na_2O contents are typically between 3 wt.% and 8 wt.%. Two-phase assemblages of garnet and clinopyroxene in which the pyroxene is not omphacitic are properly referred to as garnet clinopyroxenites. The high jadeite and low quadrilateral component contents of eclogitic clinopyroxenes are distinct from high-pressure liquidus pyroxenes produced in experiments (Figure 48). This makes an origin for eclogites as high pressure cumulates from magma unlikely. Eclogitic group I clinopyroxenes have >0.08 wt.% K_2O, which is most likely a response to high pressures of equilibration (McCandless and Gurney, 1989).

The presence of coesite and diamond together with high sodium and potassium in garnet and clinopyroxene respectively, make a clear case for the high-pressure origin of cratonic eclogites (Gurney *et al.*, 1991). In contrast to the various quantitative barometers available for peridotites,

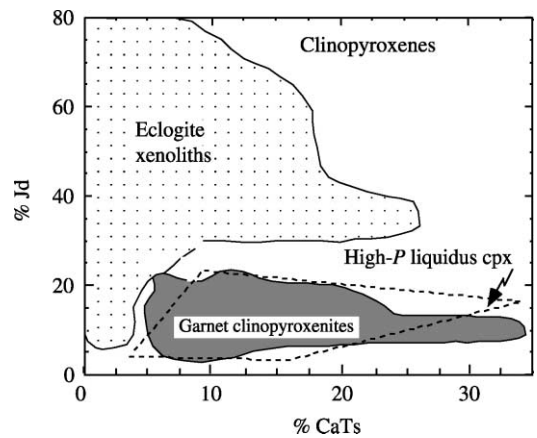

Figure 48 Molecular percent jadeite (Jd) versus Ca-Tschermak's (CaTs) of clinopyroxenes from eclogite xenoliths compared with clinopyroxene from garnet clinopyroxenite xenoliths (Irving, 1974) and from garnet clinopyroxenite layers in massif peridotites (Pearson and Nixon, 1995). Field of high-pressure liquidus clinopyroxenes from Eggins (1992). Data sources as in Figure 47.

the high thermodynamic variance of the garnet–clinopyroxene assemblage means that no barometers for eclogite xenoliths have been developed. Mukhopadhyay (1991) has proposed a barometer for garnet–clinopyroxene assemblages but this is only applicable when clinopyroxenes are enriched in quadrilateral and Tschermak components and hence it is inapplicable to true eclogites.

Equilibration temperatures are commonly calculated using the Fe–Mg exchange reaction between garnet and clinopyroxene, which is slightly pressure dependant and so an equilibration pressure must be assumed. Many thermobarometry studies of eclogites use the assumption that these rocks lie on a suitable geotherm for the region and project equilibration temperatures to the geotherm in order to derive their depth of

origin. Variations in equilibration temperatures between different eclogite suites are apparent at a given equilibration pressure. For instance, at 5 GPa the equilibration temperatures of Koidu low-MgO eclogites (Fung and Haggerty, 1995) are much lower (880–930 °C) than for Roberts Victor eclogites (~1,100 °C; Harte and Kirkley, 1997). MacGregor and Manton (1986) suggest that most cratonic eclogites originate from >150 km depth, at the base of the lithosphere. While the high sodium in garnet and high potassium in clinopyroxene, together with the presence of diamonds in group I eclogites support this notion, the absence of these features and the wide range in equilibration temperatures in group II eclogites suggest that some originate from much shallower depths.

2.05.3.3 Bulk Compositions

The bulk compositions of eclogites can be seriously affected by a combination of syn-eruption partial melting, mantle metasomatism (including invasion by their hosts) and low-*T* alteration. Omphacite is generally more affected than garnet. Kyanite-eclogites are usually the most severely altered (Harte and Kirkley, 1997). The geochemical effects are most dramatic for incompatible trace elements but major elements can be affected in some suites also (Ireland *et al.*, 1994), resulting in an increase in Mg# due to invasion of high-magnesium host melts. Accordingly, some authors have used reconstructed bulk compositions calculated from modal analyses and mineral compositions in the study of eclogite bulk rock chemistry. These compositions are subject to errors in the accuracy of modes for coarse-grained rocks. For most suites, effects on major-element compositions are relatively minor and hence their measured bulk compositions can be used to say something about their origin.

The "basaltic" compositions of eclogite xenoliths have lead to two main models of eclogite origin; that they represent the crystallized products of high-pressure mantle melting (O'Hara and Yoder, 1967; Hatton and Gurney, 1987), or that they represent the metamorphosed products of subducted oceanic crust (Helmstaedt and Doig, 1975; Jagoutz *et al.*, 1984; MacGregor and Manton, 1986; Neal *et al.*, 1990; Jacob *et al.*, 1994). A modification of the crystallized mantle melts hypothesis suggests initial crystallization at relatively low pressures (~50 km) and then burial to depths within the diamond stability field (McDade and Harte, 2000). Variations on the subduction end-member model propose that eclogites are residual slab compositions from the extraction of tonalitic magmas during Archean subduction (Ireland *et al.*, 1994; Barth *et al.*, 2001).

In discussing the relevance of eclogite bulk compositions to this argument, it is pertinent to make comparisons of their compositions with Archean basaltic/komatiitic magmatism because of the Archean age of many eclogite xenoliths (Section 2.05.3.5.3). In addition, comparisons of xenoliths with "massif" eclogites exposed in high-pressure orogenic terrains, for which an origin via metamorphism of basalt is widely accepted, are also relevant, despite the Phanerozoic age of most of these occurrences.

The MgO contents of eclogite xenoliths range from ~6% to ~20%, with a mean of 12%. This makes them basaltic to picritic in composition, rather than komatiitic. No samples extend to the very high MgO contents (>25 wt.%) of Archean komatiites (Figure 49). Some eclogite suites can be divided into low-MgO and high-MgO variants (Barth *et al.*, 2001; Barth *et al.*, 2003). Significant overlap between Archean magmatic rocks and eclogite xenoliths exists for CaO, Na_2O, and TiO_2. However, SiO_2 contents for eclogite xenoliths at a given MgO are much lower than Archean magmas while few erupted volcanic rocks reach Al_2O_3 contents of >20% observed in some eclogites. Compared to massif eclogites, there is overlap in CaO and Al_2O_3 contents, but SiO_2, Na_2O, and TiO_2 are, on average, significantly lower for the xenoliths (Figure 49). Eclogites that have been tectonically exposed in the crust in high-pressure metamorphic regions do not appear to contain the alkremite/grospdyite assemblages found in cratonic xenolith suites. This may be a function of the different depths of sampling or due to the differing ages. Orogenic eclogite suites are dominantly post-Archean, whereas cratonic eclogites are Archean in age (Section 2.05.3.5.3). Chromium contents are consistently higher in eclogite xenoliths than massif eclogites. For xenoliths, total alkalis are lower than most magmas at a given MgO content. These differences between eclogite xenolith compositions and those of Archean magmas and massif eclogites pose clear problems for a model where the xenoliths simply represent isochemically metamorphosed basalts.

McDade and Harte (2000) suggest that the major-element compositions of the Roberts Victor eclogite xenoliths are not compatible with recrystallized oceanfloor basalts although their comparisons use exclusively Phanerozoic basalt compositions. McDade and Harte (2000) and Barth *et al.* (2001, 2003) point out that most eclogite compositions are not comparable with the products of peridotite fusion at high pressures. This led McDade and Harte (2000) to appeal to low pressure (spinel-facies) mantle melting and crystallization, followed by burial to greater depths. It is not clear how crustal isotopic

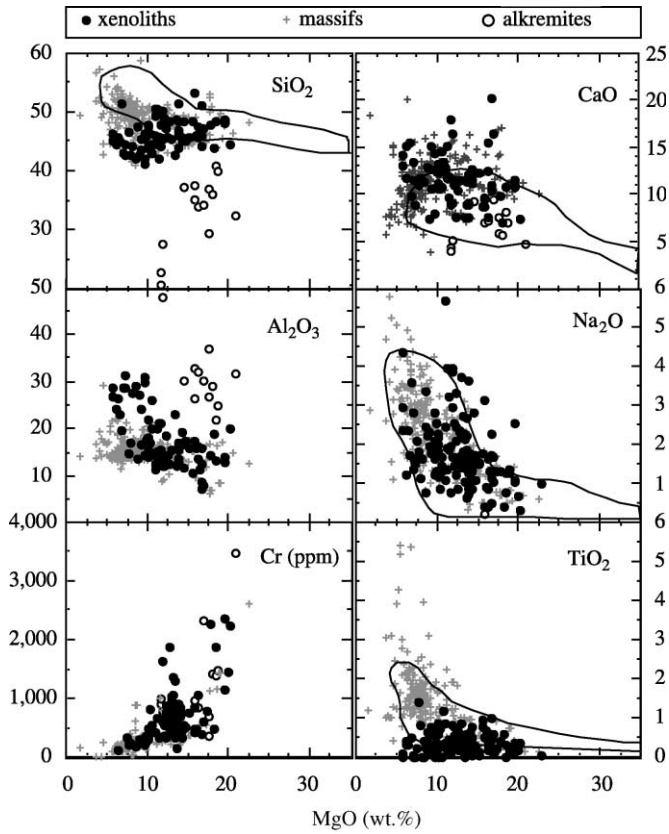

Figure 49 Bulk analyses of eclogite and alkremite (alkremite–corgaspinite–corganite; Table 1) xenoliths from kimberlites compared with massif eclogites and Archean basalts and komatiites (open field). Data sources: Kushiro and Aoki (1968), Sobolev (1974), Mazonne and Haggerty (1989), Hills and Haggerty (1989), Taylor and Neal (1989), Ireland *et al.* (1994), Pyle and Haggerty (1994), Snyder *et al.* (1993), Jacob *et al.* (1994), and Jacob and Foley (1999). Outlined field is for Archean basalts and Komatiites taken from Ireland *et al.* (1994).

signatures are acquired in this model, unless the protoliths are erupted basalts. The moderate-to-low-pressure pyroxenes on the liquidus of mantle melts are not omphacite (Figure 48) and so this must form during burial. A similar model was suggested by Barth *et al.* (2003) to explain the genesis of the Koidu high-MgO eclogite suite. High MgO and Al_2O_3 contents of the eclogites are suggestive of a cumulate origin, either as high-pressure (2–3 GPa) garnet-pyroxene cumulates or low-pressure (<1 GPa) plagioclase–pyroxene–olivine cumulates.

While differences between the major-element composition of eclogite xenoliths versus Phanerozoic *and* Archean magmas certainly exist, and the xenolith compositions also differ with massif eclogites, many of these features can be reconciled with the "residual slab" type model of eclogite xenolith origin (Ireland *et al.*, 1994; Jacob and Foley, 1999; Barth *et al.*, 2001). The relatively low SiO_2 and Na_2O contents of eclogite xenoliths compared to those of massif eclogites and Archean basalts (Figure 49) can be related to the proposed loss of a high-silicon tonalitic melt fraction during subduction. Lowering of SiO_2 during subduction zone melting can also explain the scarcity of quartz (as coesite) in some eclogite xenolith suites (Udachnaya, Koidu, Bellsbank) compared to massif eclogites (Jacob and Foley, 1999). A melting residue model would also explain the lower alkalis and titanium and the higher chromium contents of xenoliths compared with massif eclogites and Archean magmas because of the relative compatibilities of these elements during melting. Schulze *et al.* (2000) suggest that the abundance of free silica (as coesite) in Roberts Victor eclogites indicates that they have not experienced significant partial melting during subduction and represent original ocean-floor type compositions. However, Yaxley and Green (1998) showed in an experimental study that coesite is stable in eclogite until 13% melt loss and so some compositions could be residual. In slab-recycling models, the very aluminous compositions of some eclogite xenoliths, e.g., kyanite-eclogites, has led to the suggestion that they are former plagioclase-rich oceanic cumulates (Jagoutz *et al.*, 1984; Jacob and Foley, 1999).

In support of a crustal origin, Jacob *et al.* (1998b) and Barth *et al.* (2001) point out that the kyanite–eclogite assemblage is not in equilibrium with mantle peridotite at high pressure and would react with olivine to form aluminous pyroxene and garnet, further strengthening an origin via high-grade metamorphism rather than igneous processes.

The bulk compositions of alkremites and related rocks are clearly very anomalous for aluminum and silicon (Figure 49) and are largely a function of the abundance of garnet and spinel in the mode. Nixon *et al.* (1978) explain these unusual rocks in terms of high-pressure phase equilibria and their formation from mantle melts. In contrast, Mazonne and Haggerty (1989) draw attention to similarities with pelitic sediment bulk compositions and suggest an origin as high-pressure metamorphic products of melting residues from the subduction of pelitic sediments.

2.05.3.4 Trace-element Chemistry

The effects of metasomatism and invasion of the host magma alluded to above are much more significant for minor element concentrations in eclogites, particularly highly incompatible elements. For example, Barth *et al.* (2001) demonstrate that addition of ~5% host kimberlite to un-metasomatized protoliths can account for the measured whole-rock trace-element systematics of Koidu eclogites and will significantly affect incompatible element abundances and ratios. As such, our discussion will focus on those studies that have used the trace-element contents of minerals to reconstruct whole-rock trace-element abundances. Ireland *et al.* (1994) compared the trace-element systematics of inclusions in diamond with those of minerals in the host diamondiferous eclogites. They propose that the mineral compositions of the host eclogite are affected by metasomatic processes that veil the true precursor compositions. Other studies (e.g., Taylor *et al.*, 1996) have not yielded such clear results. There are issues concerned with whether the diamond-forming event in diamondiferous eclogites locally affects silicate minerals. These problems aside, there are few samples where studies of inclusions and host phases are possible. Furthermore, the extent of metasomatism by the host rock is much lower in some eclogites suites than others. Hence, we will discuss information that can be obtained from trace-element mineral studies of eclogites in general (Barth *et al.*, 2001; Harte and Kirkley, 1997; Jacob and Foley, 1999; Jerde *et al.*, 1993; Snyder *et al.*, 1997). We will describe mineral trace-element chemistry first followed by reconstructed whole-rock abundances.

Garnets from worldwide eclogite xenolith locations are typically LREE-depleted with values of $(La)_n$ as low as 0.01 (Figure 50) Most garnets have relatively unfractionated HREE abundances with $(Dy/Yb)_n$ of 0.5 to 2.5, $(Yb)_n$ values up to 50 and have small positive europium anomalies. They show variable depletion of zirconium, hafnium, and titanium (e.g., Figure 50). Barth *et al.* (2001) noted that garnets within samples possessing jadeite-poor clinopyroxenes from Koidu (Sierra Leone) show greater HFSE anomalies and less variable REE patterns than those with jadeite-rich clinopyroxenes. Nb–Ta depletions in garnet are variable. Those most deficient in niobium and tantalum are from rutile-bearing samples where these elements preferentially partition into rutile. The LREE-depleted nature of garnets from most worldwide eclogite suites contrasts markedly with the complex REE patterns shown by cratonic peridotites. This suggests that either the eclogites have been subject to much less "cryptic" metasomatism than peridotites and/or the peridotite garnet REE patterns may reflect an origin other than loosely defined metasomatic additions to an originally depleted garnet.

Clinopyroxenes in eclogite xenoliths have convex-upwards REE patterns that are LREE-enriched relative to HREE. $(La)_n$ varies from slightly below 1 to ~15, while $(Yb)_n$ varies between 0.1 and 1.5 (Figure 50). As with garnet, Nb–Ta depletions and, to some extent, other HFSE abundances depend on the coexistence of rutile (Jacob and Foley, 1999; Rudnick *et al.*, 2000; Barth *et al.*, 2001). The relatively homogenous REE patterns of eclogitic clinopyroxene contrast markedly with the wide variety of REE patterns observed in peridotitic clinopyroxene.

Rutile in eclogite xenoliths has highly variable niobium and tantalum concentrations that result in variable Nb/Ta (Rudnick *et al.*, 2000). In common with rutile in peridotites, that found within eclogites shows pronounced enrichment in tungsten, molybdenum, zirconium, and hafnium over silicate phases and this phase is clearly important in controlling the whole-rock budget of these elements plus titanium. Barth *et al.* (2001) note that secondary (metasomatic) rutiles in Koidu eclogites may be distinguished by their very high and heterogeneous niobium and tantalum contents (16,000 ppm Nb, 900–1,700 ppm Ta) plus occasional skeletal textures.

The partitioning of trace elements between clinopyroxene and garnet ($D^{cpx/gt}$) within different eclogite suites can vary by two orders of magnitude, depending on element compatibility. The correlation of $D^{cpx/gt}$ for trace elements with the molar calcium partition coefficient D_{Ca^*} indicates a high level of trace-element equilibrium in most eclogites up to the time of eruption

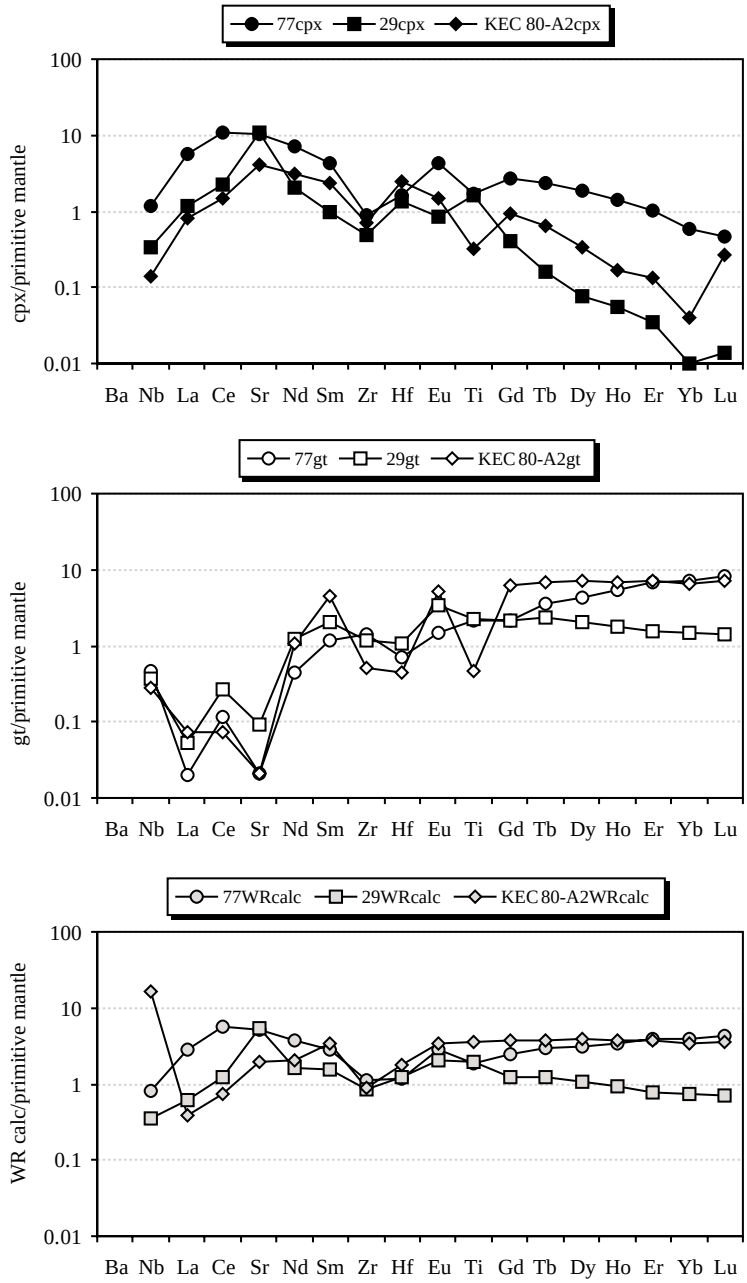

Figure 50 Garnet and clinopyroxene trace-element compositions (normalized to primitive mantle), together with their calculated whole-rock compositions (from modal data). Data sources: 77 and 29 are rutile-free eclogites from Udachnaya, Siberia (Jacob and Foley, 1999); KEC80-A-2 is a high-Nb-rutile eclogite from Koidu, Sierra Leone (Barth *et al.*, 2001).

(Harte and Kirkley, 1997). Differences in garnet–clinopyroxene partitioning behavior between the Roberts Victor and Koidu eclogite suites was attributed to the contrasting equilibration temperatures of the two suites by Barth *et al.* (2001).

Reconstructing whole-rock trace-element concentrations is the best way to avoid the effects of metasomatism, but careful account must be taken of any rutile present that can drastically affect HFSE budgets (Jacob and Foley, 1999; Rudnick *et al.*, 2000; Barth *et al.*, 2001). LREE depletion and very low HFSE abundances seem to be a characteristic of mostly rutile-free eclogites from Udachnaya (Siberia) and suggestive of protoliths originating in an island arc setting (Jacob and Foley, 1999). Positive strontium and europium anomalies and flat HREE profiles in these xenoliths are interpreted to reflect on origin as plagioclase-bearing plutonic rocks originally formed in ocean crust magma chambers

(Jacob and Foley, 1999; Barth *et al.*, 2003). Low-MgO rutile-bearing Koidu eclogites have LREE depleted but niobium-rich (up to 43 ppm) trace-element profiles (Figure 50) that Barth *et al.* (2001) cite as supporting a model where the eclogites are also residues of partial melting of altered, subducted oceanic crust, where the rutile is a residual phase during melting. Modeling of LREE/HREE systematics in the Koidu low-MgO suite suggests that they are the products of 15–40% batch melting of a basaltic protolith similar to Archean basalt. This range of melt extraction agrees with that required to produce Archean tonalitic crustal compositions as determined from eclogite melting experiments (Rapp and Watson, 1995). The relatively large degree of protolith melting also explains the lack/scarcity of coesite in Koidu low-MgO eclogites. Furthermore, the residual model firmly establishes a link between subduction and the generation of Archean continental crust (Ireland *et al.*, 1994; Rudnick *et al.*, 2000; Barth *et al.*, 2001).

For the high-MgO Koidu eclogites, trace-element modeling suggests a low-pressure origin for eclogites with flat HREE patterns and a high-pressure origin for eclogites with fractionated HREE. Flat HREE patterns, the presence of strontium anomalies, and low to moderate transition element contents in the low-*P* group are consistent with a low-pressure origin as metamorphosed olivine gabbros and troctolites (Barth *et al.*, 2003).

Calculated bulk rock trace-element systematics of eclogites have wider implications for mantle recycling models and bulk silicate earth mass balance. The subchondritic Nb/Ta, Nb/La, and Ti/Zr of both continental crust and depleted mantle require the existence of an additional reservoir with superchondritic ratios to complete the terrestrial mass balance. Rudnick *et al.* (2000) have shown that rutile-bearing eclogites from cratonic mantle have suitably superchondritic Nb/Ta, Nb/La, and Ti/Zr such that if this component formed 1–6% by weight of the bulk silicate earth, this would resolve the mass imbalance. This mass fraction far exceeds the likely mass of eclogite in the continental lithosphere and so the material is proposed to reside in the lower mantle, possibly at the core–mantle boundary.

2.05.3.5 Isotopic Characteristics

2.05.3.5.1 Stable isotopes

The small magnitude of oxygen isotope fractionation at mantle temperatures and pressures, together with the constancy of peridotite oxygen isotope compositions make oxygen isotopes a powerful tool for identifying recycled crustal material in the mantle. Although early studies found that some eclogite xenoliths had highly unusual oxygen isotope compositions (Garlick *et al.*, 1971), it was not until isotopic studies of hydrothermally altered basalts from ophiolite suites that the eclogite signatures were interpreted as an indication of a crustal prehistory for these rocks (Jagoutz *et al.*, 1984). Such data, along with their omphacitic pyroxenes, are some of the strongest evidence against models of eclogite xenoliths as directly crystallized moderate/high-pressure mantle melts. All seven suites of kimberlite-derived eclogites analyzed so far are found to have widely varying mineral $\delta^{18}O$ values that significantly exceed the range shown by olivine (5.18 ± 0.27 per mil) from mantle peridotite (Figure 51). Older analyses performed by conventional fluorination have been confirmed with laser fluorination methods, the laser-data showing more systematic garnet–clinopyroxene fractionations (Figure 51). No other mantle materials have such diverse oxygen isotopic compositions. Thus, while Snyder *et al.* (1997) choose to emphasize the great petrological and geochemical diversity shown by eclogites in general, that make their precise evolution difficult to constrain, a crustal origin for many of these rocks seems clear (Jagoutz *et al.*, 1984; MacGregor and Manton, 1986; Neal *et al.*, 1990; Jacob *et al.*, 1994, 1998b; Jacob and Foley, 1999).

The wide range in $\delta^{18}O$ is shown by both garnets and omphacite. The two minerals show the expected equilibrium fractionation relationship for both diamondiferous and nondiamondiferous samples (Figure 51). This range in $\delta^{18}O$ is considerably larger than that of garnet–diopside pairs from garnet lherzolites (Figure 51). Although it is possible to appeal to metasomatic fluids as the origin of these anomalous signatures, it is notable that metasomatic phases in mantle peridotites have oxygen isotope compositions nearly identical to nonmetasomatic minerals and in the typical mantle range. In addition, it is likely that such fluids would be rapidly buffered to the oxygen isotope composition of mantle peridotite during their movement. Hence, the generally accepted interpretation of the eclogite xenolith oxygen isotope signatures is that they represent a protolith that experienced alteration processes in the crust before subduction into the mantle.

The range in $\delta^{18}O$ values of eclogites is taken to reflect derivation from different portions of the oceanic lithosphere that underwent hydrothermal alteration at varying temperatures. Eclogites with $\delta^{18}O$ below typical mantle values are inferred to be derived from oceanic lithosphere that experienced high-temperature alteration (greenschist to amphibolite conditions; $<450\,^{\circ}C$), whereas those with $\delta^{18}O$ values above typical mantle values are interpreted as having experienced

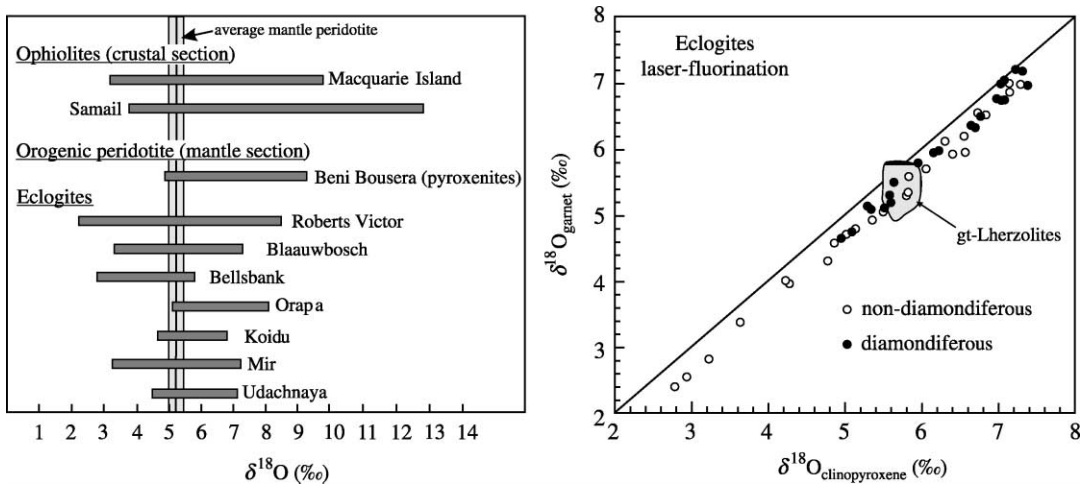

Figure 51 Figure on the left-hand side shows range in $\delta^{18}O$ values for eclogitic minerals from various kimberlites from Africa and Russia (Yakutia) compared with data for pyroxenites from the Beni Bousera peridotite massif (Pearson *et al.*, 1991) and hydrothermally altered rocks from ophiolites (after Jacob and Foley, 1999). The reference line is for average olivine from mantle peridotite (Mattey *et al.*, 1994), shaded zone is 2 SD. Data sources: Udachnaya—Jacob *et al.* (1994), Snyder *et al.* (1997), Mir—Beard *et al.* (1996), Orapa—Viljoen *et al.* (1996), Bellsbank—Neal *et al.* (1990), Blaauwbosch—Schulze *et al.* (2000), Roberts Victor—Garlick *et al.* (1971), Jagoutz *et al.* (1984), Ongley *et al.* (1987), MacGregor and Manton (1986), Schulze *et al.* (2000), Shirey *et al.* (2001), Koidu—Barth *et al.* (2001). Figure on the right-hand side shows $\delta^{18}O$ garnet versus $\delta^{18}O$ clinopyroxene for eclogites analyzed by laser-fluorination compared with the restricted field for garnet lherzolites (after Jacob *et al.*, 1998b). Garnet lherzolite field from Mattey *et al.* (1994).

low-temperature seafloor alteration prior to subduction (MacGregor and Manton, 1986; Jacob and Foley, 1999). Pearson *et al.* (1991) found similarly variable oxygen isotope compositions in garnet pyroxenites from the Beni Bousera orogenic peridotite that they also proposed reflected an origin via high-pressure crystallization from melts of subducted oceanic crust.

Correlations between $\delta^{18}O$ and major or trace elements have been observed at Udachnaya and other eclogite suites (Jacob *et al.*, 1998b) that simulate the variations expected on either side of the mantle $\delta^{18}O$ tie point for seawater alteration processes. Differences in oxygen isotope systematics between eclogite suites exist. For example, eclogites from the Udachnaya kimberlite do not have $\delta^{18}O$ values that extend to the low values found at Roberts Victor or Bellsbank, or even close-by Mir (Figure 51). Those from Orapa are predominantly higher in $\delta^{18}O$ compared to typical mantle. Coesite eclogites from Roberts Victor tend to have $\delta^{18}O$ values closer to "ordinary mantle" and are interpreted to represent the metamorphosed equivalents of deep-oceanic crustal cumulates that escaped significant hydrothermal alteration (Schulze *et al.*, 2000). In this context, Jacob and Foley (1999) point out that "ordinary mantle" oxygen isotope compositions can still be preserved in samples undergoing hydrothermal alteration when the hydrothermal fluid is in equilibrium with the rock, i.e., the system is rock-buffered.

2.05.3.5.2 Radiogenic isotopes

The high modal abundance of both garnet and clinopyroxene in eclogites combined with the appreciable amounts of neodymium that these phases contain means that the composition of both phases must be considered when discussing the Sr–Nd isotope systematics of eclogites. All data discussed here are calculated bulk rock values that account for this mass balance, but we use only the strontium isotope composition of the clinopyroxene because the very low strontium content of garnet make it susceptible to modification by the host magma. Compilation of these calculated bulk rock values show that eclogite xenoliths possess some of the most extreme radiogenic isotope compositions of terrestrial rocks. This feature is testament to their antiquity and to the variety of processes that they have experienced during their evolution. Some samples have the most radiogenic neodymium isotopic compositions of any rocks yet measured (Figure 52), with ε_{Nd} values in excess of 500 for garnets and differences of over 200ε units between coexisting garnet–pyroxene pairs (Jagoutz *et al.*, 1984). Garnet and pyroxene vary from being close to isotopic equilibrium at the time of kimberlite eruption (Snyder *et al.*, 1993) to being in gross disequilibrium. The relatively undisturbed REE systematics observed in garnet and pyroxene for most samples indicates that any isotopic disequilibrium is probably due to radiogenic in-growth following cooling through

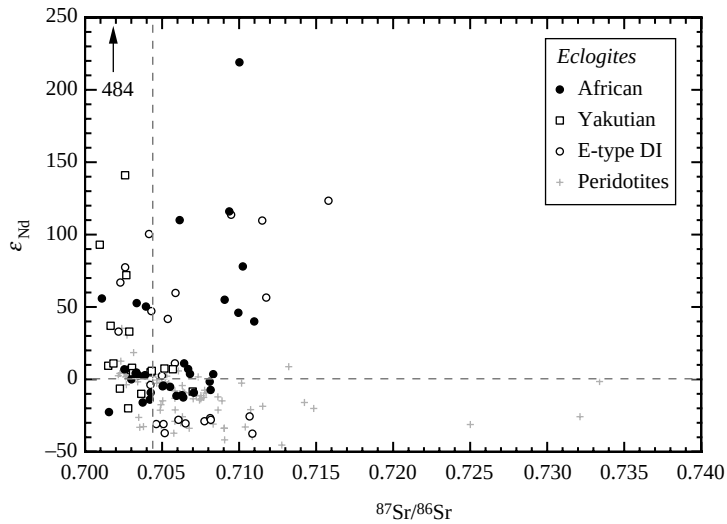

Figure 52 Initial $\varepsilon_{Nd}-\varepsilon_{Sr}$ isotope plot of calculated whole-rock eclogites from Africa (Koidu—Hills and Haggerty, 1989; Orapa—Smith *et al.*, 1989; Viljoen *et al.*, 1996; Roberts Victor—Jagoutz *et al.*, 1984; Smith *et al.*, 1989; Jacob and Jagoutz, 1994; Bellsbank—Neal *et al.*, 1990), Yakutia (Snyder *et al.*, 1993; Jacob *et al.*, 1994; Pearson *et al.*, 1995a; Snyder *et al.*, 1997), and eclogitic inclusions in diamonds (Richardson, 1986; Richardson *et al.*, 1990; 1999; Smith *et al.*, 1991). Eclogite data are initial calculated whole-rock neodymium isotope compositions. Strontium isotope compositions are from clinopyroxene only. Cratonic peridotite minerals and diamond inclusions are plotted for comparison. Arrow points to a sample from Udachnaya that has a calculated initial ε_{Nd} of 484. dashed lines are bulk Earth values.

the Sm–Nd blocking temperature for this system. This must have taken place over 2 Ga ago for some samples.

The Nd–Sr isotope variations of calculated whole-rock African and Yakutian eclogites greatly exceed those of magmas produced from the modern-day convecting mantle and occupy all four quadrants of the diagram (Figure 52). Some samples show very unradiogenic strontium and highly radiogenic neodymium that result from ancient time-integrated low Rb/Sr and high Sm/Nd that are unlike any magmatic rocks. Such characteristics might be compatible with pyroxene–garnet cumulates crystallized from high-pressure melts. However, their mineral chemistry and oxygen isotope composition make a crustal prehistory more likely. The depleted Nd–Sr isotope compositions and their calculated high bulk Sm/Nd ratios could arise if the rocks were metamorphosed oceanic-crustal cumulates, or residues from the melting of basaltic/picritic protoliths during subduction, or both.

A number of eclogites have both radiogenic neodymium isotopes and radiogenic strontium relative to bulk Earth. For these samples, some of the $^{87}Sr/^{86}Sr$ values exceed modern and Archean seawater compositions (see Chapter 6.17). Hence, in a subduction-type model, the radiogenic strontium isotopic composition of the eclogite protolith is not solely inherited from oceanic crust but is likely to be a time-integrated response to Rb/Sr enrichment during hydrothermal alteration in the oceanic crust that did not alter Sm/Nd significantly. This creates radiogenic strontium isotopic compositions without significantly altering neodymium isotopic compositions. Viljoen *et al.* (1996) propose some sediment incorporation during subduction to explain the enriched neodymium and strontium isotopic compositions of eclogites from Orapa, Botswana. Eclogite-suite inclusions in diamonds show similar variation and systematics to eclogite xenoliths. The diamond inclusions show evidence for seawater-like strontium isotope signatures and enriched neodymium isotope systematics that may be evidence of sediment incorporation (Figure 52). In contrast, inclusions in Finsch and Orapa diamonds show considerably less radiogenic neodymium isotopic compositions than xenoliths from the same locality. In these cases, the xenoliths may have been subject to open-system metasomatic behavior compared with the inclusions. Viljoen *et al.* (1996) interpret the radiogenic strontium and highly unradiogenic neodymium isotopic compositions of eclogitic diamond inclusions as a possible result of diamond genesis in a protolith consisting of subducted basalt and sediment. Although not well constrained at the moment, this interpretation is consistent with the osmium isotope systematics of eclogitic diamond inclusion sulfides (Pearson *et al.*, 1998b; Richardson *et al.*, 2001). The strontium isotope compositions of eclogite xenoliths do not extend to the extreme values observed in some peridotites, or peridotitic

mineral concentrates (Figure 52), perhaps reflecting the differing nature or extent of metasomatic processes experienced by these lithologies. These differences may also reflect the likely different origins of the phases in peridotite and eclogite xenoliths.

Mazzone and Haggerty (1989) have reported highly radiogenic $^{87}Sr/^{86}Sr$ values in garnets from alkremites of 0.780 to 0.805 that are unsupported by their Rb/Sr ratios. They propose that these compositions are inherited from pelitic crustal protoliths subducted beneath the margin of the Kaapvaal craton and the Rb/Sr lowered by partial melting during subduction. In summary, the Nd–Sr isotope compositions of eclogite xenoliths and related rocks are compatible with a varied history that likely involves crustal protoliths for many and may also reflect the superimposed effects of ancient and/or recent mantle metasomatic effects.

There are few measurements of hafnium isotopes in eclogites. The first data are for samples from the Roberts Victor kimberlite (Jacob *et al.*, 2002) and indicate extreme hafnium isotope variability. Initial ε_{Hf} values (calculated to the time of kimberlite eruption) vary from −9.2 to 166, with correspondingly variable initial ε_{Nd} values (−22 to 484). The samples mostly plot well below the mantle Nd–Hf isotope array. Jacob *et al.* (2002) point out that the good correlation between neodymium and hafnium isotopes in modern terrestrial basalts indicates that the contribution of eclogite melts from the lithosphere to these magmas has been minor. Nowell *et al.* (2003) have reported that some alkremite garnets have extremely radiogenic Hf isotopic compositions. Alkremites from South African kimberlites have ε_{Hfi} ranging from 0 to +60 at restricted ε_{Ndi} values of 0 to +2. Two alkremites from Udachnaya, Siberia have ε_{Hfi} ranging from +145 to +24,960, the latter value being the most radiogenic Hf isotope composition so far, reported for any mantle mineral. The relatively ordinary ε_{Ndi} values of −7.5 to −11 indicate that significant decoupling of Sm–Nd and Lu–Hf isotope systems has occured during alkremite formation and evolution.

Lead isotope determinations on eclogite minerals are few. Surprisingly, there are no lead isotope analyses reported for rutile within eclogites, despite the high U/Pb of this phase. Over 90% of the lead in most rutile-free eclogites is contained within their clinopyroxenes (Jacob and Foley, 1999) and hence this is the most frequently analyzed phase. $^{206}Pb/^{204}Pb$ ranges from ~15.5 to 18.5 in clinopyroxenes from Udachnaya eclogites, spanning either side of the Geochron on a $^{206}Pb/^{204}Pb$ versus $^{207}Pb/^{204}Pb$ plot (Figure 53). The correlation defines a linear array that can be interpreted as having age significance (see below).

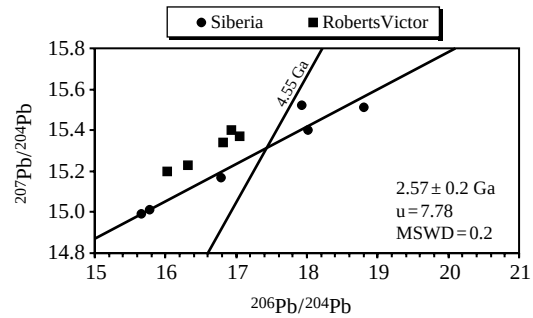

Figure 53 $^{207}Pb/^{204}Pb$ versus $^{206}Pb/^{204}Pb$ isotope compositions of eclogite xenolith clinopyroxenes. The regression line passes through clinopyroxene separates from eclogites of the Udachnaya kimberlite that define a Pb–Pb isochron age of 2.6 ± 0.2 Ga (Jacob and Foley, 1999). Other data points are clinopyroxene separates from Roberts Victor eclogites (Jacob and Jagoutz, 1994). The 4.55 Ga line is the geochron.

Clinopyroxenes from Roberts Victor eclogites generally plot to the left of the Geochron, with very unradiogenic $^{206}Pb/^{204}Pb$, indicative of time-integrated low U/Pb and consistent with the very low time-integrated Rb/Sr suggested by $^{87}Sr/^{86}Sr$ values of <0.702 for some of these samples (Jagoutz *et al.*, 1984). There is no simple relationship between lead and strontium isotopic compositions in the Udachnaya suite analyzed by Jacob *et al.* (1994) and Jacob and Foley (1999), probably reflecting the multistage histories of most of these rocks that may decouple isotope systems with differing geochemical affinities.

In addition to having the most radiogenic neodymium isotopic compositions of any mantle rocks, eclogites commonly have highly radiogenic osmium isotope signatures (Pearson *et al.*, 1992, 1995c; Menzies *et al.*, 1999; Shirey *et al.*, 2001; Barth *et al.*, 2002). Initial γ_{Os} values range from close to chondritic to >6,500 (Figure 54) are similar to values measured for Archean basalts and komatiites:

$$\gamma_{Os}(t) = \left[\left(^{187}Os/^{188}Os_{sample(t)}/ \; ^{187}Os/^{188}Os_{chondrite(t)}\right) - 1\right] \times 100$$

Eclogite osmium isotope compositions are indicative of long-term evolution with basaltic/picritic Re/Os.

2.05.3.5.3 The age of eclogites

Pioneering work by Holmes and Paneth (1936) using the U–He system first recognized that eclogites were likely to be much older than their host kimberlites. More recent work has been able to provide firmer constraints. The huge isotopic diversity of eclogites immediately suggests an

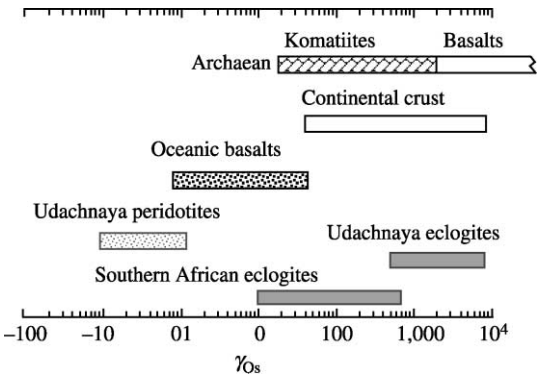

Figure 54 Comparison of present-day osmium isotopic compositions of eclogite xenoliths from Udachnaya, Yakutia (Pearson *et al.*, 1995c) and S. Africa (Pearson *et al.*, 1992; Menzies *et al.*, 1999; Shirey *et al.*, 2001) with continental crust, oceanic basalts (Shirey and Walker, 1998), and Archean komatiites and basalts (Walker *et al.*, 1989b). Udachnaya peridotite data from Pearson *et al.* (1995a).

ancient age for many samples. Jagoutz *et al.* (1984) obtained a 2.7 ± 0.1 Ga isochron age from the calculated bulk compositions of Roberts Victor eclogites. At other localities the Sm–Nd system does not yield easily interpretable age systematics, possibly due to minor metasomatic and partial melting effects during eruption. The large spread in $^{187}Os/^{188}Os$ and Re/Os within eclogite suites makes them amenable to dating using this system. Pearson *et al.* (1995c) found that whole-rock analyses of eclogites from Udachnaya (Yakutia) defined a Re–Os isochron relationship with an age equivalent to 2.9 ± 0.4 Ga. The elevated initial osmium isotope composition of the isochron is further evidence of a crustal prehistory prior to incorporation into the deep lithospheric mantle. This age is within error of the Pb–Pb isochron age defined by clinopyroxene separates from Udachnaya eclogites (Jacob and Foley, 1999; Figure 53) and confirms an Archean age for eclogites from this kimberlite. A less well-defined but clearly Archean age was also determined for eclogites from Newlands (S. Africa) by Menzies *et al.* (1999). Barth *et al.* (2002) also report a mid-Archean Re–Os isochron age for low-MgO Koidu eclogite samples. Recently, Shirey *et al.* (2001) have noted Re–Os isotope systematics of eclogite xenoliths from Roberts Victor and eclogitic-suite sulfide inclusions in diamonds from Koffiefontein, Kimberley and Orapa that are all indicative of Archean ages of ~3 Ga, implying Archean subduction and emplacement of eclogitic components into the lithosphere at this time.

The Archean age of the eclogite xenolith suites that have clear crustal signatures in their elemental, stable and radiogenic isotope compositions makes a very powerful case for plate tectonics operating in the late Archean Earth (Jagoutz *et al.*, 1984; Jacob *et al.*, 1994; Pearson *et al.*, 1995c). Late Archean ages for eclogites, coupled with their major and trace-element systematics indicating loss of a SiO_2-rich melt fraction, have provided a clearer picture of the nature of Archean continental crust generation (Ireland *et al.*, 1994; Barth *et al.*, 2001, 2002).

2.05.4 DIAMONDS

2.05.4.1 Introduction

This section is restricted to the natural occurrences of macrodiamonds from the mantle and their implications for the geochemistry and evolution of the mantle. Diamonds are discrete mantle samples, typically forming in peridotite and eclogite lithologies within the Archean subcontinental lithospheric mantle (Table 1(a)). Diamonds, occurring in kimberlite alongside xenoliths, often contain pristine inclusions of mantle minerals and thus comprise an important source of information about the mineralogy of the lithospheric mantle from which xenoliths are derived (Meyer, 1987; Section 2.05.4.5). This sample is free from the crustal alteration effects that occur in xenolith studies. The relatively recent discovery that some diamonds originate from the Earth's transition zone and the top of the lower mantle (e.g., Scott-Smith *et al.*, 1984; Kerr, 1993; Harte *et al.*, 1999b) holds the promise that diamonds will be the deepest geochemical probes of the mantle (Section 2.05.4.6).

Due to diamond's economic importance and its unique properties, a formidable literature exists with more than 3 times the number of articles published than for mantle xenoliths. Review articles on diamond include articles on diamond geology and genesis (Haggerty, 1986; Gurney, 1989; Kirkley *et al.*, 1991; Harris, 1992; Haggerty, 1999); age dating of diamond (Pearson and Shirey, 1999); diamond inclusions (Harris and Gurney, 1979; Meyer, 1987), and diamond formation in the mantle (Navon, 1999). Reviews of the very extensive literature on the physics, chemistry, economic applications and geology of diamonds can be found in Field (1979, 1992), J. Wilks and E. Wilks (1991), and Harlow (1998).

2.05.4.1.1 Occurrence

Diamond, especially micro- and nanodiamond, is a widely occurring mineral and is probably one of the most abundant forms of carbon in the Galaxy (Alexander, 2001; Allamandola *et al.*, 1993). As such, its geochemistry has implications

for both terrestrial and extraterrestrial processes. Diamond is found in meteorites as presolar grains (Fukunaga *et al.*, 1987; Lewis *et al.*, 1987) or shock-related metamorphic minerals (Lipschutz, 1964; Lipschutz and Anders, 1961) and it occurs in high-pressure metamorphic terranes (Rozen *et al.*, 1973; Sobolev and Shatsky, 1990; Xu *et al.*, 1992; Pearson *et al.*, 1995d). Macrodiamonds can occur in polycrystalline aggregates such as framesite or carbonado and as single crystals. Carbonado, a porous, black, irregularly shaped aggregate, occurs alluvially and bears an unclear relationship to the mantle (De *et al.*, 1998; Trueb and Wys, 1969). Framesite, a nonporous, polycrystalline diamond aggregate, occurs in kimberlite and has recently become recognized as a potential recorder of secondary processes in the lithosphere (Burgess *et al.*, 1998; Jacob *et al.*, 2000). Macrodiamond pseudomorphs have been found in orogenic lherzolite (Pearson *et al.*, 1989) and metamorphic eclogite (Shumilova, 2002).

Macrodiamonds occur chiefly as discrete crystals in kimberlite. The association with Archean cratons and kimberlites is strikingly clear on both a local and global scale (Janse, 1985, 1992; Levinson *et al.*, 1992), although there are isolated occurrences of diamondiferous lamproite and diamonds associated with Proterozoic cratons such as the Argyle pipe (e.g., Jaques *et al.*, 1989). Whether isolated diamonds grew in equilibrium with the kimberlite magma (as phenocrysts) or were incorporated from disaggregated lithospheric mantle country rock (as xenocrysts) remained an open question since almost the 1920s, even though the Archean cratonic association for diamond and the young eruptive age of kimberlite suggested a xenocrystal origin. The first radiometric ages on syngenetic inclusions in diamond (Kramers, 1979; Richardson *et al.*, 1984) showed that Archean diamonds occur in Cretaceous kimberlites and firmly established diamonds as xenocrysts. Subsequent work on dating diamonds over the last two decades (Section 2.05.4.5.2) has established that most, but not all, macrodiamonds are xenocrysts and are Archean or Proterozoic in age (e.g., Pearson and Shirey, 1999). An association between Archean cratons and lithospheric carbon in general, including graphite at lower pressures, has been noted by Haggerty (1986, 1999) and Pearson *et al.* (1994).

Peridotitic lithologies comprise more than 95% of the mantle lithosphere (Schulze, 1989). Thus, macrodiamonds in kimberlite are believed to come from mostly peridotitic hosts that break up during the sampling or transport that accompanies kimberlitic volcanism. Sobolev (1974) and Hatton and Gurney (1979) noted the dichotomy that peridotite xenoliths greatly outnumber eclogite xenoliths and peridotitic silicate inclusions in diamond predominate over eclogitic, yet diamondiferous eclogites are much more common than diamondiferous peridotites.

Most of the *in situ* studies of diamonds in xenolith hosts have thus been on diamondiferous eclogites. Occasional diamondiferous eclogites are so diamond-rich it is tempting to ascribe all the diamonds in some eclogite–xenolith-rich kimberlite to eclogite disaggregation alone. However, where the carbon isotopes of both diamond xenocrysts and diamonds within eclogite xenoliths have been analyzed (e.g., Deines *et al.*, 1987) it is clear there are additional noneclogite sources for the diamond xenocrysts, presumably from disaggregated peridotite. Initial studies of diamond in host eclogite concentrated on the inhomogeneities of diamond distribution and the relationship of diamond to metamorphic layering. Recent advances in computer assisted tomographic scanning have allowed diamonds to be located within an eclogite before it is sawed or crushed (e.g., Schulze *et al.*, 1996). In some eclogites, diamond lies preferentially along veins (Taylor *et al.*, 2000), which has sparked a lively debate over the degree to which diamond is a secondary phase introduced into the eclogite or a primary metamorphic phase crystallized from the originally included carbon in the eclogite.

2.05.4.1.2 Diamond morphology

The chemistry of diamond is a strong function of its growth form. The systematics of diamond growth and the factors influencing it have been reviewed by Gurney (1989), J. Wilks and E. Wilks (1991), Harris (1992), Bulanova (1995), Mendelssohn and Milledge (1995), and Harlow (1998).

Single-crystal macrodiamonds can take many forms such as the cube, the cuboctahedron, the dodecahedron and the trisoctahedron but the octahedron is the most common (Harlow, 1998). Experimental diamond synthesis has established that diamond morphology is a function of the pressure and temperature of growth. Octahedra are the high-temperature growth form, whereas cubo-octahedra grow at lower temperatures (J. Wilks and E. Wilks, 1991). An important determinant of external morphology is dissolution, presumably in the lithosphere or in kimberlitic magma during transport to the surface, which produces rounded variants of the above forms and numerous etch features on the diamond surface such as trigons (Mendelssohn and Milledge, 1995; J. Wilks and E. Wilks, 1991).

Study of the internal morphology of macrodiamond with X-ray topography (e.g., J. Wilks and E. Wilks, 1991, figures 5.32–5.36), optical microscopy and especially cathodoluminescence

(e.g., Bulanova, 1995, figures 2–9) reveals a complicated growth/resorption history in many gem-quality stones. Knowledge of such complexity has become crucial over the years as analytical sensitivity has improved and spot analyses have become possible for many spectroscopic (FTIR), crystallographic (analytical SEM), elemental (EPMA, PIXE), and isotopic (SIMS) analytical techniques. Such detail will lead to more accurate geochemical models of natural macrodiamond growth that will account for local changes in diamond-forming fluid composition (Sections 2.05.4.3 and 2.05.4.4).

2.05.4.1.3 Diamond types and classification

Diamonds can be classified by morphologic shape, size, and color (e.g., Harris, 1992). For geochemistry, the most useful classifications are those based on the content and lattice-substitutional state of the most abundant impurity in diamond, nitrogen, or the affinity of the diamond to either of the two dominant diamond host lithologies peridotite (lherzolite–harzburgite) or eclogite (Table 1(a)). The classification of diamond types by their nitrogen content is covered succinctly by Harlow (1998) and, in more detail, by Evans (1992) and J. Wilks and E. Wilks (1991). Low-nitrogen diamonds (<10 ppm) are termed type II and higher nitrogen diamonds (10–3,000 ppm) are termed type I. Type I diamonds are termed Ia if nitrogen is distributed in the crystal lattice as polyatomic aggregates and Ib if it is distributed as single atoms. Natural macrodiamonds are about 98% type Ia, 0.1% type Ib, and 2% type II. In microdiamond populations, type II is more common (Harlow, 1998). The nitrogen classification system can be applied to virtually any diamond.

To relate diamonds to their host lithologies in the lithospheric mantle, the diamond classification based on inclusion paragenesis has been the most useful. Inclusions in diamond can grow at the same time as the diamond (syngenetic) or predate the diamond (protogenetic, see Meyer, 1987; Bulanova, 1995; Pearson and Shirey, 1999). Most work has been done on inclusions thought to be syngenetic and discussions concerning inclusions in this chapter will be confined to this type. Silicates and sulfides comprise the two most abundant inclusion mineral groups and each inclusion group has affinities with the minerals in eclogite or peridotite xenoliths in kimberlite (Table 1). Diamonds are classified as peridotitic or "P-type" (or U-type by some workers, e.g., Sobolev *et al.*, 1998) when they contain Cr-pyrope, diopside, enstatite, chromite, or olivine (Harris and Gurney, 1979; Meyer, 1987; Meyer and Boyd, 1972). P-type diamonds can be further subdivided into harzburgitic or lherzolitic by the degree of depletion indicated by the Cr_2O_3 and CaO content of their included garnet (e.g., Harris and Gurney, 1979). Diamonds are classified as eclogitic or "E-type" when they contain pyrope-almandine garnet, omphacite, coesite, or kyanite. A similar E versus P paragenetic distinction has been applied to sulfide inclusions but with additional uncertainties stemming from sulfide exsolution, identification within the diamond (sulfides are opaque and also create internal fractures in the host diamond that obscure the inclusion) and rarity of coexisting silicates and sulfides. Nonetheless peridotitic sulfides from the Siberian craton typically contain nickel contents greater than 22.8 wt.%, whereas eclogitic sulfides typically have less than 8 wt.% (Yefimova *et al.*, 1983). Such a clear break between E- and P-type sulfides has not yet been established for inclusions in Kaapvaal craton diamonds (Deines and Harris, 1995; Harris and Gurney, 1979). Sulfides from pyroxenite assemblages also complicate the situation (Pearson *et al.*, 1999b).

2.05.4.2 Nitrogen in Diamond

The chief geological significance of nitrogen in diamond is because its abundance and distribution contains a record of the partitioning of nitrogen during diamond growth from the original diamond-forming fluid. Furthermore, the nitrogen aggregation state reflects a time-temperature history that relates to diamond storage in the lithospheric mantle. Diamond's resistance to metamorphism, coupled with the ancient age of many diamonds, may provide an estimate of the nitrogen content of the early Earth's mantle.

Specialized sample preparation techniques such as etching have long revealed complex zoning and resorption in natural macrodiamonds. Cathodoluminescence imaging (CL) and recent improvements in FTIR and SIMS sensitivity and resolution suggest that most macrodiamonds are zoned in nitrogen content and nitrogen aggregation (Bulanova, 1995; Bulanova *et al.*, 2002) and potentially in carbon and nitrogen isotopic composition (Hauri *et al.*, 2002; Bulanova *et al.*, 2002).

2.05.4.2.1 Nitrogen abundance

Nitrogen abundance in diamonds is an integrated reflection of the nitrogen content of the diamond-forming fluids in the mantle, changes in fluid evolution during diamond growth and possible changes in the diamond/fluid partition coefficient. Detailed studies of nitrogen abundances have been made for diamond populations

from individual kimberlite mines in southern Africa, particularly such as the De Beers Pool, Finsch, Jagersfontein, Jwaneng, Koffiefontein, Orapa, Premier, and Roberts Victor mines. These studies have shown, in general, that diamonds with E-type silicate inclusions have higher nitrogen content than diamonds with P-type silicate inclusions (Cartigny *et al.*, 1998a, 2001; Deines *et al.*, 1987, 1991a, 1993, 1989). The combined data from these mines are shown in Figure 55. Kaapvaal P-type diamonds rarely have more than 400 ppm nitrogen (Figure 55), whereas Kaapvaal E-type diamonds have almost a bimodal distribution with at least a third of the population having nitrogen concentrations above 400 ppm. Similarly, mines that have diamonds where E-types predominate have systematically lower proportions of type II diamonds (Shirey *et al.*, 2002). This difference could be due to a higher nitrogen content in the diamond source fluid of E-type diamonds. However, the high nitrogen content of fibrous diamonds (average = 900 ppm N) compared to P-type diamonds has been used to argue for strong dependence on nitrogen partitioning on diamond growth rate (Cartigny *et al.*, 2001). Using this rationale, the higher nitrogen contents of E-type diamonds would be a result of their faster growth rate compared with P-type diamonds.

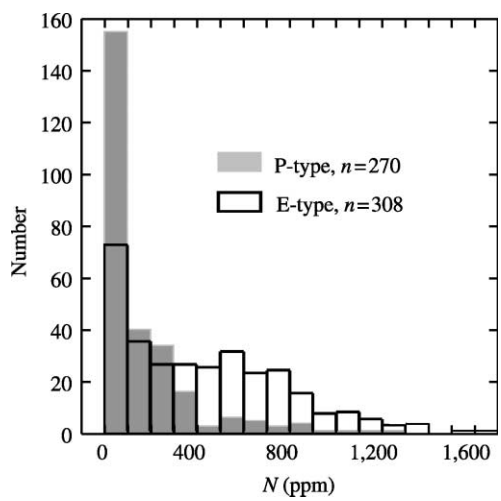

Figure 55 The nitrogen content (ppm) of diamonds of P-type and E-type parageneses. The number of total specimens is given for each group ($n = 578$). P-type diamonds (number analyzed in parens) are from these kimberlites: DO-27 (15), Finsch (66), Jagersfontein (13), Jwaneng (17), KanKan (13), Koffiefontein (27), Orapa (21), Premier (33), and Roberts Victor (65). E-type diamonds are from the following kimberlites: Argyle (20), DO-27 (10), Finsch (9), Jagersfontein (13), Jwaneng (74), KanKan (15), Koffiefontein (19), Orapa (56), Premier (76), Roberts Victor (14), and Sao Luiz (2) (sources Cartigny *et al.*, 1998a, 1999; Davies *et al.*, 1999; Deines *et al.*, 1987, 1989, 1991a,b, 1993, 1997; van Heerden *et al.*, 1995; Stachel *et al.*, 2002).

Current debate centers on whether nitrogen abundance variations in diamonds reflect the primary nitrogen content of the diamond-forming fluid or are controlled by effects more local to the site of diamond growth in the mantle, such as diamond growth rate or *in situ* changes in nitrogen content of the fluids by differentiation (see also Section 2.05.4.3.3). If nitrogen abundance is dominantly a source effect then the nitrogen content of diamonds might relate to geological processes and could lead to an understanding of the nitrogen content of the ancient mantle. If kinetic and crystallographic effects dominate then detailed nitrogen studies will lead to a better understanding of how diamonds form and grow.

In studies where nitrogen abundance has been determined by both FTIR and SIMS techniques, the agreement between the resulting concentrations is variable (Harte *et al.*, 1999a; Bulanova *et al.*, 2002; Hauri *et al.*, 1999, 2002). The agreement depends on how complex growth zonation and nitrogen distribution are and how well the sample preparation method (polished plate or fragment/chip) samples these variations. The FTIR technique provides an integrated signal through the entire thickness of the sample plate. The SIMS technique measures the signal from material sputtered from a few microns, at most, of the diamond surface. The SIMS technique thus has the potential to make more detailed studies of nitrogen distribution, but cannot measure nitrogen aggregation.

2.05.4.2.2 Nitrogen aggregation

The crystallographic distribution of nitrogen in the diamond lattice and its optical effects are described in detail by J. Wilks and E. Wilks (1991). Briefly, diamonds quenched rapidly in experiments contain single nitrogen atoms substituting randomly for single carbon atoms (diamond type Ib; Evans and Zengdu, 1982). This is extremely rare in natural diamonds. In the mantle, aggregation starts with paired nitrogen atoms (A-centers, diamond type IaA) and progresses ultimately to fourfold clusters of nitrogen atoms with an accompanying vacancy (B-centers, diamond type IaB; Evans, 1992; Evans and Zengdu, 1982; Taylor *et al.*, 1990). Many diamonds are intermediate between these two end-members and show a mix of A and B centers (diamond type IaA/B) which may be accompanied by N3 centers (threefold nitrogen and a vacancy) and platelets (Evans, 1992; Evans and Zengdu, 1982). Nitrogen aggregation is driven by time,

temperature, and nitrogen content. For diamond populations of similar nitrogen content and age, those with a lesser percentage of highly aggregated nitrogen (e.g., IaB diamonds) are more likely to have resided in cooler lithosphere, whereas diamonds with a higher type IaB nitrogen aggregation state are more likely to have resided in warmer lithosphere. Navon (1999) has made the case that, because temperature is the most important variable in nitrogen aggregation, the process of nitrogen aggregation in diamonds makes an excellent geothermometer for residence times in the upper mantle of greater than 200 Ma.

In general, temperatures for diamond storage in the lithospheric mantle obtained with nitrogen aggregation studies agree surprisingly well with traditional mineral geothermometers in the temperature range of 1,050–1,200 °C (Evans and Harris, 1989; Harris, 1992; Navon, 1999). Similarly, in studies of Archean diamonds where ages were determined on inclusions in diamond and nitrogen aggregation measured on the diamond hosting the inclusions (Pearson *et al.*, 1998, 1999a; Richardson and Harris, 1997) the ages obtained are typically supported by the advanced aggregation state of the nitrogen in the host diamond.

This applies to diamonds where inclusions give both ancient and young ages. For instance, a young P-type diamond dated from the Koffiefontein kimberlite had poorly aggregated nitrogen (Pearson *et al.*, 1998b), consistent with a short mantle residence time. Furthermore, fibrous diamond coats, thought to be much younger than their octahedral cores also have less aggregated nitrogen (Boyd *et al.*, 1987).

The chief problems with using nitrogen aggregation in natural diamonds come in accurately determining the activation energy of transition from A to B centre coupled with the time/temperature/N content tradeoffs (e.g., Evans and Harris, 1989). Also, FTIR measurements of complexly zoned diamonds, even in carefully prepared polished plates, may still integrate signals across different growth zones (e.g., Bulanova, 1995); Taylor *et al.* (1996) have quantified the kinetics of the Ib to IaA nitrogen aggregation step but further progress is required in this area.

2.05.4.3 Isotope Systematics of Diamond and its Impurities

2.05.4.3.1 Carbon isotopes

The carbon isotopic composition of diamonds has been studied for many years (e.g., Galimov *et al.*, 1978; Deines, 1980; Galimov, 1984). These early studies attempted to correlate diamond properties such as color and form with carbon isotopic composition in some form of classification scheme. These efforts have given way to using carbon isotopes in diamond to understand diamond formation and especially to examine the carbon geochemical cycle in the mantle focussing on the relative roles of recycled crustal carbon versus primordial carbon (Deines, 1980; Galimov, 1991; Gurney, 1989; Haggerty, 1999; Harris, 1992; Kirkley *et al.*, 1991; Navon, 1999).

There is a general relationship between carbon isotopic composition and diamond paragenesis as designated by inclusion chemistry (Sobolev *et al.*, 1979). Most P-type silicate inclusion-bearing diamonds show a narrow range in carbon isotopic composition of $\delta^{13}C = -5‰ \pm 4‰$ (Figure 56), a value that overlaps the carbon isotopic composition of the upper mantle as given by oceanic basalts, carbonatites, and kimberlitic carbonate (e.g., Cartigny *et al.*, 1998b). E-type diamonds show a wider range in $\delta^{13}C$ of $+3‰$ to $-34‰$ with a mode in their frequency distribution that is identical to the P-type diamonds at every locality. The carbon isotope frequency distribution of E-type diamonds at most localities is markedly skewed relative to that of P-type diamonds, usually towards isotopically light carbon values

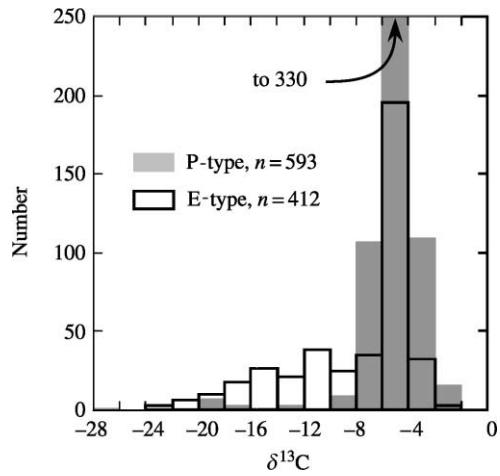

Figure 56 Comparison of the carbon isotopic composition ($\delta^{13}C$ in ‰) of diamonds of P-type and E-type parageneses. The total number of specimens is given for each group ($n = 1005$). Note that the −4 to −6 bar for P-type diamonds is off-scale at a number of 330. P-type diamonds are from these kimberlites: DeBeers Pool (125), DO-27 (14), Dokolwayo (41), Finsch (70), Jagersfontein (14), Jwaneng (20), KanKan (13), Koffiefontein (35), Orapa (22), Premier (34), Roberts Victor (65), and Venetia (140). E-type diamonds are from the following kimberlites: Argyle (24), DeBeers Pool (66), DO-27 (14), Dokolwayo (30), Finsch (10), Jagersfontein (18), Jwaneng (47), KanKan (15), Koffiefontein (20), Orapa (56), Premier (77), Roberts Victor (14), Sao Luiz (2), and Venetia (19). Data are taken from the references cited in Figure 55 caption and the following: Cartigny *et al.* (1998a), Daniels and Gurney (1999), Deines *et al.* (2001), and Hutchison *et al.* (1999).

but more rarely to isotopically heavy values. The carbon isotopic range for E-type diamonds spans a large part of the isotopic range seen for terrestrial carbon, from very light $\delta^{13}C$ values, characteristic of organic matter to heavy values similar to marine carbonate (Cartigny *et al.*, 1998b).

The carbon isotopic composition of diamonds has been explained by a variety of processes:

- intramantle isotopic fractionation during fluid transport and diamond growth (Deines, 1980; Galimov, 1991; Cartigny *et al.*, 2001);
- primoridal mantle heterogeneities (e.g., Deines *et al.*, 1987); and
- introduction of heterogeneous subducted carbon (e.g., Sobolev *et al.*, 1979; Kirkley *et al.*, 1991) as recently discussed by Navon (1999).

Carbon isotopic studies alone are not able to resolve the source of such carbon isotopic variability and the relative importance of these competing models. Thus, current approaches are to combine carbon isotopic studies with nitrogen abundance, aggregation, isotopic composition and even age determinations on the same diamonds (e.g., Hauri *et al.*, 1999, 2002).

2.05.4.3.2 Nitrogen isotopes

The application of nitrogen isotopic analyses to diamonds is well established by the early work of Javoy and co-workers (Javoy *et al.*, 1984; Javoy *et al.*, 1986), Boyd and co-workers (Boyd *et al.*, 1987, 1992; Boyd and Pillinger, 1994) and Cartigny and co-workers (Cartigny, 1998; Cartigny *et al.*, 1998a,b). The data set for nitrogen is less extensive than that for carbon, chiefly due to the lower abundance of nitrogen (nitrogen is a trace element at <10–1,000 ppm in diamond) and hence the need for lower analytical blanks (nitrogen is the major gaseous component of the atmosphere).

The nitrogen isotopic composition of diamonds shows more isotopic heterogeneity and does not display the clear paragenetic distinction evident in the frequency distribution of carbon isotopes. Except for the unusually large nitrogen isotopic range seen in P-type diamonds from Pipe 50, China (Cartigny *et al.*, 1997) and the "low $\delta^{13}C$ group" of Boyd and Pillinger (1994), P-type and E-type diamonds from many localities have an overlapping nitrogen isotopic range from $\delta^{15}N$ of −12‰ to +4‰ (Cartigny *et al.*, 1998b; Figure 57). This range is isotopically identical to that of the modern terrestrial depleted upper mantle as measured in ocean ridge basalts (Javoy *et al.*, 1986; Marty and Zimmerman, 1999). Close examination of the diamond nitrogen data allows a crude paragenetic distinction to be made. Nearly all diamonds that are light in carbon isotopic composition are E-type and it is these diamonds that comprise the bulk of diamonds with isotopically heavy nitrogen that extends towards values characteristic of sediments and granites derived from sedimentary protoliths (+5‰ to +10‰).

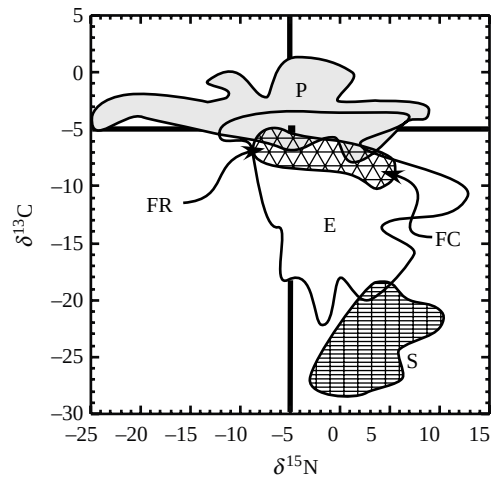

Figure 57 Carbon ($\delta^{13}C$ in ‰) and nitrogen ($\delta^{15}N$ in ‰) isotopic composition of P-type (P) and E-type (E) diamonds compared to the mantle (thick solid lines), modern sediments (S), and fibrous diamonds (FR = fibrous diamond rim; FC = fibrous diamond, non-fibrous core). Sources of data as follows: P-type diamonds (DeBeers Pool, Orapa, Pipe 50) from Cartigny *et al.* (1997, 1998a, #65; 1999), E-type diamonds (Argyle, Jwaneng, Orapa, DeBeers Pool) from Cartigny *et al.* (1998a,b, 1999) and van Heerden *et al.* (1995). Note that the "high $\delta^{13}C$"group (Finsch, Premier, Williamson, Jagersfontein, Arkansas) of Boyd and Pillinger (1994) is overlapped by the field for P-type diamonds and their "low $\delta^{13}C$" group (Argyle, Jagersfontein, Arkansas) is overlapped by the field for E-Type diamonds. Fibrous diamonds (Zaire) are from Boyd *et al.* (1987). Field for modern sediments after Navon (1999) and references therein.

2.05.4.3.3 C–N–S isotopic systematics

The combined systematics of $\delta^{13}C$–$\delta^{15}N$ and nitrogen abundance in P-type and E-type diamonds provide the strongest constraints on the abundance and ultimate sources of carbon and nitrogen in the mantle. Cartigny *et al.* (2001) estimate a diamond growth—medium C/N of 200–500 (mantle C = 400 ppm; mantle N = 1–2 ppm). C/N ratios in this medium could be as low as 10 depending on assumptions about the partitioning behavior of nitrogen. The former values would put continental lithospheric mantle C/N ratios in line with estimates for the modern depleted upper mantle from MORB analyses (Cartigny *et al.*, 2001). Based on their mantle-like carbon isotopic composition, P-type

diamonds must have predominantly mantle-derived nitrogen. Collectively, when including the diamonds from Pipe 50, China, the entire P-type diamond population shows a large range in $\delta^{15}N$ from −25‰ to +6‰ (Figure 57) that has been ascribed to primordial mantle heterogeneity in N, inherited from the large isotopic range seen in meteorites (Cartigny *et al.*, 1997). To explain the diamonds with anomalously low-$\delta^{13}C$ and high-$\delta^{15}N$ that are outside the normal mantle range (Figure 57), Cartigny and co-workers (1998a, 1999, 2001) argue for a fractionation process in the diamond-forming fluid because mixing between mantle and sedimentary end-members cannot reproduce key features of the data. Specifically, recycling of crustal material is not consistent with the occurrence of E-type diamonds with negative $\delta^{15}N$. In addition, concave upward data arrays in the $\delta^{13}C$-$\delta^{15}N$ plot would be expected for mantle–crustal fluid mixing because of by the high C/N crustal fluids. Other features that are inconsistent with a recycling model include the drop in nitrogen content of a diamond when $\delta^{15}N$ increases and the positive correlation of nitrogen content with $\delta^{13}C$, seen in some eclogitic diamond suites.

Navon (1999) objectively considered arguments against recycling models and advanced a model whereby the C–N isotope systematics of E-type diamonds can be explained as a mixture of mantle and subducted components. This model overcomes the objections of Cartigny *et al.* (1997, 1998a,b) to subduction scenarios by using mantle and sedimentary mixing end-members that have variable compositions, a variable C/N ratio of the diamond-forming fluid, and possible nitrogen isotopic fractionations during diamond growth. Such growth-related nitrogen isotopic fractionations are indicated by *in situ* nitrogen isotope determinations at high spatial resolution (Hauri *et al.*, 1999, 2002; Bulanova *et al.*, 2002). Indeed, the huge range for nitrogen isotopic composition of P-type diamonds (Cartigny *et al.*, 1997) and the lack of data on nitrogen isotopes in Archean crustal rocks require variable end-members to be considered. Future resolution of the subduction versus mantle fractionation debate for C–N isotope systematics in diamonds perhaps lies in detailed *in situ*, high spatial resolution C–N isotopic studies on typically complex zoned diamonds using cathodoluminescence, FTIR, and SIMS (Boyd and Pillinger, 1994; Bulanova, 1995; Bulanova *et al.*, 2002; Fitzsimons *et al.*, 1999; Harte *et al.*, 1999a; Hauri *et al.*, 2002). These nascent studies show large covariations in coupled C–N isotopic compositions that correlate with diamond growth zones. (e.g., Bulanova *et al.*, 2002; Fitzsimons *et al.*, 1999). Furthermore, they suggest decoupling of the carbon and nitrogen isotopic compositions and point toward temporal changes in fluid composition and/or isotopic fractionation during diamond growth (Bulanova *et al.*, 2002; Cartigny *et al.*, 2001; Fitzsimons *et al.*, 1999).

Convincing evidence of recycling of volatiles to the mantle and their incorporation into diamonds has recently been reported from sulfur isotope studies of sulfide inclusions within diamond (Farquhar *et al.*, 2002). SIMS analysis of sulfide inclusions has revealed anomalous mass-independently fractionated sulfur isotopic compositions from the Orapa kimberlite, which are explained as a consequence of the recycling of surface sulfur produced through photolytic chemistry in the Archean atmosphere. Such studies need to be extended to other diamond populations and combined with C–N isotope studies on the host diamonds.

2.05.4.4 Volatiles and Fluids in Diamonds

2.05.4.4.1 Fluid inclusions in diamonds

The first indication of the presence of fluid inclusions within diamonds was reported by Chrenko *et al.* (1967), who used infrared spectroscopy to identify the presence of water and carbonate in the fibrous coating of an octahedral diamond. Subsequent studies have recognized that fibrous diamonds contain very high densities of fluid trapped during diamond growth and hence this type of diamond offers an insight into the chemistry of deep mantle fluids from which fibrous diamonds grow (Navon *et al.*, 1988). Fibrous diamonds commonly occur either as cube-shaped crystals, where the entire diamond is fibrous throughout, or as coatings on octahedral diamonds. Fibrous diamonds are widespread and have been reported from Sierra Leone, Botswana, Zaire (Congo), India, and Yakutia (Schrauder and Navon, 1994). Although generally forming less than 1 wt.% of mine production, fibrous diamonds can represent up to 8 wt.% of production at Jwaneng, Botswana (Harris, 1992). Recently, fluid inclusions have also been found in "cloudy" monocrystalline diamonds (Izraeli *et al.*, 2001).

Analyses of the fluid inclusions within fibrous diamonds from Botswana show that the composition of fluids within individual diamonds is uniform but that significant variation exists between different diamonds. The fluids range in composition from carbonatitic to hydrous end-members, with intermediate compositions (Schrauder and Navon, 1994). The carbonatitic fluid is rich in carbonate, CaO, FeO, MgO, and P_2O_5 and the hydrous fluid is rich in SiO_2 and Al_2O_3 (Schrauder and Navon, 1994; Figure 58). K_2O contents are high and Mg# low in both end-members. In contrast, fluid inclusions from

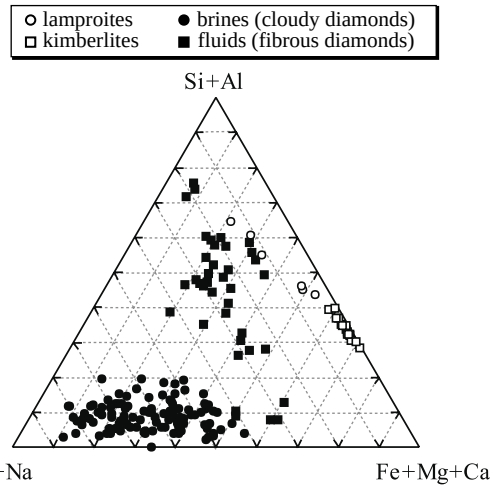

Figure 58 Major-element compositions of fluid inclusions within fibrous diamonds (squares) compared to cloudy diamonds and kimberlites/lamproites (after Izraeli *et al.*, 2001).

cloudy diamonds contain much higher chlorine contents and are classified as brines, being distinct from the other fluid types found in fibrous diamonds (Izraeli *et al.*, 2001; Figure 58). The brines carry very little SiO_2 (3–4 wt.%), possibly because of the low water content restricting the solvating capacity of the fluid.

The concentration of incompatible elements of varying geochemical affinity (potassium, sodium, bromine, rubidium, strontium, zirconium, caesium, barium, hafnium, tantalum, thorium, uranium, and LREEs) in the fluid inclusions from fibrous diamonds is higher than in typical mantle-derived magmas and melt inclusions (Schrauder *et al.*, 1996). The concentrations of most trace elements decrease by a factor of two from the carbonate-rich fluids to the hydrous fluids. REE contents of the fluid inclusions are higher than those of kimberlites and lamproites but the fluids show very similar levels of LREE/HREE fractionation to these rock types. Hence, they may be related to kimberlite-like magmas via fractionation of carbonate plus other phases such as rutile, apatite and zircon (Schrauder *et al.*, 1996). The amount of fractionation of these latter minerals must be small otherwise MREE and HREE systematics of the fluids would show distinctive fractionation effects. The link between the fluids in fibrous diamonds and kimberlite-like magmas is further supported by strontium isotope (Akagi and Masuda, 1988) and carbon isotope measurements (Boyd *et al.*, 1987, 1992) of fibrous diamonds. The incompatible-element-rich nature of the fluids in fibrous diamonds illustrate that carbonate-rich and hydrous deep mantle fluids are efficient carriers of incompatible elements.

2.05.4.4.2 Noble gases in diamonds

Diamonds provide a valuable sample of deep mantle volatiles and thus are obvious targets for noble gas analysis. Although monocrystalline (nonfibrous) diamonds have been analyzed (e.g., Honda *et al.*, 1987), noble gas abundances are very low and uncertainties very large. Far more reliable data comes from fibrous diamonds due to their high fluid inclusion contents that lead to high noble gas contents and precise analyses. Indeed, their gas-rich nature has allowed some of the most precise noble gas isotope ratio determinations of mantle materials to date. An important note here is that several studies have cited the old age of diamonds as a means of comparing mantle noble gas systematics over time. However, the very unaggregated nature of nitrogen within fibrous diamonds, which are typically analyzed in preference to monocrystalline diamonds, indicates a very young age is likely for fibrous stones, that is not much older than the host kimberlite eruption event (see Section 2.05.4.2.2). As such, fibrous diamonds provide an additional view of modern mantle to that available from volcanic rocks and not a view of the ancient mantle, as claimed by some authors. A complication to account for in the analysis of fibrous (cubic) diamonds is that the high uranium contents of their inclusions, and the high uranium-content of the host kimberlite mean that nucleogenic contributions to noble gas inventories are most likely. Cosmogenic ^{3}He may also be produced from carbon within the diamond itself.

The relatively gas-rich nature of fibrous diamonds has allowed precise analysis of helium, neon, and xenon isotopes (e.g., Ozima and Zashu, 1988, 1991; Wada and Matsuda, 1998). ^{3}He/^{4}He values are generally higher than the typical MORB value of 1×10^{-6} (Wada and Matsuda, 1998) but overlap the range of helium isotope compositions found in continental mantle xenoliths (e.g., Dunai and Baur, 1995; Section 2.05.2.9; see Chapter 2.06). Lowering of ^{3}He/^{4}He from a MORB-like value by direct decay of uranium trapped within the fluid inclusions requires time periods in excess of 1 Ga if uranium abundances are low (~0.5 ppb, Wada and Matsuda, 1998). This contrasts with the young age of fibrous diamonds indicated by nitrogen-aggregation studies. To reconcile these differences, Wada and Matsuda (1998) propose differentiation of the diamond fluid source from the mantle over 1 Ga ago followed by recent crystallization of the diamond from fluid, just before kimberlite sampling. The timescale required for modifying ^{3}He/^{4}He ratios via uranium decay is dramatically reduced if higher uranium abundances of up to 50 ppm, suggested by INAA studies (Schrauder *et al.*, 1996) are more applicable.

Fibrous diamonds have provided some of the more precise analyses of mantle neon and xenon isotopic composition and, together with MORB glass data, they have clearly revealed that the mantle is elevated in $^{20}Ne/^{22}Ne$ and $^{21}Ne/^{22}Ne$ (11–14) relative to atmosphere (9.8; Ozima and Zashu, 1988). High $^{20}Ne/^{22}Ne$ values in fibrous diamonds relative to atmosphere (9.8) are taken to indicate a primordial, Solar-like neon component in the mantle (Ozima and Zashu, 1988, 1991). Scatter in $^{21}Ne/^{22}Ne$ could be either source heterogeneity or due to nucleogenic ^{21}Ne. Wada and Matsuda (1998) have noted that many of the data points on $^{20}Ne/^{22}Ne$ versus $^{21}Ne/^{22}Ne$ correlation plots for fibrous diamonds are below the MORB regression line. This indicates greater amounts of excess ^{21}Ne (referred to as $^{21}Ne^{*}$) in cubic diamonds than the MORB source. Enrichment in ^{21}Ne due to nuclear reactions is consistent with $^{3}He/^{4}He$ values lower than MORB, since ^{21}Ne and ^{4}He are both derived from decay of uranium and thorium, via spallation. However, $^{21}Ne^{*}/^{4}He$ in cubic diamonds is significantly higher than the production rate estimated for average mantle material.

Fibrous diamonds show positively correlated excesses of ^{129}Xe and $^{131\text{-}136}Xe$ of up to 10% relative to atmospheric values, similar to the systematics shown by MORB (Figure 59). These data provide some of the best-determined mantle xenon isotope measurements. The xenon isotope excesses are attributed to decay of extinct ^{129}I and ^{244}Pu. $^{136}Xe/^{130}Xe$ versus $^{129}Xe/^{130}Xe$ correlations are identical to MORB glasses (Figure 59) and suggest that the fluid source of fibrous diamonds is very similar to the MORB/convecting mantle source (Ozima and Zashu, 1988, 1991; Wada and Matsuda, 1998). This is further supported by the uniformity and normal mantle-like carbon and nitrogen isotopic compositions of the fibrous coats of coated diamonds (Boyd *et al.*, 1987, 1992).

$^{40}Ar/^{36}Ar$ values of up to 35,000 are found in fibrous diamonds and are similar to estimates of the MORB-source mantle (e.g., Wada and Matsuda, 1998), further supporting the carbon and nitrogen isotope evidence for the involvement of this reservoir in the genesis of fibrous diamonds. Slightly elevated $^{38}Ar/^{36}Ar$ may be a product of the $^{35}Cl(\alpha,p)^{38}Ar$ reaction in the fluid phase. This is possible because of the high chlorine contents of some fibrous diamonds (>100 ppm) although levels are normally <50 ppm (Burgess *et al.*, 2002). Wada and Matsuda (1998) suggest that it is difficult for all the excess ^{38}Ar to be of nucleogenic origin and do not rule out the possibility that mantle $^{38}Ar/^{36}Ar$ is greater than atmospheric. Resolution of this possibility is needed because it has important implications for planetary–solar system noble gas reservoir requirements.

The likely young ages of fibrous diamonds mean that their isotopic compositions are directly comparable to the MORB source. When nucleogenic effects are accounted for, the isotopic signature of fibrous diamonds (as cubes or coats on octahedra) shares many similarities with the source of MORB, i.e., $\delta^{13}C$ −4 per mil to −8 per mil, $\delta^{15}N$ −2 per mill to −9 per mil, $^{40}Ar/^{36}Ar \leq 4 \times 10^{4}$, $^{3}He/^{4}He$ $4-8R_A$, $^{20}Ne/^{22}Ne$ from 10 to 14 and $^{136}Xe/^{130}Xe$ plus $^{129}Xe/^{130}Xe$ up to 10% > atmosphere. This suggests that the origin of the parental fluid forming fibrous diamonds is in the convecting mantle.

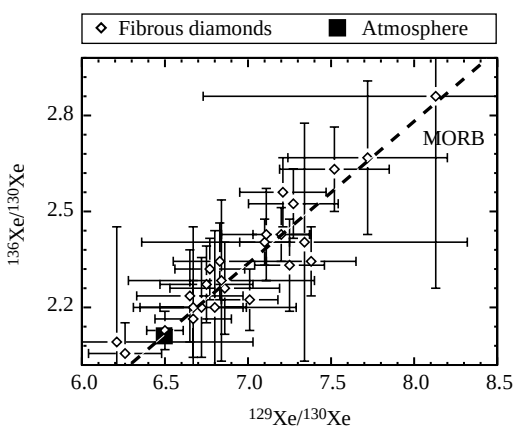

Figure 59 $^{136}Xe/^{130}Xe$–$^{129}Xe/^{130}Xe$ correlation plot of fibrous diamonds compared with the MORB correlation line and the atmospheric composition. Data and correlation line from Ozima and Zashu (1991) and Wada and Matsuda (1998). Error bars are 1σ and include blank correction.

2.05.4.4.3 Halogen contents of diamonds

Determination of the halogen content of the Earth's mantle is a difficult problem because the largest proportion of these elements is now at the Earth's surface and because seawater/surficial contamination affects recently erupted lavas such as MORB (see Chapter 2.07). Most of these problems are overcome when studying diamonds because of their deep origin and the ability to chemically remove surficial contamination before analysis. As with the noble gases, it is fluid-inclusion-rich fibrous diamonds, in the form of coated diamonds or cubes, that are the most attractive for analysis because of their high volatile contents (Burgess *et al.*, 2002). The very high chlorine contents of cloudy diamonds also make them amenable to study (Izraeli *et al.*, 2001). The Ar–Ar analytical technique can be extended for halogen analysis and enables correlation of argon isotope data with halogen contents. Burgess *et al.* (2002) have recently used this technique to study fibrous diamonds from Siberia,

Africa, and Canada. In the Siberian samples, three components have been identified with different Ar isotope compositions. Atmospheric blank is a small component present in most analyses. The major component is characterized by high $^{40}Ar/^{36}Ar$ (>11,000) and constant $^{40}Ar^{*}/Cl$ ($527 \pm 22 \times 10^{-6}$), $Br/Cl = 1.7 \times 10^{-3}$ and $I/Cl = 22 \times 10^{-6}$, indicative of a mantle fluid phase. This component is also characteristic of African and Canadian fibrous diamonds and leads to estimated mantle halogen abundances in the fluid source region of 3 ppm Cl, 11 ppb Br, and 0.4 ppb I (Burgess *et al.*, 2002). As with noble gas systematics, these data are very comparable to estimates for MORB-source mantle and implies that the mantle is >90% degassed of its halogens. A third Ar component in coated diamonds appears to be the result of ^{40}K decay since the time of kimberlite eruption.

2.05.4.5 Solid Inclusions in Diamonds

2.05.4.5.1 Geochemistry of inclusions

The P-type versus E-type paragenetic classification of diamonds based on their inclusions is introduced in Section 2.05.4.1.3. The geochemical basis for this fundamental difference between inclusion types is discussed in review articles by Meyer (1987), Harris and Gurney (1979), Gurney (1989), and Kirkley *et al.* (1991), summarized in brief here and discussed in the context of newer SIMS trace-element data on inclusions. Meyer (1987) points out the importance of inclusions in diamonds for the study of the mantle. First, inclusions are the chief way to understand the relationship of diamonds to their mantle host lithologies. Second, inclusions often represent pristine, geochemically unaltered samples that are not subject to the chemical re-equilibration and alteration that affects the minerals in xenoliths and macrocrysts.

Meyer (1987) documents nearly 20 minerals that have been proposed as protogenetic (pre-existing diamond growth) or syngenetic (forming with diamond) on the basis of modern analytical methods (X-ray or electron probe). An additional 10 minerals have been proposed to be of epigenetic origin (forming after diamond growth). In the P-type paragenesis, six minerals are typically found (sulfide, olivine, orthopyroxene, garnet, chromite, and clinopyroxene), whereas in the E-type paragenesis five minerals are typically found (sulfide, garnet, clinopyroxene, and rarely orthopyroxene and coesite; Gurney, 1989).

Olivine and orthopyroxene are generally associated with the P-type paragenesis. However, it is difficult to relate either of these two minerals specifically to a lherzolitic or harzurgitic facies because of their wide range in $(Mg/(Mg + Fe^{2+})$; 0.90–0.96; e.g., Meyer, 1987). As a general rule, highly magnesian olivines are likely to be related to the harzburgitic facies and those richer in iron to the lherzolitic facies. The difference between harzburgitic and lherzolitic garnet compositions is most easily distinguished using the relationship between calcium and chromium (e.g., Sobolev *et al.*, 1973; Gurney and Switzer, 1973) where harzburgitic garnets have much higher chromium and lower calcium contents (Figure 60). The P-type versus E-type distinction for garnet and clinopyroxene is fundamental and evident on key major-element plots (Meyer, 1987). P-type garnet inclusions have much lower FeO, CaO, and TiO_2 and much higher MgO compared to E-type garnet. P-type clinopyroxene has much lower Na_2O, Al_2O_3, and FeO and much higher MgO and Cr_2O_3 compared to E-type clinopyroxene. Sulfides that are dominantly Fe–S with minor copper and nickel follow similar paragenetic distinctions. P-type sulfides have higher nickel content, typically >13 wt.%, and E-type sulfides have lower nickel content, typically <10 wt.% (Yefimova *et al.*, 1983; Deines and Harris, 1995) but some complications exist that can be clarified using Re–Os systematics (Pearson *et al.*, 1999b). E-type sulfide inclusions have low osmium (e.g., <200 ppb to 300 ppb) and high rhenium that give combined high Re/Os compared to P-type sulfides which have lower rhenium and much higher osmium (2–30 ppm; Pearson *et al.*, 1999b).

While the major-element compositions of inclusions have served to link them to harzburgite, lherzolite or eclogite, it is their trace-element content, determined via laser ICP-MS or SIMS analysis, that has served to reveal how these

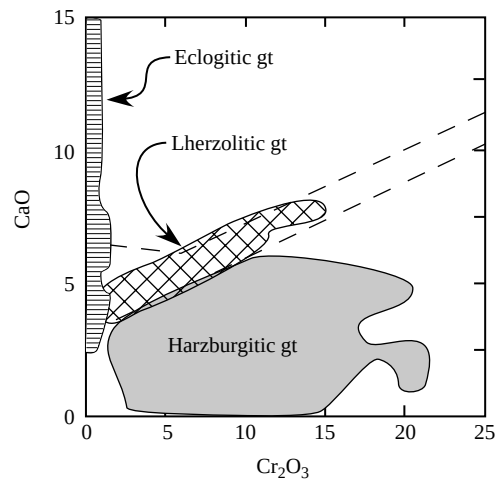

Figure 60 Cr_2O_3 versus CaO (wt.%) content of garnet inclusions in diamond. Original plot and lherzolite field (dashed) from Sobolev *et al.* (1973). This figure redrafted from plots and database of Stachel *et al.* (1997, 1998, 2000).

inclusions were formed in the mantle and the complex metasomatic processes to which they have been subjected. The first Sm–Nd isotopic analyses (Richardson *et al.*, 1984) and the first SIMS trace-element analyses on harzburgitic garnet from Finsch and Kimberley (Shimizu and Richardson, 1987) confirmed extreme light rare earth element enrichment paired with extreme depletion in major-element composition. This was recognized as a signature of ancient mantle metasomatism that preceded incorporation of the garnets in diamond (Shimizu and Richardson, 1987) and is a feature of nearly all garnets in harzburgitic xenolith suites analyzed for Sm–Nd isotopic ages (e.g., Pearson *et al.*, 1995a; Pearson and Shirey, 1999; Figure 61). Subsequent work on Udachnaya (Pearson and Milledge, 1998), Akwatia (Stachel and Harris, 1997; Stachel *et al.*, 1998), and Mwadui (Stachel *et al.*, 1999) has shown a whole range of complex (e.g., sinuous) REE patterns. Almost none are simply depleted in the LREE, as their major-element composition would indicate they should be (Figure 62). These trace-element complexities have supported the following processes in forming and metasomatising the continental lithospheric mantle:

(i) depletion by polybaric fractional melting;

(ii) enrichment during mantle metasomatism; and

(iii) slight light rare earth element depletion (e.g., La, Ce ± Pr) due to re-equilibration of the garnet with clinopyroxene (Stachel and Harris, 1997; Stachel *et al.*, 1998), all followed by diamond formation.

Similar trace-element patterns between harzburgitic garnets from xenoliths (diamondiferous and nondiamondiferous) and harzburgitic garnet inclusions (Stachel *et al.*, 1998) show that host lithologies reflect the same processes as seen in the inclusions. Lherzolitic garnets show much less complexity in their REE patterns. They are LREE depleted (Figure 62) and could have formed in equilibrium with kimberlitic/lamproitic or carbonatitic fluids (Stachel and Harris, 1997; Stachel *et al.*, 1998). The lherzolitic garnets are proposed to be distinctly different than harzburgitic garnets and are thought to be associated with additional metasomatic enrichment of the lithosphere that introduced additional calcium, iron, and silicon (Stachel *et al.*, 1998).

Eclogitic garnet and clinopyroxene inclusions studied from Udachnaya (Ireland *et al.*, 1994; Taylor *et al.*, 1996), Mwadui (Stachel *et al.*, 1999), and Kankan (Stachel *et al.*, 2000) are characterized by more "regular" REE patterns that reflect typical equilibrium distribution of the REEs between the two minerals. As is the case with the P-type paragenesis, similar trace-element patterns between garnets and clinopyroxene from eclogite xenoliths and those occurring as

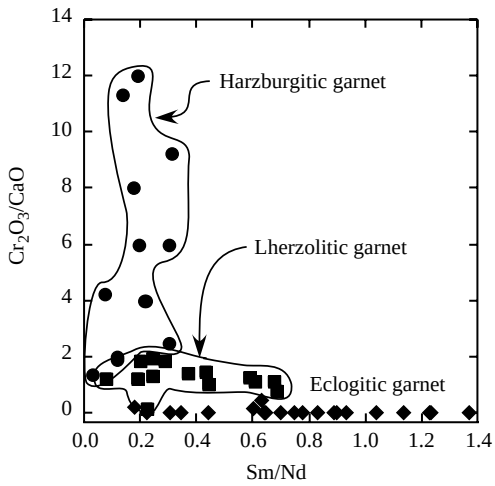

Figure 61 Cr_2O_3/CaO versus Sm/Nd for garnet inclusions in diamonds from Akwatia, Argyle, Finsch, KanKan, Kimberley Pool, Mir, Orapa, Premier, and Udachnaya (sources Richardson *et al.*, 1984, 1986, 1990; Richardson and Harris, 1993, 1997; Stachel *et al.*, 2000a, 1997; Smith *et al.*, 1991; Taylor *et al.*, 1996).

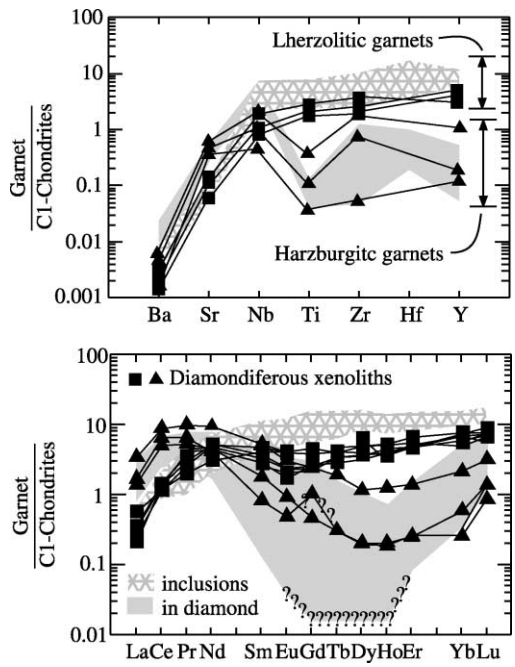

Figure 62 Trace-element plots for harzburgitic and lherzolitic diamond inclusions from Akwatia Ghana compared to harzburgitic and lherzolitic garnets from rare (<0.6% of the Roberts Victor xenolith population) diamondiferous peridotites from Roberts Victor. Ion microprobe analyses and original figures from Stachel *et al.* (1997, 1998). Labeling applies to both figure panels. Solid triangles and squares are for harzburgitic and lherzolitic (respectively) garnets in diamondiferous peridotites. Shaded and cross-hatched patterns are for harzburgitic and lherzolitic (respectively) garnet inclusions in diamond.

inclusions in diamond (Taylor *et al.*, 1996) show that the xenolith host lithologies reflect the same processes as seen in the inclusions. Since the mineral trace-element patterns are regular and eclogites are roughly 50 : 50 garnet : clinopyroxene, meaningful bulk-rock trace-element patterns can be readily constructed from trace-element analyses of the individual minerals (Ireland *et al.*, 1994; Stachel *et al.*, 1999; Taylor *et al.*, 1996). These reconstructed whole-rocks show strong light REE depletions that are interpreted by Ireland *et al.* (1994) as being consistent with those of subducted basalt residues from tonalite-trondhjemite melt extraction in the garnet stability field.

2.05.4.5.2 Ages of inclusions and their diamond hosts

The ages of diamond inclusions have been summarized by Harris (1992), Pearson and Shirey (1999), and Navon (1999). Analyses typically are performed on inclusions, thought to be syngenetic, of both E-type and P-type paragenesis in otherwise gem-quality diamonds using the following systems: Sm–Nd in garnet and clinopyroxene, Re–Os in sulfide, Ar–Ar in clinopyroxene and Pb–Pb in sulfide. Supportive age constraints can be obtained with the Rb–Sr system and nitrogen aggregation. In exploring the literature, the reader is cautioned that the ages determined do not always sample inclusion suites in the same manner and this may lead to apparent age discrepancies. For example Sm–Nd isotope studies on silicate inclusion suites typically require composites of many inclusions and provide a statistical average for many diamonds, whereas Re–Os on sulfides can be performed on single diamonds (Pearson *et al.*, 1998b). The diamond size fraction is also important. The small stones used for Sm–Nd composites need not be of the same age as the large stones used for Re–Os in sulfides.

Until the application of the Re–Os isotopic system to whole-rock peridotites (Section 2.05.2.7.4) the Archean and Proterozoic Pb–Pb and Sm–Nd model ages and isochrons obtained on diamonds were the chief constraints on the antiquity of the continental lithospheric mantle (Kramers, 1979; Richardson *et al.*, 1984). Early work, most of which was on diamonds from the Kaapvaal–Zimbabwe craton because of sample availability, suggested a simple difference from Meso-Archean P-type (harzburgitic) diamonds and Proterozoic E-type diamonds (Richardson, 1986; Richardson *et al.*, 1984, 1993). More recent Re-Os work on single sulfide inclusions from the Kaapvaal–Zimbabwe craton has underscored the importance of a Neo-Archean E-type diamond suite (Shirey *et al.*, 2001) and has resolved Proterozoic diamond populations (Pearson *et al.*, 1998b). The Neo-Archean E-type diamonds appear to be related to assembly of the Kaapvaal-Zimbabwe craton, whereas Proterozoic diamonds appear to be related to magmatic/metasomatic process by which the Archean lithosphere was modified in the Proterozoic (Shirey *et al.*, 2002).

The accuracy of diamond ages based on inclusions has sparked a lively debate in the literature (Navon, 1999; Pidgeon, 1989; Richardson, 1989; Taylor *et al.*, 2000). The main issue is to what extent the diamond ages on silicate composites are averages of many ages, and to what extent younger diamonds can encapsulate older, pre-existing inclusions. Even though some diamonds occur in fracture systems within their host lithology which must post-date the rock itself (Taylor *et al.*, 2000), there can be little doubt that diamonds can be Archean and Proterozoic in age although some are as young as the Phanerozoic age of most kimberlites (Pearson *et al.*, 1998b). Evidence for Proterozoic and Archean diamonds includes the occurrence of Proterozoic kimberlites such as Premier that carry abundant xenocrystic diamonds (Navon, 1999) and Re–Os ages of lithospheric peridotitic hosts that agree with diamond ages (Shirey *et al.*, 2001). In addition, type Ia diamonds show advanced aggregation that would take billions of years to achieve at lithospheric storage temperatures (Richardson and Harris, 1997; Pearson *et al.*, 1999a). Neodymium and strontium isotopic differences between concentrate garnets and garnets encapsulated in diamond suggest encapsulation for billion-year timescales (Richardson *et al.*, 1984; Richardson, 1989; Pearson and Shirey, 1999). Finally, diamonds occur as detrital grains in the later Archean/neo-Proterozoic Wits basin (Pearson and Shirey, 1999). The answer to the question of age accuracy must be sought in independent corroboration of the measured age (Navon, 1999). Such corroboration would come from obtaining the same age on different isotopic systems and the systematics of multiple age determinations with the same isotopic system: (i) relation of age and inclusion composition; (ii) repetition of ages in different diamonds and pipes; and (iii) agreement of ages with geological events recorded in the lithosphere or crust.

2.05.4.6 Ultradeep Diamonds

An exciting finding of the last two decades is that rare macrodiamonds occurring in kimberlites originate well below the lithosphere (Scott-Smith *et al.*, 1984; Harris, 1992) and can come from the lower mantle (McCammon, 2001). From the first reported lower mantle assemblage in a diamond

(Scott-Smith *et al.*, 1984), recognition of these ultradeep diamonds has extended to more than 12 localities on eight cratons (McCammon, 2001). The most thoroughly studied include the Slave (Davies *et al.*, 1999), Brazilian (Harte *et al.*, 1999b; Hutchison *et al.*, 1999, 2001; Kaminsky *et al.*, 2001; McCammon *et al.*, 1997; Wilding *et al.*, 1991), West African (Joswig *et al.*, 1999; Stachel *et al.*, 2000, 2002), and Kaapvaal (Deines *et al.*, 1991; McDade and Harris, 1999; Moore and Gurney, 1985; Scott-Smith *et al.*, 1984) cratons. Ultradeep mantle xenoliths are known to exist (Haggerty and Sautter, 1990; Sautter *et al.*, 1991) but ultradeep diamonds are perhaps the more revealing probes of the deep mantle. This is because, apparently, they are more widely distributed, they suffer less from retrogression and they derive from both the transition zone and the lower mantle (Harte *et al.*, 1999). Ultradeep diamonds encapsulate bonafide lower mantle mineral assemblages and allow a direct estimation of lower-mantle oxygen fugacity, carbon isotopic composition, and nitrogen abundance. However, it is important to keep in mind the potential and likely overprint of the diamond forming environment on the chemistry of these inclusions, i.e., they may be atypical samples of the ultradeep mantle environment.

Ferropericlase is the dominant ultradeep inclusion found in diamond (McCammon, 2001). Because it can be stable under upper-mantle conditions its presence alone does not signify a lower-mantle origin. The coexistence of ferropericlase with enstatite (Mg-silicate perovskite) and Ca-silicate perovskite is taken as a strong indication of lower mantle formation conditions (Stachel *et al.*, 2000). These additional ultradeep phases are the low-pressure polymorphs or exsolved multiphase chemical equivalents of their high-pressure precursors such as enstatite for $MgSiO_3$-perovskite, calcium silicates for $CaSiO_3$-perovskite and quartz/coesite for stishovite (Figure 63). A garnet composition phase, tetragonal almandine pyrope phase (TAPP; Harris *et al.*, 1997), is thought to exist at high pressure but may be a retrograde garnet (Harte *et al.*, 1999b). Nickel contents of $MgSiO_3$ inclusions in equilibrium with ferropericlase are an order of magnitude lower than typical upper-mantle enstatite and provide a ready way to establish a lower-mantle heritage for $MgSiO_3$ when it occurs in isolation (Stachel *et al.*, 2000). Recently, corundum inclusions were discovered in association with Al_2O_3-rich $MgSiO_3$-perovskite and ferropericlase, which has established that a free aluminum phase can exist in the lower mantle (Hutchison *et al.*, 2001).

The trace-element content of the ultradeep inclusion suite has been characterized by SIMS. $CaSiO_3$-perovksite is observed to have a strongly light rare earth element enriched pattern and high strontium content, whereas $MgSiO_3$-perovskite is observed to have a flat to slightly depleted rare earth element pattern (Harte *et al.*, 1999b; Hutchison *et al.*, 2001; Kaminsky *et al.*, 2001; Stachel *et al.*, 2000). These patterns have been interpreted as evidence for the presence of substantial lower-mantle/transition-zone source heterogeneity (Hutchison *et al.*, 2001) that includes nonprimitive LREE enriched sources (Stachel *et al.*, 2000). Caution must be exercised, however, in extrapolating from minute single inclusions to the entire lower mantle or transition zone. The effects of the complete mantle mineral assemblage on fractionating the trace-element patterns prior to incorporation in the diamond at these pressures and temperatures are not well-known and potential effects from the diamond-forming event also complicate interpretation.

Nearly all lower-mantle diamonds have such low nitrogen that they are classified type II (McCammon, 2001). These features are very distinctive from upper-mantle diamonds, which are chiefly type Ia and have widely variable percentages of A, A/B, and B centers. The carbon isotopic composition of ultradeep, lower-mantle diamonds is surprisingly homogeneous, most samples having typical upper-mantle values of

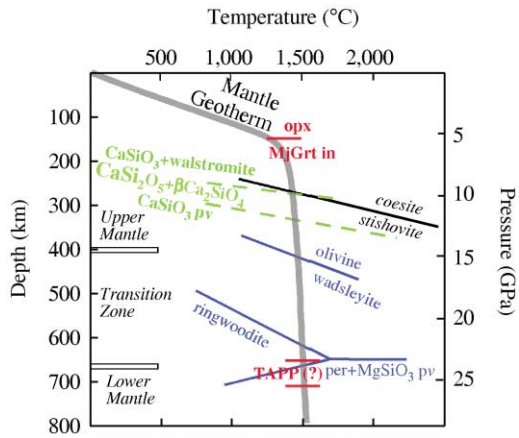

Figure 63 Mantle geotherm and $P-T$ diagram for phases included in transition zone and lower mantle diamonds. Figure modified by Joswig *et al.* (1999) to include stability fields in the Mg–Al–Si–O system for the tetragonal almandine pyrope phase (TAPP) and majorite garnet (MjGrt) using occurrences (Harte *et al.*, 1999; Stachel *et al.*, 2000), experimental data (Gasparik and Hutchison, 2000; Irifune *et al.*, 1996) and summaries of experimental work (Fei and Bertka, 1999). Si–O system in black italics; Mg–Si–O system in blue lower case; Mg–Al–Si–O system in red capitals; and the Ca–Si–O system in green boldface. Note that a higher temperature geotherm than that shown recently has been proposed (Gasparik and Hutchison, 2000).

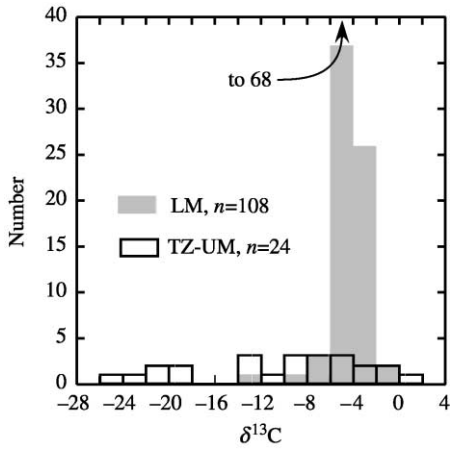

Figure 64 Comparison of the carbon isotopic composition of diamonds containing inclusions ascribed to transition zone and sublithospheric depths (TZ-UM; clear) to diamonds with inclusions derived from lower mantle depths (LM; gray). The number of specimens is given for each group ($n = 132$). Note that the -4 to -6 bar for lower mantle diamonds is off-scale at a number of 68. Transition zone and upper mantle diamonds are from these kimberlites: Jagersfontein (6), Juina (1), KanKan (5), Orapa (1), Premier (1), and Sao Luiz (10). Lower mantle diamonds (and the number analyzed from each) are from these kimberlites: Dokolwayo (1), DO-27 (5), Juina (30), KanKan (36), Koffiefontein (3), Letseng-la-Terai (1), and Sao Luiz (33) (sources Daniels and Gurney, 1999; Davies *et al.*, 1999; Deines *et al.*, 1989, 1991a, 1993; Hutchison *et al.*, 1999; Kaminsky *et al.*, 2001; McDade and Harris, 1999; Stachel *et al.*, 2000, 2002).

$\delta^{13}C = (-5 \pm 4)‰$ (Figure 64). In contrast, diamonds originating in the transition zone show considerable carbon isotopic variability, with the lightest isotopic compositions originating in the shallowest specimens, from the top of the transition zone (Davies *et al.*, 1999; Deines *et al.*, 1991; Kaminsky *et al.*, 2001; Stachel *et al.*, 2002; Wilding *et al.*, 1991).

The typical low nitrogen content of lower-mantle diamonds does not support an enhanced reservoir of nitrogen in the lower mantle (McCammon, 2001), although little is known about nitrogen partitioning during growth of diamond under these conditions. While the LREE-enriched patterns of $CaSiO_3$ perovskite could indicate a protolith subducted to transition zone depths (Stachel *et al.*, 2000), these signatures may also arise from interaction with very enriched alkaline magmas/liquids. Furthermore, the primitive and mantle-like carbon isotopic composition of many transition-zone and lower-mantle diamonds is not diagnostic of a subducted origin. Of the few ultradeep diamonds with isotopically light $\delta^{13}C$ (e.g., Deines *et al.*, 1991), most are from the transition zone as opposed to the lower mantle. Lower-mantle diamonds are characterized by restricted and heavier, mantle-like $\delta^{13}C$. This fact and a propensity for a majorite garnet and jadeitic diopside association in transition zone inclusions versus the ferropericlase-$MgSiO_3$ perovskite association with lower-mantle inclusions has led Hutchison *et al.* (2001) to suggest that the transition-zone inclusion suite is dominated by eclogitic assemblages, whereas the lower mantle is dominated by peridotitic assemblages. The ultradeep inclusion suites studied so far support a layered mantle convection model, which allows plume penetration upward through the transition zone and the accumulation of subducted slab material in the transition zone (Harte *et al.*, 1999b; Hutchison *et al.*, 2001; Stachel *et al.*, 2000) as first envisioned by Ringwood (1991). If any future lower-mantle inclusions are discovered that have isotopically light $\delta^{13}C$, then this would provide direct evidence for slab penetration into the lower mantle.

ACKNOWLEDGMENTS

The authors are very grateful to Geoff Nowell for enthusiastically helping to create many of the diagrams in this manuscript and to Dave Dowall for logistical help. Pete Nixon gave guidance with Table 1. Dmitri Ionov, Pierre Cartigny, Gordon Irvine, Roberta Rudnick, and Thomas Stachel provided assistance by donating unpublished data, database compilations, figures, and preprints. Dorrit Jacob reviewed the section on eclogites. Martin Menzies gave advice on scope and content. Comments by Nina Simon, Rick Carlson, and Tony Irving helped to create a much more readable manuscript. We acknowledge the inspiration provided by Pete Nixon and Joe Boyd in the pursuit of xenolith studies across the world.

REFERENCES

Akagi T. and Masuda A. (1988) Isotopic and chemical evidence for a relationship between kimberlite and Zaire cubic diamonds. *Nature* **336**, 665–667.

Alard O., Griffin W. L., Lorand J. P., Jackson S. E., and O'Reilly S. Y. (2000) Non-chondritic distribution of the highly siderophile elements in mantle sulphides. *Nature* **407**, 891–894.

Alexander C. M. O. D. (2001) Inherited material from the protosolar cloud: composition and origin. *Phil. Trans. Roy. Soc. London A* **359**, 1973–1989.

Allamandola L. J., Sandford S. A., Tielens A. G. G. M., and Herbst T. M. (1993) Diamonds in dense molecular clouds: a challenge to the standard interstellar medium paradigm. *Science* **260**, 64–66.

Aoki K. (1968) Petrogenesis of ultrabasic and basic inclusions in Iki Island, Japan. *Am. Mineral.* **53**, 241–256.

Arai S. (1994) Characterization of spinel peridotites by olivine-spinel compositional relationships: review and interpretation. *Chem. Geol.* **113**, 191–204.

Arndt N. T. and Christensen U. (1992) The role of lithospheric mantle in flood volcanism: thermal and geochemical constraints. *J. Geophys. Res.* **97**, 10967–10981.

Ave Lallement H. L., Carter N. L., Mercier J. C., and Ross J. V. (1980) Rheology of the uppermost mantle: inferences from peridotite xenoliths. *Tectonophysics* **70**, 221–234.

Baker M. B. and Stolper E. M. (1994) Determining the composition of high-pressure mantle melts using diamond aggregates. *Geochim. Cosmochim. Acta* **58**, 2811–2827.

Ballhaus C., Berry R. F., and Green D. H. (1991) High pressure experimental calibration of the olivine-orthopyroxene-spinel oxygen barometer: implications for the oxidation state of the upper mantle. *Contrib. Mineral. Petrol.* **107**, 27–40.

Barnes S. J. and Roeder P. L. (2001) The range of spinel compositions in terrestrial mafic and ultramafic rocks. *J. Petrol.* **42**, 2279–2302.

Barth M. G., Rudnick R. L., Horn I., McDonough W. F., Spicuzza M. J., Valley J. W., and Haggerty S. E. (2001) Geochemistry of xenolithic eclogites from West Africa: Part I. A link between low MgO eclogites and Archean crust formation. *Geochim. Cosmochim. Acta* **65**, 1499–1527.

Barth M. G., Rudnick R. L., Carlson R. W., Horn I., and McDonough W. F. (2003) Re–Os and U–Pb geochronological constraints on the eclogite-tonalite connection in the Archean Man Shield, West Africa. *Precamb. Res.* **118**, 267–283.

Barth M. G., Rudnick R. L., Horn I., McDonough W. F., Spicuzza M. J., Valley J. W., and Haggerty S. E. (2002) Geochemistry of xenolithic eclogites from West Africa: Part II. Origins of the high MgO eclogites. *Geochim. Cosmochim. Acta* **66**, 4325–4345.

Basu A. R. and Murthy V. R. (1977) Ancient lithospheric lherzolite xenoliths in alkali basalt from Baja California. *Earth Planet. Sci. Lett.* **35**, 239–246.

Basu A. R. and Tatsumoto M. (1980) Nd isotopes in selected mantle-derived rocks and minerals and their implications for mantle evolution. *Contrib. Mineral. Petrol.* **75**, 43–54.

Beard B. L., Fraracci K. N., Taylor L. A., Snyder G. A., Clayton R. N., Mayeda T., and Sobolev N. V. (1996) Petrography and geochemistry of eclogites from the Mir kimberlite, Yakutia, Russia. *Contrib. Mineral. Petrol.* **125**, 293–310.

Bedini R. M. and Bodinier J. L. (1999) Distribution of incompatible trace elements between the constituents of spinel peridotite xenoliths: ICP–MS data from the east African rift. *Geochim. Cosmochim. Acta* **63**, 3883–3900.

Bedini R. M., Blichert-Toft J., Boyet M., and Albarede F. (2002) Lu–Hf isotope geochemistry of garnet-peridotite xenoliths from the Kaapvaal craton and the thermal regime of the lithosphere. *Geochim. Cosmochim. Acta (Spec. Suppl.)* **66S1**, A61.

Beeson M. H. and Jackson E. D. (1970) Origin of the garnet pyroxenite xenoliths from Salt Lake Crater Oahu. *Spec. Pap. Min. Soc. Am.* **3**, 95–112.

Ben Othman D., Tilton G. R., and Menzies M. A. (1990) Pb–Nd–Sr isotopic investigations of kaersutite and clinopyroxene from ultramafic nodules and their host basalts: the nature of the subcontinental mantle. *Geochim. Cosmochim. Acta* **54**, 3449–3460.

Binns R. A., Duggan M. B., and Wilkinson J. F. G. (1970) High pressure megacrysts in alkaline lavas from northeastern New South Wales. *Am. J. Sci.* **269**, 132–168.

Blichert-Toft J., Ionov D. A., and Albarede F. (2000) The nature of the sub-continental lithospheric mantle: Hf isotope evidence from garnet peridotite xenoliths from Siberia. *J. Conf. Abstr.* **5**, 217.

Bodinier J. L., Merlet C., Bedini R. M., Simien F., Remaidi M., and Garrido C. J. (1996) Distribution of niobium, tantalum, and other highly incompatible trace elements in the lithospheric mantle: the spinel paradox. *Geochim. Cosmochim. Acta* **60**, 545–550.

Boettcher A. L. and O'Neill J. R. (1980) Stable isotope, chemical, and petrographic studies of high-pressure amphiboles and micas: evidence for metasomatism in the mantle source regions for alkali basalts and kimberlites. *Am. J. Sci.* **280A**, 594–621.

Boullier A. M. and Nicolas A. (1975) Classification of textures and fabrics of peridotite xenoliths from South African kimberlites. *Phys. Chem. Earth* **9**, 467–475.

Boyd F. R. (1969) Electron-probe study of diopside inclusions from kimberlite. *Am. J. Sci.* **267A**, 50–69.

Boyd F. R. (1970) Garnet peridotites and the system $CaSiO_3$–$MgSiO_3$–Al_2O_3. *Min. Soc. Am. Spec. Publ.* **3**, 63–75.

Boyd F. R. (1973) A pyroxene geotherm. *Geochim. Cosmochim. Acta* **37**, 2533–2546.

Boyd F. R. (1989) Compositional distinction between oceanic and cratonic lithosphere. *Earth Planet. Sci. Lett.* **96**, 15–26.

Boyd F. R. (1997) Origins of peridotite xenoliths: major element considerations. In *Short Course on High P and T Research on the Lithosphere*. U. Siena. pp. 89–106.

Boyd F. R. and McAllister R. H. (1976) Densities of fertile and sterile garnet peridotites. *Geophys. Res. Lett.* **3**, 509–512.

Boyd F. R. and Mertzman S. A. (1987) Composition and structure of the Kaapvaal lithosphere, Southern Africa. In *Magmatic Processes: Physicochemical Principles* (ed. B. O. Mysen). The Geochemical Society, Houston, vol. 1, pp. 3–12.

Boyd F. R. and Nixon P. H. (1978) Ultramafic nodules from the Kimberley pipes, South Africa. *Geochim. Cosmochim. Acta* **42**, 1367–1382.

Boyd F. R., Jones R. A., and Nixon P. H. (1983) Mantle metasomatism: the Kimberley dunites. *Carneg. Inst. Wash. Yearb.* **82**, 330–336.

Boyd F. R., Dawson J. B., and Smith J. V. (1984a) Granny Smith diopside megacrysts from the kimberlites of the Kimberley area and Jagersfontein, South Africa. *Geochim. Cosmochim. Acta* **48**, 381–384.

Boyd F. R., Nixon P. H., and Boctor N. Z. (1984b) Rapidly crystallised garnet pyroxenite xenoliths possibly related to discrete nodules. *Contrib. Mineral. Petrol.* **86**, 119–130.

Boyd F. R., Pearson D. G., Nixon P. H., and Mertzman S. A. (1993) Low Ca garnet harzburgites from southern Africa: their relation to craton structure and diamond crystallisation. *Contrib. Mineral. Petrol.* **113**, 352–366.

Boyd F. R., Pokhilenko N. P., Pearson D. G., Mertzman S. A., Sobolev N. V., and Finger L. W. (1997) Composition of the Siberian cratonic mantle: evidence from Udachnaya peridotite xenoliths. *Contrib. Mineral. Petrol.* **128**, 228–246.

Boyd F. R., Pearson D. G., and Mertzman S. A. (1999) Spinel-facies peridotites from the Kaapvaal root. In *Proc. 7th Int. Kimb. Conf.* (eds. J. J. Gurney, J. L. Gurney, M. D. Pascoe, and S. H. Richardson). National Book Printers, Red Roof Design, Cape Town, vol. 1, pp. 40–48.

Boyd S. R. and Pillinger C. T. (1994) A preliminary study of $^{15}N/^{14}N$ in octahedral growth form diamonds. *Chem. Geol.* **116**(1–2), 43–59.

Boyd S. R., Mattey D. P., Pillinger C. T., Milledge H. J., Mendelssohn M., and Seal M. (1987) Multiple growth events during diamond genesis: an integrated study of carbon and nitrogen isotopes and nitrogen aggregation state in coated stones. *Earth Planet. Sci. Lett.* **86**(2), 341–353.

Boyd S. R., Pillinger C. T., Milledge H. J., and Seal M. J. (1992) C and N isotopic composition and the infrared absorption spectra of coated diamonds: evidence for the regional uniformity of CO (sub 2)-H (sub 2) O rich fluids in lithospheric mantle. *Earth Planet. Sci. Lett.* **108**, 139–150.

Brandon A. D., Becker H., Carlson R. W., and Shirey S. B. (1999) Isotopic constraints on timescales and mechanisms of slab material transport in the mantle wedge: evidence from the Simcoe mantle xenoliths, Washington USA. *Chem. Geol.* **160**, 387–407.

Brandon A. D., Snow J. E., Walker R. J., Morgan J. W., and Mock T. D. (2001) ^{190}Pt–^{186}Os and ^{187}Re–^{187}Os systematics of abyssal peridotites. *Earth Planet. Sci. Lett.* **177**, 319–335.

Brey G. P. (1990) Geothermobarometry for lherzolites: experiments from 10 kb to 60 kb, new thermobarometers and application to natural rocks. Habil. Thesis, University of Aarmstadt, Germany, 227pp.

Brey G. and Köhler T. (1990) Geothermobarometry in four-phase lherzolites: II. New thermobarometers, and practical assessment of existing thermobarometers. *J. Petrol.* **31**, 1353–1378.

Brey G., Köhler T., and Nickel K. G. (1990) Geothermobarometry in four-phase lherzolites: I. Experimental results from 10 to 60 kb. *J. Petrol.* **31**, 1313–1352.

Bruekner H. K. (1974) Mantle Rb/Sr and $^{87}Sr/^{86}Sr$ ratios from clinopyroxenes from Norwegian garnet peridotites and pyroxenites. *Earth Planet. Sci. Lett.* **24**, 26–32.

Bulanova G. P. (1995) The formation of diamond. Diamond Exploration into the 21st Century. *J. Geoch. Explor.* **53**(1–3), 1–23.

Bulanova G. P., Pearson D. G., Hauri E. H., and Griffin William L. (2002) Carbon and nitrogen isotope systematics within a sector-growth diamond from the Mir kimberlite, Yakutia. *Chem. Geol.* **188**, 105–123.

Bulatov V., Brey G. P., and Foley S. F. (1991) Origin of low-Ca, high-Cr garnets by recrystallization of low-pressure harzburgites. *Fifth International Kimberlite Conference, Extended Abstracts,* CPRM Spec. Publ., 2/91, CPRM, Brasilia, pp. 29–31.

Burgess R., Johnson L. H., Mattey D. P., Harris J. W., and Turner G. (1998) He, Ar and C isotopes in coated and polycrystalline diamonds. *Chem. Geol.* **146**(3–4), 205–217.

Burgess R., Layzelle E., Turner G., and Harris J. W. (2002) Constraints on the age and halogen composition of mantle fluids in Siberian coated diamonds. *Earth Planet. Sci. Lett.* **197**, 193–203.

Burgess S. R. and Harte B. (1999) Tracing lithosphere evolution through the analysis of heterogeneous G9/G10 garnets in peridotite xenoliths: I. Major element analysis. In *Proc. 7th Int. Kimberlite Conf.* (eds. J. J. Gurney, J. L. Gurney, M. D. Pascoe, and S. H. Richardson). Red Roof Design, Cape Town, vol. 1, pp. 66–80.

Burnham O. M., Rogers N. W., Pearson D. G., van calsteren P. W., and Hawkesworth C. J. (1998) The petrogenesis of the eastern Pyrenean peridotites: an integrated study of their whole-rock geochemistry and Re–Os isotope composition. *Geochim. Cosmochim. Acta* **62**, 2293–2310.

Burton K. W., Schiano P., Birck J.-L., Allegre C. J., Rehkämper M., Halliday A. N., and Dawson J. B. (2000) The distribution and behaviour of rhenium and osmium amongst mantle minerals and the age of the lithospheric mantle beneath Tanzania. *Earth Planet. Sci. Lett.* **183**, 93–106.

Canil D. (1990) Experimental study bearing on the absence of carbonate in mantle-derived xenoliths. *Geology* **18**, 1011–1013.

Canil D. (1991) Experimental evidence for the exsolution of cratonic peridotite from high temperature harzburgite. *Earth Planet. Sci. Lett.* **106**, 64–72.

Canil D. (1992) Orthopyroxene stability along the peridotite solidus and the origin of cratonic lithosphere beneath southern Africa. *Earth Planet. Sci. Lett.* **111**, 83–95.

Canil D. (1999) The Ni-in-garnet geothermometer: calibration at natural abundances. *Contrib. Mineral. Petrol.* **136**, 240–246.

Canil D. (2002) Vanadium in peridotites, mantle redox and tectonic environments: Archean to present. *Earth Planet. Sci. Lett.* **195**, 75–90.

Canil D. and Fedortchouk Y. (2000) Clinopyroxene-liquid partitioning for vanadium and the oxygen fugacity during formation of cratonic and oceanic mantle lithosphere. *J. Geophys. Res.* **105**, 26003–26016.

Canil D. and O'Neill H. S. C. (1996) Distribution of ferric iron in some upper mantle assemblages. *J. Petrol.* **37**, 609–635.

Canil D. and Wei K. (1992) Constraints on the origin of mantle-derived low Ca garnets. *Contrib. Mineral. Petrol.* **109**, 421–430.

Canil D., O'Neill H. S. C., Pearson D. G., Rudnick R. L., McDonough W. F., and Carswell D. A. (1994) Ferric iron in peridotites and mantle oxidation states. *Earth Planet. Sci. Lett.* **123**, 205–220.

Carlson R. W. and Irving A. J. (1994) Depletion and enrichment history of sub-continental lithospheric mantle: Os, Sr, Nd and Pb evidence for xenoliths from the Wyoming Craton. *Earth Planet. Sci. Lett.* **126**, 457–472.

Carlson R. W., Irving A. J., and Hearn B. C., Jr. (1999a) Chemical and isotopic systematics of peridotite xenoliths from the Williams kimberlite, Montana: clues to processes of lithospheric formation, modification and destruction. In *Proc. 7th Int. Kimberlite Conf.* (eds. J. J. Gurney, J. L. Gurney, M. D. Pascoe, and S. H. Richardson). Red Roof Design, Cape Town, vol. 1, pp. 90–98.

Carlson R. W., Pearson D. G., Boyd F. R., Shirey S. B., Irvine G., Menzies A. H., and Gurney J. J. (1999b) Regional age variation of the southern African mantle: significance for models of lithospheric mantle formation. In *Proc. 7th Int. Kimberlite Conf.* (eds. J. J. Gurney, J. L. Gurney, M. D. Pascoe, and S. H. Richardson). Red Roof Design, Cape Town, vol. 1, pp. 99–108.

Cartigny P. (1998) Carbon isotopes in diamond. PhD Thesis, Universite de Paris VII.

Cartigny P., Boyd S. R., Harris J. W., and Javoy M. (1997) Nitrogen isotopes in peridotitic diamonds from Fuxian, China: the mantle signature. *Terra Nova* **9**(4), 175–179.

Cartigny P., Harris J. W., and Javoy M. (1998a) Eclogitic diamond formation at Jwaneng: no room for a recycled component. *Science* **280**, 1421–1424.

Cartigny P., Harris J. W., Phillips D., Girard M., and Javoy M. (1998b) Subduction-related diamonds? The evidence for a mantle-derived origin from coupled delta (^{13}C-delta ^{15}N determinations. In *The Degassing of the Earth* (eds. M. R. Carroll, S. C. Kohn, and B. J. Wood). Elsevier, Amsterdam, vol. 147(1–2), pp. 147–159.

Cartigny P., Harris J. W., and Javoy M. (1999) Eclogitic, peridotitic and metamorphic diamonds and the problems of carbon recycling: the case of Orapa (Botswana). In *Proc. 7th Int. Kimberlite Conf.* (eds. J. J. Gurney, J. L. Gurney, M. D. Pascoe, and S. H. Richardson). Red Roof Design, Cape Town, vol. 1, pp. 117–124.

Cartigny P., Harris J. W., and Javoy M. (2001) Diamond genesis, mantle fractionations and mantle nitrogen content: a study of d^{13}C–N concentrations in diamonds. *Earth Planet. Sci. Lett.* **185**, 85–98.

Carswell D. A. (1975) Primary and secondary phlogopites and clinopyroxenes in garnet lherzolite xenoliths. *Phys. Chem. Earth* **9**, 417–429.

Carswell D. A. (1991) The garnet-orthopyroxene Al barometer: problematic application to natural garnet lherzolite assemblages. *Mineral. Mag.* **55**, 19–31.

Carswell D. A., Griffin W. L., and Kresten P. (1984) Peridotite nodules from the Ngopetsoeu and Lipelaneng kimberlites. Lesotho: a crustal or mantle origin. In *Kimberlites II: The Mantle and Crust-mantle Relationships* (ed. J. Kornprobst). Elsevier, Amsterdam, pp. 229–243.

Carter J. L. (1970) Mineralogy and chemistry of the earth's upper mantle based on partial fusion-partial crystallisation model. *Geol. Soc. Am. Bull.* **81**, 2021–2034.

Chaussidon M., Albarède F., and Sheppard S. M. F. (1989) Sulfur isotope variations in the mantle from ion-microprobe analyses of micro-sulfide inclusions. *Earth Planet. Sci. Lett.* **92**, 144–156.

Chazot G., Menzies M. A., and Harte B. (1996) Determination of partition coefficients between apatite, clinopyroxene, amphibole and melt in natural spinel lherzolites from Yemen: implications for wet melting of the lithospheric mantle. *Geochim. Cosmochim. Acta* **60**, 423–437.

Chazot G., Lowry D., Menzies M. A., and Mattey D. (1997) Oxygen isotopic composition of hydrous and anhydrous mantle peridotites. *Geochim. Cosmochim. Acta* **61**, 161–169.

Chesley J. T., Rudnick R. L., and Lee C. T. (1999) Re–Os systematics of mantle xenoliths from the East African Rift: age, structure and history of the Tanzanian craton. *Geochim. Cosmochim. Acta* **63**, 1203–1217.

Chrenko R. M., McDonald R. S., and Darrow K. A. (1967) Infra-red spectrum of diamond coat. *Nature* **214**, 474–476.

Ciuff S., Rivalenti G., Vannucci R., Zanetti A., Mazzucchelli M., and Cingolani C. A. (2002) Are the glasses in mantle xenoliths witness of the metasomatic agent composition? *Geochim. Cosmochim. Acta (Spec. Suppl.)* **66S1**, A143.

Cohen R. S., O'Nions R. K., and Dawson J. B. (1984) isotope geochemistry of xenoliths from East Africa: implications for development of mantle reservoirs and their interaction. *Earth Planet. Sci. Lett.* **68**, 209–220.

Coleman R. G. and Keith T. E. (1971) A chemical study of serpentinization—Burro Mountain, California. *J. Petrol.* **12**, 311–329.

Coltorti M., Bonadiman C., Hinton R. W., Siena F., and Upton B. G. J. (1999) Carbonatite metasomatsim of the oceanic upper mantle: evidence from clinopyroxenes and glasses in ultramafic xenoliths of Grande Comore, Indian Ocean. *J. Petrol.* **40**, 133–165.

Cox K. G., Smith M. R., and Beswetherick S. (1987) Textural studies of garnet lherzolites: evidence of exsolution origin from high-temperature harzburgites. In *Mantle Xenoliths* (ed. P. H. Nixon). Wiley, Chichester, pp. 537–550.

Daniels L. R. M. and Gurney J. J. (1999) Dokolwayo diamond carbon isotopes. In *The J. B. Dawson Volume: Proceedings of the VIIth International Kimberlite Conference* (eds. J. J. Gurney, J. L. Gurney, M. D. Pascoe, and S. H. Richardson). Red Roof Designs, Cape Town, vol. 1, pp. 143–147.

Davies R. M., Griffin W. L., Pearson N. J., Andrew A. S., Doyle B. J., and O'Reilly S. Y. (1999) Diamonds from the deep: pipe DO-27, Slave Craton, Canada. In *The J. B. Dawson Volume: Proceedings of the VIIth International Kimberlite Conference* (eds. J. J. Gurney, J. L. Gurney, M. D. Pascoe, and S. H. Richardson). Red Roof Designs, Cape Town, vol. 1, pp. 148–155.

Dawson J. B. and Smith J. V. (1975) Occurrence of diamond in a mica-garnet lherzolite xenolith from kimberlite. *Nature* **254**, 580–58.

Dawson J. B. and Smith J. V. (1977) The MARID (mica-amphibole-rutile-ilmenite-diopside) suite of xenoliths in kimberlite. *Geochim. Cosmochim. Acta* **41**, 309–323.

De S., Heaney P. J., Hargraves R. B., Vicenzi E. P., and Taylor P. T. (1998) Microstructural observations of polycrystalline diamond: a contribution to the carbonado conundrum. *Earth Planet. Sci. Lett.* **164**(3–4), 421–433.

Deines P. (1980) The carbon isotopic composition of diamonds: relationship to diamond shape, color, occurrence and vapor composition. *Geochim. Cosmochim. Acta* **44**(7), 943–962.

Deines P. and Haggerty S. (2000) Small-scale oxygen isotope variations and petrochemistry of ultradeep (>300 km) and transition zone xenoliths. *Geochim. Cosmochim. Acta* **64**, 117–131.

Deines P. and Harris J. W. (1995) Sulfide inclusion chemistry and carbon isotopes of African diamonds. *Geochim. Cosmochim. Acta* **59**(15), 3173–3188.

Deines P., Harris J. W., and Gurney J. J. (1987) Carbon isotopic composition, nitrogen content and inclusion composition of diamonds from the Roberts Victor Kimberlite, South Africa: evidence for ^{13}C depletion in the mantle. *Geochim. Cosmochim. Acta* **51**, 1227–1243.

Deines P., Harris J. W., Spear P. M., and Gurney J. J. (1989) Nitrogen and ^{13}C content of Finsch and Premier diamonds and their implications. *Geochim. Cosmochim. Acta* **53**, 1367–1378.

Deines P., Harris J. W., and Gurney J. J. (1991a) The carbon isotopic composition and nitrogen content of lithospheric and asthenospheric diamonds from the Jagersfontein and Koffiefontein Kimberlite, South Africa. *Geochim. Cosmochim. Acta* **55**, 2615–2625.

Deines P., Harris J. W., Robinson D. N., Gurney J. J., and Shee S. R. (1991b) Carbon and oxygen isotope variations in diamond and graphite eclogites from Orapa, Botswana, and the nitrogen content of their diamonds. *Geochim. Cosmochim. Acta* **55**(2), 515–524.

Deines P., Harris J. W., and Gurney J. J. (1993) Depth-related carbon isotope and nitrogen concentration variability in the mantle below the Orapa Kimberlite, Botswana, Africa. *Geochim. Cosmochim. Acta* **57**, 2781–2796.

Deines P., Harris J. W., and Gurney J. J. (1997) Carbon isotope ratios, nitrogen content and aggregation state, and inclusion chemistry of diamonds from Jwaneng, Botswana. *Geochim. Cosmochim. Acta* **61**(18), 3993–4005.

Deines P., Viljoen F., and Harris J. W. (2001) Implications of the carbon isotope and mineral inclusion record for the formation of diamonds in the mantle underlying a mobile belt: Venetia, South Africa. *Geochim. Cosmochim. Acta* **65**(5), 813–838.

Dick H. J. B. and Sinton J. M. (1979) Compositional layering in Alpine peridotites: evidence for pressure solution creep in the mantle. *J. Geol.* **87**, 403–416.

Downes H. and Dupuy C. (1987) Textural, isotopic and rare earth variations in spinel peridotites xenoliths, Massif Central, France. *Earth Planet. Sci. Lett.* **82**, 121–135.

Ducea M., Sen G., Eiler J., and Fimbres J. (2002) Melt depletion and subsequent metasomatism in the shallow mantle beneath Koolau volcano (Hawaii). *Geochem. Geophys. Geosys.* **3** 10.1029/2001GC000184.

Dunai T. J. and Baur H. (1995) Helium, neon, and argon systematics of the European subcontinental mantle: implications for its geochemical evolution. *Geochim. Cosmochim. Acta* **59**, 2767–2783.

Eggins S. M. (1992) Petrogenesis of Hawaiin tholeiites: 1. Phase equilibria constraints. *Contrib. Mineral. Petrol.* **110**, 387–397.

Eggins S. M., Rudnick R. L., and McDonough W. F. (1998) The composition of peridotites and their minerals: a laser-ablation ICP–MS study. *Earth Planet. Sci. Lett.* **154**, 53–71.

Eggler D. H., McCallum M. E., and Smith C. B. (1979) Megacryst assemblages in kimberlite from northern Colorado and southern Wyoming: petrology, geothermometry–barometry and areal distribution. In *Kimberlites, Diatremes, and Diamonds: Their Geology, Petrology, and Geochemistry* (eds. F. R. Boyd and H. O. A. Meyer). American Geophysical Union, Washington, DC, vol. 1, pp. 213–226.

Ehrenberg S. N. (1982a) Petrogenesis of garnet lherzolite and megacrystalline nodules from the Thumb, Navajo Volcanic Field. *J. Petrol.* **23**, 507–47.

Ehrenberg S. N. (1982b) Rare earth element geochemistry of garnet lherzolite and megacrystalline nodules from minette of the Colorado Plateau province. *Earth Planet. Sci. Lett.* **57**, 191–210.

Erlank A. J., Waters F. G., Hawkesworth C. J., Haggerty S. E., Allsopp H. L., Rickard R. S., and Menzies M. A. (1987) Evidence for mantle metasomatism in peridotite nodules from the Kimberley pipes, South Africa. In *Mantle Metasomatism* (eds. C. J. Hawkesworth and M. A. Menzies). Academic Press, London, pp. 221–311.

Evans T. (1992) Aggregation of nitrogen in diamond. In *The Properties of Natural and Synthetic Diamond* (ed. J. E. Field). Academic Press, London, pp. 259–290.

Evans T. and Harris J. W. (1989) Nitrogen aggregation, inclusion equilibration temperatures and the age of diamonds. In *Kimberlites and Related Rocks* (ed. N. Ross). Spec. Publ. Geol. Soc. Austral. No. 14, IGSA, Perth, vol. 2, pp. 1001–1006.

Evans T. and Zengdu Q. (1982) The kinetics of the aggregation of nitrogen atoms in diamond. *Proc. Roy. Soc. London, Ser. A: Math. Phys. Sci.* **381**(1780), 159–178.

Farquhar J., Wing B. A., McKeegan K. D., Harris J. W., Cartigny P., and Thiemens M. H. (2002) Anomalous sulfur isotope compositions of inclusions from diamonds: evidence

for recycling of sulfur to the mantle on early Earth. *Science* **298**, 2369–2372.

Fei Y. and Bertka C. M. (1999) Phase transitions in the Earth's mantle and mantle mineralogy. In *Mantle Petrology: Field Observations and High-pressure Experimentation; a Tribute to Francis R. (Joe) Boyd* (eds. Y. Fei, M. Bertka Constance, and O. Mysen Bjorn). Geochemical Society, Houston, vol. 6, pp. 189–207.

Fermor L. L. (1913) Preliminary note on garnet as a geological barometer and on an infra-plutonic zone in the Earth's crust. *Geol Surv. India, Records* **43**, 41–47.

Field J. E. (1979) *The Properites of Diamond*. Academic Press, London, 674pp.

Field J. E. (1992) *The Properties of Natural and Synthetic Diamond*. Academic Press, London 710pp.

Finnerty A. A. (1989) Xenolith-derived mantle geotherms: whither the inflection? *Contrib. Mineral. Petrol.* **102**, 367–375.

Finnerty A. A. and Boyd F. R. (1987) Thermobarometry for garnet peridotite xenoliths: a basis for upper mantle stratigraphy. In *Mantle Xenoliths* (ed. P. H. Nixon). Wiley, Chichester, pp. 381–402.

Fitzsimons I. C. W., Harte B., Chinn I. L., Gurney J. J., and Taylor W. R. (1999) Extreme chemical variation in complex diamonds from George Creek, Colorado: a SIMS study of carbon isotope composition and nitrogen abundance. *Min. Mag.* **63**(6), 857–878.

Foley S. F. (1992) Vein-plus-wall-rock melting mechanisms in the lithosphere and the origin of potassic alkaline magmas. *Lithos* **28**, 435–453.

Francis D. (1976) The origin of amphibole in lherzolite xenoliths from Nunivak Island, Alaska. *J. Petrol.* **17**, 357–78.

Franz L., Brey G., and Okrusch M. (1996a) Steady state geotherm, thermal disturbances and tectonic development of the lower lithosphere underneath the Gibeon Kimberlite Province, Namibia. *Contrib. Mineral. Petrol.* **126**, 181–198.

Franz L., Brey G. P., and Okrusch M. (1996b) Re-equilibration of ultramafic xenoliths from Namibia by metasomatic processes at the mantle boundary. *J. Geol.* **104**, 599–615.

Frey F. A. (1980) The origin of pyroxenites and garnet pyroxenites from Salt Lake Crater, Oahu, Hawaiii: trace element evidence. *Am. J. Sci* **280**, 427–449.

Frey F. A. and Green D. H. (1974) The mineralogy, geochemistry and origin of lherzolite inclusions in Victorian basanites. *Geochim. Cosmochim. Acta* **38**, 1023–1059.

Frey F. A. and Prinz M. (1978) Ultramafic inclusions from San Carlos, Arizona: petrological and geochemical data bearing on their petrogenesis. *Earth Planet. Sci. Lett.* **38**, 129–176.

Fukunaga K., Matsuda J. i., Nagao K., Miyamoto M., and Ito K. (1987) Noble-gas enrichment in vapour-growth diamonds and the origin of diamonds in ureilites. *Nature* **328**(6126), 141–143.

Fung A. T. and Haggerty S. E. (1995) Petrography and mineral composition of eclogites from the Koidu kimberlite complex, Sierra Leone. *J. Geophys. Res. B.* **100**(10), 20451–20473.

Galer S. J. G. and O'Nions R. K. (1989) Chemical and isotopic studies of ultramafic inclusions from the San Carlos Volcanic Field, Arizona: a bearing on their petrogenesis. *J. Petrol.* **30**, 1033–1064.

Galimov E. M. (1984) The relation between formation conditions and variations in isotope composition of diamonds. *Geochemistry* **8**, 1091–1118.

Galimov E. M. (1991) Isotope fractionation related to kimberlite magmatism and diamond formation. *Geochim. Cosmochim. Acta* **55**(6), 1697–1708.

Galimov E. M., Kaminskiy F. V., and Ivanovskaya I. N. (1978) Carbon isotope compositions of diamonds from the Urals, Timan, Sayan, the Ukraine, and elsewhere. *Geochem. Int.* **15**(2), 11–18.

Garlick G. D., MacGregor I. D., and Vogel D. E. (1971) Oxygen isotope ratios in eclogites from kimberlites. *Science* **172**, 1025–1027.

Gao S., Rudnick R. L., Carlson R. W., McDonough W. F., and Liu Y.-S. (2002) Re–Os evidence for replacement of ancient mantle lithosphere beneath the North China craton. *Earth Planet. Sci. Lett.* **198**, 307–322.

Gasparik T. and Hutchison M. T. (2000) Experimental evidence for the origin of two kinds of inclusions in diamonds from the deep mantle. *Earth Planet. Sci. Lett.* **181**(1–2), 103–114.

Gautheron C. and Moreira M. (2002) Helium isotopic signature of the subcontinental lithospheric mantle. *Earth Planet. Sci. Lett.* **199**, 39–47.

Girnis A. V. and Brey G. P. (1999) Garnet-spinel-olivine-orthopyroxene equilibria in the $FeO–MgO–Al_2O_3–SiO_2–Cr_2O_3$ system: II. Thermodynamic analysis. *Euro. J. Mineral.* **11**, 619–636.

Glaser S. M., Foley S. F., and Gunther D. (1999) Trace element compositions of minerals in garnet and spinel peridotite xenoliths from the Vitim volcanic field, Transbaikalia, eastern Siberia. *Lithos* **48**, 263–285.

Goetze C. (1975) Sheared lherzolites: from the point of view of rock mechanics. *Geology* **3**, 172–173.

Green D. H. and Hibberson W. (1970) The instability of plagioclase in peridotite at high pressure. *Lithos* **3**, 209–221.

Green D. H. and Ringwood A. E. (1970) Mineralogy of peridotitic compositions under upper mantle conditions. *Phys. Earth Planet. Int.* **3**, 359–371.

Gregoire M., Bell D. R., and Roux A. P. L. (2002) Trace element geochemistry of phlogopite-rich mafic mantle xenoliths: their classification and their relationship to phlogopite-bearing peridotites and kimberlites revisited. *Contrib. Mineral. Petrol.* **142**, 603–625.

Gregory R. T. and Taylor H. P. (1986) Non-equilibrium metasomatic $^{18}O/^{16}O$ effects in upper mantle mineral assemblages. *Contrib. Mineral. Petrol.* **93**, 124–135.

Griselin M. and Lassiter J. C. (2002) Extreme unradiogenic Os isotopes in Hawaiin mantle xenoliths: implications for mantle convection. *Geochim. Cosmochim. Acta. (Spec. Suppl.)* **66**(**S1**), A292.

Griffin W. L., Cousens D. R., Ryan C. G., and Suter G. F. (1989) Ni in chrome garnet: a new geothermometer. *Contrib. Mineral. Petrol.* **103**, 199–202.

Griffin W. L., Sobolev N. V., Ryan C. G., Pokhilenko N. P., Win T. T., and Yefimova E. S. (1993) Trace elements in garnets and chromites: diamond formation in the Siberian lithosphere. *Lithos* **29**, 235–256.

Griffin W. L., O'Reilly S. Y., and Stabel C. G. (1988) Mantle metasomatism beneath western Victoria, Australia: II. isotopic geochemistry of Cr-diopside lherzolites and Al-augite pyroxenites. *Geochim. Cosmochim. Acta.* **52**, 449–459.

Griffin W. L., Fisher N. I., Friedman J., Ryan C. G., and O'Reilly S. Y. (1999a) Cr-pyrope garnets in the lithospheric mantle: I. Compositional systematics and relations to tectonic setting. *J. Petrol.* **40**, 679–704.

Griffin W. L., O'Reilly S. Y., and Ryan C. G. (1999b) The composition and origin of sub-continental lithospheric mantle. In *Mantle Petrology: Field Observations and High Pressure Experimentation* (eds. Y. Fei, C. M. Bertka, and B. O. Mysen). The Geochemical Society, Houston, vol. 6, pp. 13–45.

Griffin W. L., Shee S. R., Ryan C. G., Win T. T., and Wyatt B. A. (1999c) Harzburgite to lherzolite and back again: metasomatic processes in ultramafic xenoliths from the Wesselton kimberlite. Kimberley, South Africa. *Contrib. Mineral. Petrol.* **134**, 232–250.

Gudmundsson G. and Wood B. J. (1995) Experimental tests of garnet peridotite oxygen barometry. *Contrib. Mineral. Petrol.* **199**, 56–67.

Gunther M. and Jagoutz E. (1994) isotopic disequilibria (Sm/Nd, Rb/Sr) between minerals of coarse grained, low temperature peridotites from Kimberely floors, southern Africa. In *Kimberlites, Related Rocks and Mantle Xenoliths, Proc. 5th Int. Kimberlite Conf., Araxa, Brazil. CPRM*. Spec.

Publ. 1/a (eds. H. O. A. Meyer and O. H. Leonardos). CPRM, Brasilia, pp. 354–356.

Gunther M. and Jagoutz E. (1997) The meaning of Sm/Nd apparent ages from kimberlite-derived coarse grained low temperatures peridotites from Yakutia. *Russian Geol. Geophys.* **38**, 229–239.

Gurney J. J. (1989) Diamonds. *Kimberlites and Related Rocks*. Spec. Publ. Geol. Soc. Austral., No. 14, vol. 2, pp. 935–965.

Gurney J. J. and Harte B. (1980) Chemical variations in upper mantle nodules from southern African kimberlites. *Phil. Trans. Roy. Soc. London* **A297**, 273–293.

Gurney J. J. and Switzer G. S. (1973) The discovery of garnets closely related to diamonds in the Finsch pipe, South Africa. *Contrib. Mineral. Petrol.* **39**, 103–116.

Gurney J. J., Harte B., and Cox K. G. (1975) Mantle xenoliths in the Matsoku kimberlite pipe. *Phys. Chem. Earth* **9**, 507–523.

Gurney J. J., Jacob W. R. O., and Dawson J. B. (1979) Megacrysts from the Monastery kimberlite pipe, South Africa. In *Kimberlites, Diatremes and Diamonds: Their Geology, Petrology and Geochemistry* (eds. F. R. Boyd and H. O. A. Meyer). American Geophysical Union, Washington, DC, vol. 1, pp. 222–243.

Gurney J. J., Moore R. O., Otter M. L., Kirkley M. B., Hops J. J., and McCandless T. E. (1991) Southern African kimberlites and their xenoliths. In *Magmatism in Extensional Structural Settings* (eds. A. B. Kampunzu and R. T. Lubala). Springer, Berlin, pp. 495–536.

Haggerty S. E. (1986) Diamond genesis in a multiply-constrained model. *Nature* **320**, 34–38.

Haggerty S. E. (1987) Metasomatic mineral titanates in upper mantle xenoliths. In *Mantle Xenoliths*. (ed. P. H. Nixon), Wiley, Chichester, pp. 671–690.

Haggerty S. E. (1989) Upper mantle opaque mineral stratigraphy and the genesis of metasomites and alkali-rich melts. In *Kimberlites and Related Rocks*. Geological Society of Australia Special Publication No. 14 (ed. J. Ross). Blackwell, Perth, vol. 2, pp. 687–699.

Haggerty S. E. (1999) A diamond trilogy: superplumes, supercontinents, and supernovae. *Science* **285**, 851–860.

Haggerty S. E. and Sautter V. (1990) Ultradeep (greater than 300 kilometers), ultramafic upper mantle xenoliths. *Science* **248**, 993–996.

Haggerty S. E., Smyth J. R., Erlank A. J., Rickard R. S., and Danchin R. V. (1983) Lindsleyite (Ba) and Mathiasite (K): two new chromium titanates in the crichtonite series from the upper mantle. *Am. Mineral.* **68**, 494–505.

Hamilton M. A., Pearson D. G., Stern R. A., and Boyd F. R. (1998) Constraints on MARID petrogenesis: SHRIMP II U–Pb zircon evidence for pre-eruption metasomatism at Kampfersdam. *7th Int. Kimberlite. Conf. (Ext. Abstr.)* Cape Town, 296–298.

Handler M. R. and Bennett V. C. (1999) Behaviour of platinum-group elements in the subcontinental mantle of eastern Australia during variable metasomatism and melt depletion. *Geochim. Cosmochim. Acta* **63**, 3597–3618.

Handler M. R., Bennett V. C., and Esat T. Z. (1997) The persistence of off-cratonic lithospheric mantle: Os isotopic systematics of variably metasomatised southeast Australian xenoliths. *Earth Planet. Sci. Lett.* **151**, 61–75.

Handler M. R., Bennett V. C., and Dreibus G. (1999) Evidence from correlated Ir/Os and Cu/S for late-stage Os mobility in peridotite xenoliths: implications for Re–Os systematics. *Geology* **27**, 75–78.

Hanghoj K., Kelemen P. B., Bernstein S., Blusztajn J., and Frei R. (2001) Osmium isotopes in the Wiedemann Fjord mantle xenoliths: a unique record of cratonic mantle formation by melt depletion in the Archaean. *Geochem. Geophys. Geosys.* **2** (20010109): 2000GC000085.

Harley S. L. (1984) An experimental study of the partitioning of Fe and Mg between garnet and orthopyroxene. *Contrib. Mineral. Petrol.* **86**, 359–373.

Harlow G. E. (1998) *The Nature of Diamonds*. Cambridge University Press, Cambridge, UK.

Harris J., Hutchison M. T., Hursthouse M., Light M., and Harte B. (1997) A new tetragonal silicate mineral occurring as inclusions in lower-mantle diamonds. *Nature (London)* **387**(6632), 486–488.

Harris J. W. (1987) Recent physical, chemical and isotopic research of diamond. In *Mantle Xenoliths* (ed. P. H. Nixon). Wiley, Chichester, pp. 477–500.

Harris J. W. (1992) Diamond geology. In *The Properties of Natural and Synthetic Diamond* (ed. J. E. Field). Academic Press, London, pp. 345–393.

Harris J. W. and Gurney J. J. (1979) Inclusions in diamond. In *The Properties of Diamond* (ed. J. E. Field). Academic Press, London, pp. 555–591.

Hart S. R. and Ravizza G. E. (1996) Os partitioning between phases in lherzolite and basalt. In *Earth Processes: Reading the isotopic Code*, Geophysical Monograph 95 (eds. A. Basu and S. R. Hart). American Geophysical Union, Washington, DC, pp. 123–134.

Hart S. R. and Zindler A. (1986) In search of a bulk Earth composition. *Chem. Geol.* **57**, 247–267.

Harte B. (1977) Rock nomenclature with particular relation to deformation and recrystallisation textures in olivine-bearing xenoliths. *J. Geology* **85**, 279–288.

Harte B. (1983) Mantle peridotites and processes—the kimberlite sample. In *Continental Basalts and Mantle Xenoliths* (eds. C. J. Hawkesworth and M. J. Norry). Shiva, Nantwich, pp. 46–91.

Harte B. and Hawkesworth C. J. (1989) Mantle domains and mantle xenoliths. In *Kimberlites and Related Rocks,* Geol. Soc. Austral. Spec. Publ., No. 14 (ed. J. Ross). Blackwell, Perth, vol. 2, pp. 649–686.

Harte B. and Kirkley M. B. (1997) Partitioning of trace elements between clinopyroxene and garnet: data from mantle eclogites. *Chem. Geol.* **136**, 1–24.

Harte B., Cox K. G., and Gurney J. J. (1975) Petrography and geological history of upper mantle xenoliths from the Matsoku kimberlite pipe. *Phys. Chem. Earth* **9**, 477–506.

Harte B., Winterburn P. A., and Gurney J. J. (1987) Metasomatic and enrichment phenomena in garnet peridotite facies mantle xenoliths from the Matsoku kimberlite pipe, Lesotho. In *Mantle Metasomatism* (eds. C. J. Hawkesworth and M. A. Menzies). Academic Press, London, pp. 145–220.

Harte B., Fitzsimons I. C. W., Harris J. W., and Otter M. L. (1999a) Carbon isotope ratios and nitrogen abundances in relation to cathodoluminescence characteristics for some diamonds from the Kaapvaal Province S. Africa. *Mineral. Mag.* **63**(6), 829–856.

Harte B., Harris J. W., Hutchison M. T., Watt G. R., and Wilding M. C. (1999b) Lower mantle mineral associations in diamonds from Sao Luiz, Brazil. In *Mantle Petrology; Field Observations and High-pressure Experimentation: A Tribute to Francis R. (Joe) Boyd* (eds. Y. Fei, M. Bertka Constance, and O. Mysen Bjorn). Geochemical Society, Houston, vol. 6, pp. 125–153.

Hassler D. R. and Shimizu N. (1998) Osmium isotopic evidence for ancient sub-continental lithospheric mantle beneath the Kerguelen Islands, southern Indian Ocean. *Science* **280**, 418–420.

Hatton C. J. and Gurney J. J. (1979) Eclogites and peridotites from kimberlites. In *The Mantle Sample: Inclusions in Kimberlites and Other Volcanics* (eds. F. R. Boyd and H. O. A. Meyer). American Geophysical Union, Washington, DC, pp. 29–36.

Hatton C. J. and Gurney J. J. (1987) Roberts Victor eclogites and their relation to the mantle. In *Mantle Xenoliths* (ed. P. H. Nixon). Wiley, Chichester, pp. 453–463.

Hauri E. and Hart S. R. (1993) Re–Os isotope systematics in HIMU and EMII Ocean island basalts. *Earth Planet. Sci. Lett.* **114**, 253–271.

Hauri E. H., Shimizu N., Dieu J. J., and Hart S. R. (1993) Evidence for hotspot-related carbonatite metasomatism in the oceanic upper mantle. *Nature* **365**, 221–227.

Hauri E. H., Pearson D. G., Bulanova G. P., and Milledge H. J. (1999) Microscale variations in C and N isotopes within mantle diamonds revealed by SIMS. *Proc. 7th Int. Kimberlite Conf.* (eds. J. J. Gurney, J. L. Gurney, M. D. Pascoe, and S. H. Richardson). Red Roof Design, Cape Town, vol. 1, pp. 341–347.

Hauri E. H., Wang J., Pearson D. G., and Bulanova G. P. (2002) Microanalysis $\delta^{15}C$, $\delta^{15}N$, and N abundances in diamonds by secondary ion mass spectrometry. *Chem. Geol.* **185**(1–2), 149–163.

Hawkesworth C. J., Erlank A. J., Marsh J. S., Menzies M. A., and van Calsteren P. (1983) Evolution of the continental lithosphere: evidence from volcanics and xenoliths from Southern Africa. In *Continental Basalts and Mantle Xenoliths* (eds. C. J. Hawkesworth and M. J. Norry). Shiva, Nantwich, pp. 111–138.

Helmstaedt H. and Doig R. (1975) Eclogite nodules from kimberlite pipes in the Colorado plateau-samples of subducted Franciscan type oceanic lithosphere. In *Phys. Chem. Earth* (eds. L. H. Ahrens, J. B. Dawson, A. R. Duncan, and A. J. Erlank). Pergamon, Oxford, vol. 9, pp. 95–111.

Hergt J. M., Peate D. W., and Hawkesworth C. J. (1991) The petrogenesis of Mesozoic Gondwana low-Ti flood basalts. *Earth Planet. Sci. Lett.* **105**, 134–148.

Herzberg C. (1999) Phase equilibrium constraints on the formation of cratonic mantle. In *Mantle Petrology: Field Observations and High Pressure Experimentation*, Spec. Publ. Geochem. Soc. (eds. Y. Fei, C. Bertka, and B. O. Mysen) Geochemical Society, Houston, vol. 6, pp. 241–250.

Hills D. V. and Haggerty S. E. (1989) Petrochemistry of eclogites from the Koidu Kimberlite Complex, Sierra Leone. *Contrib. Mineral. Petrol.* **103**, 397–422.

Hirschmann M. M. (2000) Mantle solidus: experimental constraints and the effects of peridotite composition. *Geochem. Geophys. Geosys.* **1** (20001024).

Hoal K. E. O., Hoal B. G., Erlank A. J., and Shimizu N. (1994) Metasomatism of the mantle lithosphere recorded by rare earth elements in garnets. *Earth Planet. Sci. Lett.* **126**, 303–313.

Holmes A. and Paneth F. A. (1936) Helium ratios of rocks and minerals from the diamond pipes of South Africa. *Proc. Roy. Soc. Ser.* **154A**, 385–413.

Honda M., Reynolds J. H., Roedder E., and Epstein S. (1987) Noble gases in diamonds: occurrences of solarlike helium and neon. *J. Geophys. Res.* **92**, 12507–12521.

Hops J., Gurney J. J., and Harte B. (1992) The Jagersfontein Cr-poor megacryst suite-towards a model for megacryst petrogenesis. *J. Volcanol. Geotherm. Res.* **50**, 143–160.

Horn I., Foley S. F., Jackson S. E., and Jenner G. A. (1994) Experimentally determined partitioning of high field strength and selected transition elements between spinel and basaltic melt. *Chem. Geol.* **117**, 193–218.

Hutchison M. T., Cartigny P., and Harris J. W. (1999) Carbon and nitrogen compositions and physical characteristics of transition zone and lower mantle diamonds from Sao Luiz, Brazil. In *The J. B. Dawson Volume: Proceedings of the VIIth International Kimberlite Conference* (eds. J. J. Gurney, J. L. Gurney, M. D. Pascoe, and S. H. Richardson), Red Root Designs, Cape Town, vol. 1, pp. 372–382.

Hutchison M. T., Hursthouse M. B., and Light M. E. (2001) Mineral inclusions in diamonds: associations and chemical distinctions around the 670-km discontinuity. *Contrib. Mineral. Petrol.* **142**(1), 119–126.

Hurley P. M., Fairburn H. W., and Pinson W. H. (1964) Rb–Sr relationships in serpentine from Mayaguez, Puerto Rico and dunite from St. Paul's rocks: a progress report. In *A Study of Serpentinite: The AMSOC Core Hole near Mayaguez, Puerto Rico*. (ed. C. A. Burke) Natl. Tes. Counc. vol. 1118, pp. 149–151.

Ionov D. (1998) Trace element composition of mantle-derived carbonates and coexisting phases in peridotite xenoliths from alkali basalts. *J. Petrol.* **39**, 1931–1941.

Ionov D. A. (1996) Distribution and residence of lithophile trace element in minerals of garnet and spinel peridotites: an ICP–MS study. *J. Conf. Abstr.* **1**, 278.

Ionov D. A. (2004) Chemical variations in peridotite xenoliths from Vitim, Siberia: inferences for REE and Hf behaviour in the garnet facies upper mantle. *J. Petrol.* **45**.

Ionov D. A. and Harmer R. E. (2002) Trace element distribution in calcite-dolomite carbonatites from Spitskop: inferences for differentiation of carbonatite magmas and the origin of carbonates in mantle xenoliths. *Earth Planet. Sci. Lett.* **198**, 495–510.

Ionov D. A. and Hofmann A. W. (1995) Nb–Ta–rich mantle amphiboles and micas: implications for subduction-related metasomatic trace element fractionations. *Earth Planet. Sci. Lett.* **131**, 341–356.

Ionov D. A., and Weis D. (2002) Hf isotope composition of mantle peridotites: first results and inferences for the age and evolution of the lithospheric mantle. *Abstract, 4th Int. Workshop on Orogenic Lherzolites and Mantle Processes*, Samani, Japan, pp. 56–57.

Ionov D. A., Ashchepkov I. V., Stosch H.-G., Witt-Eickschen G., and Seck H. A. (1993a) Garnet peridotite xenoliths from the Vitim volcanic field, Baikal Region: the nature of the garnet-spinel peridotite transition zone in the continental mantle. *J. Petrol.* **34**, 1141–1175.

Ionov D. A., Dupuy C., O'Reilly S., Kopylova M. G., and Genshaft Y. S. (1993b) Carbonated peridotite xenoliths from Spitsbergen: implications for trace element signature of mantle carbonate metasomatism. *Earth. Planet. Sci. Lett.* **119**, 283–297.

Ionov D. A., Griffin W. L., and O'Reilly S. Y. (1997) Volatile-bearing minerals and lithophile trace elements in the upper mantle. *Chem. Geol.* **141**, 153–184.

Ionov D. A., Bodinier J.-L., Mukasa S. B., and Zanetti A. (2002a) Mechanisms and sources of mantle metasomatism: major and trace element compositions of peridotite xenoliths from Spitsbergen in the context of numerical modelling. *J. Petrol.* **43**, 2219–2259.

Ionov D. A., Mukasa S. B., and Bodinier J.-L. (2002b) Sr–Nd–Pb isotopic compositions of peridotite xenoliths from Spitsbergen: numerical modelling indicates Sr–Nd decoupling in the mantle by melt percolation metasomatism. *J. Petrol.* **43**, 2261–2278.

Ireland T. R., Rudnick R. L., and Spetsius Z. (1994) Trace elements in diamond inclusions from eclogites reveal link to Archean granites. *Earth Planet. Sci. Lett.* **128**, 199–213.

Irifune T., Koizumi T., and Ando J.-I. (1996) An experimental study of the garnet-perovskite transformation in the system $MgSiO_3$–$MgAl_2SiO1_2$. *Phys. Earth Planet. Inter.* **96**, 147–157.

Irvine G. J. (2002) Time constraints on the formation of lithospheric mantle beneath cratons: a Re–Os isotope and Platinum Group Element study of peridotite xenoliths from Northern Canada and Lesotho, PhD Thesis, University of Durham.

Irvine G. J., Carlson R. W., Kopylova M. G., Pearson D. G., Shirey S. B., and Kjarsgaard B. A. (1999) Age of the lithospheric mantle beneath and around the Slave craton: a rhenium-osmium isotopic study of peridotite xenoliths from the Jericho and Somerset Island kimberlites. In *Abst. Ninth Annual V. M. Goldschmidt Conference* LPI contribution no. 971. Lunar and Planetary Institute, Houston, pp. 134–135.

Irvine G. J., Pearson D. G., and Carlson R. W. (2001) Lithospheric mantle evolution in the Kaapvaal craton: A Re-Os isotope study of peridotite xenoliths from Lesotho kimberlites. *Geophys. Res. Lett.* **28**, 2505–2508.

Irvine G. J., Pearson D. G., Carlson R. W., Kjarsgaard B. A., Dreibus G. E., and Kopylova M. G. (2003) A PGE and

Re–Os isotope study of mantle xenoliths from Somerset Island. *Lithos*.

Irving A. J. (1974) Geochemical and high pressure experimental studies of garnet pyroxenite and pyroxene granulite xenoliths from the Delegate basaltic pipes. *Australia. J. Petrol.* **15**, 1–40.

Irving A. J. (1980) Petrology and geochemistry of composite ultramafic xenoliths in alkalic basalts and implications for magmatic processes in the mantle. *Am. J. Sci.* **280A**, 389–426.

Irving A. J. and Frey F. A. (1984) Trace element abundances in megacrysts and their host basalts: constraints on partition coefficients and megacryst genesis. *Geochim. Cosmochim. Acta* **48**, 1201–1221.

Irving A. J. and Price R. C. (1981) Geochemistry and evolution of high pressure phoonolitic lavas from Nigeria,Australia, Eastern Germany and New Zealand. *Geochim. Cosmochim. Acta* **45**, 1309–1320.

Izraeli E. S., Harris J. W., and Navon O. (2001) Brine inclusions in diamonds: a new upper mantle fluid. *Earth Planet. Sci. Lett.* **187**, 323–332.

Jackson E. D. and Wright T. L. (1970) Xenoliths in the Honolulu volcanic series, Hawaii. *J. Petrol.* **11**, 405–430.

Jacob D. and Jagoutz E. (1994) A diamond-graphite bearing eclogite xenolith from Roberts Victor (South Africa): implications for petrogenesis from Pb-, Nd-, and Sr isotopes. In *Kimberlites, Related Rocks and Mantle Xenoliths* (eds. H. O. A. Meyer and O. H. Leonardos) CPRM Spec. Publ. CPRM, Brasilia, vol. 1, pp. 304–317.

Jacob D., Jagoutz E., Lowry D., Mattey D., and Kudrjavtseva G. (1994) Diamondiferous eclogites from Siberia: remnants of Archean oceanic crust. *Geochim. Cosmochim. Acta* **58**, 5191–5207.

Jacob D. E., Jagoutz E., and Sobolev N. V. (1998a) Neodymium and strontium isotopic measurements on single subcalcic garnet grains from Yakutian kimberlites. *Neus. Jahrb. Mineral. Abh.* **172**, 357–379.

Jacob D., Jagoutz E., Lowry D., and Zinngrebe E. (1998b) Comments on "The origins of Yakutian Eclogite Xenoliths" by G. A. Snyder L. A. Taylor G. Crozaz A. N. Halliday B. L. Beard V. N. Sobolev and N. V. Sobolev. *J. Pet.* **39**, 1527–1533.

Jacob D. E. and Foley S. F. (1999) Evidence for Archean ocean crust with low high field strength element signature from diamondiferous eclogite xenoliths. *Lithos* **48**, 317–336.

Jacob D. E., Viljoen K. S., Grassineau N., and Jagoutz E. (2000) Remobilization in the cratonic lithosphere recorded in polycrystalline diamond. *Science* **289**, 1182–1185.

Jacob D. E., Bizinis M., and Salters V. J. M. (2002) Lu–Hf isotope systematics of subducted ancient oceanic crust: Roberts Victor eclogites. *Geochim. Cosmochim. Acta (Spec. Suppl.)* **66S1**, A360.

Jagoutz E. (1988) Nd and Sr systematics in an eclogite xenolith from Tanzania: evidence for frozen mineral equilibria in the continental lithsphere. *Geochim. Cosmochim. Acta* **52**, 1285–1293.

Jagoutz E., Palme H., Baddenhausen H., Blum K., Cendales M., Dreibus G., Spettel B., Lorenz V., and Wanke H. (1979) The abundances of major, minor and trace elements in the Earth's mantle as derived from primitive ultramafic nodules. In *Proc. 10th Lunar and Planetary Science Conference*, Pergamon, Houston, pp. 2031–2050.

Jagoutz E., Carlson R. W., and Lugmair G. W. (1980) Equilibrated Nd-, unequilibrated Sr isotopes in mantle xenoliths. *Nature* **296**, 708–710.

Jagoutz E., Dawson J. B., Hoernes S., Spettel B., and Wanke H. (1984) Anorthositic oceanic crust in the Archean Earth. In *Abstr. 15th Lunar and Planetary Science Conf.* pp. 395–396. Lunar and Planetary Science Institute, Houston.

Janse A. J. A. (1985) Kimberlites; where and when. In *Kimberlite Occurrence and Origin; a Basis for Conceptual Models in Exploration* (eds. J. E. Glover and P. G. Harris). University of Western Australia, Geology Department and Extension Service, Perth, West, vol. 8, pp. 19–61.

Janse A. J. A. (1992) New ideas in subdividing cratonic areas. *Russian Geol. Geophys.* **33**(10), 9–25.

Jaques A. L., Haggerty S. E., Lucas H., and Boxer G. L. (1989) Mineralogy and petrology of the Argyle (AK1) lamproite pipe, Western Australia. In *Kimberlites and Related Rocks* (eds. J. Ross, A. L. Jaques, J. Ferguson, D. H. Green, O'Reilly S. Y., R. V. Danchin, and A. J. A. Janse). Geological Society of Australia, Perth, vol. 14(12), pp. 153–188.

Javoy M., Pineau F., and Demaiffe D. (1984) Nitrogen and carbon isotopic composition in the diamonds of Mbuji Mayi (Zaire). *Earth Planet. Sci. Lett.* **68**(3), 399–412.

Javoy M., Pineau F., and Delorme H. (1986) Carbon and nitrogen isotopes in the mantle. In *Isotopes in Geology: Picciotto Volume* (eds. S. Deutsch and A. W. Hofmann). Elsevier, Amsterdam, vol. 57(1–2), pp. 41–62.

Jerde E. A., Taylor L. A., Crozaz G., Sobolev N. V., and Sobolev V. S. (1993) Diamondiferous eclogites from Yakutia, Siberia: evidence for a diversity of protoliths. *Contrib. Mineral. Petrol.* **114**, 189–192.

Jochum K. P., McDonough W. F., Palme H., and Spettel B. (1989) Compositional constraints on the continental lithospheric mantle from trace elements in spinel peridotite xenoliths. *Nature* **340**, 548–550.

Johnson K. E., Davis A. M., and Bryndzia L. T. (1996) Contrasting styles of hydrous metasomatism in the upper mantle: an ion microprobe investigation. *Geochim. Cosmochim. Acta* **60**, 1367–1385.

Jones A. P., Smith J. V., and Dawson J. B. (1982) Mantle metasomatism in 14 veined peridotites from Bultfontein Mine, South Africa. *J. Geology* **90**, 435–453.

Joswig W., Stachel T., Harris J. W., Baur W. H., and Brey G. P. (1999) New Ca-silicate inclusions in diamonds-tracers from the lower mantle. *Earth Planet. Sci. Lett.* **173**(1–2), 1–6.

Kalfoun F., Ionov D., and Merlet C. (2002) HFSE residence and Nb/Ta ratios in metasomatised rutile-bearing mantle peridotites. *Earth Planet. Sci. Lett.* **199**, 49–65.

Kaminsky F. V., Zakharchenko O. D., Davies R., Griffin W. L., Khachatryan B. G. K., and Shiryaev A. A. (2001) Superdeep diamonds form the Juina area, Mato Grosso State, Brazil. *Contrib. Mineral. Petrol.* **140**(6), 734–753.

Kelemen P. B., Hart S. R., and Bernstein S. (1998) Silica enrichment in the continental upper mantle via melt/rock reaction. *Earth Planet. Sci. Lett.* **164**, 387–406.

Kerr R. A. (1993) Bits of the lower mantle found in Brazilian diamonds. *Science* **261**(5127), 1391.

Kinny P. D. and Dawson J. B. (1992) A mantle metasomatic injection event linked to late Cretaceous kimberlite magmatism. *Nature* **360**, 726–728.

Kirkley M. B., Gurney J. J., and Levinson A. A. (1991) Age, origin, and emplacement of diamonds; scientific advances in the last decade. *Gems and Gemology* **27**, 2–25.

Koga K. T., Shimizu N., and Grove T. L. (1999) Disequilibrium trace element redistribution during garnet to spinel facies transformation. In *Proceedings of the VIIth International Kimberlite Conference* (eds. J. Gurney John, L. Gurney James, D. Pascoe Michelle, and H. Richardson Stephen). Red Roof Designs, Cape Town, vol. 1, pp. 444–451.

Köhler T. and Brey G. P. (1990) Calcium exchange between olivine and clinopyroxene calibrated as a geothermobarometer for natural peridotites from 2–60 kb with applications. *Geochim. Cosmochim. Acta* **54**, 2375–2388.

Konzett J., Armstrong R. A., Sweeney R. J., and Compston W. (1998) The timing of MARID metasomatism in the Kaapvaal mantle: an ion probe study of zircons from MARID xenoliths. *Earth Planet. Sci. Lett.* **160**, 133–145.

Konzett J., Armstrong R. A., and Gunther D. (2000) Modal metasomatism in the Kaapvaal craton lithosphere: constraints on timing and genesis from U–Pb zircon dating of

metasomatised peridotites and MARID xenoliths. *Contrib. Mineral. Petrol.* **139**, 704–719.

Kopylova M. G. and Russell J. K. (2000) Chemical stratification of cratonic lithosphere: constraints from the Northern Slave craton, Canada. *Earth Planet. Sci. Lett.* **181**, 71–87.

Kopylova M. G., Russell J. K., and Cookenboo H. (1999) Petrology of peridotite and pyroxenite xenoliths from the Jericho kimberlite: implications for the thermal state of the mantle beneath the Slave craton, northern Canada. *J. Petrol.* **40**, 79–104.

Kopylova M. G., Russell J. K., Stanley C., and Cookenboo H. (2000) Garnet from Cr- and Ca-saturated mantle: implications for diamond exploration. *J. Geochem. Explor.* **68**, 183–199.

Kramers J. D. (1977) Lead and strontium isotopes in Cretaceous kimberlites and mantle-derived xenoliths from Southern Africa. *Earth Planet. Sci. Lett.* **34**, 419–431.

Kramers J. D. (1979) Lead, uranium, strontium, potassium and rubidium in inclusion-bearing diamonds and mantle-derived xenoliths from southern Africa. *Earth Planet. Sci. Lett.* **42**(1), 58–70.

Kramers J. D., Roddick J. C. M., and Dawson J. B. (1983) Trace element and isotope studies on veined, metasomatic and "MARID" xenoliths from Bultfontein, South Africa. *Earth Planet. Sci. Lett.* **65**, 90–106.

Krogh E. J. (1988) The garnet-clinopyroxene Fe–Mg geothermometer—a reinterpretation of existing experimental data. *Contrib. Mineral. Petrol.* **99**, 44–48.

Kuno H. and Aoki K. (1970) Chemistry of ultramafic nodules and their bearing on the origin of basaltic magmas. *Phys. Earth Planet. Int.* **3**, 273–301.

Kurat G., Palme H., Spettel B., Baddenhausen H., Hofmeister H., Palme C., and Wanke H. (1980) Geochemistry of ultramafic xenoliths from Kapfenstein, Austria: evidence for a variety of upper mantle processes. *Geochim. Cosmochim. Acta* **44**, 45–60.

Kushiro I. and Aoki K. (1968) Origin of some eclogite inclusions in kimberlite. *Am. Mineral.* **53**, 1347–1367.

Kyser T. K. (1990) Stable isotopes in the continental lithospheric mantle. In *Continental Mantle* (ed. M. A. Menzies). Clarendon Press, Oxford, pp. 127–156.

Kyser T. K., O'Neill J. R., and Carmichael S. E. (1981) Oxygen isotope thermometry of basic lavas and mantle nodules. *Contrib. Mineral. Petrol.* **77**, 11–23.

Lacroix A. (1893) Les enclaves des roches volcaniques. Protat Freres, Macon, 710pp.

Lanphere M. (1968) Sr–Rb–K and Sr isotopic ratios in ultramafic rocks S. E. Alaska. *Earth Planet. Sci. Lett.* **9**, 247–256.

Lawless P. J., Gurney J. J., and Dawson J. B. (1979) Polymict peridotites from the Bultfontein and De Beers mines, Kimberley, South Africa. In *The Mantle Sample: Inclusions in Kimberlites and other Volcanics* (eds. F. R. Boyd and H. O. A. Meyer). American Geophysical Union, Washington, DC, pp. 144–155.

Lee C., Rudnick R. L., and Jacobsen S. (2001) Preservation of ancient and fertile lithospheric mantle beneath the southwestern United States. *Nature* **411**, 69–73.

Lee C. T. (2002) Platinum-group element geochemsitry of peridotite xenoliths from the Sierra Nevada and the Basin and Range, California. *Geochim. Cosmochim. Acta* **66**, 3987–4006.

Lee C. T., Yin Q., Rudnick R. L., Chesley J. T., and Jacobsen S. B. (2000a) Osmium isotopic evidence for Mesozoic removal of lithospheric mantle beneath the Sierra Nevada. *Science* **289**, 1912–1916.

Lee C. T., Rudnick R. L., McDonough W. F., and Horn I. (2000b) Petrologic and geochemical investigation of carbonates in peridotite xenoliths from northeastern Tanzania. *Contrib. Mineral. Petrol.* **139**, 470–484.

Lee D.-C., Halliday A. N., Davies G. R., Essene E. J., Fitton J. G., and Temdjim R. (1996) Melt enrichment of shallow depleted mantle: a detailed petrological, trace element and isotopic study of mantle-derived xenoliths and megacrysts from the Cameroon Line. *J. Petrol.* **37**, 415–441.

Lee H.-Y. and Ganguly J. (1988) Equilibrium composition of coexisting garnet and orthopyroxene: experimental determinations in the system $FeO–MgO–Al_2O_3–SiO_2$ and applications. *J. Petrol.* **29**, 93–113.

Levinson A. A., Gurney J. J., and Kirkley M. B. (1992) Diamond sources and production; past, present, and future. *Gems and Gemology* **28**(4), 234–254.

Lewis R. S., Ming T., Wacker J. F., Anders E., and Steel E. (1987) Interstellar diamonds in meteorites. *Nature (London)* **326**(6109), 160–162.

Liang Y. and Elthon D. (1990) Evidence from chromium abundances in mantle rocks for extraction of picrite and komatiite melts. *Nature* **343**, 551–553.

Lipschutz M. E. (1964) Origin of diamonds in the ureilites. *Science* **143**(3613), 1431–1434.

Lipschutz M. E. and Anders E. (1961) The record in the meteorites: Part 4. Origin of diamonds in iron meteorites. *Geochim. Cosmochim. Acta* **24**, 83–105.

Lorand J.-P. and Alard O. (2001) Platinum-group element abundances in the upper mantle: new constraints from *in situ* and whole-rock analyses of Massif Central xenoliths. *Geochim. Cosmochim. Acta* **65**, 2789–2806.

Lorand J.-P., Pattou L., and Gros M. (1999) Fractionation of platinum-group elements and gold in the upper mantle: a detailed study in Pyrenean orogenic lherzolites. *J. Petrol.* **40**, 957–981.

Lovering J. F. and White A. J. R. (1969) Granulitic and eclogitic inclusions from basic pipes at Delegate, Australia. *Contrib. Mineral. Petrol.* **21**, 9–52.

Lowry D., Mattey D. P., and Harris J. W. (1999) Oxygen isotope composition of syngenetic inclusions in diamond from the Finsch Mine, RSA. *Geochim. Cosmochim. Acta* **63**, 1825–1836.

Luth R. W. and Canil D. (1993) Ferric iron in mantle-derived pyroxenes and a new oxybarometer for the upper mantle. *Contrib. Mineral. Petrol.* **113**, 236–248.

Luth R. W., Virgo D., Boyd F. R., and Wood B. J. (1990) Ferric iron in mantle derived garnets: implications for thermobarometry and for the oxidation state of the mantle. *Contrib. Mineral. Petrol.* **104**, 56–72.

Maaloe S. and Aoki K. (1977) The major element composition of the upper mantle estimated from the composition of lherzolites. *Contrib. Mineral. Petrol.* **63**, 161–173.

Macdougal J. D. and Haggerty S. F. (1999) Ultradeep xenoliths from African kimberlites: Sr and Nd isotopic compositions. *Earth Planet. Sci. Lett.* **170**, 73–82.

MacGregor I. D. (1974) The system $MgO–Al_2O_3–SiO_2$: solubility of Al_2O_3 in enstatite for spinel and garnet peridotite compositions. *Am. Mineral.* **59**, 110–119.

MacGregor I. D. and Carter J. L. (1970) The chemistry of clinopyroxenes and garnets of eclogite and peridotite xenoliths from the Roberts Victor Mine, South Africa. *Phys. Earth Planet. Int.* **3**, 391–397.

MacGregor I. D. and Manton W. I. (1986) Roberts Victor Eclogites: ancient oceanic crust. *J. Geophys. Res.* **91**, 14063–14079.

MacKenzie J. M. and Canil D. (1999) Composition and thermal evolution of cratonic mantle beneath the central Archean Slave Province, NWT, Canada. *Contrib. Mineral. Petrol.* **134**, 313–324.

Marty B. and Zimmerman L. (1999) Volatiles (He, C, N, Ar) in mid-ocean ridge basalts: assessment of shallow-level fractionation and characterization of source composition. *Geochim. Cosmochim. Acta* **63**, 3619–3633.

Mattey D. P., Lowry D., and Macpherson C. (1994) Oxygen isotope composition of mantle peridotite. *Earth Planet. Sci. Lett.* **128**, 231–241.

Matsumoto T., Honda M., McDougall I., Yatsevich I., and O'Reilly S. Y. (1997) Plume-like neon in a metasomatic

apatite from the Australian lithospheric mantle. *Nature* **388**, 162–164.

Matsumoto T., Honda M., McDougall I., O'Reilly S. Y., Norman M., and Yaxley G. (2000) Noble gases in pyroxenites and metasomatised peridotites from the Newer Volcanics, southeastern Australia: implications for mantle metasomatism. *Chem. Geol.* **168**, 49–73.

Mazonne P. and Haggerty S. E. (1989) Peraluminous xenoliths in kimberlite: metamorphosed restites produced by partial melting of pelites. *Geochim. Cosmochim. Acta* **53**, 1551–1561.

McCammon C. (2001) Geophysics—Deep diamond mysteries. *Science* **293**(5531), 813–814.

McCammon C. A., Hutchinson M., and Harris J. (1997) Ferric iron content of mineral inclusions in diamonds from Sao Luiz: a view into the lower mantle. *Science* **278**(5337), 434–436.

McCandless T. E. and Gurney J. J. (1989) Sodium in garnet and potassium in clinopyroxene: criteria for classifying mantle eclogites. In *Kimberlites and Related Rocks*, Geol. Soc. Austral. Spec. Publ. No. 14 (ed. J. Ross). Blackwell, Perth, vol. 2, pp. 827–832.

McCulloch M. T. (1989) Sm–Nd systematics in eclogite and garnet peridotite nodules from kimberlites: implications for the early differentiation of the earth. In *Kimberlites and Related Rocks*, Geol. Soc. Austral. Spec. Publ. No. 14 (ed. J. Ross). Blackwell, Perth, vol. 2, pp. 864–876.

McDade P. and Harris J. W. (1999) Syngenetic inclusion bearing diamonds from Letseng-la-Terai, Lesotho. In *Proceedings of the VIIth International Kimberlite Conference* (eds. J. Gurney John, L. Gurney James, D. Pascoe Michelle, and H. Richardson Stephen). Red Roof Designs, Cape Town, vol. 2, pp. 557–565.

McDade P. and Harte B. (2000) Roberts Victor eclogites with a spinel-facies mantle signature. *J. Conf. Abstr.* **5**, 690.

McDonough W. F. (1990) Constraints on the composition of the continental lithospheric mantle. *Earth Planet. Sci. Lett.* **101**, 1–18.

McDonough W. F. and Frey F. A. (1989) Rare earth elements in upper mantle rocks. In *Geochemistry and Mineralogy of Rare Earth Elements*. Mineral. Soc. Am.—Rev. Mineral. Ser. (eds. B. R. Liplin and G. A. McKay) AGU, Washington, DC, vol. 21, pp. 99–145.

McDonough W. F. and McCulloch M. T. (1987) The southeast Australian lithospheric mantle: isotopic and geochemical constraints on its growth and evolution. *Earth. Planet. Sci. Lett.* **86**, 327–340.

McDonough W. F. and Sun S. S. (1995) The composition of the earth. *Chem. Geol.* **120**, 223–253.

McDonough W. F., Stosch H. G., and Ware N. G. (1992) Distribution of titanium and rare earth elements between peridotitic minerals. *Contrib. Mineral. Petrol.* **110**, 321–328.

McInnes B. I. A. and Cameron E. M. (1994) Carbonated alkaline hybridising melts from a sub-arc environment: mantle wedge samples from the Tabar-Lihir-Tanga-Feni arc, Papua New Guinea. *Earth Planet. Sci. Lett.* **122**, 125–141.

McKay D. B. and Mitchell R. H. (1988) Abundance and distribution of gallium in some spinel and garnet lherzolites. *Geochim. Cosmochim. Acta* **52**, 2867–2870.

McKenzie D. (1989) Some remarks on the movement of small melt fractions in the mantle. *Earth. Planet. Sci. Lett.* **95**, 53–72.

Meijer A., Kwon S. T., and Tilton G. R. (1990) U–Th–Pb partitioning behavior during partial melting in the upper mantle; implications for the origins of high mu components and the "Pb-paradox". *J. Geophys. Res.* **95**, 433–448.

Meisel T., Walker R. J., Irving A. J., and Lorand J.-P. (2001) Osmium isotopic compositions of mantle xenoliths: a global perspective. *Geochim. Cosmochim. Acta* **65**, 1311–1323.

Mendelssohn M. J. and Milledge H. J. (1995) Morphological characteristics of diamond populations in relation to temperature-dependent growth and dissolution rates. *Int. Geol. Rev.* **37**(4), 285–312.

Menzies A. H., Shirey S. B., Carlson R. W., and Gurney J. J. (1999) Re–Os systematics of Newlands peridotite xenoliths: implications for diamond and lithosphere formation. In *Proc. 7th Int. Kimberlite Conf.* (eds. J. J. Gurney, J. L. Gurney, M. D. Pascoe, and S. H. Richardson). Red Roof Design, Cap Town, pp. 566–583.

Menzies M. and Chazot G. (1995) Fluid processes in diamond to spinel facies shallow mantle. *J. Geodyn.* **20**, 387–415.

Menzies M. and Halliday A. N. (1988) Lithospheric mantle domains beneath the Archean and Proterozoic crust of Scotland. In *Oceanic and Continental Lithosphere: Similarities and Differences*, J. Petrology (Spec. volume) (eds. M. A. Menzies and K. G. Cox). Oxford University Press, Oxford, pp. 275–302.

Menzies M. and Murthy V. R. (1980a) Enriched mantle: Nd and Sr isotopes in diopsides from kimberlite nodules. *Nature* **283**, 634–636.

Menzies M. and Murthy V. R. (1980b) Nd and Sr isotope geochemistry of hydrous mantle nodules and their host alkali basalts; implications for local heterogeneities in metasomatically veined mantle. *Earth Planet. Sci. Lett.* **46**, 323–334.

Menzies M. and Wass S. Y. (1983) CO_2 rich mantle beneath eastern Australia: REE, Sr and Nd isotopic study of Cenozoic alkaline magmas and apatite-rich xenoliths, southern Highlands Province, New South Wales, Australia. *Earth Planet. Sci. Lett.* **65**, 287–302.

Menzies M. A. (1983) Mantle ultramafic xenoliths in alkaline magmas: evidence for mantle heterogeneity modified by magmatic activity. In *Continental Basalts and Mantle Xenoliths* (eds. C. J. Hawkesworth and M. J. Norry). Shiva, Nantwich, pp. 92–110.

Menzies M. A. (1990a) Archaean, proterozoic and phanerozoic lithospheres. In *Continental Mantle*. (ed. M. A. Menzies). Clarendon Press, Oxford, pp. 67–86.

Menzies M. A. (1990b) Petrology and geochemistry of the continental mantle: an historical perspective. In *Continental Mantle* (ed. M. A. Menzies). Clarendon press, Oxford, pp. 31–54.

Menzies M. A. (1992) The lower lithosphere as a major source for continental flood basalts: a re-appraisal. In *Magmatism and the Causes of Continental Break-up*, Geol. Soc. Spec. Publ. (eds. B. C. Storey, T. Alabaster, and R. J. Pankhurst). The Geological Society, London, vol. 68, pp. 31–40.

Menzies M. A. and Hawkesworth C. J. (1987) *Mantle Metasomatism*. Academic Press, London, 472pp.

Menzies M. A., Kempton P. D., and Dungan M. (1985) Interaction of continental lithosphere and asthenospheric melts below the Geronimo volcanic field, Arizona USA. *J. Petrol.* **26**, 663–693.

Menzies M. A., Halliday A. N., Hunter R. H., MacIntyre R. M., and Upton B. J. G. (1989) The age, composition and significance of a xenolith-bearing monchiquite dike, Lewis, Scotland. In *Kimberlites and Related Rocks*, Geol. Soc. Austral. Spec. Publ. No. 14 (ed. J. Ross). Blackwell, Perth, vol. 2, pp. 843–852.

Mercier J. C. (1980) Magnitude of continental lithospheric stresses inferred from rheomorphic petrology. *J. Geophys. Res.* **85**, 6293–6303.

Meyer H. O. A. (1987) Inclusions in diamond. In *Mantle Xenoliths* (ed. Peter H. Nixon). Wiley, Chichester, pp. 501–523.

Meyer H. O. A. and Boyd F. R. (1972) Composition and origin of crystalline inclusions in natural diamonds. *Geochim. Cosmochim. Acta* **36**(11), 1255–1273.

Mitchell R. H. (1977) Ultramafic xenoliths from the Elwin bay kimberlite: the first Canadian paleogeotherm. *Can. J. Earth Sci.* **14**, 1202–1210.

Mitchell R. H. (1984) Garnet lherzolites from the Hanaus-1 and Louwrensia kimberlites of Namibia. *Contrib. Mineral. Petrol.* **86**, 178–188.

Mitchell R. H. and Keays R. R. (1981) Abundance and distribution of gold, palladium and iridium in some spinel and garnet lherzolites: implications for the nature and origin of precious metal-rich intergranular components in the upper mantle. *Geochim. Cosmochim. Acta* **45**, 2425–2442.

Mitchell R. M. (1995) *Kimberlites, Orangeites and Related Rocks*. Plenum, New York.

Moore R. O. and Gurney J. J. (1985) Pyroxene solid solution in garnets included in diamond. *Nature (London)* **318**(6046), 553–555.

Moore R. O., Griffin W. L., Gurney J. J., Ryan C. G., Cousens D. R., Shee S. H., and Suter G. F. (1992) Trace element geochemistry of ilmenite megacrysts from the Monastery kimberlite, South Africa. *Lithos* **29**, 1–16.

Morgan J. W. (1986) Ultramafic xenoliths: clues to Earth's late accretionary history. *J. Geophys. Res.* **91**(B12), 12375–12387.

Morgan J. W., Wandless G. A., Petrie R. K., and Irving A. J. (1981) Composition of the Earth's upper mantle: I. Siderophile trace elements in ultramafic nodules. *Tectonophysics* **75**, 47–67.

Mukhopadhyay B. (1991) Garnet-clinopyroxene geobarometry: the problems, a prospect and an approximate solution. *Am. Mineral.* **76**, 512–529.

Navon O. (1999) Diamond formation in the Earth's mantle. In *The P. H. Nixon Volume* (eds. J. J. Gurney, J. L. Gurney, M. D. Pascoe, and S. H. Richardson). Red Roof Design, Cape Town, pp. 584–604.

Navon O., Hutcheon I., Rossman G. R., and Wasserburg G. J. (1988) Mantle-derived fluids in diamond micro-inclusions. *Nature* **335**, 784–789.

Neal C. R., Taylor L. A., Davidson J. P., Holden P., Halliday A. N., Nixon P. H., Paces J. B., Clayton R. N., and Mayeda T. (1990) Eclogites with oceanic crustal and mantle signatures from the Bellsbank kimberlite, South Africa: Part 2. Sr, Nd and O isotope geochemistry. *Earth Planet. Sci. Lett.* **99**, 362–379.

Neumann E. R., Wulff P. E., Johnsen K., Andersen T., and Krogh E. (1995) Petrogenesis of spinel harzburgite and dunite suite xenoliths from Lanzarote, eastern Canary Islands: implications for the upper mantle. *Lithos* **35**, 83–107.

Nickel K. G. (1986) Phase equilibria in the system SiO_2–MgO–Al_2O_3–CaO–Cr_2O_3 (SMACCR) and their bearing on the spinel/garnet lherzolite relationships. *Neus. Jahrb. Mineral. Abh.* **155**, 259–287.

Nickel K. G. and Green D. H. (1985) Empirical geothermobarometry for garnet peridotites and implications for the nature of the lithosphere, kimberlites and diamonds. *Earth Planet. Sci. Lett.* **73**, 158–170.

Nimis P. and Taylor W. R. (2000) Single clinopyroxene thermobarometry for garnet peridotites: Part 1. Calibration and testing of a Cr-in-cpx barometer and enstatite-in-cpx thermometer. *Contrib. Mineral. Petrol.* **139**, 541–554.

Nixon P. H. (1987) *Mantle Xenoliths*. Wiley, Chichester.

Nixon P. H. and Boyd F. R. (1973a) Petrogenesis of the granular and sheared ultrabasic nodule suite in kimberlite. In *Lesotho Kimberlites* (ed. P. H. Nixon). Cape and Transvaal, Maseru, pp. 48–56.

Nixon P. H. and Boyd F. R. (1973b) The discrete nodule association in kimberlites from northern Lesotho. In *Lesotho Kimberlites*, (ed. P. H. Nixon) Lesotho National Development Corporation, Maseru, Lesotho, 67–75.

Nixon P. H. and Boyd F. R. (1979) Garnet bearing lherzolites and discrete nodules from the Malaita alnoite, Solomon Islands S. W. Pacific, and their bearing on oceanic mantle composition and geotherm. In *The Mantle Sample: Inclusions in Kimberlites and Other Volcanics* (eds. F. R. Boyd and H. O. A. Meyer). American Geophysical Union, Washington, DC, pp. 400–423.

Nixon P. H., Chapman N. A., and Gurney J. J. (1978) Pyrope-Spinel (Alkremite) xenoliths from kimberlite. *Contrib. Mineral. Petrol.* **65**, 314–346.

Nixon P. H., Rogers N. W., Gibson I. L., and Grey A. (1981) Depleted and fertile mantle xenoliths from southern African kimberlites. *Ann. Rev. Earth Planet. Sci.* **9**, 285–309.

Norman M. (2001) Applications of laser-ablation ICPMS to the trace element geochemistry of basaltic magmas and mantle evolution. In *Min. Assoc. Can. Short Course Series* (ed. P. Sylvester). Ottawa, vol. 29, pp. 163–184.

Norman M. D. (1998) Melting and metasomatism in the continental lithosphere: laser ablation ICPMS analysis of minerals in spinel lherzolites from eastern Australia. *Contrib. Mineral. Petrol.* **130**, 240–255.

Nowell G. M., Kempton P. D., Noble S. R., Fitton J. G., Saunders A. D., Mahoney J. J., and Taylor R. N. (1998) High precision Hf isotope measurements of MORB and OIB by thermal ionisation mass spectrometry: insights into the depleted mantle. *Chem. Geol.* **149**, 211–233.

Nowell G. M., Pearson D. G., Jacob D. J., Spetsius Z. V., Nixon P. H., and Haggerty S. E. (2003). The origin of alkremites and related rocks: Lu–Hf, Rb–Sr and Sm–Nd isotope study. Abstr. 8th Int. Kimberlite Conference, Victoria, FLA 0271.

Nowell G. M., Pearson D. G., Bell D. R., Carlson R. W., Smith C. B., Kempton P. D., and Noble S. R. (2004) Hf isotope systematics of kimberlites and their megacrysts: new constraints on their source regions. *J. Petrol.* (in press).

O'Hara M. J. and Yoder H. S. (1967) Formation and fractionation of basic magmas at high pressures. *Scott. J. Geol.* **3**, 67–117.

O'Hara M. J., Saunders M. J., and Mercy E. L. P. (1975) Garnet-peridotite, primary ultrabasic magma and eclogite: interpretation of upper mantle processes in kimberlite. *Phys. Chem. Earth* **9**, 571–604.

O'Neill H. S. C. (1980) The transition between spinel lherzolite and garnet lherzolite and its use as a geobarometer. *Contrib. Mineral. Petrol.* **77**, 185–194.

O'Neill H. S. C. (1991) The origin of the Moon and early history of the Earth—a chemical model: Part 2. The Earth. *Geochim. Cosmochim. Acta* **55**, 1159–1172.

O'Neill H. S. C. and Wood B. J. (1979) An experimental study of Fe–Mg partitioning between garnet and olivine and its calibration as a geothermometer. *Contrib. Mineral. Petrol.* **70**, 59–70.

O'Neill H. S. C., Rubie D. C., Canil D., Geiger C. A., Ross C. R. I., Seifert F., and Woodland A. B. (1993) Ferric iron in the upper mantle and in transition zone assemblages: implications for relative oxygen fugacities in the mantle. In *Evolution of the Earth and Planets*, Geophys. Monogr. 74 (eds. E. Takahashi, R. Jeanloz, and D. Rubie). American Geophysical Union, Washington, DC, pp. 73–87.

Ongley J. S., Basu A. R., and Kyser T. K. (1987) Oxygen isotopes in coexisting garnets, clinopyroxenes and phlogopites of Roberts Victor eclogites: implications for petrogenesis and mantle metasomatism. *Earth Planet. Sci. Lett.* **83**, 80–84.

O'Reilly S. Y., Griffin W. L., and Ryan C. G. (1991) Residence of trace elements in metasomatized spinel lherzolite xenoliths: a proton-microprobe study. *Contrib. Mineral. Petrol.* **109**, 98–113.

Ozima M. and Zashu S. (1988) Solar-type neon in Zaire cubic diamonds. *Geochim. Cosmochim. Acta* **52**, 19–25.

Ozima M. and Zashu S. (1991) Noble gas state of the ancient mantle as deduced from noble gases in coated diamonds. *Earth Planet. Sci. Lett.* **105**, 13–27.

Palme H. and Nickel K. (1985) Ca/Al ratio and composition of the Earth's mantle. *Geochim. Cosmochim. Acta* **49**, 2123–2132.

Pearson D. G. (1999a) The age of continental roots. *Lithos* **48**, 171–194.

Pearson D. G. (1999b) Evolution of cratonic lithospheric mantle: an isotopic perspective. In *Mantle Petrology: Field Observations and High Pressure Experimentation* (eds. Y. Fei, C. M. Bertka, and B. O. Mysen). The Geochemical Society, Houston, vol. 6, pp. 57–78.

Pearson D. G. and Milledge H. J. (1998) Diamond growth conditions and preservation: inferences from trace elements in a large garnet inclusion in a Siberian diamond. Extended Abstracts of 7th Int. Kimb. Conf., Cape Town, pp. 667–669.

Pearson D. G. and Nixon P. H. (1995) Diamonds in young orogenic belts: graphitised diamonds from Beni Bousera N. Morocco, a comparison with kimberlite-derived diamond occurrences and implications for diamond genesis and exploration. *Africa Geosci. Rev.* **3**, 295–316.

Pearson D. G. and Nowell G. M. (2002) The continental lithospheric mantle: characteristics and significance as a mantle reservoir. *Proc. Roy. Soc. Ser. A.* **360**, 2383–2410.

Pearson D. G. and Nowell G. M. (2003) Dating mantle differentiation: a comparison of the Lu–Hf, Re–Os and Sm–Nd isotope systems in the Beni Bousera peridotite massif and constraints on the Nd–Hf composition of the lithospheric mantle. *Geophys. Res. Abstr.* **5**, 05430.

Pearson D. G. and Shirey S. B. (1999) Isotopic dating of diamonds. In *Application of Radiogenic isotopes to Ore Deposit Research and Exploration* (eds. D. D. Lambert and Ruiz J.). Society of Economic Geologists, Boulder, vol. 12, pp. 143–172.

Pearson D. G. and Woodland S. J. (2000) Carius tube digestion and solvent extraction/ion exchange separation for the analysis of PGEs (Os, Ir, Pt, Pd, Ru) and Re–Os isotopes in geological samples by isotope dilution ICP-mass spectrometry. *Chem. Geol.* **165**, 87–107.

Pearson D. G., Davies G. R., Nixon P. H., and Milledge H. J. (1989) Graphitized diamonds from a peridotite massif in Morocco and implications for anomalous diamond occurrences. *Nature (London)* **338**(6210), 60–62.

Pearson D. G., Davies G. R., Nixon P. H., Greenwood P. B., and Mattey D. P. (1991) Oxygen isotope evidence for the origin of pyroxenites in the Beni Bousera peridotite massif N. Morocco: derivation from subducted oceanic lithosphere. *Earth Planet. Sci. Lett.* **102**, 289–301.

Pearson D. G., Shirey S. B., Carlson R. W., and Taylor L. R. (1992) Os isotope constraints on the origin of eclogite xenoliths. *EOS, Trans. Am. Geophys. Union* **73**(14), 376.

Pearson D. G., Davies G. R., and Nixon P. H. (1993) Geochemical constraints on the petrogenesis of diamond facies pyroxenites from the Beni Bousera peridotite massif, north Morocco. *J. Petrology* **34**, 125–172.

Pearson D. G., Boyd F. R., Haggerty S. E., Pasteris J. D., Field S. W., Nixon P. H., and Pokhilenko N. P. (1994) The characterisation and origin of graphite in cratonic lithospheric mantle: a petrological carbon isotope and Raman spectroscopic study. *Contrib. Mineral. Petrol.* **115**, 449–466.

Pearson D. G., Shirey S. B., Carlson R. W., Boyd F. R., Pokhilenko N. P., and Shimizu N. (1995a) Re–Os, Sm–Nd and Rb–Sr isotope evidence for thick Archaean lithospheric mantle beneath the Siberia craton modified by multi-stage metasomatism. *Geochim. Cosmochim. Acta* **59**, 959–977.

Pearson D. G., Carlson R. W., Shirey S. B., Boyd F. R., and Nixon P. H. (1995b) The stabilisation of Archaean lithospheric mantle: a Re–Os isotope study of peridotite xenoliths from the Kaapvaal craton. *Earth Planet. Sci. Lett.* **134**, 341–357.

Pearson D. G., Snyder G. A., Shirey S. B., Taylor L. A., Carlson R. W., and Sobolev N. V. (1995c) Archaean Re–Os age for Siberian eclogites and constraints on Archaean tectonics. *Nature* **374**, 711–713.

Pearson D. G., Davies G. R., and Nixon P. H. (1995d) Orogenic ultramafic rocks of UHP (Diamond Facies) origin. In *Ultrahigh Pressure Metamorphism* (eds. R. G. Coleman and X. Wang). Cambridge University Press, Cambridge, pp. 456–510.

Pearson D. G., Ionov D., Carlson R. W., and Shirey S. B. (1998a) Lithospheric evolution in circum-cratonic settings: a Re–Os isotope study of peridotite xenoliths from the Vitim region, Siberia. *Mineral. Mag.* **62A**, 1147–1148.

Pearson D. G., Shirey S. B., Harris J. W., and Carlson R. W. (1998b) A Re–Os isotope study of sulfide diamond inclusions from the Koffiefontein kimberlite S. Africa: constraints on diamond crystallisation ages and mantle Re–Os systematics. *Earth Planet. Sci. Lett.* **160**, 311–326.

Pearson D. G., Shirey S. B., Bulanova G. P., Carlson R. W., and Milledge H. J. (1999a) Re–Os isotope measurements of single sulfide inclusions in a Siberian diamond and its nitrogen aggregation systematics. *Geochim. Cosmochim. Acta* **63**(5), 703–711.

Pearson D. G., Shirey S. B., Bulanova G. P., Carlson R. W., and Milledge H. J. (1999b) Dating and paragenetic distinction of diamonds using the Re–Os isotope system. In *Proc. 7th Int. Kimberlite Conf.* (eds. J. J. Gurney, J. L. Gurney, M. D. Pascoe, and S. H. Richardson). Red Roof Design, Cape Town, vol. 2, pp. 637–643.

Pearson D. G., Irvine G. J., Carlson R. W., Kopylova M. G., and Ionov D. A. (2002) The development of lithospheric mantle keels beneath the earliest continents: time constraints using PGE and Re–Os isotope systematics. In *The Early Earth* (eds. M. Fowler, C. J. Ebinger, and C. J. Hawkesworth). Geological Society of London Special Publication, London, vol. 199, pp. 65–90.

Pearson D. G., Irvine G. J., Ionov D. A., Boyd F. R., and Dreibus G. E. (2004) Re–Os isotope systematics and platinum group element fractionation during mantle melt extraction: a study of massif and xenolith peridotite suites. *Chem. Geol.* (special volume): *Highley Siderophile Elements* (in press).

Pearson N. J., Alard O., Griffin W. L., Jackson S. E., and O'Reilly S. (2002) *In situ* measurement of Re–Os isotopes in mantle sulfides by laser ablation multicollector inductively coupled plasma mass spectrometry: anaytical methods and preliminary results. *Geochim. Cosmochim. Acta* **66**, 1037–1050.

Peslier A. H., Reisberg L. R., Ludden J., and Francis D. (2000) Os isotope systematics in mantle xenoliths: age constraints on the Canadian Cordillera lithosphere. *Chem. Geol.* **166**, 85–101.

Pidgeon R. T. (1989) Archaean diamond xenocrysts in kimberlites: how definitive is the evidence?. In *Kimberlites and Related Rocks* (eds. J. Ross, A. L. Jaques, J. Ferguson, D. H. Green, S. Y. O'Reilly, R. V. Danchin, and A. J. A. Janse). Geological Society of Australia, Perth, vol. 14, pp. 1006–1011.

Pokhilenko N. P., Sobolev N. V., Boyd F. R., Pearson D. G., and Shimizu N. (1993) Megacrystalline pyrope peridotites in the lithosphere of the Siberian platform: mineralogy, geochemical peculiarities and the problem of their origin. *Russian J. Geol. Geophys.* **34**(1–12), 56–67.

Porcelli D., Nions R. K. O., and O'Reilly S. Y. (1986) Helium and strontium isotopes in ultramafic xenoliths. *Chem. Geol.* **54**, 237–250.

Porcelli D., O'Nions R. K., Galer S. J. G., Cohen A. S., and Mattey D. P. (1992) isotopic relationships of volatile and lithophile trace elements in continental ultramafic xenoliths. *Contrib. Mineral. Petrol.* **110**, 528–538.

Poreda R. J. and Farley K. A. (1992) Rare gases in Samoan xenoliths. *Earth Planet. Sci. Lett.* **113**, 129–144.

Pyle J. M. and Haggerty S. E. (1994) Silicate-carbonate liquid immiscibility in upper mantle eclogites: evidence of natrosilicic and carbonatitic conjugate melts. *Geochim. Cosmochim. Acta* **58**, 2997–3011.

Pyle J. M. and Haggerty S. E. (1998) Eclogites and the metasomatism of eclogites from the Jagersfontein kimberlite: punctuated transport and implications for alkali magmatism. *Geochim. Cosmochim. Acta* **62**, 1207–1231.

Rapp R. P. and Watson E. B. (1995) Dehydration melting of metabasalt at 8–32 kbar: implications for continental growth and crust-mantle recycling. *J. Petrol.* **36**, 891–932.

Rehkämper M., Halliday A. N., Barford D., Fitton J. G., and Dawson J. B. (1997) Platinum-group element abundance

patterns in different mantle environments. *Science* **278**, 1595–1598.

Rehkämper M., Halliday A. N., Alt J., Fitton J. G., Zipfel J., and Takazawa E. (1999) Non-chondritic platinum-group element ratios in oceanic mantle lithosphere: petrogenetic signature or melt percolation? *Earth Planet. Sci. Lett.* **172**, 65–81.

Reisberg L. and Lorand J. P. (1995) Longevity of sub-continental mantle lithosphere from osmium isotope systematics in orogenic peridotite massifs. *Nature* **376**, 159–162.

Reisberg L. and Zindler A. (1986) Extreme isotopic variations in the upper mantle: evidence from Ronda. *Earth Planet. Sci. Lett.* **81**, 29–45.

Rhodes J. M. and Dawson J. B. (1975) Major and trace element chemistry of peridotite inclusions from the Lashaine volcano, Tanzania. *Phys. Chem. Earth* **11**, 545–555.

Richardson S. H. (1986) Latter-day origin of diamonds of eclogitic paragenesis. *Nature* **322**, 623–626.

Richardson S. H. (1989) As definitive as ever: a reply to Archean diamond xenocrysts in kimberlites: how definitive is the evidence? by R. T. Pidgeon. In *Kimberlites and Related Rocks* (eds. J. Ross, A. L. Jaques, J. Ferguson, D. H. Green, S. Y. O'Reilly, R. V. Danchin, and A. J. A. Janse). Geological Society of Australia, Perth, vol. 14, pp. 1070–1072.

Richardson S. H. and Harris J. W. (1997) Antiquity of peridotitic diamonds from the Siberian Craton. *Earth Planet. Sci. Lett.* **151**(3–4), 271–277.

Richardson S. H., Gurney J. J., Erlank A. J., and Harris J. W. (1984) Origin of diamonds in old enriched mantle. *Nature* **310**, 198–202.

Richardson S. H., Erlank A. J., and Hart S. R. (1985) Kimberlite-borne garnet peridotite xenoliths from old enriched subcontinental lithosphere. *Earth Planet Sci. Lett.* **75**, 116–128.

Richardson S. H., Erlank A. J., Harris J. W., and Hart S. R. (1990) Eclogitic diamonds of Proterozoic age from Cretaceous kimberlites. *Nature* **346**, 54–56.

Richardson S. H., Harris J. W., and Gurney J. J. (1993) Three generations of diamonds from old continental mantle. *Nature* **366**, 256–258.

Richardson S. H., Chinn I. L., and Harris J. W. (1999) Age and origin of eclogitic diamonds from the Jwaneng kimberlite, Botswana. *Proc. 7th Int. Kimberlite Conf.* (eds. J. J. Gurney, J. L. Gurney, M. D. Pascoe, and S. H. Richardson). Red Roof Design, Cape Town, vol. 2, pp. 709–713.

Richardson S. H., Shirey S. B., Harris J. W., and Carlson R. W. (2001) Archean subduction recorded by Re–Os isotopes in eclogitic sulfide inclusions in Kimberley diamonds. *Earth Planet. Sci. Lett.* **191**, 257–266.

Ringwood A. E. (1966) The chemical composition and origin of the Earth. In *Advances in Earth Science* (ed. P. M. Hurley). MIT press, Cambridge, Massachusetts, pp. 287–356.

Ringwood A. E. (1991) Phase transformations and their bearing on the constitution and dynamics of the mantle. *Geochim. Cosmochim. Acta* **55**, 2083–2110.

Robinson D. N., Gurney J. J., and Shee S. R. (1984) Diamond eclogite and graphite eclogite xenoliths from Orapa. Botswana. In *Kimberlites: II. The Mantle and Crust-Mantle Relationships* (ed. J. Kornprobst). Elsevier, Amsterdam, pp. 11–24.

Robinson J. A. C., Wood B. J., and Blundy J. D. (1998) The beginning of melting of fertile and depleted peridotite at 1.5 GPa. *Earth Planet. Sci. Lett.* **155**, 97–111.

Roe G. D. (1964) Rubidium-strontium analyses of ultramafic rocks and the origin of peridotites. DPhil. Thesis, Massachusetts Institute of Technology.

Roeder P. L. (1994) Chromite: from the fiery rain of chondrules to the Kilauea Iki lava lake. *Can. Mineral.* **32**, 729–746.

Rosenbaum J. M. (1993) Mantle phlogopite: a significant lead repository? *Chem. Geol.* **106**, 475–483.

Rosenbaum J. M., Zindler A., and Rubenstone J. L. (1996) Mantle fluids: evidence from fluid inclusions. *Geochim. Cosmochim. Acta* **60**, 3229–3252.

Ross J. V. (1983) The nature and rheology of the Cordilleran upper mantle of British Columbia: inferences from peridotite xenoliths. *Tectonophysics* **100**, 321–357.

Ross J. V., Ave Lallement H. G., and Carter N. L. (1980) Stress dependence of recrystallized grain and subgrain size in olivine. *Tectonophysics* **70**, 147–158.

Rozen O. M., Zorin Y. M., and Zayachkovskiy A. A. (1973) A diamond find in Precambrian eclogite of the Kokchetav Block. *Trans. (Doklady) USSR Acad. Sci.: Earth Sci. Sec.* **203**(1–6), 163–165.

Rudnick R. L. and Nyblade A. A. (1999) The thickness and heat production of Archean lithosphere: constraints from xenolith thermobarometry and surface heat flow. In *Mantle Petrology: Field Observations and High Pressure Experimentation* (eds. Y. Fei, C. Bertka, and B. O. Mysen). The Geochemical Society, Houston, vol. 6, pp. 3–12.

Rudnick R. L., McDonough W. F., and Chappell B. W. (1993) Carbonatite metasomatism in the Northen Tanzanian mantle: petrographic and geochemical characteristics. *Earth. Planet. Sci. Lett.* **114**, 463–475.

Rudnick R. L., McDonough W. F., and Orpin A. (1994) Northern Tanzanian peridotite xenoliths: a comparison with Kaapvaal peridotites and inferences on metasomatic interactions. In *Proc. 5th Int. Kimberlite Conf.* (eds. H. O. A. Meyer and O. H. Leonardos). CRPM, vol. 1, pp. 336–353.

Rudnick R. L., McDonough W. F., and O'Connell R. J. (1998) Thermal structure, thickness, and composition of continental lithosphere. *Chem. Geol.* **145**, 395–411.

Rudnick R. L., Ireland T. R., Gehrels G., Irving A. J., Chesley J. T., and Hanchar J. M. (1999) Dating mantle metasomatism: U–Pb geochronology of zircons in cratonic mantle xenoliths from Montana and Tanzania. In *Proc. 7th Int. Kimberlite Conf.* (eds. J. J. Gurney, J. L. Gurney, M. D. Pascoe, and S. H. Richardson). Red Roof Design, Cape Town, vol. 2, pp. 728–735.

Rudnick R. L., Barth M. G., Horn I., and McDonough W. F. (2000) Rutile-bearing refractory eclogites: missing link between continents and depleted mantle. *Science* **287**, 278–281.

Russell J. K. and Kopylova M. G. (1999) A steady state conductive geotherm for the north central Slave, Canada: inversion of petrological data from the Jericho kimberlite pipe. *J. Geophys. Res.* **104**, 7089–7101.

Russell J. K., Dipple G. M., and Kopylova M. G. (2001) Heat production and heat flow in the mantle lithosphere, Slave craton, Canada. *Phys. Earth Planet. Int.* **123**, 27–44.

Sachtleben T. H. and Seck H. A. (1981) Chemical control of Al-solubility in orthopyroxene and its implications on pyroxene geothermometry. *Contrib. Mineral. Petrol.* **78**, 157–165.

Salters V. J. M. and Zindler A. (1995) Extreme $^{176}Hf/^{177}Hf$ in the sub-oceanic mantle. *Earth Planet. Sci. Lett.* **129**, 13–30.

Saltzer R. L., Chatterjee N., and Grove T. L. (2001) The spatial distribution of garnets and pyroxenes in mantle peridotites: pressure-temperature history of peridotites from the Kaapvaal craton. *J. Petrol.* **42**, 2215–2229.

Sautter V., Haggerty S. E., and Field S. W. (1991) Ultradeep (>300 kilometers) ultramafic xenoliths: petrological evidence from the transition zone. *Science* **252**, 827–830.

Schiano P. and Clocchiatti R. (1994) Worldwide occurrence of silicate-rich melts in sub-continental and sub-oceanic mantle minerals. *Nature* **368**, 621–624.

Schmidberger S. S. and Francis D. (1999) Nature of the mantle roots beneath the North American craton: mantle xenolith evidence from Somerset Island kimberlites. *Lithos* **48**, 195–216.

Schmidberger S. S. and Francis D. (2001) Constraints on the trace element composition of the Archean mantle root

beneath Somerset Island, Arctic Canada. *J. Petrol.* **42**, 1095–1117.

Schmidberger S. S., Simonetti A., and Francis D. (2001) Sr–Nd–Pb isotope systematcis of mantle xenoliths from Somerset Island kimberlites: evidence for lithosphere stratification beneath Arctic Canada. *Geochim. Cosmochim. Acta* **65**, 4243–4255.

Schmidberger S. S., Simonetti A., Francis D., and Gariepy C. (2002) Probing Archean lithosphere using the Lu–Hf isotope systematics of peridotite xenoliths from Somerset Island kimberlites, Canada. *Earth Planet. Sci. Lett.* **197**, 245–259.

Schrauder M. and Navon O. (1994) Hydrous and carbonatitic mantle fluids in fibrous diamonds from Jwaneng, Botswana. *Geochim. Cosmochim. Acta* **58**, 761–771.

Schrauder M., Koeberl C., and Navon O. (1996) Trace element analyses of fluid-bearing diamonds from Jwaneng, Botswana. *Geochim. Cosmochim. Acta* **60**, 4711–4724.

Schulze D. J. (1986) Calcium anomalies in the mantle and a subducted metaserpentinite origin for diamonds. *Nature* **319**, 483–485.

Schulze D. J. (1987) Megacrysts from alkalic volcanic rocks. In *Mantle Xenoliths* (ed. P. H. Nixon). Wiley, Chichester, pp. 433–451.

Schulze D. J. (1989) Constraints on the abundance of eclogite in the upper mantle. *J. Geophys. Res.* **94**, 4205–4212.

Schulze D. J. (1995) Low-Ca garnet harzburgites from Kimberley, South Africa: abundance and bearing on the structure and evolution of the lithosphere. *J. Geophys. Res.* **100**(12), 513–526.

Schulze D. J., Wiese D., and Steude J. (1996) Abundance and distribution of diamonds in eclogite revealed by volume visualization of CT X-ray scans. *J. Geol.* **104**(1), 109–113.

Schulze D. J., Valley J. W., and Spicuzza M. (2000) Coesite eclogites from the Roberts Victor kimberlite, South Africa. *Lithos* **54**, 23–34.

Scott-Smith B. H., Danchin R. V., Harris J. W., and Stracke K. J. (1984) Kimberlites near Orroroo, South Australia. In *Kimberlites II: the Mantle and Crust-mantle Relationships (Proc. Third Int.l Kimberlite Conf.)* (ed. J. Kornprobst). Elsevier, Amsterdam, pp. 121–142.

Sen G. (1988) Petrogenesis of spinel lherzolite and pyroxenite suite xennoliths from the Koolau shield, Oahu, Hawaii: implications for petrology of the post-eruptive lithosphere beneath Oahu. *Contrib. Mineral. Petrol.* **100**, 61–91.

Sen G. and Leeman W. P. (1991) Iron-rich lherzolite xenoliths from Oahu: origin and implications for Hawaiian magma sources. *Earth Planet. Sci. Lett.* **102**, 45–57.

Shi L., Francis D., Ludden J., Frederiksen A., and Bostock M. (1998) Xenolith evidence for lithospheric melting above anomalously hot mantle under the northern Canadian Cordillera. *Contrib. Mineral. Petrol.* **131**, 39–53.

Shimizu N. (1975) Rare earth elements in garnets and clinopyroxenes from garnet lherzolite nodules in kimberlites. *Earth Planet. Sci. Lett.* **25**, 26–35.

Shimizu N. (1999) Young geochemical features in cratonic peridotites from southern Africa and Siberia. In *Mantle Petrology: Field Observations and High Pressure Experimentation* (eds. Y. Fei, C. M. Bertka, and B. Mysen). The Geochemical Society, Houston, vol. 6, pp. 47–55.

Shimizu N. and Richardson S. H. (1987) Trace element abudance patterns of garnet inclusions in peridotite suite diamonds. *Geochim. Cosmochim. Acta* **51**, 755–758.

Shimizu N., Sobolev N. V., and Yefimova E. S. (1997) Chemical heterogeneities of inclusion garnets and juvenile character of peridotitic diamonds from Siberia. *Russian J. Geol. Geophys.* **38**(2), 356–372.

Shirey S. B. and Walker R. J. (1998) The Re–Os isotope system in cosmochemistry and high-temperature geochemistry. *Ann. Rev. Earth Planet. Sci.* **26**, 423–500.

Shirey S. B., Carlson R. W., Richardson S. H., Menzies A., Gurney J. J., Pearson D. G., Harris J. W., and Wiechert U. (2001) Archean emplacement of eclogitic components into the lithospheric mantle during formation of the Kaapvaal craton. *Geophys. Res. Lett.* **28**, 2509–2512.

Shirey S. B., Harris J. W., Richardson S. H., Fouch M. J., James D. E., Cartigny P., and Viljoen F. (2002) Seismic structure, diamond geology and evolution of the Kaapvaal-Zimbabwe craton. *Science* **297**, 1683–1686.

Shumilova T. G. (2002) Carbynoid carbon and its pseudomorphs after diamond in the eclogitization zone—(Shumikha complex, central Urals). *Doklady—Earth Sciences* **383**(2), 222–224.

Simon N. S. C., Carlson R. W., Pearson D. G., and Davies G. R. (2002) The Lu–Hf isotope composition of cratonic lithosphere: disequilibrium between garnet and clinopyroxene in kimberlite xenoliths. *Geochim. Cosmochim. Acta* **6651**, A717.

Simon N. S. C., Irvine G. J., Davies G. R., Pearson D. G., and Carlson R. W. (2003) The origin of garnet and clinopyroxene in "depleted" Kaapvaal peridotites. *Lithos* (in press).

Smith C. B., Gurney J. J., Harris J. W., Robinson D. N., Shee S. R., and Jagoutz E. (1989) Sr and Nd isotopic systematics of diamond-bearing eclogite xenoliths and eclogite inclusions in diamond from southern Africa. *Kimberlites and Related Rocks*. Spec. Pub. Geol. Soc. Austral., no. 14, vol. 2, pp. 853–863.

Smith C. B., Gurney J. J., Harris J. W., Otter M. L., Kirkley M. B., and Jagoutz E. (1991) Neodymium and strontium isotope systematics of eclogite and websterite paragenesis inclusions from single diamonds, Finsch and Kimberley Pool, RSA. *Geochim. Cosmochim. Acta* **55**, 2579–2590.

Smith D. (1977) The origin and interpretation of spinel-pyroxene clusters in peridotite. *J. Geol.* **85**, 476–482.

Smith D. (1999) Temperatures and pressures of mineral equilibration in peridotite xenoliths: review, discussion and implications. In *Mantle Petrology: Field Observations and High Pressure Experimentation* (eds. Y. Fei, C. Bertka, and B. O. Mysen). The Geochemical Society, Houston, vol. 6, pp. 171–188.

Smith D. and Barron B. R. (1991) Pyroxene-garnet equilibration during cooling in the mantle. *Am. Mineral.* **76**, 1950–1963.

Smith D. and Boyd F. R. (1992) Compositional zonation in garnets of peridotite xenoliths. *Contrib. Mineral. Petrol.* **112**, 134–147.

Smith D., Griffin W. L., Ryan C. G., and Sie S. H. (1991) Trace element zonation in garnets from the thumb: heating and melt infiltration below the Colorado Plateau. *Contrib. Mineral. Petrol.* **107**, 60–79.

Smith D., Riter J. C. A., and Mertzman S. A. (1999) Water rock interactions, orthopyroxene growth and Si-enrichment in the mantle: evidence in xenoliths from the Colorado Plateau, southwestern United States. *Earth Planet. Sci. Lett.* **167**, 347–356.

Snow J. E. and Dick H. J. B. (1995) Pervasive magnesium loss by marine weathering of peridotite. *Geochim. Cosmochim. Acta* **59**, 4219–4235.

Snow J. E. and Reisberg L. C. (1995) Erratum of "Os isotopic systematics of the MORB mantle: results from altered abyssal peridotites. *Earth Planet. Sci. Lett.* **136**, 723–733.

Snyder G. A., Jerde E. A., Taylor L. A., Halliday A. N., Sobolev V. N., and Sobolev N. V. (1993) Nd and Sr isotopes from diamondiferous eclogites, Udachnaya kimberlite pipe, Yakutia, Siberia: evidence of differentiation in the early Earth? *Earth. Planet. Sci. Lett.* **118**, 91–100.

Snyder G. A., Taylor L. A., Crozaz G., Halliday A. N., Beard B., Sobolev V., and Sobolev N. (1997) The origins of Yakutian eclogite xenoliths. *J. Petrol.* **38**, 85–113.

Sobolev N. V. (1974) Deep-seated Inclusions in Kimberlites and the Problem of the Composition of the Upper Mantle. Nauka, Novosibirsk, 264pp (in Russian).

Sobolev N. V. and Shatsky V. S. (1990) Diamond inclusions in garnets from metamorphic rocks. *Nature* **343**, 742–746.

Sobolev N. V., Lavrent'yev Y. G., Pokhilenko N. P., and Usova L. V. (1973) Chrome-rich garnets from the kimberlites of Yakutia and their paragenesis. *Contrib. Mineral. Petrol.* **40**, 39–52.

Sobolev N. V., Galimov E. M., Ivanovskaya I. N., and Yefimova E. S. (1979) isotopic composition of carbon of diamonds containing crystalline inclusions. *Akad. Nauk SSSR Doklady* **249**, 1217–1220.

Sobolev N. V., Yefimova E. S., Channer D. M. D., Anderson P. F. N., and Barron K. M. (1998) Unusual upper mantle beneath Guaniamo, Guyana Shield, Venezuela: evidence from diamond inclusions. *Geology* **26**, 971–974.

Stachel T. and Harris J. W. (1997) Diamond precipitation and mantle metasomatism: evidence from the trace element chemistry of silicate inclusions in diamonds from Akwatia, Ghana. *Contrib. Min. Petrol.* **129**(2–3), 143–154.

Stachel T., Viljoen K. S., Brey G., and Harris J. W. (1998) Metasomatic processes in lherzolitic and harzburgitic domains of diamondiferous lithospheric mantle. *Earth Planet. Sci. Lett.* **159**, 1–12.

Stachel T., Harris J. W., and Brey G. P. (1999) REE patterns of peridotitic and eclogitic inclusions in diamonds from Mwadui (Tanzania). In *Proceedings of the VIIth International Kimberlite Conference* (eds. J. Gurney, J. L. Gurney, M. D. Pascoe, and S. H. Richardson), Red Roof Designs, Cape Town, vol. 2, pp. 829–835.

Stachel T., Harris J. W., Brey G. P., and Joswig W. (2000) Kankan diamonds (Guinea): II. Lower mantle inclusion parageneses. *Contrib. Min. Petrol.* **140**(1), 16–27.

Stachel T., Harris J. W., Aulbach S., and Deines P. (2002) Kankan diamonds (Guinea): III. $\delta^{13}C$ and nitrogen characteristics of deep diamonds. *Contrib. Min. Petrol.* **142**(4), 465–475.

Stern C. R., Saul S., Skewes M. A., and Futa K. (1989) Garnet peridotite xenoliths from the Pali-Aike alkali basalts of southernmost South America. In *Kimberlites and Related Rocks*. Geol. Soc. Austral. Spec. Publ. No. 14 (ed. J. Ross). Blackwell, Perth, vol. 2, pp. 735–744.

Stolz A. J. and Davies G. R. (1988) Chemical and isotopic evidence from spinel lherzolite xenoliths for episodic metasomatism of the upper mantle beneath southeast Australia. In *Oceanic and Continental Lithosphere: Similarities and Differences* J. Petrology (Spec. volume) (eds. M. A. Menzies and K. G. Cox). Oxford University Press, Oxford, pp. 303–330.

Stosch H. G. and Lugmair G. W. (1986) Trace element and Sr and Nd isotope geochemistry of peridotite xenoliths from the Eifel (West Germany) and their bearing on the evolution of the sub-continental lithosphere. *Earth Planet. Sci. Lett.* **80**, 281–298.

Stosch H. G. and Seck H. A. (1980) Geochemistry and mineralogy of two spinel peridotite suites from Dreiser-Weiher, West Germany. *Geochim. Cosmochim. Acta* **44**, 457–470.

Streckeisen A. (1976) To every plutonic rock its proper name. *Earth Sci. Rev.* **12**, 1–33.

Stueber A. M. and Murthy V. R. (1966) Sr isotope and alkali element abundances in ultramafic rocks. *Geochim. Cosmocim. Acta* **33**, 543–553.

Sun S. S. (1982) Chemical composition and origin of the Earth's primitve mantle. *Geochim. Cosmochim. Acta* **46**, 179–192.

Tatsumoto M., Basu A. R., Wankang H., Junwen W., and Guanhong X., Sr (1992) Nd and Pb isotopes of ultramafic xenoliths in volcanic rocks of eastern China: enriched components, EMI and EMII in sub-continental lithosphere. *Earth Planet. Sci. Lett.* **113**, 107–128.

Taylor L. A. and Neal C. R. (1989) Eclogites with oceanic crustal and mantle signatures from the Bellsbank kimberlite, South Africa: Part 1. Mineralogy, Petrography, and whole rock chemistry. *J. Geol.* **97**, 551–567.

Taylor L. A., Snyder G. A., Crozaz G., Sobolev V. N., Yefimova E. S., and Sobolev N. V. (1996) Eclogitic inclusions in diamonds: evidence of complex mantle processes over time. *Earth Planet. Sci. Lett.* **142**(3–4), 535–551.

Taylor L. A., Keller R. A., Snyder G. A., Wang W. Y., Carlson W. D., Hauri E. H., McCandless T., Kim K. R., Sobolev N. V., and Bezborodov S. M. (2000) Diamonds and their mineral inclusions, and what they tell us: a detailed "pull-apart" of a diamondiferous eclogite. *Int. Geol. Rev.* **42**(11), 959–983.

Taylor W. R. (1998) An experimental test of some geothermometer and geobarometer formulations for upper mantle peridotites with application to the thermobarometry of fertile lherzolite and garnet websterite. *Neus. Jahrb. Mineral. Abh.* **172**, 381–408.

Taylor W. R., Jaques A. L., and Ridd M. (1990) Nitrogen-defect aggregation characteristics of some Australasian diamonds: time-temperature constraints on the source regions of pipe and alluvial diamonds. *Am. Min.* **75**, 1290–1310.

Thompson R. N., Morrison M. A., Hendry G. L., and Parry S. L. (1983) Continental flood basalts…arachnids rule OK? In *Continental Flood Basalts and Mantle Xenoliths* (eds. C. J. Hawkesworth and M. J. Norry). Shiva, Nantwich, pp. 158–185.

Tompkins L. A. and Haggerty S. E. (1984) The Koidu Kimberlite Complex, Sierra Leone: geological setting, petrology and mineral chemistry. In *Kimberlites II: the Mantle and Crust-Mantle Relationships* (ed. J. Kornprobst). Elsevier, Amsterdam, pp. 83–105.

Trueb L. F. and Wys E. C. d. (1969) Carbonado: natural polycrystalline diamond. *Science* **165**(2895), 799–802.

Twiss R. J. (1977) Theory and applicability of a recrystallized grain size paleopiezometer. *Pure Appl. Geophys.* **115**, 227–244.

van Heerden L. A., Boyd S. R., Milledge H. J., and Pillinger C. T. (1995) The carbon- and nitrogen isotope characteristics of the Argyle and Ellendale diamonds, Western Australia. *Int. Geol. Rev.* **37**(1), 39–50.

Van Orman J. A., Grove T. L., and Shimizu N. (2001) Rare earth element diffusion in diopside: influence of temperature, pressure, and ionic radius, and an elastic model for diffusion in silicates. *Contrib. Min. Petrol.* **141**, 687–703.

Van Orman J. A., Grove T. L., Shimizu N., and Layne G. D. (2002) Rare Earth element diffusion in a natural pyrope single crystal at 2.8 GPa. *Contrib. Min. Petrol.* **142**, 416–424.

Vance D., Stone J. O. H., and O'Nions R. K. (1989) He, Sr and Nd isotopes in xenoliths from Hawaii and other oceanic islands. *Earth Planet. Sci. Lett.* **96**(1–2), 147–160.

Vannucci R., Piccardo G. B., Rivalenti G., Zanetti A., Rampone E., Ottolini L., Oberti R., Mazzucchelli M., and Bottazzi P. (1995) Origin of LREE-depleted amphiboles in the sub-continental mantle. *Geochim. Cosmochim. Acta* **59**, 1763–1771.

Vaselli O., Downes H., Thirwall M. F., Dobosi G., Coradossi N., Seghedi I., Szakacs A., and Vannucci R. (1995) Ultramafic xenoliths in Plio-pleistocene alkali basalts from the eastern Transylvanian Basin: depleted mantle enriched by vein metasomatism. *J. Petrol.* **36**, 23–53.

Verhoogen J. (1956) Temperatures within the earth. *Phys. Chem. Earth* **1**, 17–43.

von Seckendorff V. and O'Neill H. S. C. (1993) An experimental study of Fe–Mg partitioning between olivine and orthopyroxene at 1173, 1273 and 1423 K and 1.6 GPa. *Contrib. Min. Petrol.* **113**, 196–207.

Viljoen K. S., Smith C. B., and Sharp Z. D. (1996) Stable and radiogenic isotope study of eclogite xenoliths from the Orapa kimberlite, Botswana. *Chem. Geol.* **131**, 235–255.

Wada N. and Matsuda J. (1998) A noble gas study of cubic diamonds from Zaire: constraints on their mantle source. *Geochim. Cosmochim. Acta* **63**, 2335–2345.

Wagner P. A. (1914) *The Diamond Fields of Southern Africa*. Transvaal Leader, Johannesburg 347pp.

Walker R. J., Carlson R. W., Shirey S. B., and Boyd F. R. (1989a) Os, Sr, Nd, and Pb isotope systematics of southern African peridotite xenoliths: implications for the chemical evolution of sub-continental mantle. *Geochim. Cosmochim. Acta* **53**, 1583–1595.

Walker R. J., Shirey S. B., Horan M. F., and Hanson G. N. (1989b) Re—Os, Rb–Sr, and O isotopic systematics of the Archean Kolar schist belt, Karnataka, India. *Geochim. Cosmochim. Acta.* **53**, 3005–3013.

Walter M. J. (1998) Melting of garnet peridotite and the origin of komatiite and depleted lithosphere. *J. Petrol.* **39**, 29–60.

Walter M. J. (1999) Melting residues of fertile peridotite and the origin of cratonic lithosphere. In *Mantle Petrology: Field Observations and High Pressure Experimentation* (eds. Y. Fei, C. Bertka, and B. O. Mysen). The Geochemical Society, Houston, vol. 6, pp. 225–240.

Wilding M. C., Harte B., and Harris J. W. (1991) Evidence for a deep origin for Sao Luiz diamonds. In *Fifth International Kimberlite Conference; Extended Abstracts* (ed. Anonymous), vol. 5, pp. 456–458 [publisher varies].

Wilks J. and Wilks E. (1991) *Properties and Applications of Diamond*. Heinemann, Oxford.

Wilshire H. G. and Shervais J. W. (1975) Al-augite and Cr-diopside ultramafic xenoliths in basaltic rocks from the Western United States. *Phys. Chem. Earth* **9**, 257–272.

Wilson M. R., Kyser T. K., and Fagan R. (1996) Sulfur isotope systematics and platinum group element behavior in REE-enriched metasomatic fluids: a study of mantle xenoliths from Dish Hill, California, USA. *Geochim. Cosmochim. Acta* **60**, 1933–1942.

Winterburn P. A., Harte B., and Gurney J. J. (1990) Peridotite xenoliths from the Jagersfontein kimberlite pipe: I. Primary and primary-metasomatic mineralogy. *Geochim. Cosmochim. Acta* **54**, 329–341.

Witt-Eickschen G. and Harte B. (1994) Distribution of trace elements between amphibole and clinopyroxene from mantle peridotites of the Eifel (western Germany): an ion microprobe study. *Chem. Geol.* **117**, 235–250.

Witt-Eickschen G. and Seck H. A. (1991) Solubility of Ca and Al in orthopyroxene from spinel peridotite: an improved version of an empirical thermometer. *Contrib. Mineral. Petrol.* **106**, 431–439.

Wood B. J. and Nicholls J. (1978) The thermodynamic properties of reciprocal solid solutions. *Contrib. Mineral. Petrol.* **66**, 389–400.

Wood B. J. and Virgo D. (1989) Upper mantle oxidation state: ferric iron contents of lherzolite spinels by ^{57}Fe Mössbauer spectroscopy and resultant oxygen fugacities. *Geochim. Cosmochim. Acta* **53**, 1277–1291.

Wood B. J., Bryndzia L. T., and Johnson K. E. (1990) Mantle oxidation state and its relationship to tectonic environment and fluid speciation. *Science* **248**, 337–345.

Xu S., Okay A. I., Ji S., Sengor A. M. C., Su W., Liu Y., and Jiang L. (1992) Diamond from the Dabie Shan metamorphic rocks and its implication for tectonic setting. *Science* **256**(5053), 80–82.

Xu Y., Menzies M. A., Vroon P., Mercier J. C., and Lin C. (1998) Texture-temperature-geochemistry relationships in the upper mantle as revealed from spinel peridotite xenoliths from Wanqing, NE China. *J. Petrol.* **39**, 469–493.

Yaxley G. M. and Green D. H. (1998) Reactions between eclogite and peridotite: mantle refertilisation by subduction of oceanic crust. *Schweitz. Mieral. Petrogr. Mitt.* **78**, 243–255.

Yaxley G. M., Green D. H., and Kamenetsky V. (1998) Carbonatite metasomatism in the southeastern Australian lithosphere. *J. Petrol.* **39**, 1917–1930.

Yefimova E. S., Sobolev N. V., and Pospelova L. N. (1983) Sulfide inclusions in diamond and specific features of their paragenesis. *Zap. Vsesoy. Mineral. Obsh.* **112**, 300–310.

Yoder H. S. J. (1976) *Generation of Basaltic Magma*. National Academy of Sciences, Washington, DC.

Zanetti E., Vannucci R., Botazzi P., Oberi R., and Ottolini L. (1996) Infiltration metasomatism at Lherz as monitored by systematic ion-microprobe investigations close to a hornblendite vein. *Chem. Geol.* **134**, 113–133.

Zhuravlev A. Z., Laz'ko Y. Y., and Ponomarenko A. I. (1991) Radiogenic isotopes and REE in garnet peridotite xenoliths from the Mir kimberlite pipe, Yakutia. *Geokhimiya* **7**, 982–994.

Zipfel J. and Wörner G. (1992) Thermobarometry on four- and five-phase periodotites from a continental rift system: evidence for upper mantle uplift and cooling at the Ross Sea margin (Antartica). *Contrib. Mineral. Petrol.* **111**, 24–36.

Zindler A. and Hart S. R. (1986) Chemical geodynamics. *Ann. Rev. Earth Plan. Sci.* **14**, 493–571.

Zindler A. and Jagoutz E. (1988) Mantle cryptology. *Geochim. Cosmochim. Acta.* **52**, 319–333.

Treatise on Geochemistry
ISBN (set): 0-08-043751-6
Volume 2; (ISBN: 0-08-044337-0); pp. 171–275